SOUTH AMERICAN SEISMOTECTONICS FROM SAAS DATA

by

JESUS BERROCAL

B.Sc. (U.N.S.A. - Peru)

M.Sc. (Edinburgh - U.K.)

Thesis submitted for the degree of

Doctor of Philosophy

in the University of Edinburgh

January 1974

ABSTRACT

The study of the principal tectonic features of South America, by using seismic data recorded at SAAS, is the main objective of this research.

Over 200 events, which occurred in 1972 within 95° of distance from SAAS, were analysed in order to obtain the following observed parameters which refer to the main P phase: travel time, magnitude, azimuth and apparent velocity. These parameters were compared with expected values, which were computed by using NOAA epicentral data and, as a result, four different kind of residuals were obtained.

The analysis of the distribution of these residuals, especially the distribution of residuals in azimuth and apparent velocity, allowed the identification of the following important tectonic features in South America:

1) a lateral discontinuity under the central part of western South America with a NW-SE orientation and dipping slightly to the SW; 2) a lateral discontinuity, although less well defined, under the Amazon Basin, perhaps dipping to the South; and 3) a horizontal discontinuity at around 650 km of depth, having a high velocity property.

Other characteristics of South American tectonics that it was possible to identify in this study are the existence of defined areas with different degree of amplitude attenuation, and a correspondence between this attenuation and the travel time of the seismic waves when recorded at SAAS. This, together with the distribution of the

P phase velocity, at both sides of the suggested lateral discontinuities, (necessary to explain the observed values of the residuals in azimuth and in apparent velocity), permitted the division of South America into three tectonic provinces, with their boudaries coinciding with the lateral discontinuities, and having different tectonic characteristics.

The main arguments used to explain the existence of the suggested lateral discontinuities are based on the basic concept of the plates tectonic theory, and it was found that the results presented in this study agree perfectly with the axioms of plate tectonics. The history of the formation of the principal physiographic features of South America has been correlated with the origin of the lateral discontinuities, which were explained as a result of the change in the directions of continental drift and different convergence rates at different latitudes of South America.

Further evidence, which supports the results of this work, has been found by analysing the vertical distribution of the South American seismicity reported in the last 10 years: several sections at different latitudes of western South America have been plotted in vertical planes, at right angles with the orientation of the subduction zone between the South American and the Eastern Pacific plates, showing the existence of the suggested lateral discontinuities. The sections also show a downgoing slab reaching under 600Km of depth

with a dipping angle of 47^{o}, under the western side of the central tectonic province. The slabs under the western side of the other two provinces are smaller and have dipping angles other than 47^{o}: smaller in the southern province and larger in the northern province.

Another supporting piece of evidence was found by analysing, in time and space, the distribution of the deep events which occurred in South America in the last 10 years. The events occurring at the southernmost end of the slab are followed, after several weeks or several months, by fewer but larger shocks at the northernmost deep end. Some shallower large shocks, which occurred in the Andean area of the central province, also agree with the pattern shown by the deep events. This proves the continuity of this slab and provides a means for earthquake forecasting.

This work represents the first results obtained with SAAS data and reports the activity involved in the development and installation of SAAS since 1968.

LIST OF CONTENTS

LIST OF ILLUSTRATIONS

LIST OF TABLES

CHAPTER 1

INTRODUCTION

The Andean region of Latin America is one of the most seismically active areas of the world. Very destructive earthquakes occurring in this region have killed many thousands of people and have affected the growing economy of the countries in which these disasters took place, causing serious problems in their development. Some examples of these destructive shocks are those which occurred in Chile in May 1960 (M=8.3)[1], with damage in the southern central area of the country and over 1,500 persons killed, in Peru in May 1970 (m_b=6.6)[2], with damage in the central area of the country and over 70,000 people killed, and in Guatemala in December 1972 (m_b=5.6)[2], with great damage in Managua and the loss of over 6,000 people. In spite of its great seismic activity, very little seismic research has been carried out in South America compared to similar regions in the world.

The main reason for this deficiency is the lack of necessary support from Latin American governments to execute seismological research, and the small number of good quality seismic stations. Most of the stations in South America are located in the Andes and two on the eastern coast. Most of them have to operate with very low gain due to their proximity to the oceans. This is a great disadvantage in the determination of the focal parameters of earthquakes which occur within this region and in the study of its seismicity.

---

(1) Calculated by Duda (1965) from surface waves data

(2) NOAA m_b magnitude

The creation of the Centro Regional de Sismologia para America del Sur (CERESIS) was intended to organise the dispersed efforts in each country of its region in such a way that regional studies and collaboration between the seismological institutions of Latin America could take place. A very sensitive seismic station was planned to work attached to CERESIS, and to be installed in the most convenient place of South America. This station was intended to be the field laboratory of the centre and to improve the number of seismic observations on the eastern side of the Andes.

The installation of the South American Array System (SAAS) in Brasilia, as the attached station of CERESIS,has given seismologists a very powerful tool to increase their knowledge of South American seismicity; it is also a means of studying the internal constitution of the Earth in this region by using high quality data, with the advantages offered by seismic arrays and by the handling of data recorded on multichannel magnetic tape. The very low noise of the site occupied by SAAS and its position in relation to the seismic areas of Latin America are also advantages that increase the quality and importance of the data recorded at SAAS.

With the development of the plate tectonics theory, new ideas to explain the seismic activity in the modern orogenic belts have arisen. The knowledge of the structure of the Earth's interior under the seismic areas of the plates and the study of other tectonic features around these seismic areas will lead to a better understanding of the mechanism (or mechanisms) which produce earthquakes in these areas. The South American plate is the most characteristic example of the plate tectonics theory. It is surrounded almost completely

by seismic areas, with a relatively stable central shield constituting most of the South American continent. SAAS is located in the central part of this shield.

Since the appearance of seismic arrays in 1961, as a tool to provide means for the detection and identification of nuclear explosions, a great deal of research has been carried out by using array data in the study of natural seismic events. The most important contribution in the study of the Earth's interior that seismic arrays can provide, is the possibility of determining the azimuth and the apparent velocity (function of $dT/d\Delta$) that the seismic waves present during their passage through the array. Other contributions that arrays can offer to seismology are the improvement of the signal/noise ratio by the insertion of proper delays between sensors before summing their signals to enhance a particular signal coming from a given azimuth and distance (velocity filtering), and the possibility of correlating its data in such a way that other features, among the signal of one single event or between signals of events from different areas, can be compared from the resulting correlograms, which otherwise would not have been possible to notice in a traditional seismogram.

The azimuth and apparent velocity calculated from array data are affected by refractions of the seismic waves in lateral and horizontal discontinuities of the Earth's interior. This effect is greater for near events, when the horizontal layering of the crust has a considerable effect especially in the apparent velocity, and in cases with complicated internal structure near the source of the event or near the site of the recording station. If the

array is located on a site with uniform internal structure or if the structure under the array can be assessed, this disadvantage can be turned into a very useful tool to study the lateral and horizontal discontinuities through which the seismic waves have to travel to reach the array. Very useful information can also be obtained in this way regarding the structure of the seismic source and its surroundings.

A large number of researchers have used $dT/d\Delta$ from array data which has been inverted with the Herglotz-Wiechert technique and have found the velocity distribution for P phases in the Earth's interior, determining in this way several horizontal and lateral discontinuities in different parts of the Earth's mantle; some examples of these studies can be found in Niazi and Anderson (1965), Johnson (1966, 1967, 1969), Chinnery and Toksöz (1967), Kanamori (1967), Hales et al (1968), Husebye et al (1971), and Simpson (1973).

Although a great deal of attention has been given to the variations of $dT/d\Delta$, very few studies have used the azimuth departures observed in array studies. Departures in observed azimuths were used by Niazi (1966) to study the local structure under the Tonto Forest Seismological Observatory array in U.S.A. and have been mentioned very briefly by Simpson (1973) as possibly resulting from the effect of lateral variations in structure along the ray paths, although his observation was referred to the differences in the azimuth departures for different arrivals from the same event.

It is assumed in this work that departures in the azimuth and apparent velocity ($dT/d\Delta$) observed at an array are due to refractions

of the ray paths in lateral and horizontal discontinuities and that lateral discontinuities affect mostly the observed azimuth and the horizontal ones affect mostly the observed apparent velocity ($dT/d\Delta$). If these departures could be identified with the structure belonging to different seismic paths, it would then be possible to get appropriate corrections for known seismic areas. These corrections will permit reliable epicentral determinations of events within those areas by using array data, especially in the case of undetermined events. Hence an improvement in the knowledge of the seismicity of those areas is possible.

Another means of studying the internal constitution of the Earth, is by the distribution of the time residuals of the P phase at different azimuths and epicentral distances from one station or network of stations. The time residual is the difference between the observed time at one point and its expected time calculated by using appropriate travel time tables. The tables which are most commonly used are the Jeffreys-Bullen tables originally published in 1940. Since then, the existence of regional deviations from the J-B tables have been noticed, which have led to the construction of regional travel time tables in some parts of the world; and have also given rise to speculation that internal discontinuities exist either in the ray paths or under the stations.

Another way of studying the Earth's internal constitution is by analysing the azimuthal-distance distribution of the amplitude of the observed P phase, and noticing any existing anomaly in the distribution of Q values in the mantle by comparing the observed amplitudes with the expected ones. In this way it may

not be possible to find small discontinuities, but large differences in amplitude can be caused by important heterogenities inside the Earth.

Time residuals and amplitude anomalies observed at SAAS are studied in this work, with the hope of finding some relationship with the results obtained by using the observed departures in azimuth and apparent velocity calculated from SAAS data. All these methods of studying the Earth's interior are used in the present research, by employing SAAS data, to give a general idea of the main tectonic features of Latin America, with the hope that this knowledge may help future research leading to the minimization of the disastrous effects that earthquakes cause in this part of the world.

1.1 Summarized History of SAAS

The South American Array System was originally suggested at the Conference of Latin American Experts on Seismology which was held in Lima in December 1963 with the objective of discussing the creation of a regional seismological centre for South America. The experts recommended the establishment of a highly sensitive seismic station, attached to the projected centre, in the most convenient place in South America.

A portable magnetic tape recording seismograph which was being developed at the Seismological Unit of the University of Edinburgh was offered by Dr. P.L. Willmore to be taken to South America to constitute the preliminary stage of the station recommended at the Conference of Experts. The Instituto Geofisico del Peru gave all its cooperation towards the realization of this project since 1964, when the author was sent to Edinburgh to participate in the organisation of an experimental expedition to South America, taking the portable magnetic tape recording seismograph of the University of Edinburgh.

In July 1966 the experimental expedition set out for Brasilia (Brazil) where a temporary small array (experimental SAAS) was installed with 12 points forming an asymmetrical cross. Two different distributions of the points were tested during the four months that the recording period of the expedition lasted (November 1966 - February 1967). This expedition was successful thanks to the cooperation of the Observatorio Nacional do Rio de Janeiro, the University of Brasilia and other official Brazilian Institutions.

After the preliminary analysis of some records of the experimental SAAS, the excellent quality of the occupied quiet mid-continental site in the detection of small Andean events was verified, and the advantages of using radio links and portable equipment in array installations were shown. In December 1966, Dr. Willmore, as the Director of the Seismology Unit of the University of Edinburgh, organised a meeting in Brasilia with the assistance of representatives of CERESIS, Instituto Geofisico del Peru, UNESCO, United States Coast and Geodetic Survey (now NOAA), and University of Brasilia (UnB), to discuss the establishment of a permanent array in place of the experimental one. This idea was supported by all the participants of the meeting and it was decided that a permanent SAAS would be installed in Brasilia, with its equipment and technical assistance supplied by the British Institute of Geological Sciences (IGS) and with its operation and organisation supplied by the South American institutions. It was also decided to install a standard seismograph system (WWSS) supplied by NOAA at the recording vault of the array. It was decided that part of the equipment used in the experimental SAAS was to be left in Brasilia to link the experimental stage of the operation with the permanent installations and to enhance the Brazilian interest in this project.

The linking stage of SAAS started in June 1967, with a small array of 4 points. Since then, up to the installation of the permanent SAAS, there has been continuous recording at Brasilia, although most of the time with only one or two points in operation. In March 1968 continuous preliminary readings of the records started

to be made and since then seismic messages were sent to CERESIS, NOA, and ISC under the code BAE ($15^{o}50'$ 24.9"S, $47^{o}49'$ 05.3"W).

During 1969 and part of 1970 the installations to accommodate the permanent SAAS and the WWSS system were prepared. Topographic locations for the array points were made and proper underground pits were constructed to house the SAAS recording equipment and the WWSSS equipment. Details of the permanent SAAS installations and other information related to the array are given in Chapter 2.

In September 1970 the permanent SAAS started to operate with five points but it has only been in continuous operation since November of that year and SAAS seismic bulletins since then referred to the point E4 of the new array, under the code BDF ($15^{o}39'$ 51.1"S and $47^{o}54'$ 11.2"W). Most of the remaining points were installed during 1971 and 1972, so that now, in November 1973, SAAS is operating with all its elements.

In September 1972 the WWSSS equipment was installed in the vault constructed at E4, but its operation has been discontinued many times because of failures of the equipment.

The IGS contribution to the establishment of SAAS is in the form of all its equipment, technical staff, financial support for its installation and supplies of magnetic tape, batteris, paper and ink for jet pen recorder, etc..

The Departamento de Geociencias of the University of Brasilia (formerly Instituto Central de Geo-ciencias) participates in the project by providing the necessary staff to operate the station, premises for analysis and electronic laboratories, administration of the station, and financial support. Other Brazilian Institutions like

the Conselho Nacional de Pesquisas (National Research Council) have participated in the project with financial support to help in the construction of the recording vault and with fellowships for SAAS staff and UnB students interested in seismological research.

CERESIS and Instituto Geofisico del Peru (IGP) have continued their contribution to SAAS through two members of IGP staff, financial support for SAAS installations and training the Brazilian staff of SAAS.

The USCGS (now NOAA) contribution to the Seismological Station of Brasilia is through the WWSSS equipment and necessary photographic material, financial help in the construction of the recording vault at E4 and technical assistance during the installation and operation of the standard system installed in Brasilia.

At present, SAAS is in full operation, the installation period is finished, the next stage will be the improvement of analysis and processing facilities in South America to enable Latin American seismologists to use SAAS data with all its advantages. Negotiations to make this possible are being carried on between CERESIS and IGS.

1.2 The Scope of the Present Study

The main objective of this work is to use modern array processing techniques to study South American seismotectonics by using SAAS data, and to define the contribution of SAAS in the improvement of the knowledge of South American seismicity. Since 1968 the author has been involved in the installation and organization of the permanent SAAS and, since October 1972, has been working at the Geophysical Laboratories of IGS in Edinburgh. This research has been carried out mainly by processing SAAS data employing the techniques developed by IGS seismologists.

Chapters 2 and 3 of this thesis deal with the characteristics of SAAS and with an estimate of its capability in the detection of South American events. More than 200 events have been analysed for this research and their observed arrival times and amplitudes have been used to study anomalies which had been observed during the analysis of early SAAS records. The results of the travel-time residuals distribution observed at SAAS appear in Chapter 4 together with some peculiarities in the distribution of the amplitudes observed at SAAS.

The array processing techniques available at present in Edinburgh are described in Chapter 5; here are also presented the reasons for the selection of one of these techniques in the calculation of observed azimuth and apparent velocity from SAAS data. The effect of the structure under SAAS is discussed and the results obtained for the observed azimuth and apparent velocity by using SAAS data are presented in this chapter.

In Chapter 6 the departures in azimuth and apparent velocity

of the observed values obtained in SAAS are analysed for seismic events in all azimuths and up to 95° of epicentral distance. In this chapter also, the departures in azimuth and apparent velocity are compared with other results obtained in this research and related to possible South American tectonic features.

Finally, in Chapter 7, further evidences supporting the results discussed in Chapter 6, are presented.

CHAPTER 2

SAAS CHARACTERISTICS

2.1 Introduction

Seismic arrays have been used in Seismology since 1961 when the United Kingdom Atomic Energy Authority (UKAEA) installed a linear array at Pole Mountain Wyoming (USA), to record signals from the Gnome atomic explosion. Since then, many other arrays have been installed, especially by British and USA seismologists, and can be arranged into three categories according to their size:-

a) Small aperture arrays, only a few Km in aperture, such as the ones installed by the U.S. Air Force.

b) Medium aperture arrays, up to 20Km in aperture, like the ones operated by UKAEA.

c) Large aperture arrays, up to 200Km in aperture, such as LASA and NORSAR.

Linear arrays with equidistant seismometers installed in two perpendicular lines, have been favoured by British seismologists, and fulfil the requirements expected from an array as follows:-

a) Improvement in the signal/noise ratio.

b) Identification of seismic phases.

c) Determination of azimuth and apparent velocity.

Assuming that all n sensors of an array have the same response, the improvement in the signal to noise ratio by summing the delayed outputs, is proportional to $n^{\frac{1}{2}}$. The delays used in this process can be found directly from the array data, or can be calculated independently for a given signal. Improvements in the signal to noise ratio are important when considering very small

events which are hidden by background noise.

The identification of seismic phases is carried out by inserting delays belonging to a given phase at the appropriate azimuth and distance. This will enhance the amplitude of this particular phase, and minimise the amplitudes belonging to noise and other different phases. The output can be the summation of all points of the array or a correlogram of the product of the sums of the two lines of a linear array.

The determination of azimuth and apparent velocity from array data can be carried out by different methods, some of which are described in Chapter 5. Observed azimuth and apparent velocity at an array are very useful in the study of the Earth's structure. By comparing the observed values at these parameters with the expected ones from great circle paths, some deviations are obtained. These deviations are caused by the discontinuities encountered by the seismic rays on their journey to the station. The apparent velocity varies with the epicentral distance, therefore approximate epicentral locations can be carried out by using the azimuth and apparent velocity observed at an array.

The transmission of data from the points of an array to the recorder can be made by means of multicore cable buried underground or suspended from poles above the surface. Radio links are used as an alternative method of data transmission, giving a great flexibility to the array and easier installation.

Array data is recorded on multichannel magnetic tape, either in analogue form or digital form. The advantages of digital recordings are well known but its high cost and the large quantity

of magnetic tape required makes analogue recording more attractive.

The packing density on the magnetic tape determines the speed of the tape for a given carrier frequency when a frequency modulated recording system is used, and the width of the tape and quality of the recording head determine the number of tracks. There have been later improvements in the quality of magnetic tape recording equipment such that it is now possible to record up to 14 tracks on ½ inch magnetic tape at speeds as low as 15/640 ins/Sec. Improvements of magnetic tape recording systems are expected in the future.

2.2 SAAS Location

SAAS is located on the Central Plateau of Brazil and its central point (CP) is situated 28 Km to the Northwest of Brasilia. See Figure 1.

The main advantages offered by the site occupied by SAAS are:-

a) An optimum position regarding the seismic areas surrounding South America. Most of the Andean region is between 15^{o} and 35^{o} from SAAS. Most of the Middle and Southern parts of the Mid Atlantic Ridge are between 25^{o} and 50^{o}. The seismic areas of the Eastern South Pacific are between 30^{o} and 65^{o}. The seismic areas of the Caribbean Sea, Central America and Mexico are between 30^{o} and 70^{o} from SAAS.

b) Stability and low noise. The Central Plateau, where SAAS is located, is in the middle of the Brazilian shield which has a low level of seismicity. The site is 900 Km away from the Atlantic Ocean and 400 Km from the nearest large lake and dam. The nearest large river is 200 Km away. The artificial lake surrounding Brasilia does not increase the background noise of the area as it has very smooth edges. There is no heavy industry in Brasilia but the high frequency cultural noise, produced mainly by construction works in the city during working hours of the day is noticeable only on the points which are located on sediments and close to the city (i.e. S1, S3, S4). The vegetation is mainly indigenous small trees, with

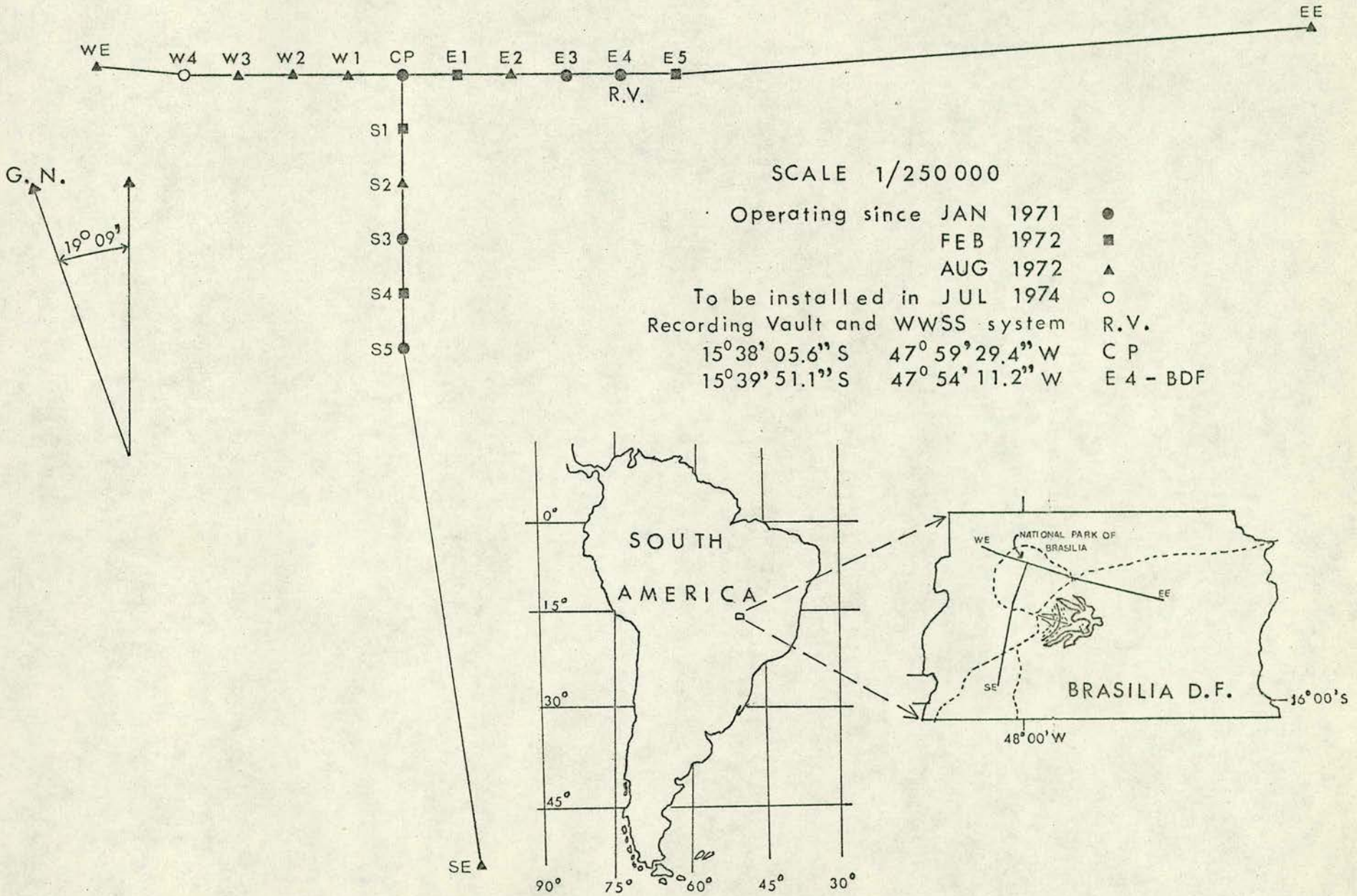

FIG. 1 THE SOUTH AMERICAN ARRAY SYSTEM (SAAS)

large areas of grassland and small shrubs; tall trees are found only near the streams. Most of the points of the array (13 out of 18) are inside the National Park of Brasilia which is completely fenced and guarded, thus impeding any disturbance to the instrumentation by people or vehicles. Occasional lightning during the rainy season produces some interference to the radio transmissions and also localised vibrations in parts of the array, but can be easily identified.

c) Appropriate topography to offer good line of sight for radio transmission and for accessibility. The Central Plateau is a large almost flat tableland, with an altitude between 1,000 and 1,350 metres. Smooth low hills and a few small valleys are the main features of the topography of the area occupied by SAAS. Old tracks made by explorers cross the area in various directions, facilitating easy access to many points. New tracks have been made to reach some of them, and all points are accessible with a four-wheel-drive vehicle, which is only necessary during the rainy season.

d) Simple surface geology and structural features, in the area occupied by SAAS. The basement rock, which is part of the Brazilian shield, is mainly formed by quartzite and other metamorphic rocks outcropping in many points of the plateau. Most of the hills are formed by thick deposits of recent unconsolidated sediments. The outcrops

of the basement rock appear to be largely affected by surface erosion. Many fissures are noticeable, which increases the permeability of these formations to water, which in turn affects the velocity of seismic waves travelling through them.

e) Good logistic facilities offered by the proximity to Brasilia, which now is a large city, with good commercial suppliers.

f) The existence of academic and research facilities offered by the University of Brasilia, which also administers SAAS.

TABLE 1

SAAS Coordinates as from January 1971

POINT	LAT.	LONG.	HEIGHT	CODE
CP	15 38 05.6 S	47 59 29.4 W	1211 m	BAO
E1	38 33.2 S	58 07.9 W	1170 m	
E2	39 00.3 S	56 49.0 W	1110 m	
E3	39 25.0 S	55 34.0 W	1150 m	
E4	39 51.1 S	54 11.2 W	1258 m	BDF
E5	40 20.9 S	52 51.2 W	1260 m	
EE*	44 18.5 S	37 11.8 W	1130 m	
S1	39 22.1 S	59 58.9 W	1145 m	
S2	40 40.5 S	48 00 25.1 W	1060 m	
S3*	41 55.1 S	00 52.7 W	1120 m	
S4*	43 08.9 S	01 20.2 W	1140 m	
S5	44 31.2 S	01 49.5 W	1150 m	
SE*	57 00 S	04 00 W	1185 m	
W1	37 41.7 S	00 46.5 W	1150 m	
W2	37 16.7 S	01 07.9 W	1260 m	
W3	36 45.4 S	03 27.0 W	1265 m	
W4	36 18.7 S	04 46.6 W	1260 m	
WE*	35 27.4 S	06 50.1 W	1340 m	

* Not final coordinates

2.3 SAAS Layout and Constructions

SAAS is a linear array with two perpendicular lines almost North-South and East-West, in the shape of an asymmetrical T, with maximum extension of 14 Km to the West, 42 Km to East and 37 Km to the South. See Figure 1.

The coordinates of the points occupied by SAAS are listed in Table 1. The internal points are at approximately 2.5 Km spacing and are named according to their direction and distance from the central point (CP), so E1 means that the point is to the East and at approximately 2.5 Km from CP, whereas S4 means that the point is at approximately 10 Km to the South of CP. The extreme points have been located as near as possible to the projection of the lines of the internal points and, as far as the topography permitted, in order to obtain a reasonable line of sight to the recording vault.

The old North-South line of the experimental array was used for the new S points but new locations were necessary for the East-West line and for the extreme points. The geographical coordinates cor CP of the experimental SAAS, were obtained from a geodetic triangulation carried out by members of the Conselho Nacional de Geografia of Brazil and from this the geographical coordinates for the new locations were calculated.

In order to find suitable places for the construction of seismometer pits, it was necessary at some points to diverge as much as 100 metres from the surveyed positions, and for which the appropriate corrections were made to the coordinates.

Each point of the array contains a vertical short period seismometer, therefore a similar pit was constructed in all points

except in E4 where the recording vault was constructed. A typical SAAS pit is illustrated in Figure 2. Whenever possible, preliminary excavations were made near outcrops of hard rock, and final excavations were made where the bedrock was between 1 to 2 metres from the surface. Concrete pillars were then built up from the bedrock to about 0.5 metres from the surface to accommodate the seismometer. Where bedrock could not be found in the upper layers, a 0.3 metres diameter hole was excavated to a depth of 7 metres and a concrete pillar constructed. In both cases excavation was carried out with hand tools.

At each site waterproofed concrete rings were placed around the pillars to a depth of 1.5 to 2 metres from the surface to isolate the pillar laterally. A thick layer of pitch (0.5 metres) was poured on to the bottom of each pit to prevent water entering from below.

The top part of each pit rises no more than 0.20 metres above the surface and is covered by a waterproof iron lid. The seismometer pits also house an amplifier-modulator unit. Nearby and usually at 5 metres from the pits, a brick box has been constructed to accommodate the caustic soda cells for power supply and a control unit.

At around 10 metres from the pits, tubular masts were erected. These masts, stand on a concrete base and are supported by steel guys also fixed to concrete. The height of these masts varies between 5 and 10 metres depending on the topography. The transmitter and directional antenna are fixed to the top of the masts and the cable runs down the inside of the masts and then underground to the

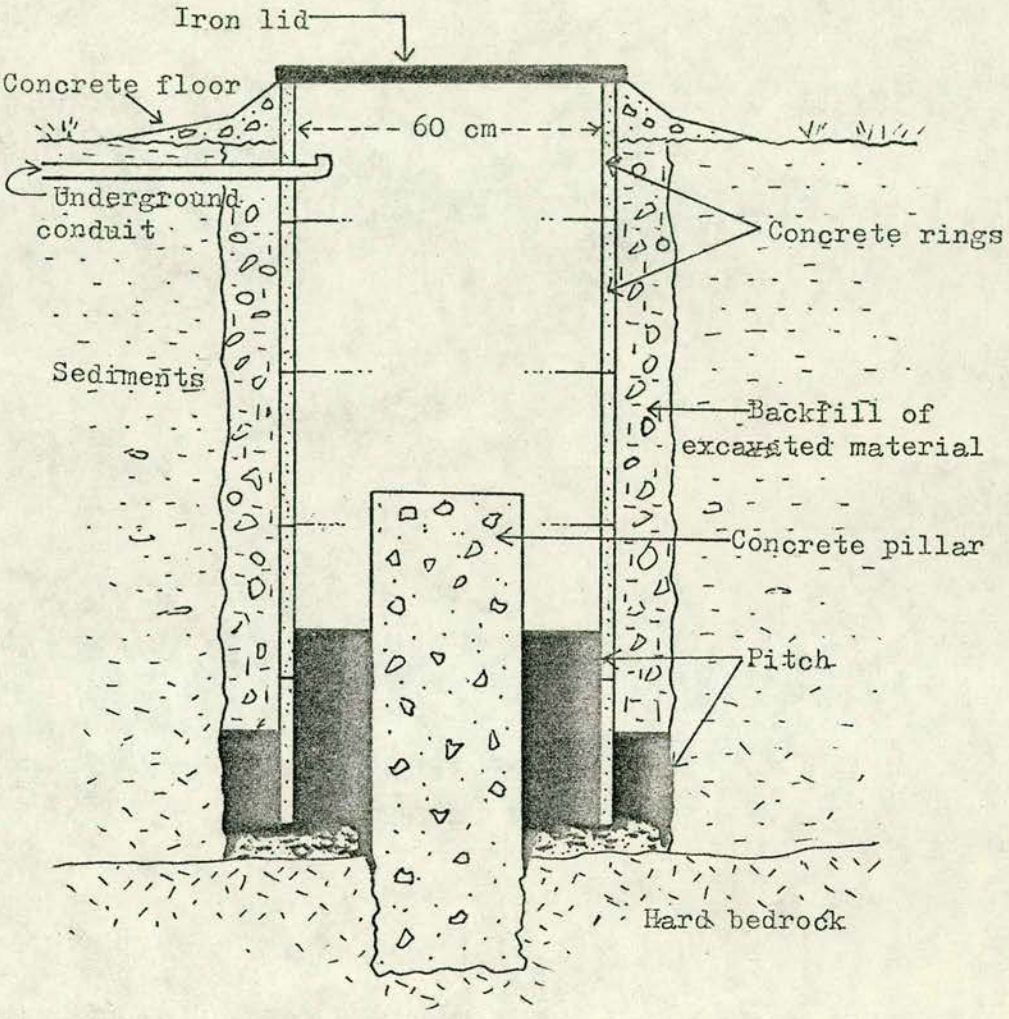

Figure 2.- A TYPICAL SEISMOMETER PIT AT SAAS

control unit. The cables connecting the seismometer pit and the control unit at the batteries box are also underground.

It was originally planned to have the recording vault at the central point (CP), but as CP is approximately 7 Km from the nearest limit of the National Park of Brasilia, permission for an access road and power lines was not possible. The recording vault was built in the position of the point E4, which is 1 Km from the North limit of the referred park. It is an underground, waterproofed, concrete, semi-circular vault of 14 X 6 X 3 metres. See Figure 3.

To construct this vault on hard rock it was necessary to remove more than 600 cubic metres of eroded quartzite and surface soil by means of a "caterpillar" and hand tools. No explosives were used in the excavation. After finishing the construction the remaining cavities were filled with earth so that the complete structure was underground. Around 20 metres from the vault a scaffold type structure was erected to hold all the directional receiving antennas and some receivers.

The vault houses the WWSSS equipment, a three component set belonging to E4 and SAAS recording equipment.

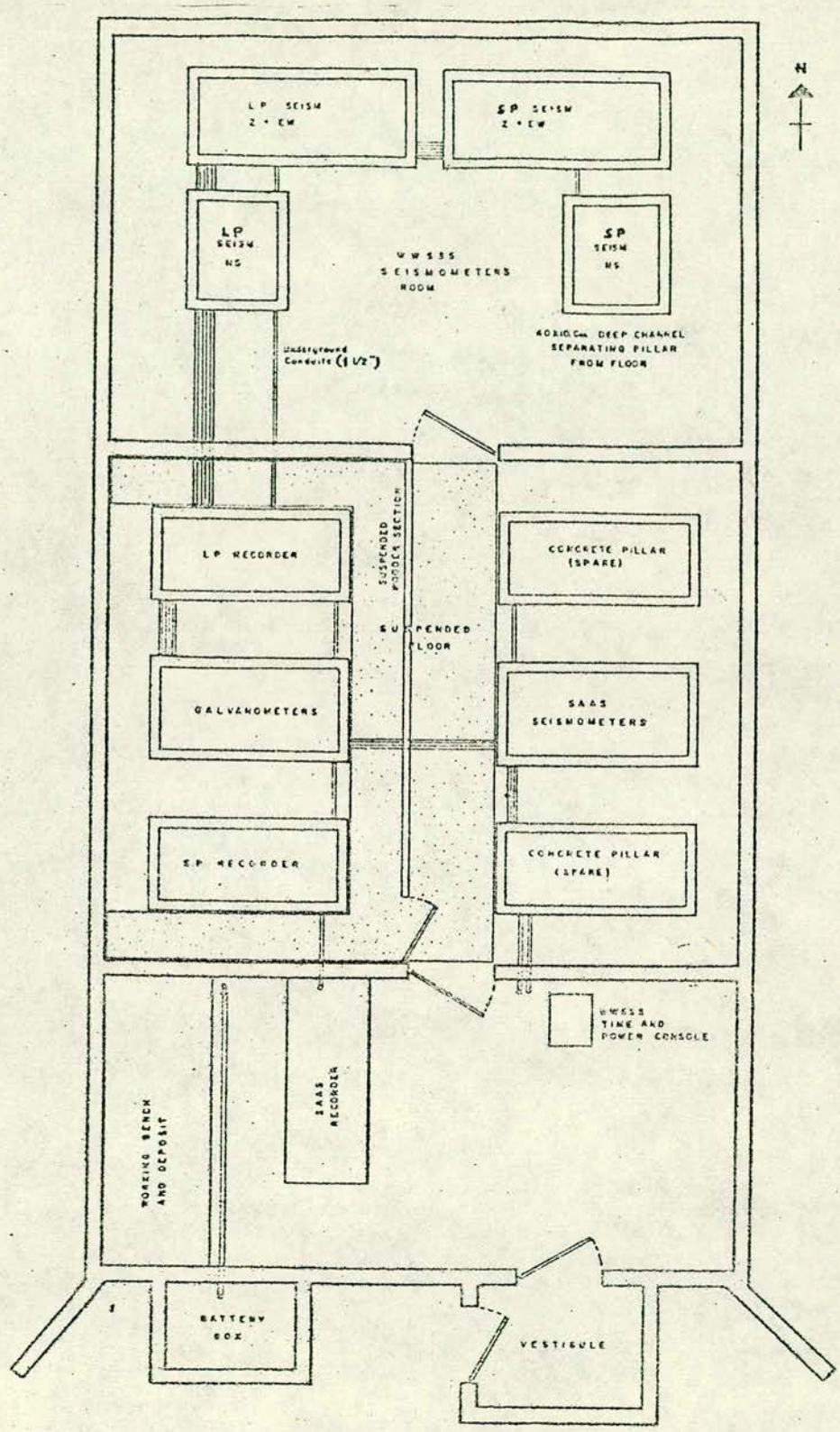

Figure 3.- SAAS VAULT PLANT

2.4 SAAS Equipment

2.4.1 Detecting Equipment (Outstations)

Each point of the array, except E4, has a vertical short period component with the following units (see Figure 4).

- A short period Willmore MK II seismometer set at 1 sec natural period. This seismometer is an electromagnetic transducer, with an approximate sensitivity of 5.7 volts/cm/sec. when fitted with a 3,300 ohm coil.
- An amplifier-modulator unit (Racal-Thermionic D 4980), which amplifies and converts to a series of pulses (frequency modulated) the output signal from the seismometer. The frequency of these pulses at any time depends on the polarity and amplitude of the input signal. An autocalibration circuit in this unit can be activated by momentarily reversing the polarity of the power supply to the unit. Power can be fed along the same pair of wires that carry the output signal. Power consumption is of the order of 40 mA. Five switched gain positions are provided in this unit (x100, x200, x400, x1,000, x2,000). The centre carrier frequency of the modulator is 210 Hz. with maximum deviations of $\pm$ 40% for a $\pm$ 1.0 volt signal from the output of the amplifier.
- A battery termination unit, to provide an easy interconnection of power supply and signal between the amplifier-modulator unit and the UHF radio transmitter. A switch to calibrate the system is also in this unit.
- An UHF Pye Pocketfone transmitter, enclosed in an aluminium canister, installed at the top of a 5 metre mast along with

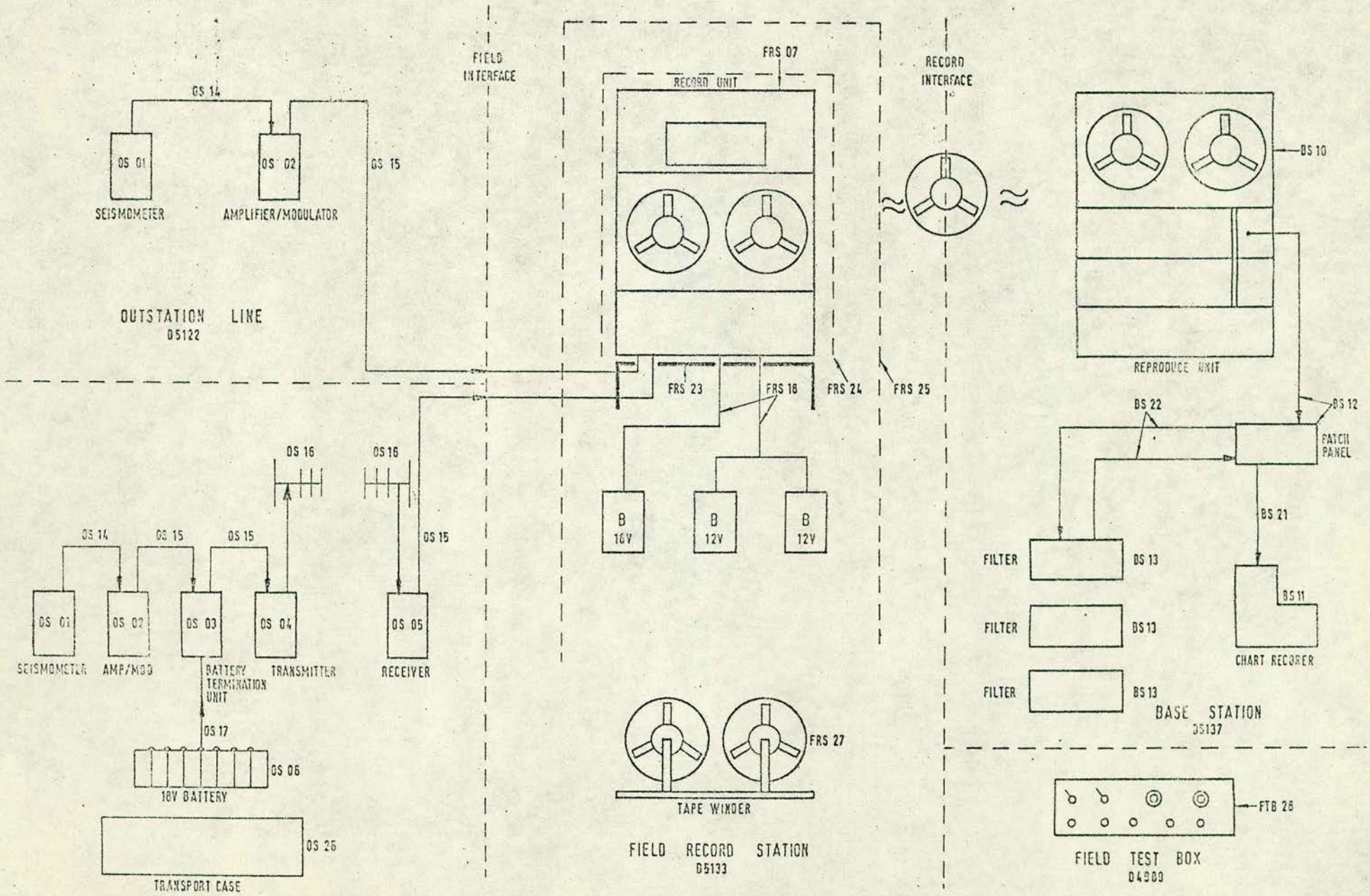

Figure 4.- SAAS EQUIPMENT DIAGRAM

a 12 element UHF Yagi antenna. The frequency range of these transmitters is between 450 and 470 MHz, with channel separation of 25 KHz. Power output is 100 mW fed into a directional antenna with 12 db gain.

- A set of 12 to 16 air depolarized primary cells, type EMU 1. Each cell has a voltage of approximately 1.4 volts, and are activated on site, by adding water. These cells will run the equipment continuously at each site for a period of nine months. At the point E4 (Recording vault) there is a three component set of short period detectors, linked by cable to the record unit, consequently each member of the set has only a seismometer and an amplifier modulator unit, which takes its supply from the record unit.

2.4.2 Recording Equipment

The recording equipment of SAAS is installed in the underground vault constructed at E4 and has the following units (see Figure 4):-

- UHF receivers of two kinds: PYE Pocketfone type PF1 which are modified to suit field continuous operation. These receivers are fitted with an interface, for supply and signal to the record unit. Each receiver is fitted into a cylindrical aluminium canister and is installed on the masts' structure (built outside the vault) beside the Yagi antenna. The other type of receivers used are the PYE L 470 which are rack mounted beside the record unit and connected directly to the record unit via their 600 ohms outputs. The PYE L 470 receiver offers many advantages compared to the PF1, such as: signal monitoring facilities, better stability and signal to noise

ratio, audio output and 600 ohms output. These receivers are used in SAAS when line of sight or signal strength are poor. Their cost, size and power consumption are the main disadvantages when compared with the PF1 type.

- A Racal-Thermion T8100 record unit (see Figure 4), composed of a tape deck with 2 x 12 track interlaced recording heads, operating at a speed of 15/128 inches/second, with 1" magnetic tape on 8" diameter spools (1,800 feet of tape gives 52 hours of recording). An extra tape deck is operated in parallel to obtain duplicate records. The unit has 24 channels of preamplifiers and auxiliary interface circuits (two channels are used for flutter compensation and one for time signal). A crystal oscillator drives a time encoder which produces second marks and identifies every minute up to 32 days. The signals for flutter compensation and 60 Hz for the capstan motor are derived from the crystal.
- An EC10 Eddystone short wave radio receiver for time signals to control the time encoder. It operates in any band between 550 KHz and 30 MHz.
- The recording system is operated from two 12 volts lead acid batteries, on continuous charge from the mains, thus allowing a 24 hour break in the mains supply.

2.4.3 Reproduction Equipment

This equipment operates at the seismological laboratories of the Departamento de Geosciencias of the University of Brasilia. It is installed in a sound-proof cabin and is composed of the following parts (see Figure 4).

- A Racal-Thermionic T8100 replay unit with 2 x 12 track interlaced heads, 24 channels of demodulators, filters and pre-amplifiers (to operate at 7 1/2 inches/second); a tape deck with a selection of running speeds (from 15/64 to 30 inches/second), and an audio amplifier with a small speaker. Tape capacity of this unit is similar to the record unit.
- A set of three band pass Krohn-Hite variable frequency filters, which can be continuously adjusted in the range 0.2 to 20,000 Hz real time (0.003-333 Hz recording time).
- Two (8 and 16 channel) ink jet pen chart recorders, which register visual playouts of filtered or unfiltered signals from the tapes. The choice of channels and filters to be recorded on the jet pens is made via a distribution patch panel. The charts can be produced at 9 different paper speeds from 2.5mm/sec up to 1,000 mm/sec (at maximum paper speed, 1 sec. of recorded time measures around 16 mm). The gain of each jet pen can be independently adjusted in 8 steps from 100 up to 0.025 volts/cm.
- A quality loud-speaker system for the audio analysis of the tapes.

2.4.4 Maintenance Equipment

The following instruments were essential for the routine maintenance of SAAS: a battery mains portable oscilloscope, a multimeter, a digital voltmeter, a frequencymeter and a good kit of tools. Without the necessary instruments, only a limited amount of repairs and maintenance can be carried out on radio links,

and the following additional instruments would be required:-

- RF power output meter
- FM signal generator
- AF oscillator
- Deviation meter
- 10.7 MHz marker oscillator

Another useful instrument in the field, especially to see "in situ" the seismic background noise, is the Field Test Box (FTB), which can demodulate and produce a visual record of the signal being detected, taken from the output of the amplifier-modulator unit.

2.4.5 Transcription Facilities

A transcription unit has been developed and is being tested in Edinburgh before sending it to Brasilia. It connects directly into the T8100 replay unit and, besides copying of data from tape to tape, can also help the replaying of original analogue tapes. This unit will be mainly used to build up a library of events on magnetic tape in the analogue form.

2.5 SAAS Magnification Curve

The following factors govern the overall magnification of the system:

- Velocity sensitivity of the seismometer
- Amplifier gain
- Amplifier response
- Replay Unit gain
- Replay Unit response
- Replay Unit speed
- Ink jet pen gain
- Ink jet pen response

Some of these factors have set values which are kept constant unless special circumstances require them to be changed. These constant values, during the period of operation of SAAS considered in this study, are:-

- Amplifier gain : x 2,000
- Replay speed : 7.5 inches/second

The replay units in Brasilia and Edinburgh have different gains, in such a proportion that 40% deviation from the centre carrier frequency will produce the following outputs:-

- EMI replay unit in Edinburgh	6.0 volts
- T8100 replay units in Edinburgh	5.0 volts
- T8100 replay unit in Brasilia	0.5 volts

The ink jet pen gain can be changed according to the size of the signal being reproduced, but the results can be normalised to

a standard gain (i.e. 1 volt/cm). Knowing the values of the amplifier gain, the gain and speed of the replay unit and the gain of the jet pen, the other factors governing the magnification of the system (i.e. the response of the amplifier, replay unit and ink jet pen, and the velocity sensitivity of the seismometer), have been found experimentally.

The response curve for the amplifier, replay unit and ink jet pen was obtained by Miller (1973) by using sinewave signals of constant amplitude over the range 0 to 30 Hz, fed into an amplifier-modulator unit and recorded directly on to tape using a T8100 record unit. The tape was replayed at 7.5 inches/sec. on a T8100 replay unit and the signals recorded on paper using an ink jet recorder. The values used to construct the response curve were obtained from the visual playouts.

A typical velocity sensitivity curve for a Willmore MK II seismometer was obtained by Crampin and Morgan (1971). At any given frequency the product of the response curve mentioned above and the velocity sensitivity of the seismometer gives the velocity sensitivity of the whole seismographic system used in SAAS.

The amplitude magnification curve of the system is obtained by multiplying together the velocity sensitivity and the angular frequency. See Figure 5.

In Table 2 the values of K, to be used in magnitude determination for SAAS recordings replayed on different replay units, are listed.

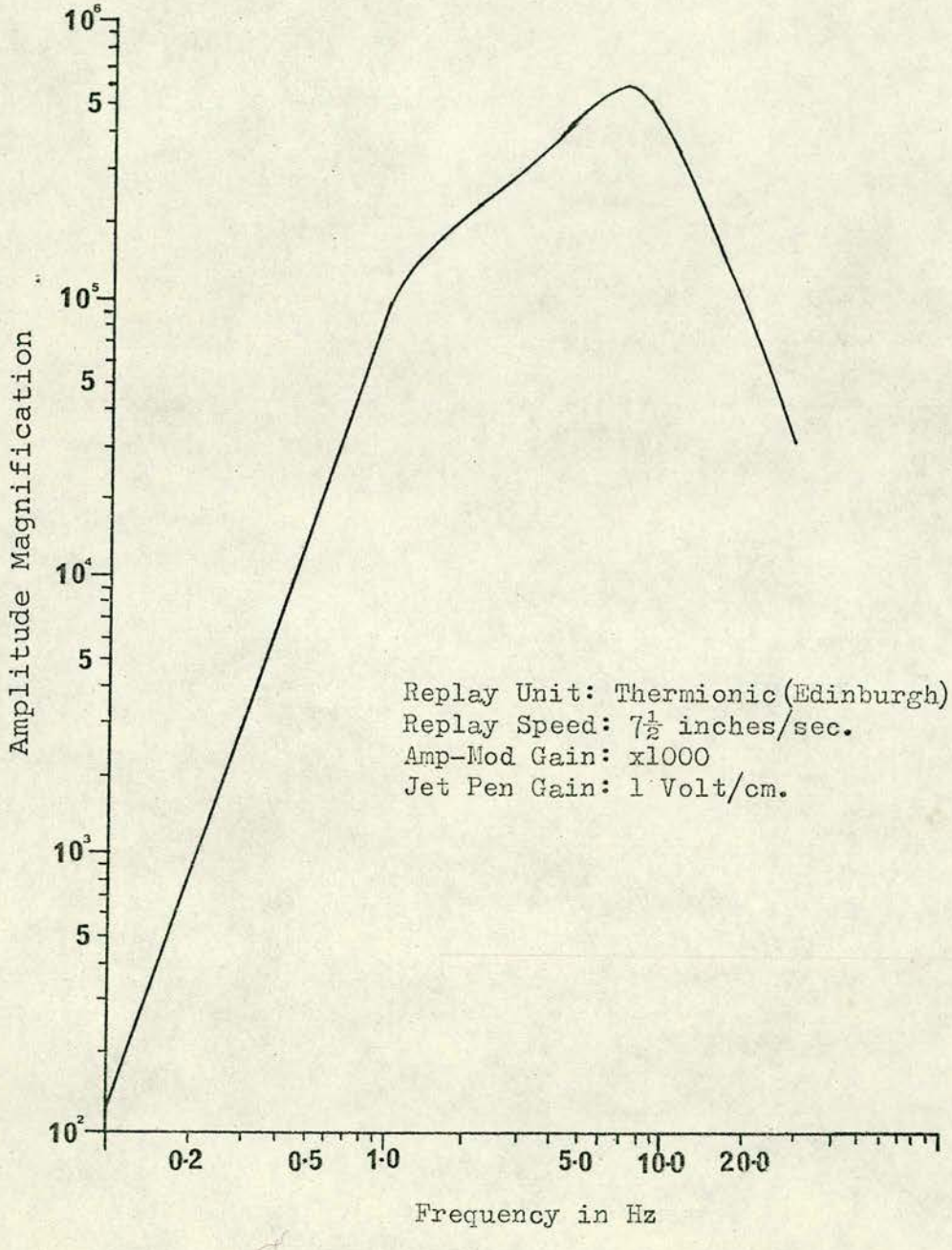

Figure 5.- SAAS MAGNIFICATION CURVE

TABLE 2

VALUE OF K AND KT FOR SAAS SYSTEM (AMP-MOD GAIN = x2000)

PERIOD (SEC)	FREQUENCY (Hz)	EMI EDINBURGH		T8100 EDINBURGH		T8100 BRASILIA	
		K	KT	K	KT	K	KT
0.2	5.00	1176	235	980	196	98.0	19.6
0.3	3.33	792	238	660	198	66.0	19.8
0.4	2.50	619	248	516	206	51.6	20.6
0.5	2.00	518	259	432	216	43.2	21.6
0.6	1.66	446	268	372	223	37.2	22.3
0.7	1.43	384	269	320	224	32.0	22.4
0.8	1.25	319	255	266	213	26.6	21.3
0.9	1.11	276	248	230	207	23.0	20.7
1.0	1.00	230	230	192	192	19.2	19.2
1.1	0.91	192	211	160	176	16.0	17.6
1.2	0.83	154	185	128	154	12.8	15.4
1.3	0.77	122	159	102	133	10.2	13.3
1.4	0.71	98	137	82	115	8.2	11.5
1.5	0.67	82	123	68	102	6.8	10.2
1.6	0.62	65	104	54	86	5.4	8.6
1.7	0.59	55	94	46	78	4.6	7.8
1.8	0.56	46	83	38	68	3.8	6.8
1.9	0.53	41	78	34	65	3.4	6.5
2.0	0.50	34	68	28	56	2.8	5.6

K = magnification in thousands

T = period in seconds

CHAPTER 3

SAAS CAPABILITY

3.1 Introduction

The capability of a seismic station in the detection of natural and man made seismic events depends mainly on the following factors:-

a) Location of the station regarding regional and local sources of noise, and

b) type of instrumentation used for detecting and recording seismic signals, and the method of analysis of the records.

The advantages of quiet sites are obvious, being able at the mid-continental locations, to increase the magnification of the station up to a level limited only by the instrumental capacity.

Data from seismic arrays is recorded on magnetic tape either in digital or analogue form. Analysis of the records is carried out either on line, as in LASA or NORSAR, or it is performed after the tape has been recorded and replayed on a separate unit.

Real time on-line analysis requires data recorded in digital form, to make use of large fast digital computers in order to take advantage of the properties of array processing.

Several hundreds of array beams may be formed, which are steered towards the most important seismic regions of the Earth. The identification of events is made by the control of the amplitude of the ratio "short-term average/long-term average" signals. The short-term average signal results from the integration (sliding window of around 2 sec) of the rectified beam. The long-term average gives

an estimate of the noise which is based on the history of the beam since the system was activated (Bungum et al, 1971). An event is declared when the ratio mentioned above exceeds a certain threshold for a predefined time interval. This can occur on several beams; in such a case, the beam which has the largest amplitude of the ratio is chosen as the answer. Subsequently, the event is further analysed either automatically or manually to produce the parameters of the event to be included in a bulletin.

When the analysis of array records is carried out off-line, this may be done either in an audio or in a visual way. In the audio method of analysis, the records must be replayed at faster speeds than those used during recording to bring the typical short period seismic frequencies (0.3-10 Hz) into the human audio band. Any sudden change in the amplitude of the signal, produced by the larger amplitude of a seismic event as compared with the noise amplitude, will produce a change in sound which indicates the presence of a seismic event on the tape. In this analysis one listens to the filtered signal (0,5-2 Hz) of a quiet point of the array and every time that the operator believes he has found an event on the tape, a paper playout of the filtered output of the array components is produced.

Large and medium magnitude events are easily found in this way, but very small ones are frequently missed. The most important factors in the audio method magnetic tape analysis are:-

a) Quality of audio equipment and amount of external noise during the playing back sessions. A proper soundproof room, and high quality sound amplifier and speaker improve this type of analysis.

b) Experience and concentration of the operator, and

c) Quality of recorded signal, which must be free from instrumental noise.

Listening to summed signal outputs of nearby array points (filtered but without delays), does not increase the number of events detected over those obtained by using a filtered signal of a single quiet point. Other audio techniques to search for recorded events on array magnetic tapes have been suggested, such as to listen to the separate signals of several selected points and arranging the speakers in such a way that the direction of approach of the event can be assessed.

The visual method of searching for events contained in magnetic tapes is done by producing a continuous slow playout of the whole tape with the signals of as many points as possible passed through an appropriate band pass frequency filter (1-4 Hz). The possible events are found visually on this slow playout and faster playouts, with more convenient band pass frequency filters and jet pen gains if necessary, are obtained for further analysis. This visual method has shown better results than the single channel audio method.

An automatic method (AUTOREAD) of finding the events contained on analogue magnetic tape is being developed in Edinburgh (see Crampin et al, 1973). In this method the tape is replayed at 8 or 16 times the recording speed, the signals of as many as 16 tracks are continuously digitized after being passed in a broad band pass frequency filter (DC-10 Hz). The signal of each track

is processed by three triggering mechanisms having different frequency and amplitude characteristics. An event is delcared when there are more than a specified number of different signals triggered in an appropriate time window. This method detects more events contained in the tapes than the single channel audio method but it requires the use of a PDP15 or a similar computer on-line with a complete replay unit for 24 channels which must be able to operate at low speeds. The main advantage of this method is the automation of the analysis and the production of a digital record of the events which can be used in further array processing analysis.

All these methods have been used on one SAAS tape and the results are presented in this chapter. It is necessary to make clear that these methods of searching for events on analogue records do not make use of the signal/noise ratio improvement offered by seismic arrays, which is useful to detect very small events obscured by the background noise. A very quiet site for an array can reduce in part this disadvantage.

To estimate the capability of a station in the detection of seismic events, it is necessary to compare, for a given time period, the number of recorded events with the number of reported events in the bulletins of international agencies such as NOAA (U.S. National Oceanic and Atmospheric Administration) or ISC (International Seismological Centre). In the case of SAAS, it is not possible to do such a comparison by considering the preliminary readings obtained in Brasilia, for the following reasons:-

a) The audio method of tape analysis in use in Brasilia does not detect several small earthquakes which can be seen with the visual method.

b) SAAS reported data extracted from the NOAA Earthquake Data Report bulletins do not show all the events reported in SAAS preliminary bulletins. This could be due to the delay in producing the messages sent to NOAA especially during the installation period of the array, when the tapes were reanalysed every four days and with a delay in producing the messages of up to eight days.

c) Human errors in the reported arrival times and misidentifications of phase during the training period of SAAS operators.

In order to estimate the capability of SAAS some records have been reanalysed and the results compared with NOAA data in the following ways:-

a) Visual analysis of 1 SAAS tape (4 days of recording) in which all events were found by the visual method described before, and the results are compared with NOAA bulletin for that period. These results are also compared with the preliminary audio analysis carried out in Brasilia, with an audio analysis made in Edinburgh and with the AUTOREAD method presently being developed in Edinburgh.

b) All events reported by NOAA with body wave magnitude (m_b) equal to or larger than 4, and epicentral distance equal to or smaller than 95 degrees from SAAS, have been searched in the records of a 66-day period of SAAS operation, and

the results have been compared with NOAA reports.

These ways of assessing the capability of SAAS in the detection of seismic events do not represent the real capacity of the station because no array processing methods have been used during these analyses, therefore some very small events which could be brought out by array processing have not been found. It would have been desirable to analyse longer periods of recording than those used in the present study, but the periods chosen represent typical periods of world seismic activity, therefore they are a good example of SAAS capability in detecting seismic events.

It is important to emphasise that any improvement in the knowledge of South American seismicity expected from SAAS data depends mainly on the ability to detect all or most of the seismic events of this region contained in SAAS tapes.

3.2 Visual Analysis Results

The data used for this analysis is contained in the tape DF 41/72, for the following period:-

SIDE A:	ON	14 h	32 m	10 JUN 1972
	OFF	15 h	28 m	12 JUN 1972
SIDE B:	ON	15 h	29 m	12 JUN 1972
	OFF	17 h	23 m	14 JUN 1972

A continuous slow playout on a 16-channel jet pen recorder, paper speed 50 mm/sec, was obtained by using the EMI reproduction system at Edinburgh, with the following distribution of channels:-

PEN	SIGNAL	FREQ.FILTER	GAIN
1	TE	Unfiltered	10 v/cm
2	E4	0.5-2Hz	1 v/cm
3	E3	"	"
4	E1	"	"
5	CP	"	"
6	S1	"	"
7	S3	"	"
8	S4	"	"
9	E4	Unfiltered	"
10	CP	"	"
11	S4	"	"
12	E4	1-4Hz	0.25 v/cm
13	CP	"	"
14	S4	"	"
15	RADIO	Unfiltered	10 v/cm
16	TE	"	"

TE = Time encoder

The two bands used for the frequency filters were intended to show the teleseisms better in the band 0.5-2 Hz, and local events better in the band 1-4 Hz, but it has been found that the band 1-4 Hz shows small teleseisms more clearly than the other band. Large and medium size events are also easily identified in the 1-4 Hz band.

Faster playouts were obtained of all suspected events found in the slow playout analysis, a paper speed of 250 mm/sec being used for small signals and 1,000 mm/sec for the clear large signals. The jet pen gains were changed according to the size of the signals.

All the events found on this tape and their observed arrival times at E4 (BDF) are listed in Table 3, together with NOAA, LASA, and NORSAR reported events that should have been detected on SAAS records. Table 3 also shows the result of the preliminary audio analysis made in Brasilia, and the audio and AUTOREAD analysis made in Edinburgh.

An inspection of Table 3 and NOAA, LASA, and NORSAR reports shows the following comparative results:

A. Events Recorded by SAAS

a) Clear Events, Range P (IP,EP,I(P))

SAAS + NOAA	10	
SAAS + LASA	5	
SAAS	10	*

b) Possible Events, Range P (E(P)$^{+}_{-}$)

SAAS	2	*

c) Clear Events, Range PKP (IPKP, EPKP)

SAAS + NOAA	6	
SAAS + LASA	1	
SAAS	9	*

d) Possible Events, Range PKP ((PKP))

SAAS + NOAA	4	
SAAS + LASA	1	
SAAS + NORSAR	1	
SAAS	3	*

e) Local Events

SAAS-EP	12	*
SAAS-E (P)	6	*

f) Doubtful Events (E(P))

SAAS	10	*

B. Events Not Recorded by SAAS

a) From all events Reported by NOAA

P Range ($m_b > 4$)	1	!	(10 Tons UK Explosion $\Delta > 80^{o}$)
P Range ($m_b < 4$)	3		$\Delta \approx 83^{o}$, m = 0.0
PKP Range	2	!	$\Delta \approx 144^{o}$, $m_b = 4.7$
Shadow Zone	18		$95^{o} < \Delta < 125^{o}$

TABLE 3

ANALYSIS OF SAAS TAPE OF 41/72

N.	DATE	VISUAL AND OTHER ANALYSIS					NOAA REPORTS			REGION AND COMMENTS
		PHASE	ARRIV. TIME	AU	PA	AA	MB	DEP.	DIST.	
01	10JUN	EP	14 39 02							LOCAL EVENT
02		E(P)	15 07 04							
03		E(P)	15 29 06							
04		EP	17 03 18							LOCAL
05		EP	17 29 28.6	X	X	X	3.4			N.C.OF C.CHILE(LASA)
06			19 35			X				AUT.ANALYSIS ONLY
07		PKP	19 44 30	X			3.7			KURILE I. (LASA)
08		E(P)	20 29 40							
09		EP	21 13 31.5							SW AZIMUTH
10		EP	23 42 54.6	X	X	X	3.6			NORTHERN CHILE(LASA)
11	11JUN	EP*	00 28 33							SE AZIMUTH
12		PKP	04 49 58				5.1	33	117.3	TONGA I.
13		EPKP	06 05 15.8							W AZIMUTH
14		E(P)	06 40 42	X						
15		IP	10 23 31.0	X	X	X	4.3	88	21.9	N.C.OF N.CHILE
16		EP	11 12 38							LOCAL EVENT
17							4.7	55	141.3	SALOMON I.(H 11 24)
18		IP	12 04 59.8	X	X	X	4.9	28	24.6	N.C.OF C.CHILE
19		E(P)	14 20 28							LOCAL EVENT
20		E(P)	15 46 10	X	X	X				LOCAL EVENT
21							4.2			N.COLOM.(LASA, 16 05)
22							4.4	0	80.3	U.K.EXP.(H 16 08)
23		EPKP	16 43 18.3	X	X	X				
24		E(P)	16 46 56	X		X				LOCAL EVENT
25		IPKP	17 00 29.6	X	X	X	5.8	325	166.1	CELEBES SEA
26		PKP	17 29 24		X	X				AUT.& PRE.ANALY.ONLY
27		I(P)	17 37 52.5	X	X	X				SE AZIMUTH
28		IPKP	17 44 02.9	X	X	X	5.1			MINDANO P.I. (LASA)
29							5.1			BOLIV.(NORSAR 17 40)
30		EPKP	17 59 42.3	X		X				SE AZIMUTH
31		EP	18 30 16.6	X	X	X	5.1	52	51.2	N.C.OF GUATEMALA
32		IPKP	18 56 25.4	X	X	X	5.2	154	154.4	E.NEW GUINEA R.
33		EP	19 18 08.1	X		X	4.4	79	51.2	N.C.OF GUATEMALA
34		EPKP	21 32 45.6	X			4.6	98	154.3	N.C.OF HONSU, JAPAN
35		PKP	22 16 43							
36		E(P)	23 17 54							LOCAL EVENT
37		EPKP	23 46 02.8	X		X				SE AZIMUTH
38		PKP	23 53 12				4.0			KURILE I. (NORSAR)
39	12JUN						4.6			S.SANDW.IS.(NORSAR 00 55)
40		PKP	01 04 24.5	X	X	X	5.5	245	135.6	S.CRUZ I.R.
41		E(P)	01 16 48	X						
42		EP	03 48 53.4			X				SW AZIMUTH
43		EPKP	07 10 32.4	X						SE AZIMUTH

N.	DATE	VISUAL AND OTHER ANALYSIS PHASE	ARRIV.TIME	AU	PA	AA	NOAA REPORTS MB	DEP.	DIST.	REGION AND COMMENTS
44	12JUN	E(P)	08 44 20							LOCAL EVENT
45		IP	10 03 26.2	X	X	X	5.6	27	36.5	S.OF PANAMA
46		EP	11 23 56	X						LOCAL EVENT
47		PKP	11 39 53				5.2	33	170.6	LUZON, P.I.
48		EP	14 04 54		X	X				LOCAL EVENT
49		EP	14 15 10	X	X	X				LOCAL EVENT
50							4.0			PERU (NORSAR 16 05)
51		EP	17 40 55							LOCAL EVENT
52		EPKP	20 06 23.7	X	X	X	5.8	44	119.6	FOX I., ALEUTIAN I.
53		EPKP	20 16 36.4	X		X				
54		EP	20 54 06							LOCAL EVENT
55	13JUN	EP*	01 11 25							SW AZIMUTH
56		EP	01 57 53.0	X		X				SW AZIMUTH
57		EP	02 38 30.7	X						SW AZIMUTH
58		E(P)	04 01 08	X						
59		EP	04 02 18.0	X						SW AZIMUTH
60		IP	04 39 06.0	X	X	X				SE-S AZIMUTH
61							4.6			GUATEM.(LASA 05 17)
62		IP	07 54 37.5	X	X	X	5.0	159	33.4	NORTHERN COLOMBIA
63		EP	09 36 48.4	X		X	4.2	110	26.5	CHILE-ARGENT.B.R.
64		EP	10 23 53.2	X	X	X	4.2			S.BOLIVIA (LASA)
65		PKP	11 04 32				4.8	33	140.6	EASTERN RUSSIA
66		EPKP	13 16 30.7	X	X	X				E AZIMUTH
67		IP	14 42 26.2	X	X	X	4.9	16	23.9	CHILE-ARGENT.B.R.
68		EPKP	17 27 57.0							
69		EP	18 50 56	X		X				LOCAL EVENT
70		IP	19 53 44.7	X	X	X	4.4	127	53.5	N.C.CHIAPAS, MX.
71		IP	19 54 42.8	X	X	X	4.0			N.CHILE (LASA)
72		EP	20 37 23.5	X						SE AZIMUTH
73							4.7	108	141.3	KURILE I(H 21 41)
74	14JUN	EP	01 12 07.1	X						SE AZIMUTH
75		E(P)	01 21 59							
76		EPKP	01 38 42.7							W AZIMUTH
77		PKP	03 19 38	X						N AZIMUTH
78		EPKP	04 13 15.0	X			4.6	25	132.0	N, HEBRIDES I.
79		E(P)	04 52 27							
80		EPKP	05 11 17.4	X	X	X	5.4	83	141.3	SALOMON I.
81		IP	05 15 29.2	X	X	X	4.5	89	22.2	N.CHILE
82		IP	07 07 38.5	X		X	4.3			SALTA, P.ARGEN.(LASA)
83		EP	13 11 25	X						LOCAL EVENT
84		E(P)	19 39			X				
85		EP	13 57 26	X	X	X				LOCAL EVENT
86		EP	14 03 42.7	X		X				SW AZIMUTH
87		EP	14 19 41	X	X	X				LOCAL EVENT
88		E(P)	14 22 16	X	X	X				LOVAL EVENT

AU = AUDIO ANALYSIS (EDINBURGH)
PA = PRELIMINARY AUDIO ANALYSIS (BRASILIA)
AA = AUTOREAD ANALYSIS (EDINBURGH)
MB = BODY WAVE MAGNITUDE REPORTED BY NOAA (OR LASA OR NORSAR AS INDICATED)

COMMAND:

b) SAAS P Range Events Reported by LASA

$m_b > 4$	3	!
$m_b < 4$	17	

c) SAAS P Range Events Reported by NORSAR

$m_b = 5.1$	1	!	Bolivia
$m_b = 4.6$	1	!	S. Sandwich Is.

Results marked with '*' are events found in SAAS tape DF 41/72 that were not reported by NOAA, LASA or NORSAR. The results marked with '!' are events reported by the agencies named above which might have been recorded by SAAS, and which were not found in the present analysis.

Concentrating attention on the P range events of Table 3, it is clearly seen that there is a large number of events which belong mainly to South America or neighbouring regions that are not reported by NOAA. Only 10 events out of 25 found in this analysis were reported by NOAA in the P range, and 10 events (or 12 if the E(P)$^+$ events are included) were found only in the SAAS tape used in the present visual analysis. Therefore, it may be concluded that the contribution of SAAS to the knowledge of South American seismicity could be very substantial, bearing in mind that the events recorded at SAAS and not reported by other agencies could be processed to calculate their epicentral parameters. The majority of the events not detected on SAAS records but reported by NOAA are located in the shadow region for SAAS, and 3 events in the P range $\Delta \approx 83^o$ do not have magnitude determinations (it is assumed, therefore, that they are very small). Only one event in the P range, a 10 Tons UK explosion ($\Delta = 80.3^o$; $m_b = 4.4$), reported by NOAA

was not seen on SAAS records; this could be due to some peculiarities in the path of this event, because a similar event of 20th July 1971 in the North Sea ($\Delta = 82.7^{o}$; $m_b = 4.3$) was recorded by SAAS (see Jacob and Willmore, 1972).

The events reported by LASA that were not found in the present analysis of a SAAS record are mostly of magnitude smaller than 4, except for two reported in the northern region of South America (Colombia, Guatemala) - from which it is supposed that there exists an amplitude attenuation anomaly (see Chapter 4) - and one seismic event reported in Peru. From the 17 events reported by LASA with $m_b < 4$, 6 belong to the northern region of South America, 5 to the Middle-western and North-western region of that continent. Signals from some of these events were perhaps received at recordable amplitude by SAAS but may be lost in the background noise and it was not possible to identify them by the methods used during the present analysis.

From Table 3, it can be concluded that the detection magnitude threshold for SAAS is under $m_b = 4$ (for the Southern part of the Andean Region), being able to detect events of $m_b = 3.4$ (LASA magnitude) in this region. It seems that for other regions of South America the magnitude threshold is larger, esepcially for the Northern region.

From this analysis, it can also be concluded that the audio method of detection being used in Brasilia is needing an improvement. Some suggestions for this are given in Appendix 4.

3.3 SAAS Capability up to 95° from comparison with NOAA Data

One hundred and seventy one events reported by NOAA during 66 days of SAAS operation, with epicentral distances less than 95° from Brasilia, have been searched in the tapes covering the following periods:-

a) 09 MAR 72 - 01 APR 1972

b) 15 APR 72 - 28 MAY 1972

All events reported by NOAA up to 50° from SAAS were considered in this analysis, including one event of $m_b = 3.9$ with $\Delta = 50.4$. For distances greater than 50° only events with $m_b \geq 4$ were considered.

The events found in this analysis are included in Appendix 1, but the ones that have a weak signal or that were not found during a visual analysis of paper playouts are listed in Table 4.

The results of this analysis have been plotted in Figure 6. From an inspection of Figure 6 and Table 4, the following conclusions, regarding SAAS capability to record seismic events as compared with NOAA bulletins, can be arrived at:-

a) From 171 events reported by NOAA considered for this analysis, 137 were visually detected on SAAS records from which 13 events have a poor signal (5 with $\Delta < 65°$ and 8 with $\Delta > 65°$)

b) The 34 visually undetected events are distributed as follows:-

- 5 events, $\Delta < 65°$ and $300° < Az < 16°$
- 24 events, $\Delta > 65°$ mainly from North America, Europe and Africa.
- 5 events (marked with * in Table 4) occurred when the station was not in operation.

Figure 6.- SAAS CAPABILITY FROM NOAA REPORTS

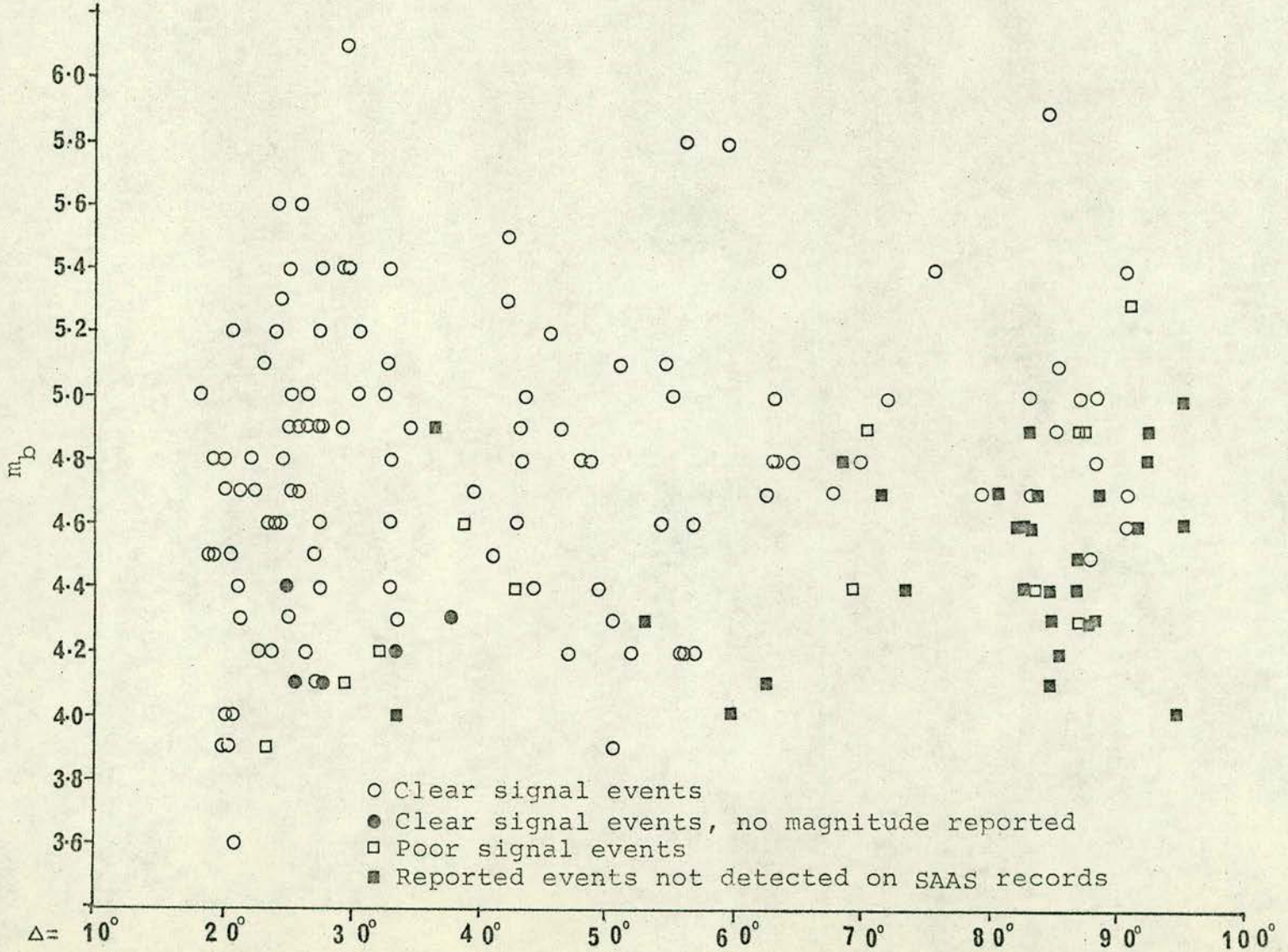

TABLE 4

DATE	ORIG. TIME	MB	DEPTH	DIST.	REGION	SAAS
09MAR	23 07 45.3	4.9	33	70.3	U.S.Africa	E(P)
15MAR	01 42 07.8	4.4	33	73.1	N.Rhodesia	-
16MAR	03 35 36.6	4.2	146	85.4	Greece	-
	21 31 33.4	4.8	33	68.1	Spain	-
17MAR	00 29 01.0	4.9	33	87.1	Iceland Region	E(P)
21MAR	04 29 33.0	4.2	67	32.2	Off.Coast C. Chile	E(P)
	13 10 27.7	3.9	106	23.2	S.Juan,Prov.Argentina	E(P)
22MAR	07 16 52.1	4.3	16	52.9	Mexico-Guatemala	-
	16 33 32.4	5.3	33	90.9	Jan Mayen Isl. Region	E(P)
23MAR	04 49 43.5	4.1	39	29.5	N. Peru	E(P)
	21 25 40.3	4.9	33	92.2	Off Coast Oregon	-
24MAR	02 50 25.4	4.8	33	92.2	Off Coast Oregon	-
25MAR	06 16 06.6	4.3	33	87.8	Dodecanese Isl.	-
26MAR	03 54 46.3	4.4	33	42.6	N.Atlantic Region	E(P)
28MAR	10 40 52.0	4.4	5	86.5	Montana	-
29MAR	23 04 37.6	4.7	51	35.9	Near C. Venezuela	*
30MAR	21 00 01.2	4.6	10	82.7	S. Nevada	-
31MAR	20 04 32.5	4.3	33	87.7	Dodecanese Isl.	-
01APR	05 51 48.8	4.9	33	82.9	Yugoslavia	-
15APR	17 37 26.0	4.9	42	36.4	Colombia	-
17APR	01 39 55.6	4.6	33	83.3	Adriatic Sea	-
	14 38 56.9	5.0	33	95.0	Off C. Oregon	-
	23 29 33.2	4.6	33	95.0	Off C. Oregon	-
18APR	15 07 49.1	5.4	5	76.3	Lake Tanganyika	*
	18 27 27.3	5.2	33	63.0	S.W.Africa	*
19APR	03 39 19.9	4.1	4	84.6	Greece	-
	16 32 00.0	4.6	0	82.6	S.Nevada	-
21APR	13 33 25.9	4.9	33	87.5	Norwegian Sea	E(P)
23APR	05 13 33.0	4.7	39	83.6	Greece	-
	11 18 05.9	4.7	33	80.3	B.California	-
25APR	02 26 31.3	4.2	8	88.2	California-Mexico B.Reg.	*
	17 26 27.6	5.5	33	70.5	U.S.Africa	*
26APR	21 14 06.3	4.4	33	84.5	Greece	-
29APR	01 00 16.7	4.0	9	33.5	Venezuela	-
30APR	10 33 45.0	4.3	81	84.6	Crete	-
03MAY	00 29 53.0	4.6	33	91.3	Off C.N.California	-
	08 52 53.0	4.1	33	62.4	N.Atlantic Region	-
07MAY	14 43 49.9	4.4	57	83.6	Yugoslavia	E(P)
08MAY	08 58 06.0	4.5	33	86.7	Greece	-
09MAY	17 40 25.1	4.7	37	88.1	Turkey	-
13MAY	13 58 50.6	4.4	33	69.2	N.Atlantic Ocean	E(P)
14MAY	07 20 43.0	4.0	33	59.6	N.C.Guerrero, Mexico	-
15MAY	01 51 01.4	4.7	33	71.3	S.Rhodesia	E(P)
17MAY	14 10 00.2	4.4	0	82.8	S.Nevada	-
18MAY	05 08 47.8	4.0	33	94.9	Q.Elizabeth Isl.	-
23MAY	02 35 18.4	4.6	38	38.8	Mona Pass.	E(P)
	03 14 28.2	4.3	5	87.1	Greece-Bulgaria B.Reg.	E(P)

c) Excluding the 5 events visually undetected on SAAS records with $\Delta < 65^{o}$, coming from a region where it is suspected that an amplitude attenuation anomaly exists, it can be stated that all events reported by NOAA up to $\Delta = 50^{o}$ and all events with $m_b \geqslant 4$ with Δ between 50^{o} and 65^{o}, for the period considered in this analysis, have been visually detected on SAAS records.

d) In the range between 65^{o} and 91^{o} of epicentral distance from SAAS, it appears that the magnitude threshold is $m_b = 4.4$, although there are several events with $m_b \geqslant 4.4$ occurring in this range and even in the same seismic area as some of the detected events, which were not seen on SAAS records.

e) None of the 6 reported events, during the period being studied, with m_b between 4.0 and 5.0 for the range of Δ between 91^{o} and 95^{o} from Brasilia, were seen on SAAS records.

f) There were five events with no magnitude reported by NOAA (with $\Delta < 50^{o}$) during the period of study, which are also shown in Figure 6, with their magnitude value calculated from SAAS data.

It is important to bear in mind that the events considered in this analysis do not include the events recorded by SAAS but not reported by NOAA. Hence this analysis cannot be used to determine the magnitude threshold for SAAS for events with $\Delta < 65^{o}$. Some of the events recorded by SAAS with poor signals (marked E(P) in Table 4)

might have been enhanced by beam forming but this has not been considered.

The peculiarities presented by the events used in this analysis regarding their travel time and observed amplitudes at SAAS are discussed in Chapter 4, together with data of some other events recorded at SAAS.

3.4 Epicentral Determinations from SAAS Data

The azimuth and the apparent velocity observed at an array provide the means of calculating the epicentral coordinates by using the following equations (Berrocal, 1968):-

a) The geographic latitude of the epicentre ϕ_e is deduced from

$$\phi_e = \arctan\left[\tan(\phi'_e)/0.993277\right] \quad (1)$$

where ϕ'_e is the epicentre geocentric latitude determined by

$$\phi'_e = \arctan\left[\sin(\phi'_e)/\sqrt{1-\sin^2(\phi'_e)}\right] \quad (2)$$

and where

$$\mathrm{Sin}(\phi'_e) = C\cos(\Delta) - K\sin(\Delta)\cos(Az) \quad (3)$$

The value of Az is the observed azimuth at an array and Δ is the epicentral distance found from the J-B seismic tables (by using the observed apparent velocity and the reported epicentral depth).

$$C = \sin(\phi'_s) \quad (4)$$

$$K = -\cos(\phi'_s) \quad (5)$$

where ϕ'_s is the geocentric latitude of the station, deduced from the station geographic latitude ϕ_s as follows:

$$\phi'_s = \arctan\left[0.993277\ \tan(\phi_s)\right] \quad (6)$$

b) The geographic latitude of the epicentre λ_e is calculated as follows:

$$\lambda_e = \lambda_s + \arctan(\gamma) \quad (7)$$

where λ_s is the station geographic longitude, and

$$\sin(\gamma) = -\sin(\Delta)\ \sin(Az)/K \quad (8)$$

$$\cos(\gamma) = C\sin(\phi'_e) - \cos(\Delta)/K\ \cos(\phi'_e) \quad (9)$$

The other variables are the same as those used to calculate ϕ_e.

The azimuth is given in degrees from 0^o to 360^o to the East from North and the distance is given also in degrees, subtended at the Earth's centre. The geographic latitude is positive if it is North and negative if it is South of the equator, the geographic longitude is positive if it is East and negative if it is West of the 0^o longitude meridian.

The azimuth and apparent velocity used in these calculations should be those obtained after proper corrections are introduced allowing for structural differences under the array and for lateral and horizontal discontinuities that cause refraction in the seismic ray paths and which are discussed in Chapters 5 and 6.

3.5 Seismic Activity in some Areas of Brazil detected by SAAS

Since the end of 1966, when the experimental stage of SAAS was installed, many seismic events occurred in Brazil were recorded by the array. The majority of these events have been located in areas close to dam sites.

Over 200 Brazilian events have been recorded in the period August 1967 - February 1972 and detected during the preliminary audio analysis of SAAS records (see Appendix 5). Most of these events were preliminary, located by using the method suggested in 3.4 but without using corrections. From these events, 178 have been located in the Southern central area of the state of Minas Gerais and 17 in the South of the state of Ceara (see Figure 7). Only one of these events has been located by NOAA (23 February, 1968, 14 23 03.3, m_b 4.5, damage at Pereiro).

The 17 events located in the South of Ceara occurred in January and February, 1968, and they are relevant because of the existence of the Oros dam in the vicinity of their epicentral area.

There are several indications that the Oros reservoir may not be the cause of the seismic activity of the South of Ceara:

- Seismic activity in this area is reported since 1810
- Large fault systems crossing the area
- No seismic activity was reported during the impounding of the reservoir
- The activity recorded by SAAS has characteristics of tectonic events, a main shock with several foreshocks and aftershocks which occurred in a short period of time (two months).

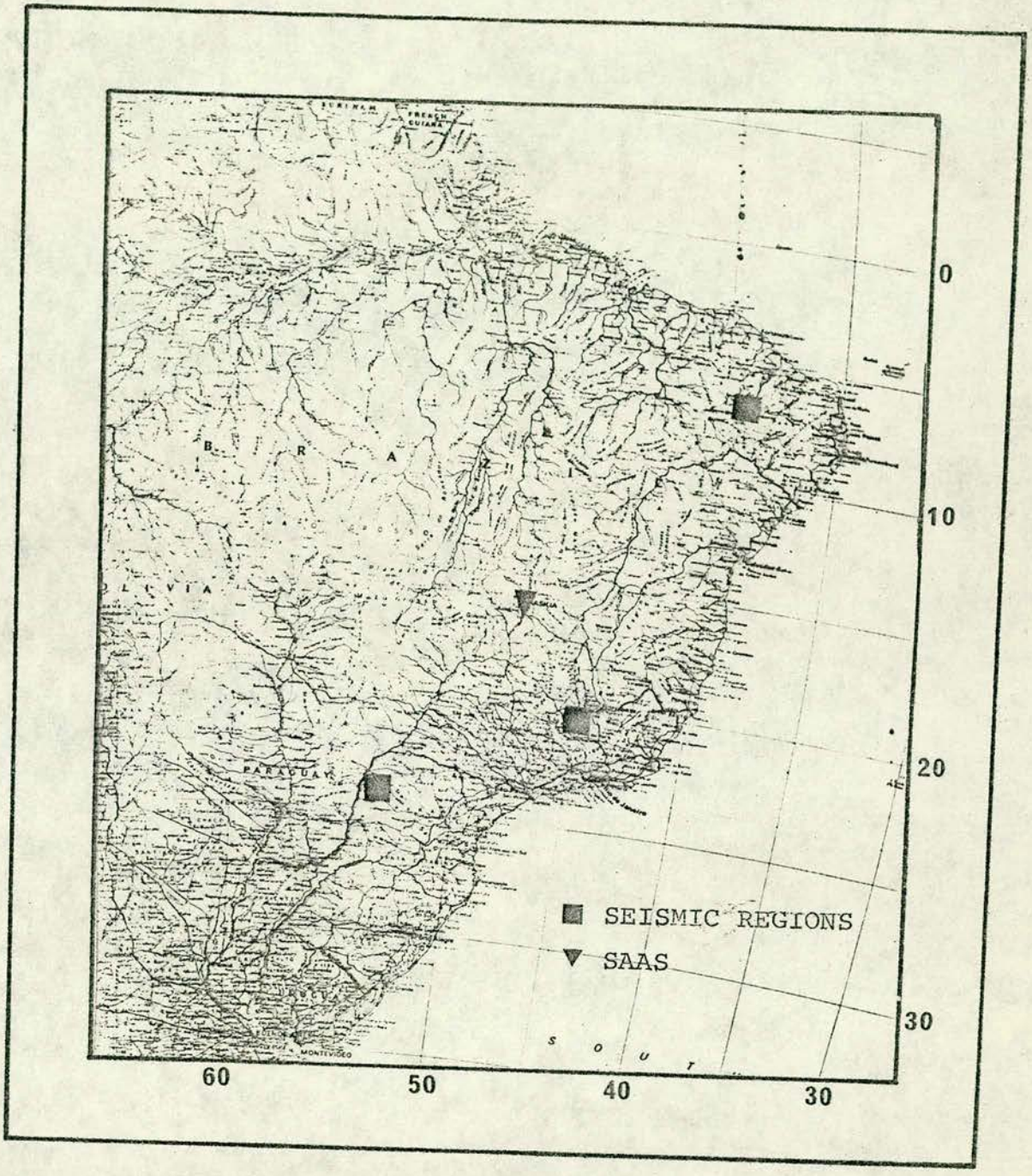

Figure 7.- REGIONS OF SEISMIC ACTIVITY IN BRAZIL

Nevertheless, a possible relationship between the Oros reservoir and the seismic activity in the South of Ceara cannot be completely excluded until further investigation is made.

The seismicity observed in the Southern central area of Minas Gerais started to be recorded by SAAS in April, 1970, and up to February, 1972 178 events were studied having magnitudes (SAAS m_b) between 3.5 and 4.8.

The most peculiar characteristic of these events is that 68% of them occurred between 13.00 and 15.00 GMT (10 and 12 hours local time) and 20% occurred between 18.00 and 21.00 GMT (15 and 18 hours local time). See Figure 8.

The two largest events (m_b 4.8 and 4.6) occurred in periods of the highest and of the lowest rainfall of that area, and these events were also widely felt in Minas Gerais.

Over 20 small and large dams are in operation in the state of Minas Gerais, the majority of which are located in its southern part. There is no means of relating with certainty the seismic activity observed in the southern central area of Minas Gerais with any of the reservoirs of that area until further studies are made, but the characteristics mentioned above indicate a good possibility of such a relationship.

It is important to mention also that the structural features of the area do not present very large fault systems to make a tectonic origin of these events likely.

On the other hand, the area is located only 100 km from Bom Sucesso where there has been a high degree of seismic activity

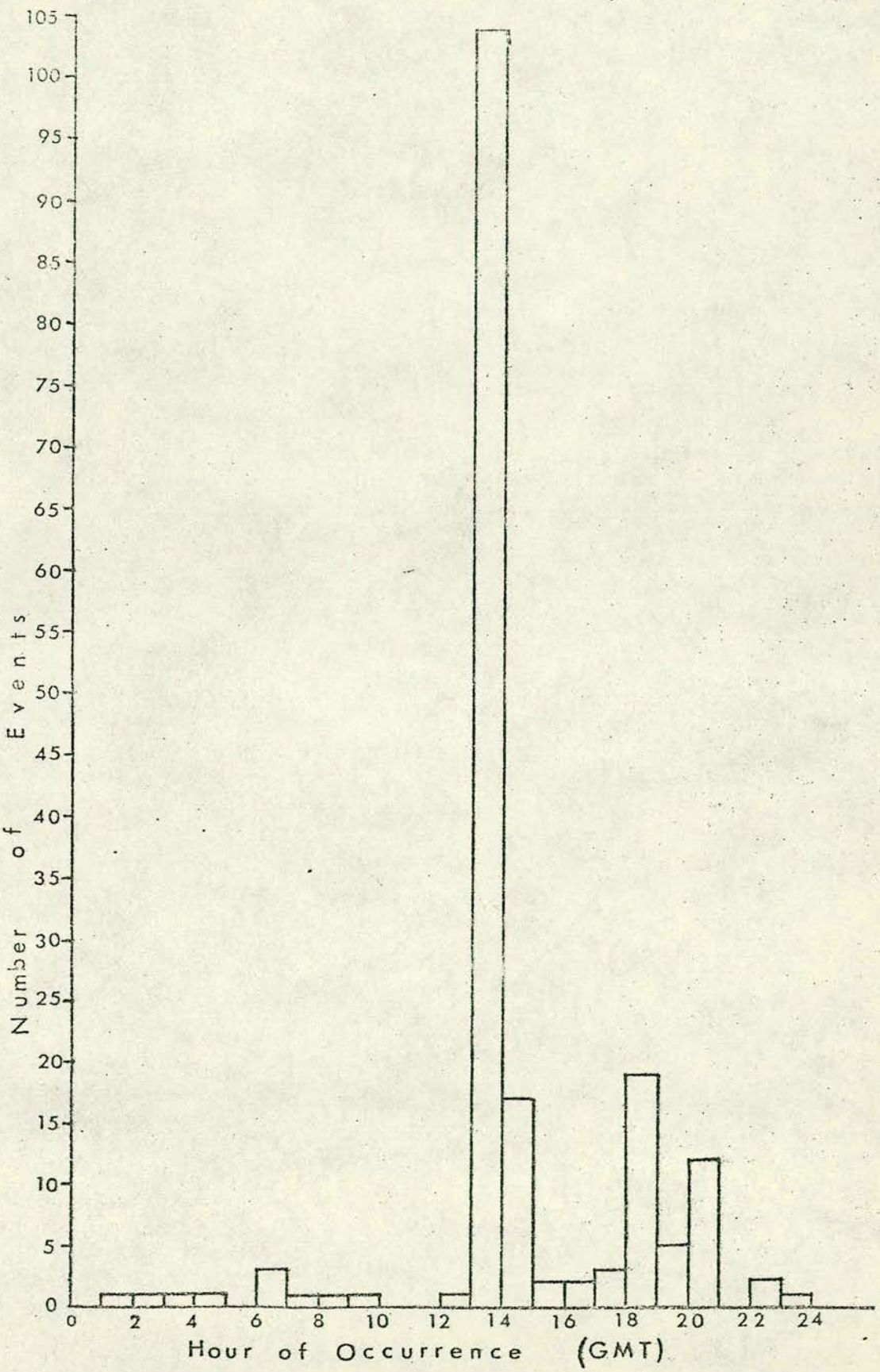

FIG. 8 TIME OF OCCURRENCE OF MINAS GERAIS EVENTS.

since 1824 with a peak in 1920 and gradually coming to a halt around 1950. Nowadays, it is very seldom that someone reports the occurrence of seismic tremors in Bom Sucesso.

Another area in Brazil from which shocks have been reported is in the state of Parana (see Fig. 7). No one of these events was recorded at SAAS or at least they were not identified as such during the preliminary analysis of the records.

Several other small seismic events have been recorded at SAAS with characteristics of having occurred at several hundred of kilometres away from Brasilia, but coming from different azimuths.

The Brazilian seismic activity detected by SAAS shows that there exists, at least in some areas, evidences of instability within the Brazilian shield. In other areas of Brazil, SAAS can detect small disturbances in the Earth's crust which could have been caused by the impounding of water reservoirs.

CHAPTER 4

ARRIVAL TIMES AND AMPLITUDES OF P PHASES OBSERVED AT SAAS

4.1 Introduction

One of the most direct and exact parameters than can be obtained from a seismic signal is the arrival time of the onset at the recording seismic stations. In the past few years there have been great advances in seismic recording instrumentation (1) so that now it is possible to read the arrival time of first onsets in most seismic events with an accuracy of 1/10 of a second. For large, clear signals recorded on magnetic tape and replayed at high paper speeds, this accuracy can be 1/100 of a second.

Other parameters that are observed fairly well are the amplitude and period of some of the seismic phases observed in the seismograms. At present the majority of seismic stations report these parameters for the largest longitudinal short period signal (P phase) recorded at the vertical short period component of the station. Latest advances in recording instrumentation have also enhanced the accuracy of the observation of these parameters, and the use of reliable electronic amplifiers makes the characteristics of the instrumentation less able to be affected by minor changes of the surrounding climatic conditions; this permits a continuous reliable observation of the amplitude and period of P phases which are used to determine the body wave magnitude (m_b) of the earthquakes.

Travel-time and magnitude residuals of over 200 events, with Δ up to 95^{o} from SAAS, have been recalculated and are presented in this chapter. A review of some work involving travel-time residuals

---

(1) Magnetic tape permits preparation of paper records of optimum speed and gain, and the signal can be passed through appropriated frequency filters which enhances the onset.

and amplitudes of P phases is also presented in this chapter. An interpretation of the distribution of the travel-time and magnitude residuals observed at SAAS is also discussed.

4.2 Brief Review of Studies on Travel-Time Residuals

Since the publication of the seismological travel-time tables by Jeffreys and Bullen in 1940, it has been possible to obtain more accurate epicentral determinations, and further improvements have arisen from the increase in quality and number of seismic observatories in different parts of the Earth and from the use of high speed digital computers.

Large departures from the travel-times predicted by the J-B tables have been observed at many stations in most parts of the world. These travel-time residuals have been used by many research workers to study peculiarities of the Earth's interior or to improve local and regional travel-time tables to be used in refined epicentral determinations.

Some of these studies have found regional differences of P travel-time residuals up to 11 seconds, such as in the eastern and western United States of America. Herrin and Taggart (1962) explained this difference in the USA by variations in the seismic velocity of the upper mantle; Hales *et al*, (1968) explained the same difference more specifically, as a result of the variation in the thickness of the low velocity layer which they fixed at 130 Km of depth. Similar differences for the P phase residuals were observed in the USA by Romney *et al* (1962) by using recordings of the Gnome nuclear explosion obtained at distances up to 25^{o}; this anomaly suggested to them a systematic relationship to crustal thickness.

Cleary and Hales (1966) used a technique similar to the "time term" method of refraction seismology to study the residuals observed

at USA stations from events in the distance range 32° to 100°. In this way, they claim to have separated the deviations from the J-B tables from the effects of station and source structure; they concluded that negative residuals are related to shield areas where there is low heat flow and positive residuals to continental areas which have uplifted since the Tertiary Era and where there is a large heat flow.

Travel-time station corrections for 321 seismological stations were calculated by Herrin and Taggart (1968) which were dependent on azimuth. These corrections were calculated by using 400 large earthquakes and 30 large explosions. Herrin (1968) and his group produced a new set of travel-times tables for P,PP,pP,PcP and PKP phases with the hope that they might become a new standard for epicenter determinations and studies of regional variations in travel-times. Herrin et al (1968) pointed out that it has become apparent that the J-B tables are generally 2 to 4 seconds slow for both oceanic and continental sources.

The Herrin (1968) travel-time table for P phases was closely fitted by the following second degree parabola (Lomnitz and Vargas, 1969):

$$t = 67.35 + 11.14\Delta - 0.0356\,\Delta^2 \qquad (10)$$

which has obvious advantages over the 1968 table, especially in computer calculations. Lomnitz (1971) explains why the 1968 table did not meet the objective that had been expected: only 278 events were utilized to deal with 963 station correction constants, which means an average of less than 1/3 event per station constant to be

estimated, therefore a large feedback from station corrections into the travel-times could be expected. Most information was absorbed by the corrections, therefore possible source effects, systematic errors and effects of the structure under stations were not descriminated from the effects of true Earth inhomogeneity, even by using the successive iterations that were necessary to reach a stable solution for the Herrin tables.

By using exact travel-time data from 42 explosions (true origin time and location), Lomnitz (1971) pointed out that the J-B tables predict later arrivals at all distances of the P range, (i.e. negative station residuals), which could be corrected by the mean values that are listed in Table 5; on the other hand, he shows that the negative skew observed in his study was not wholly an effect of the J-B error but also a result of the Earth structure covered by the observed seismic paths of these explosions. Finally, to quote from Lomnitz (1971), "Since the J-B error is within the natural Earth "noise", it is conceivable that it might change sign or disappear with a more representative body of data. Unfortunately, no such data are presently available; hence, current attempts at improving or correcting the J-B tables must be regarded as premature, or of restricted regional validity at best".

A method to determine epicentres and travel times simultaneously (Joint Epicentre Method) has been described by Lilwall and Douglas (1970). They claim that regional variations of travel-times are not revealed when epicentres are computed singly, and that azimuthally varying source terms of smaller value (than claimed elsewhere) can be found if these regional variations are included as station corrections.

TABLE 5

TRAVEL-TIME TABLE FOR SURFACE FOCUS FROM AVAILABLE CALIBRATED SOURCES*

Distance (deg)	Correction (sec)	Distance	Correction (sec)
0-30	-1.1	61	-4.1
31	-1.2	62	-4.1
32	-1.2	63	-4.0
33	-1.3	64	-3.7
34	-1.4	65	-3.4
35	-1.5	66	-3.2
36	-1.6	67	-3.0
37	-1.6	68	-2.9
38	-1.7	69	-2.8
39	-1.8	70	-2.7
40	-1.9	71	-2.6
41	-2.0	72	-2.5
42	-2.1	73	-2.4
43	-2.2	74	-2.3
44	-2.3	75	-2.2
45	-2.4	76	-2.1
46	-2.5	77	-2.0
47	-2.6	78	-1.9
48	-2.7	79	-1.9
49	-2.8	80	-1.9
50	-3.0	81	-1.9
51	-3.1	82	-1.8
52	-3.2	83	-1.8
53	-3.3	84	-1.8
54	-3.4	85	-1.8
55	-3.5	86	-1.8
56	-3.6	87	-1.8
57	-3.8	88	-1.8
58	-4.0	89	-1.8
59	-4.1	90	-1.8
60	-4.1		

* Mean corrections to be added to J-B travel times. (After Lomnitz, 1971)

By using the Joint Epicentral Method and the data of 81 shallow events recorded by 146 stations, Lilwall and Douglas obtained a travel-time curve which has almost the same shape of the Herrin (1968) curve rotated 0.5 sec towards the J-B reference line.

From the foregoing review it may be seen that the relationship between travel-time residuals and major discontinuities in the Earth's structure is observed in some regions, although the interpretations of these discontinuities made by different researchers do not often agree. It can also be seen that although the J-B tables predict late time arrivals and therefore a great amount of the observed negative travel-time residuals, they cannot be improved, to be used in every region of the Earth, because the present available explosion data is restricted to few areas of the Earth and earthquake data could give bias results. For this reason all data used in this chapter (NOAA epicentral locations and time residuals) are referred to the J-B 1940 travel-time tables.

4.3 Travel-Time residuals Observed at SAAS

4.3.1 Data

The arrival times of more than 200 events detected by SAAS and reported by NOAA have been re-analysed for this study. These events have occurred in different periods of 1971 (JUL) and 1972 (MAR,APR,MAY,OCT,NOV)[1] at distances up to 92° from SAAS. The observed arrival times of these events are listed in Appendix 1.

The playouts obtained for the analysis of these events have at least 1/40 sec. of reading accuracy (for events replayed at 250 mm/sec paper speed); readings up to 1/10 sec. were easily obtained, even in the case of events with doubtful onset, in which case the onset was localised by correlating visually the signal recorded at several points of the array. Some events with poor signal were not considered. All readings have been referred to E4, which was the SAAS reference point during the period of study.

The Earthquake Data Reports (EDR) bulletins from NOAA have been used to obtain epicentral distances and travel-time residuals for SAAS events (BDF code) included in the EDR bulletins. For the remaining events (not included in the EDR bulletins) distances and residuals have been obtained from the GEDESS (which calculates expected seismic parameters for some British stations from NOAA reports) bulletins of UKAEA. Both bulletins, EDR and GEDESS, use the J-B travel-time tables, therefore the residuals used in this analysis are referred to the J-B tables. Travel-time residual (ΔTT) is defined in this study by:

$$\Delta TT = \text{Observed arrival time} - \text{Expected arrival time}. \quad (11)$$

(1) The events used in this research were chosen from SAAS tapes available at Edinburgh, which belong to the permanent stage of the array.

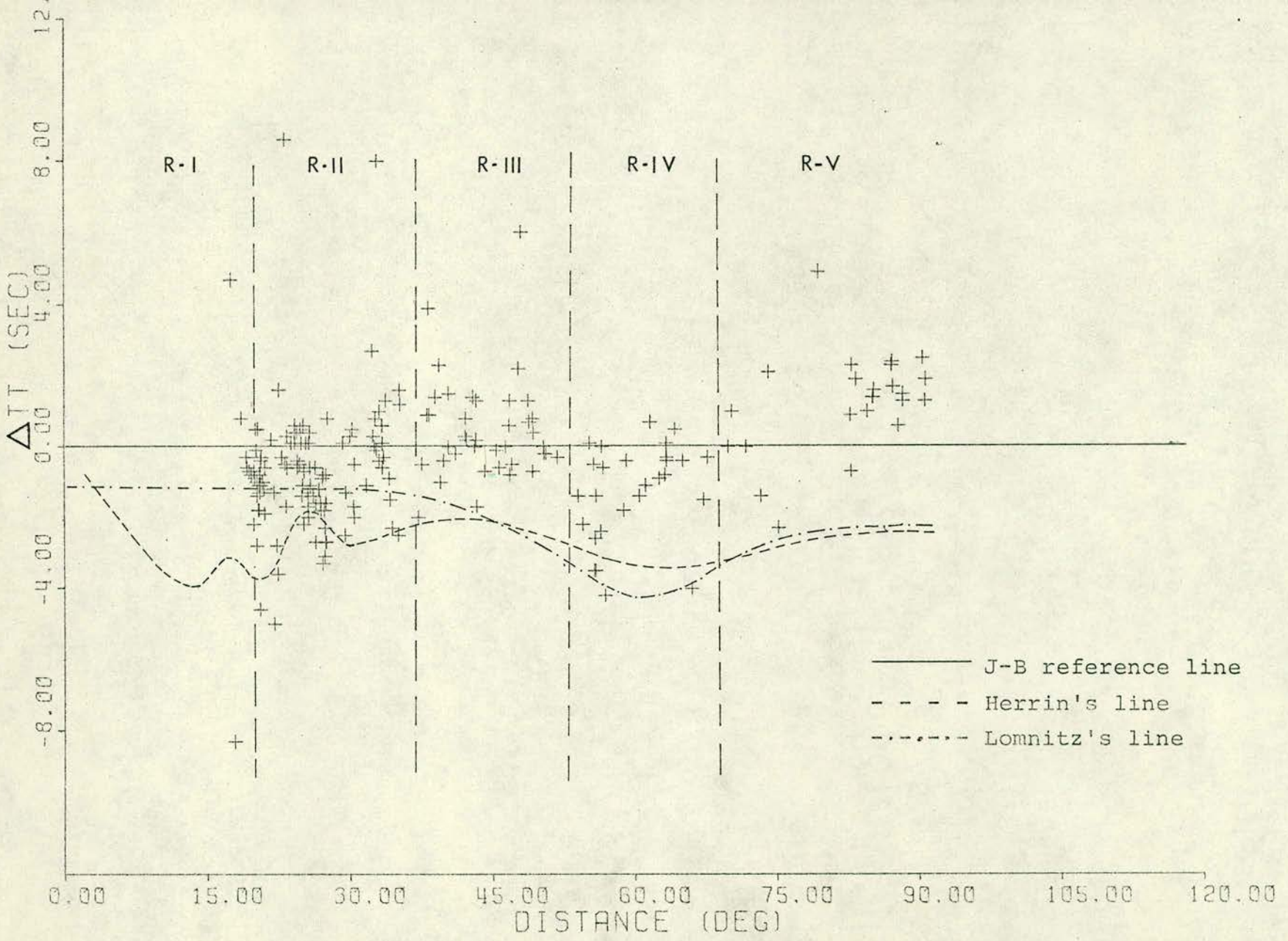

Figure 9.- DISTRIBUTION OF ΔTT AGAINST EPICENTRAL DISTANCE, SHOWING RANGES OF CONCENTRATION OF RESIDUALS

4.3.2 The Variation of ΔTT with Distance

All observed ΔTT values with reference to J-B travel-time tables have been plotted in Figure 9 against epicentral distances. Also displayed are the Herrin 1968 travel-times reference line and the corrections to J-B travel-times suggested by Lomnitz (1971).

The distribution of ΔTT values with distance allows them to be grouped in several ranges of distances as shown in Figure 9.

In Range I, ΔTT values reveal a tendency for late arrivals to appear for the nearest events. See also Table 6. It appears that these events also present a relationship with the depth of their foci, as shown in Figure 10 (late arrivals for deeper events), however, more events would be necessary to confirm this possible relationship. The events from this range occurred in Bolivia and Northwest of Argentina.

TABLE 6

RANGE I EVENTS

EVENT	PHASE	DIST.	DEPTH	ΔTT	REGION
E17	EP	17.6°	275Km	4.7 sec	Southern Bolivia
E57	IP	18.7	191	0.8	Southern Bolivia
A41	IP	18.8	215	1.8	Jujuy, Argentina
A64	IP	19.2	209	-0.3	Jujuy, Argentina
A65	IP	19.2	195	-0.6	Jujuy, Argentina
E36	EP	19.4	201	-0.7	Jujuy, Argentina
E56	IP	19.7	197	-0.8	Salta, Argentina
A51	IP	18.0	102	-8.3	Bolivia

Ranges II and IV in Figure 9 have ΔTT with mainly negative values. Range II comprises mainly the Andean region of South

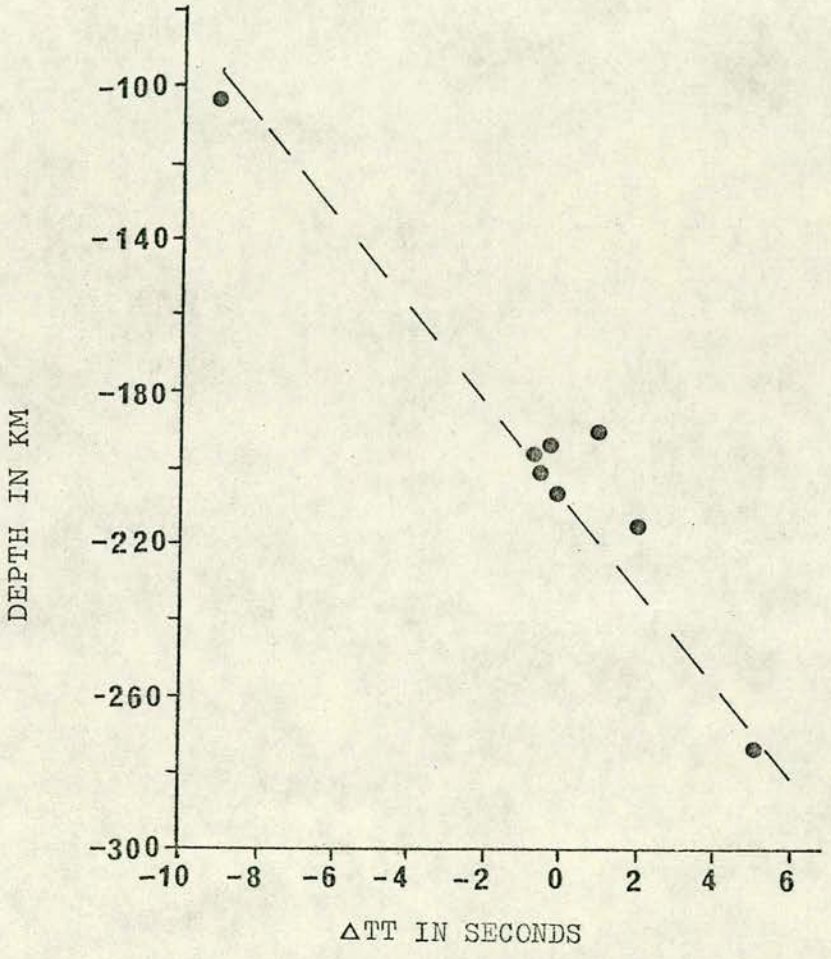

Fig.10.- DISTRIBUTION OF ΔTT OF EVENTS WITH $\Delta < 20^{\circ}$ FROM SAAS, AGAINST DEPTH

America and the central part of the Mid Atlantic Ridge (see Figure 11). Range IV includes the events occurred in the Eastern Pacific Ocean, Mexico, part of the Northern Mid Atlantic Ridge and Southern Atlantic ridge.

Ranges III and V (see Figure 9) have events with ΔTT having mainly positive value. Range III covers mainly Central America and the Caribbean region and the South Sandwich Islands region. Range V comprises mainly the eastern Europe and Middle East region; and the seismic regions of Africa.

In Figure 9 it can be seen that the ΔTT values observed at SAAS are mainly positive with respect to the Herrin (1968) and Lomnitz (1971) reference lines. If a mean line were to be fitted to these residuals in Figure 9, it would follow approximately the Herrin's reference line but with a shift ranging between 2 and 3 seconds towards the J-B reference line. This positive shift of the travel-time residuals observed at SAAS (with respect to Lomnitz and Herrin's reference lines), could correspond to the shift of these lines with respect to the J-B reference line. If the epicentres were determined by using Herrin's or Lomnitz's travel-times, the positive shift of 2 or 3 seconds referred to above would disappear or become small.

SAAS ΔTT have mainly negative values with reference to the J-B travel times, which agrees with the expected by Cleary and Hales (1966), with two clear groups of exceptions in the Ranges III and V of Figure 9.

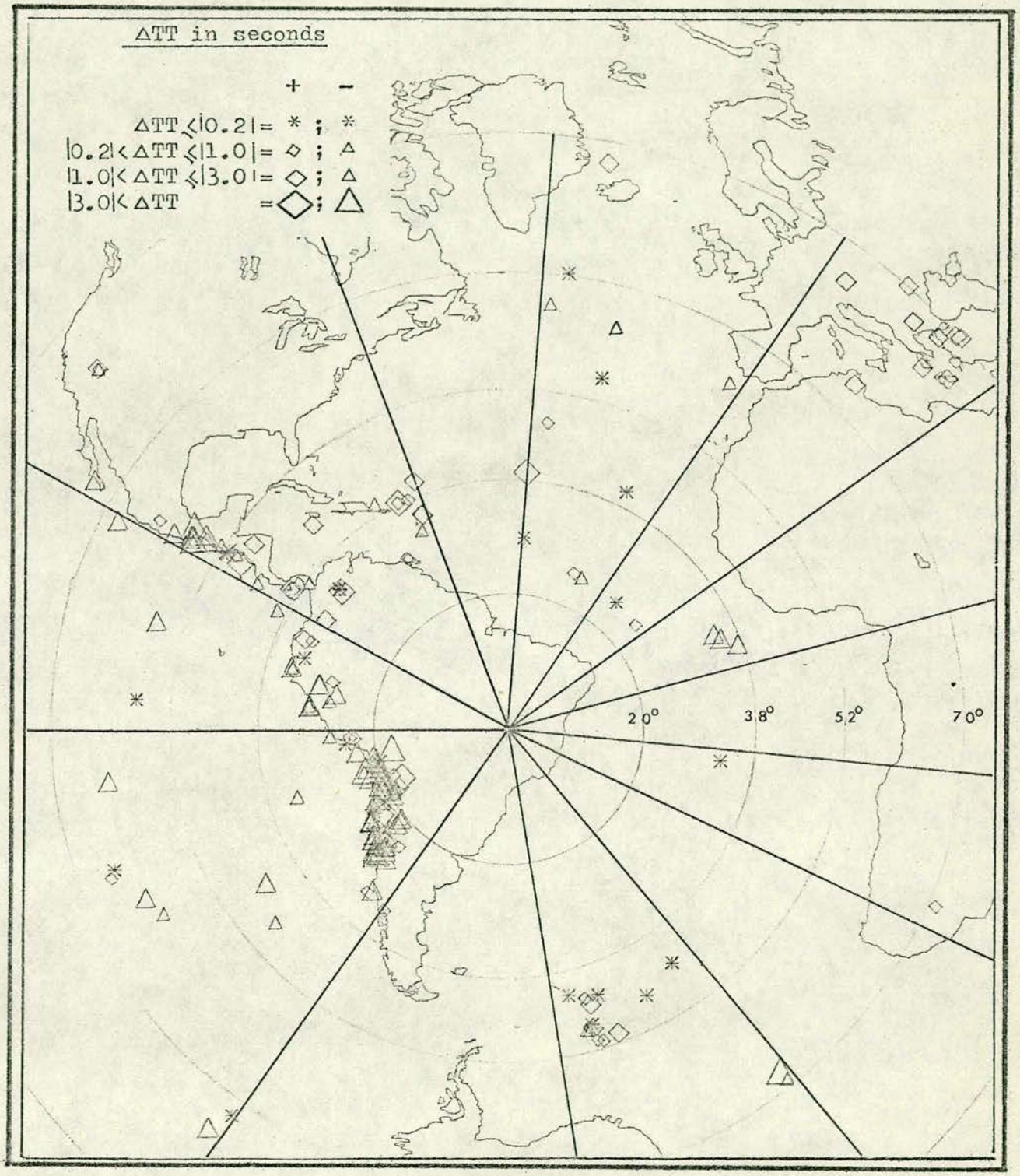

Figure 11.- AZIMUTHAL DISTRIBUTION OF ΔTT CENTRED AT SAAS, SHOWING ZONES OF CONCENTRATION OF RESIDUALS

4.3.3 The Variation of ΔTT with Azimuth

The ΔTT values with reference to J-B tables, observed at SAAS and being used in the present study, have been plotted in Figure 11 in a polar projection of the Earth centred in SAAS. The distribution of ΔTT in Figure 11 allows them to be grouped in 8 zones of azimuth.

ΔTT of Zones I,II and III are plotted against epicentral distance in Figure 12, showing that the value of the residuals is similar for each region included in these zones, regardless of the distance of their events (especially in the case of the Mid Atlantic Ridge residuals).

ΔTT of Zones IV and V are plotted against epicentral distance in Figure 13. The events of zone V are mainly from the South Sandwich Islands Region and show a similar behaviour. Most events of Africa and of the South of Africa were recorded at SAAS with a poor signal, therefore their residuals should not be considered in the present analysis.

In Figure 14, the ΔTT values of Zone VI have been plotted against epicentral distance. In this figure can be seen a smaller scatter of the residuals of the East Pacific Ocean events as compared with the residuals of the Andean events. In Figure 15 the residuals of the Andean events of Zone VI are plotted in a larger scale map of that region. In this figure one can observe the following regionalization on the distribution of ΔTT:

- Southern Peru (14^{o}S to 18^{o}S): small negative or small positive residuals.
- Northern Chile, Chile-Bolivia Border (18^{o}S to 25^{o}S, West of medidian 67^{o}W): mainly negative residuals.

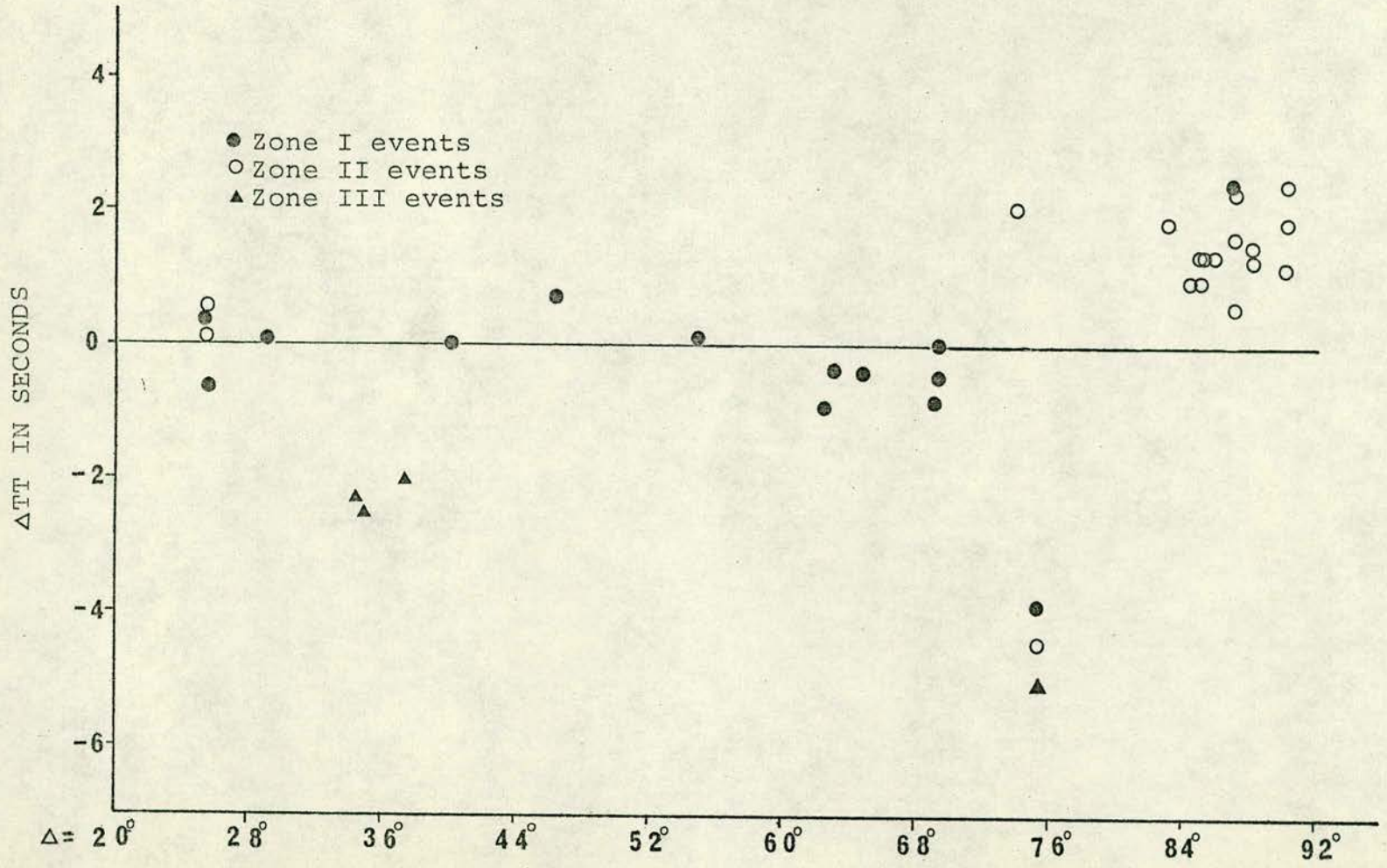

Figure 12.- ΔTT FOR EVENTS FROM ZONES I, II, AND III AGAINST EPICENTRAL DISTANCE

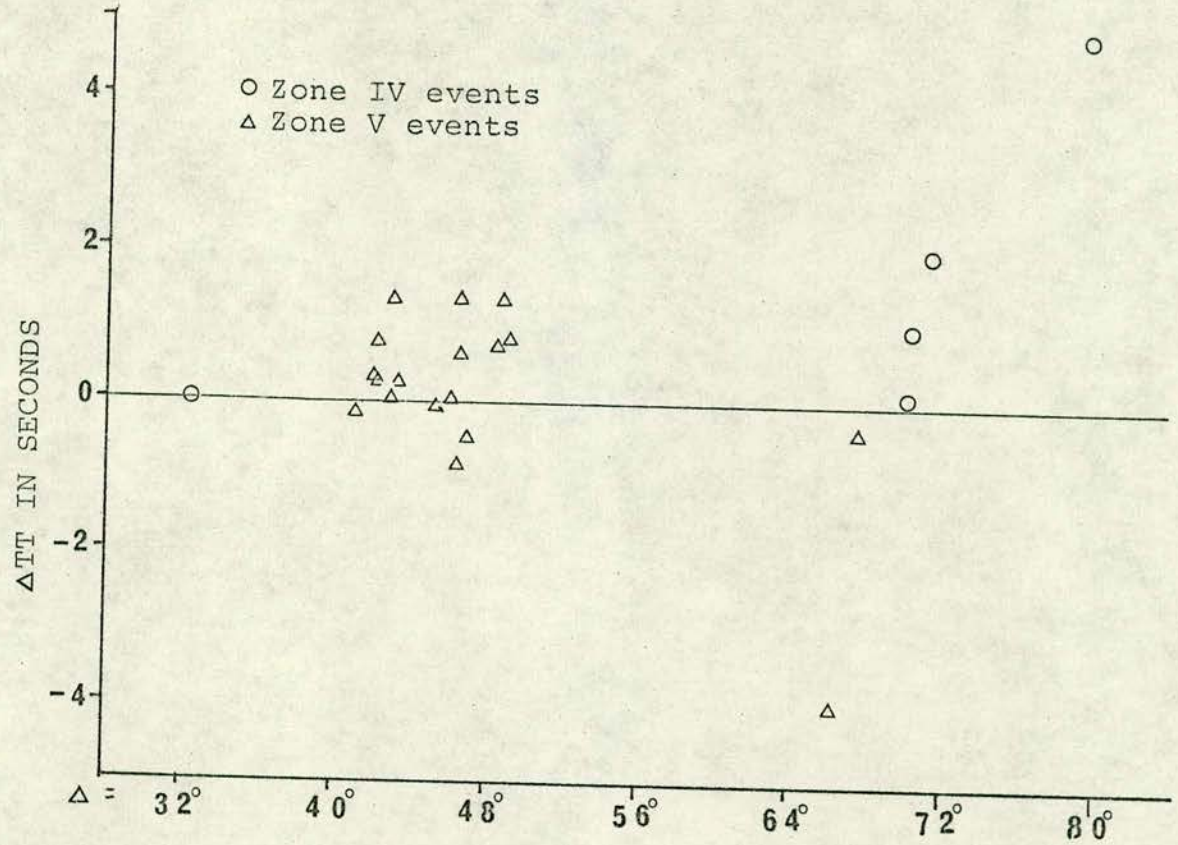

Figure 13.- ΔTT FOR EVENTS FROM ZONES IV AND V AGAINST EPICENTRAL DISTANCE

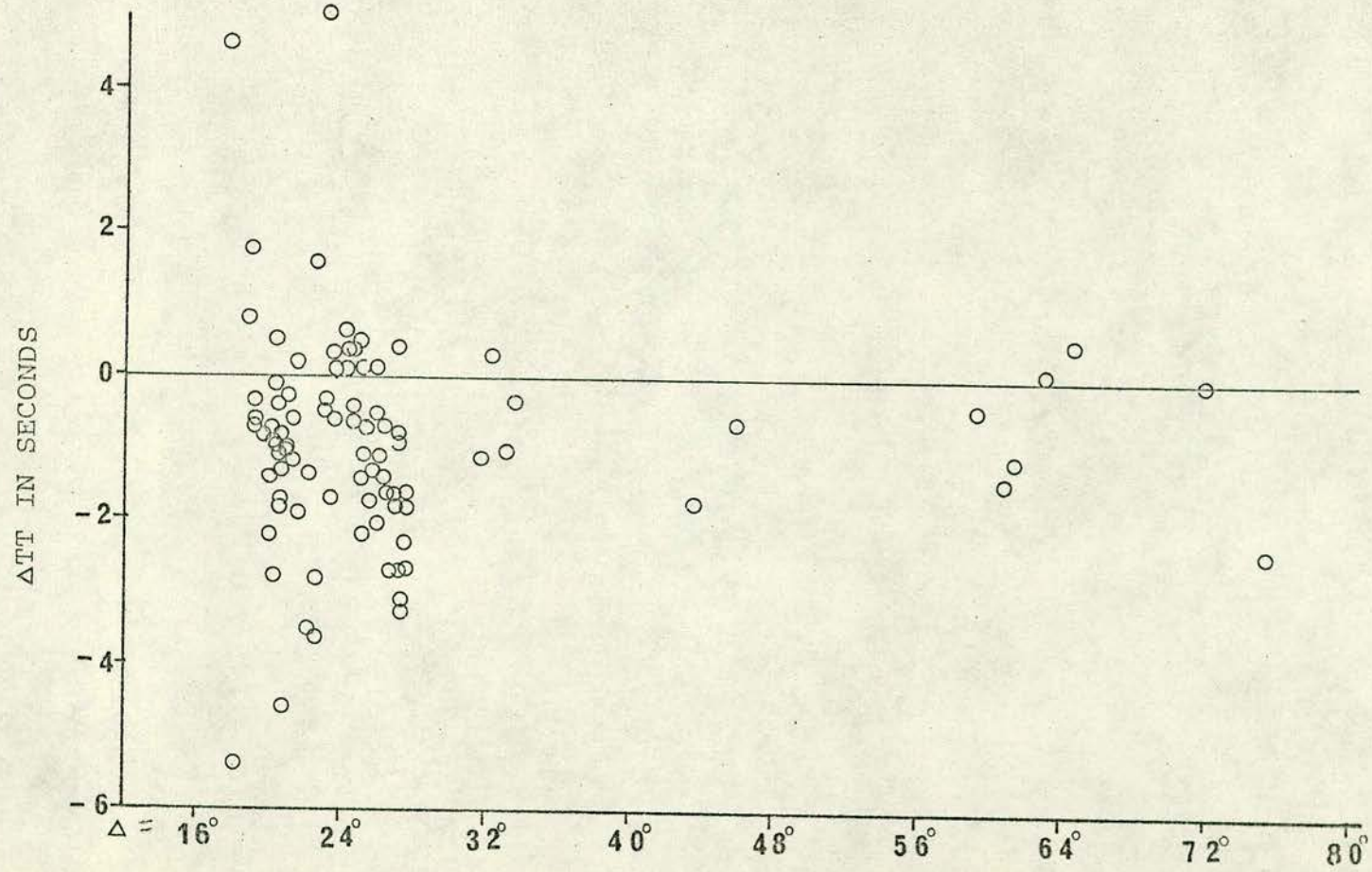

Figure 14.- ΔTT FOR EVENTS FROM ZONE VI AGAINST EPICENTRAL DISTANCE

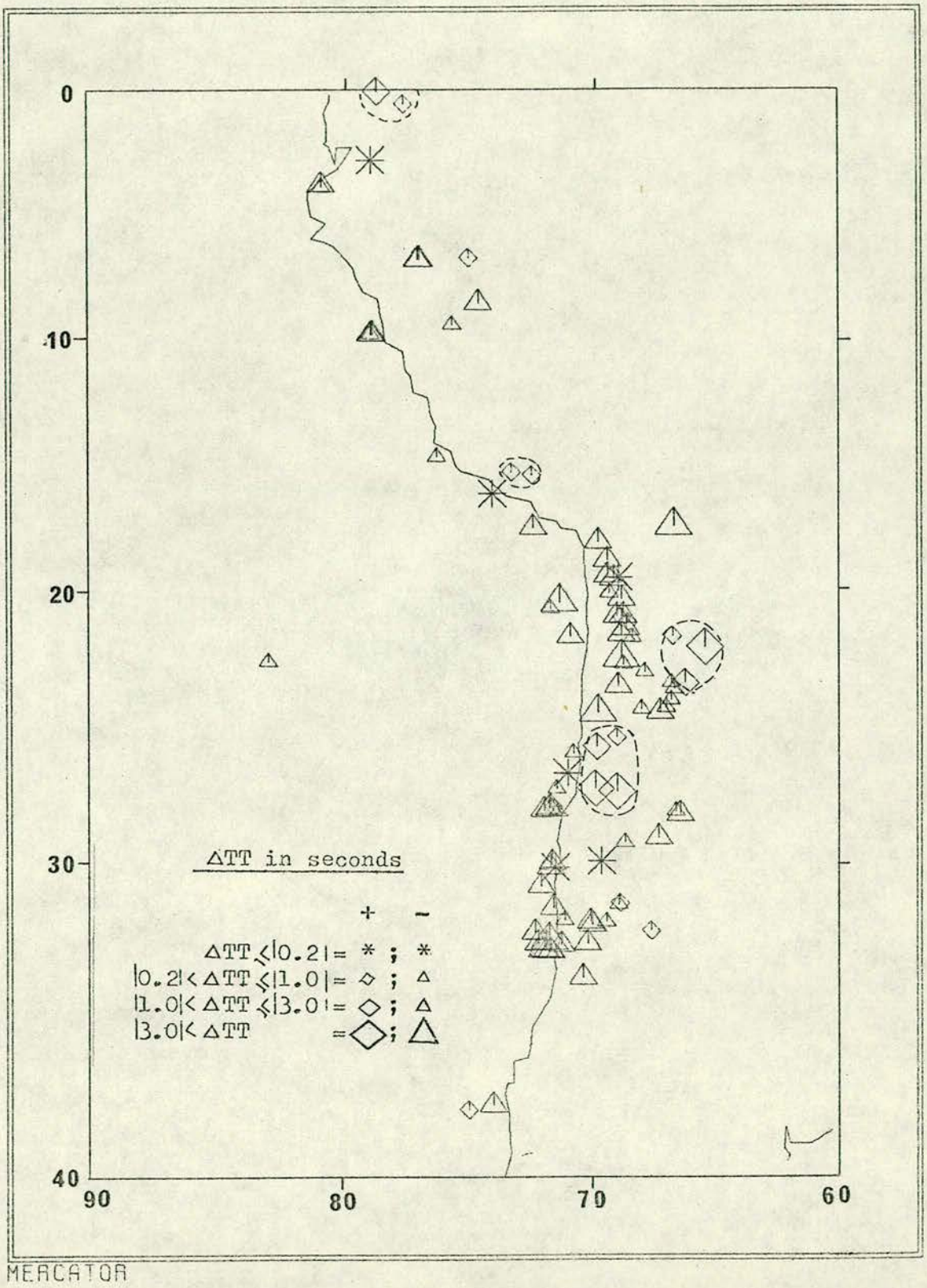

Figure 15.- DISTRIBUTION OF ΔTT IN WESTERN SOUTH AMERICA

- Southern Bolivia (around 22°S and 66°W): positive residuals.
- Jujuy Province, Argentina (around 24°S and 67°W): small negative residuals.
- Chile and Chile-Argentina Border (between 25°S and 30°S): residuals mainly close to zero, with very large positive residuals at around 27°S latitude.
- San Juan and Mendoza Provinces, Argentina (around 32°S and 68°W): positive or small negative residuals.
- Near the Coast of Chile (below 27°S): negative residuals.

ΔTT values belonging to zones VII,VIII and IX have been plotted against epicentral distances in Figure 16. The events of Zone VII belong mainly to the Peruvian and Ecuatorian Andes (dominant negative residuals). The events of Zone VIII can be grouped in three areas: Colombia and Central America (mainly positive residuals); Mexico (mainly negative residuals); Nevada (residuals betweeen -0.9 and 2.3 sec). Zone IX comprises events from the Caribbean Sea (mainly positive residuals and similar to those of events occurred in Colombia and Central America). See also Figure 17, which shows ΔTT values distributed in the Colombia, Central America, Caribbean Sea and Mexico region.

4.3.4 Discussion

ΔTT values observed at SAAS for events with epicentral distances of up to 92°from the station, show some peculiarities which are worthy to point out.

First of all, the distribution of ΔTT against epicentral distances show that seismic events reported by NOAA during the period of study occur at every distance between 17° and 92° from SAAS, except for a clear gap in the range between 74° - 82°.

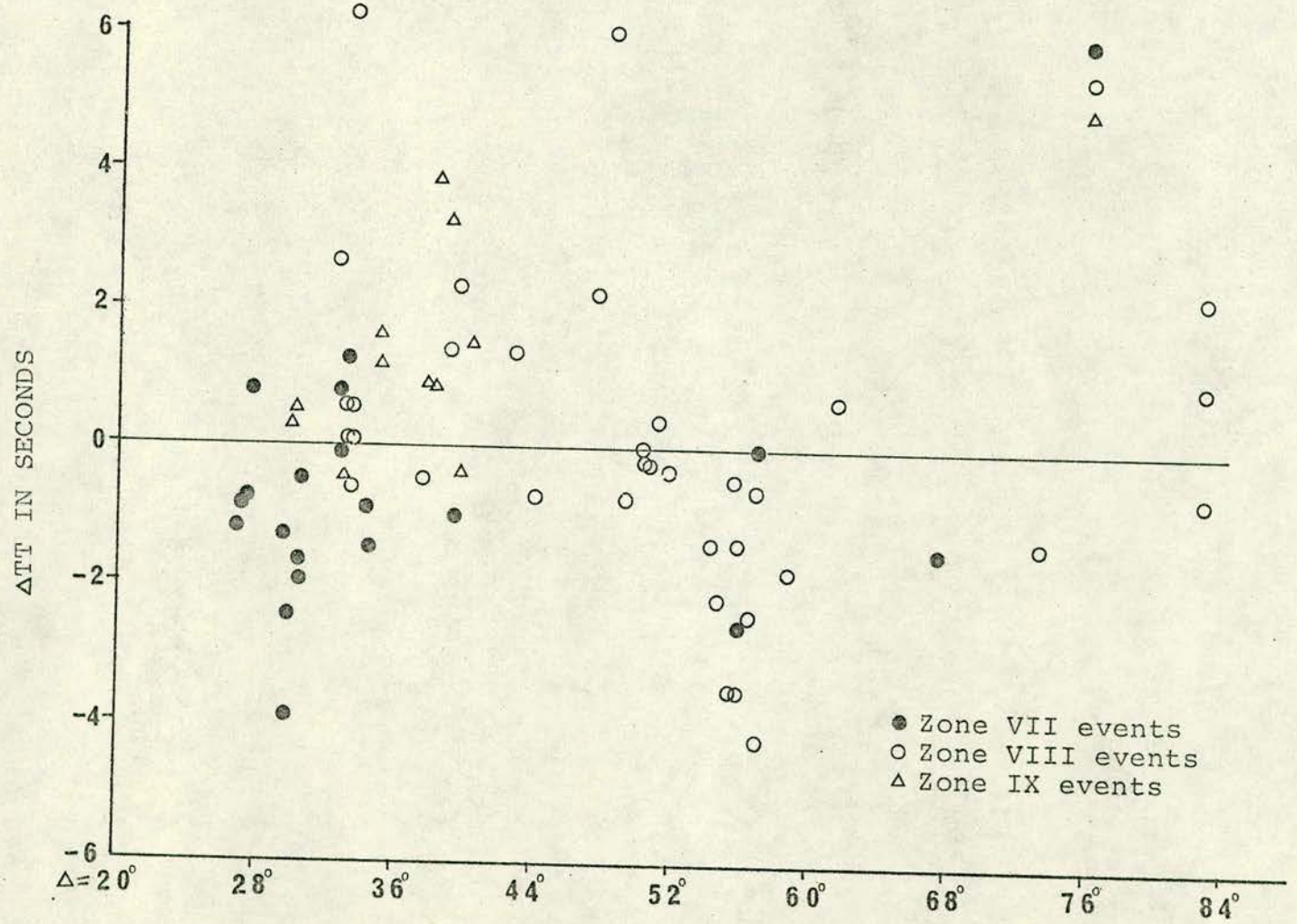

Figure 16.- ΔTT FOR EVENTS FROM ZONES VII, VIII and IX AGAINST EPICENTRAL DISTANCE

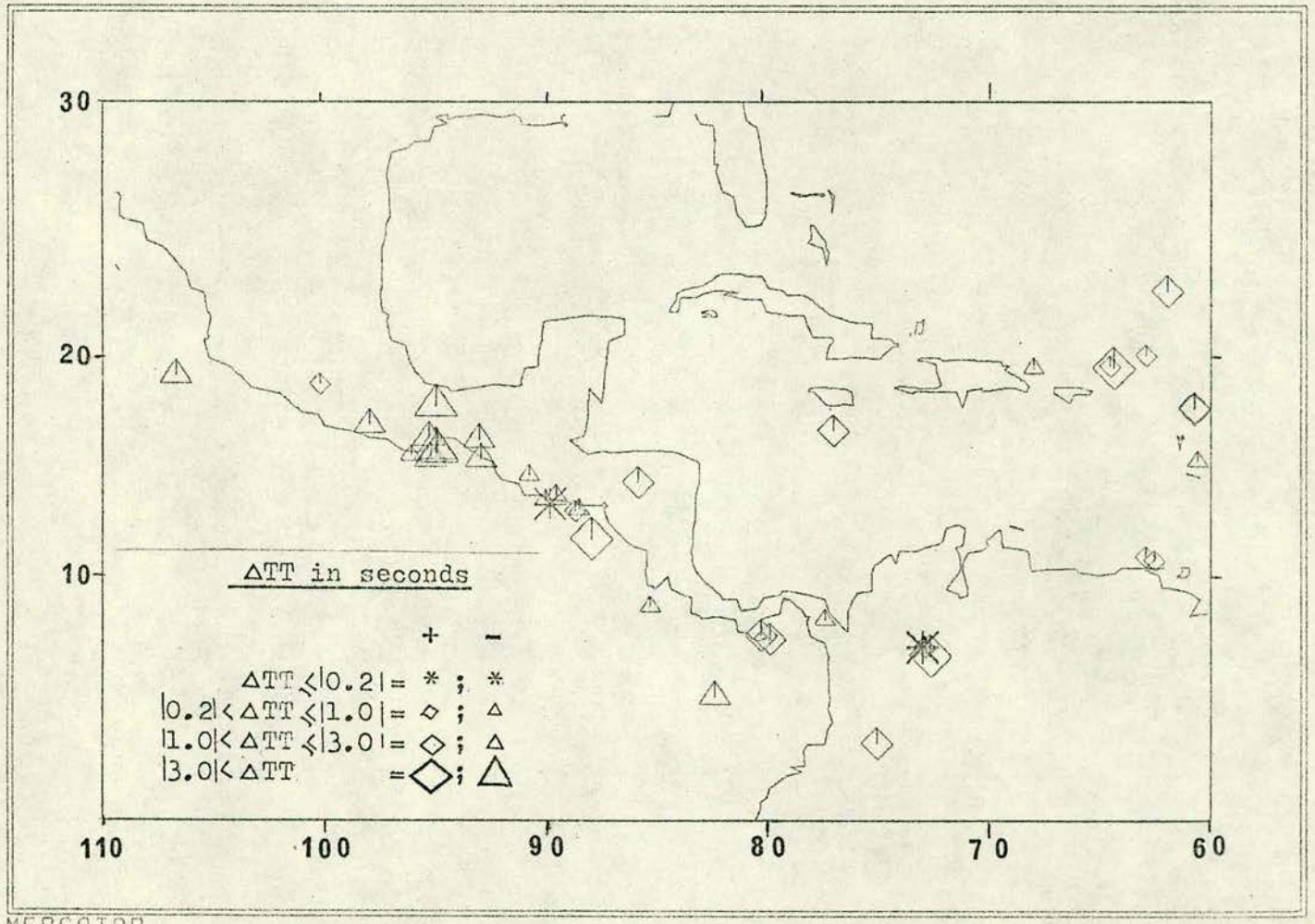

Figure 17.- DISTRIBUTION OF ΔTT IN NORTHERN LATIN AMERICA

No events were reported by NOAA with epicentral distances smaller than 17^{o} from SAAS. Events reported by NOAA beyond 92^{o} and up to 95^{o} were not detected on SAAS records. The travel-time residuals are mainly negative in relation to J-B Tables, with two ranges of distances which have ΔTT with mainly positive value (38^{o} to 52^{o} and 70^{o} to 92^{o}). ΔTT values are mainly positive (relatively positive only) with regard to the correction line suggested by Lomnitz (1971) and to the Herrin (1968) tables, by almost the same amount as the shift of these travel-times from the J-B reference line; they follow closely the shape of Herrin's reference line. There appears to be a relationship between depth and the sign of ΔTT: in general, for similar distances, deeper events have more negative residuals; this relationship appears to be inverted for events with $\Delta < 20^{o}$ (i.e. deeper events have more positive residuals).

The scatter and some exceptionally large values of ΔTT observed at SAAS could be due to error in epicentral location, which could arise from the use of doubtful arrival times at few stations in case of the smaller events, or by the use of good arrival times but from stations now evenly distributed in azimuth and distance, producing appreciable shifts from the true epicentre, as it was suggested by Lomnitz (1971). See, for example, the events A51, E17 and E55 of Figure 46 which have ΔTT equal to -8.3, 4.7 and -2.8 seconds respectively. These events have a relatively clear onset which allow good time readings, therefore the observed residuals have to be caused by possible mislocation of the hypocentres or by genuine departures of the J-B tables from the true P phase velocity distribution in the paths followed by these events before they were recorded at SAAS.

Consequently, it is not advisable to obtain a mean curve to fit the residuals observed at SAAS, in order to get station corrections for SAAS, until more refined epicentral locations are made or explosion data can be used as source of data.

The distribution of SAAS ΔTT values against the azimuth of seismic signal approach to the station offers a better regionalization of the studied events, as can be seen in Figures 11 to 17. There are zones up to 95° of distance in which no events have been either reported by NOAA or detected by SAAS during the periods of study. These zones are (see Figure 11):

a) From 75° to 95° of azimuth

b) From 115° to 140° of azimuth

c) From 170° to 215° of azimuth

d) From 340° to 5° of azimuth

The redistribution of ΔTT against distance for events of each zone of azimuth from Figure 11 shows clear differences in the value of the residuals for events of the same azimuth, and similar residuals for events of the same region, irrespective of their azimuth (i.e. Mid-Atlantic Ridge), indicating a possible influence of the source region in the travel time of P phases. This is contrary to the conclusions of Bolt and Nuttli (1966), who eliminated the influence of the source region on seismic travel times. The source region effect on seismic travel times makes ineffective any attempt to obtain station corrections dependent only on azimuth as was suggested by Herrin and Taggart (1968). It would be more useful to find regional corrections for select seismographic station from explosions

which could be of low charge size (i.e. 10 tons; see Willmore, 1972) or from very refined epicentral locations of natural events. By using such data and a method similar to that suggested by Lilwall and Douglas (1970), uniform travel-time curves and regionalized station corrections could be obtained.

The peculiarities of the travel-time residuals distribution just described, which concern more the present research, are the following:

a) Small residuals (close to zero) associated with the Mid-Atlantic Ridge at any distance or azimuth considered.

b) Positive and small negative residuals observed for the events of Central America, Caribbean Sea and Northern South America. Negative residuals produced by the Mexican events. (See Figure 17).

c) Concentration of residuals with similar values in different areas of the Andes shown in Figure 15.

d) Different value for residuals of events with similar azimuth and different distance, showing that the residuals are related to the source structure or to discontinuities encountered by the seismic waves travelling in different paths.

4.4 Brief Review of Studies on Seismic Amplitudes

The amplitudes of some recorded seismic phases have been used since the 1930s to calculate the magnitude of seismic events, which in turn is used as a measure of the relative energy rating of earthquakes. Originally, the concept of magnitude was due to Richter (1935) when the local magnitude (M_L) was defined. Later, studies were concentrated on surface waves of around 20 seconds period to determine the magnitude (M_S of just M) of shallow teleseisms. For deep events, Gutenberg and Richter (1956), suggested the use of P,PP,S and SS phases with appropriate factors to account for the depth distance function, to calculate the body phases magnitude (m_b). The unified magnitude (m) has been later suggested as an averaging of the various magnitude values.

In this work, only magnitudes m_b (or MB for computer listings) from P phases as defined by Gutenberg and Richter (1956) will be considered:

$$m_b = Q + \log_{10} (A/KT) + s \qquad (12)$$

A = peak to peak amplitude in mm.

T = signal period in seconds.

K = magnification factor in thousands (for T).

Q = depth-distance factor.

s = station correction

Initially, it was recommended that the maximum values of amplitude and period should be read in the first few cycles after the P onset. Now it appears that better results are obtained by choosing the maximum amplitude in the first 20 or 25 sec of the seismic signal (Bune et al, 1970).

At present the most common source of information regarding seismic parameters are the NOAA and ISC bulletins. Both institutions use the Gutenberg and Richter (1956) formula and Q values to calculate body wave magnitudes. Bune et al (1970), by comparing NOAA reports with USSR determinations of magnitude, showed that NOAA m_b values were significantly lower than the corresponding USSR determinations. This was explained by Bune et al (1970) as due to the strong influence of the USA array stations TFO, WMO, UBO and BMO which were found to report comparatively low values of m_b parameters. Later, Jordan and Hunter (1972), by comparing USSR and NOAA data in two different ways, concluded that there appears to be little difference between NOAA m_b values and the USSR surface wave magnitudes on a worldwide basis; they also found selected seismic regions with significant differences and that both institutions surface wave magnitudes give similar results for shallow events. NOAA m_b values cover the range from just under 4.0 to over 6.0, while its M_s determinations are usually on events over magnitude 5. For these reasons, and because ISC bulletins do not cover the period of the data used in this research, the values of m_b reported by NOAA are taken as reference.

Study of the Gnome explosion data (Romney et al, 1962) showed that Pn amplitudes were dependent upon the path of propagation and associated directly with the time residuals (earlier arrivals produce larger amplitudes), suggesting a systematic relationship to crustal thickness.

Velocity-depth curves in the upper mantle were determined by Asbel et al (1966) by a joint interpretation of travel-time and

amplitude residuals of P waves. Julian and Anderson (1968) presented some models of the Earth's structure obtained by considering the variations in travel times, apparent velocities and amplitudes of P phases, at different distances, as the result of anomalies of the velocity distribution in the mantle.

Amplitude ratios between seismographic stations can be used to determine anomalies in the upper mantle. By studying data at five USA array stations, McGinley and Anderson (1969) found areas with high attenuation of P waves, indicating a low Q upper mantle or a very high Poisson's ratio or both, under these areas.

By studying the amplitude and period of P phases recorded on long period seismographs from signals of some nuclear explosions, Nuttli (1972) found Q values that yield, in some cases differences of up to 0.4 units of magnitude compared with Gutenberg-Richter (1956) values. By comparing the short and long period body-wave magnitude for the 1966 Novaya Zemlya explosion, Nuttli (1972) concluded that the anelastic attenuation of P waves is greater in the upper than in the lower mantle, and that for waves with periods of 1 sec or greater, the effect of anelastic attenuation on the amplitudes is less than the effect of geometric spreading. From his study he also suspects the existence of a second-order discontinuity at a depth of about 2300 Km.

An attempt to improve the Gutenberg and Richter (1956) amplitude distance curve was made by Carpenter et al (1967) by using the amplitudes of explosion signals detected by up to 65 stations in the range 30° to 102° of epicentral distance. They suggest a sharp maximum at $\Delta = 35^{\circ}$, a minimum followed by a sharp increase at $\Delta = 75^{\circ}$ and a sharp minimum at $\Delta = 93^{\circ}$.

Gupta and Rastogi (1972) studied the relationship between M_S and m_b for events detected at the Hyderabad observatory and found some indication of complexity for events of a given ratio between the two observed magnitudes. Complex events were considered by these authors, when there were clear later phases after the P onset observed on short period seismograms. Simple events have quite small energies in surface waves and long period body-waves. They suggested the multiplicity of the earthquake source as the major factor responsible for the scatter in the relationship between m_b and M_S.

Complex longitudinal signals from seismic events, including explosions have been observed to present smaller values of magnitude (m_b) (Key, 1968). Complexity has been attributed to the effect of regions with low Q values crossed by direct P or pP phases, while the clear later arrivals that form the complex signal have crossed regions with high Q and hence with little attenuation (Douglas et al 1971, 1973).

4.5 Magnitude Values Observed at SAAS

4.5.1 Data

The body waves magnitude (m_b) of 200 events recorded at SAAS, at epicentral distances of up to 92°, were calculated by using the Gutenberg and Richter (1956) equation (see 4.4) and their Q values. NOAA epicentral parameters were used to find the corresponding value of Q. Playouts from the tapes were obtained using maximum paper speed (1000 mm/sec) to obtain a high degree of precision for amplitude and period readings. The reported and computed m_b values for these events are listed in Appendix 1.

To make a comparative analysis between SAAS and NOAA m_b values, the difference of both magnitudes were calculated and are called "magnitude residuals" (Δm):

$$\Delta m = (SAAS)m_b - (NOAA)m_b \qquad (13)$$

These residuals are shown in Figure 18 together with the events, reported by NOAA, with $m_b \geq 4$ and distances of up to 95° from SAAS, that have signals which are too small to allow reliable measurements of amplitude and periods, or which have not been found in the SAAS playouts.

4.5.2 Regions with Low Detection Capability at SAAS

There are some regions from which SAAS has low detection capability. The events from these regions are recorded at SAAS with smaller amplitude than expected producing, therefore, a Δm with negative value or, in some cases, with amplitudes smaller than the noise level that these events cannot be detected by the visual method of analysis used in this study. These regions are:

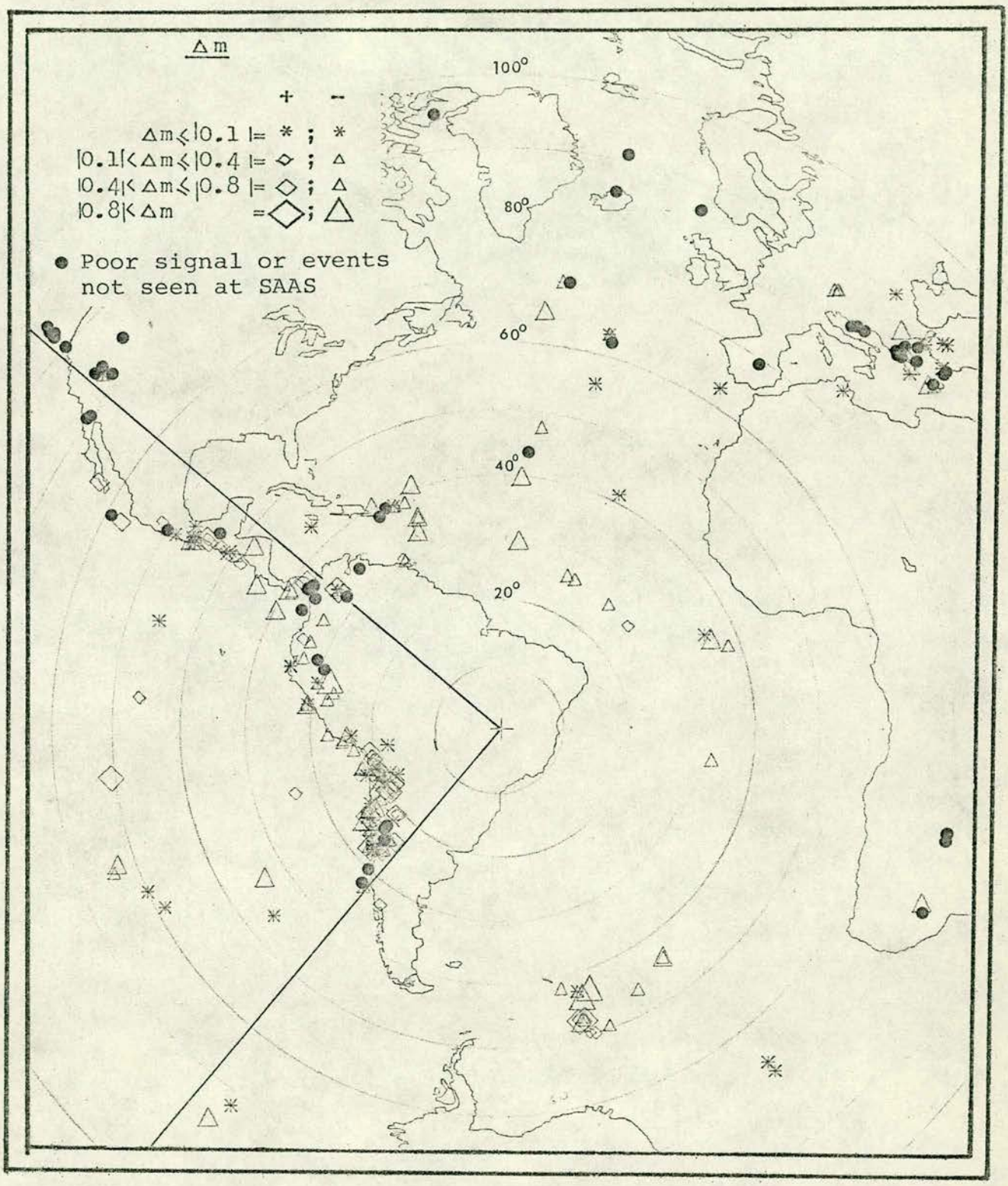

Figure 18.- AZIMUTHAL DISTRIBUTION OF Δm CENTRED AT SAAS SHOWING THE EVENTS NOT DETECTED OR DETECTED BUT GIBING A POOR SIGNAL ON SAAS RECORDS

- Western Side of USA ($\Delta > 80$), only 3 events ($m_b > 4.9$, Nevada explosions) out of 14 reported by NOAA ($m_b > 4.0$) were detected.
- Northern Region of the Atlantic Ocean, no events reported by NOAA with $m_b < 4.8$ and $\Delta > 60^o$ were seen on SAAS records.
- Eastern Mediterranean Sea, most events (m_b between 4.1 and 4.9) from the Adriatic Sea, Greece and Dodecanese Islands (see Figure 19) were not seen on SAAS records but other events of $m_b > 4.5$ in either side of the area mentioned above, were detected, although with smaller amplitude than expected. LASA and NORSAR recorded some of these events with also smaller amplitudes than expected (LASA and NORSAR m_b were in most cases 0.2 and 0.5 units lower than NOAA m_b, respectively).
- Southern Region of Africa, only events with $m_b > 4.7$ were recorded at SAAS with clear signal (smaller than expected) to allow reliable measurement of amplitude and period.
- Northwestern South America, Panama and Caribbean Sea, (see Figure 20) several events in this region with m_b between 4.3 and 4.9 reported by NOAA, were not seen on SAAS records and most of the detected events have smaller amplitude than expected, except for some deep events ($h \approx 170$km) in the Santander Province of Colombia and one deep event ($h = 140$km) in the coast of Venezuela.
- San Juan Province, Argentina, (see Figure 21) three events reported by NOAA with m_b between 3.9 and 4.1 ($h > 60$km) were

Figure 19.- DISTRIBUTION OF Δm IN EASTERN EUROPE-MIDDLE EAST

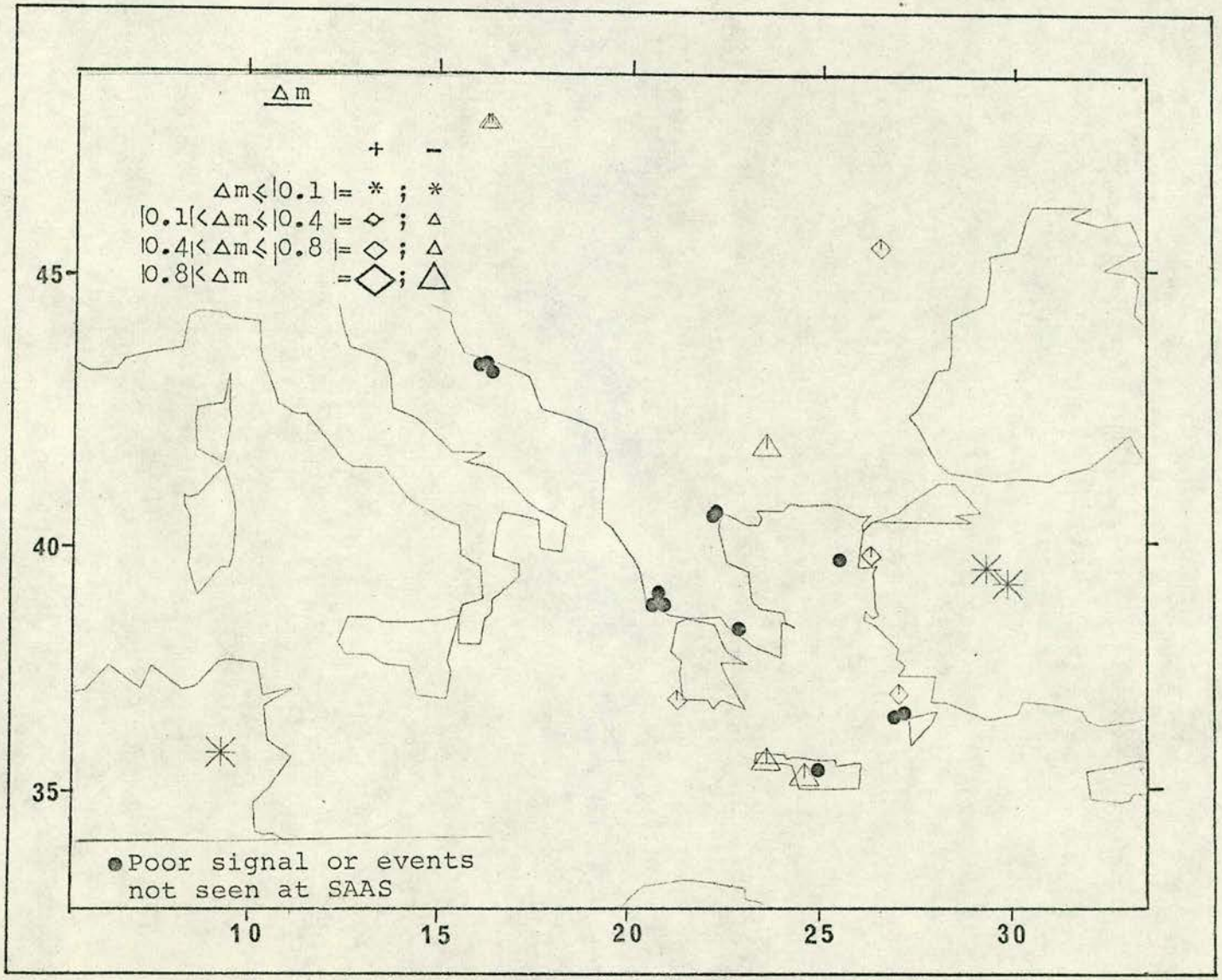

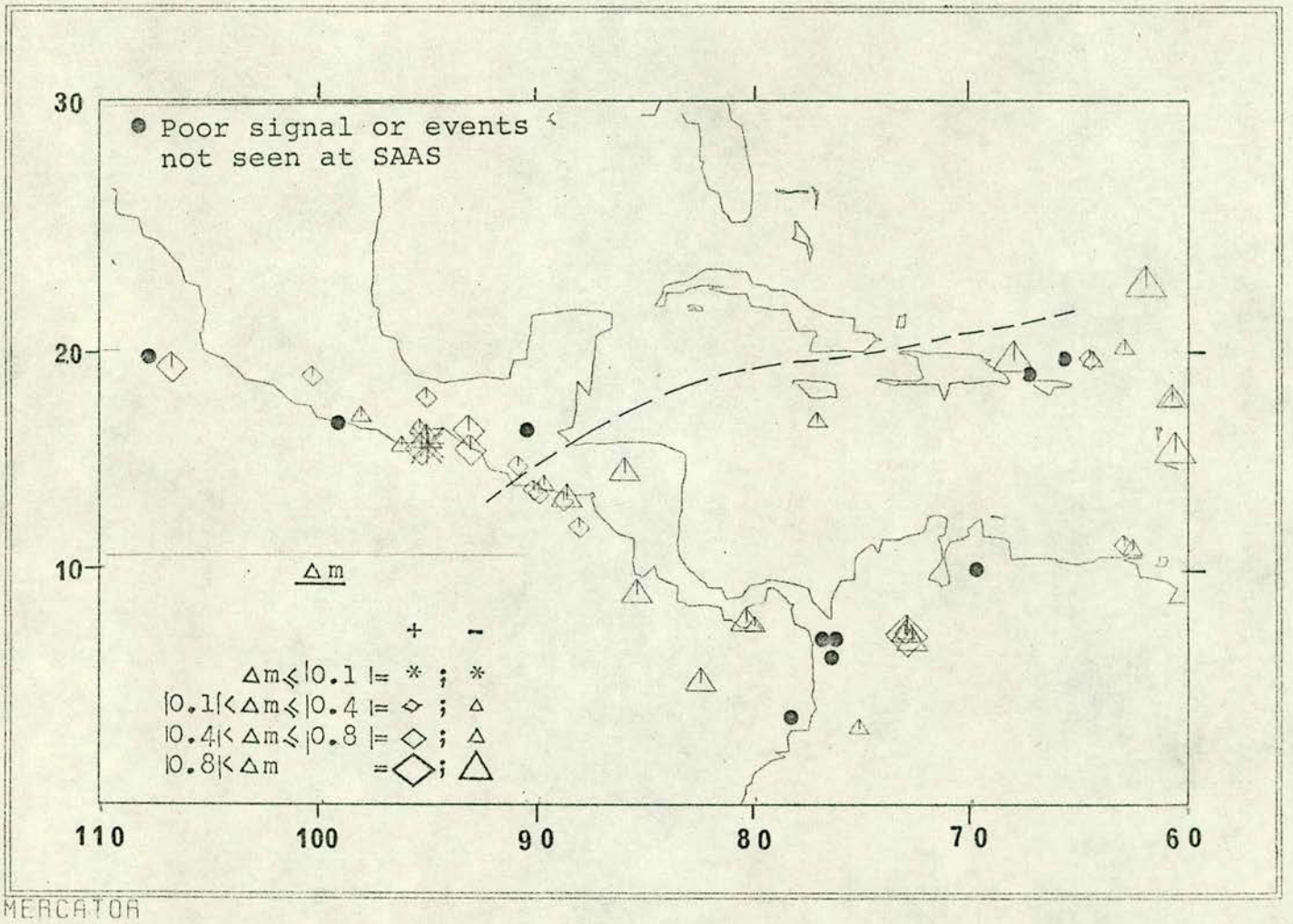

Figure 20.- DISTRIBUTION OF Δm IN NORTHERN LATIN AMERICA

recorded by SAAS with poor signals not allowing magnitude determination. The other events in this area (h > 100km) were recorded by SAAS with smaller amplitude than expected.

- Central Coast of Chile (below 35°S latitude), two events reported by NOAA with m_b 4.1 and 4.2, were recorded at SAAS with poor signals (see Figure 21).

Most of the other regions, within 95° of distance from SAAS, had events which were recorded at SAAS with smaller amplitude than expected, therefore producing Δm with negative values. These regions are: central and southern Mid-Atlantic Ridge, South Sandwich Islands Region (two Δm with a positive value shown for this region in Figure 18 are for events with m_b not reported by NOAA but calculated with SAAS data), southern part of Eastern Pacific Ocean, Peru, and western Chile between 25° and 28° South latitude.

4.5.3 Regions with Δm having Positive Values Observed at SAAS

The regions from which SAAS has recorded events with mainly larger amplitudes than expected, are the following:

- Western regions of Mexico, Guatemala, El Salvador and Nicaragua.
  See Figure 20.
- Santander Province, Colombia, Δm with relatively positive values, with reference to the regional large negative magnitude residuals.
  See Figure 20.
- Eastern Pacific Ocean facing Peru. See Figure 18.

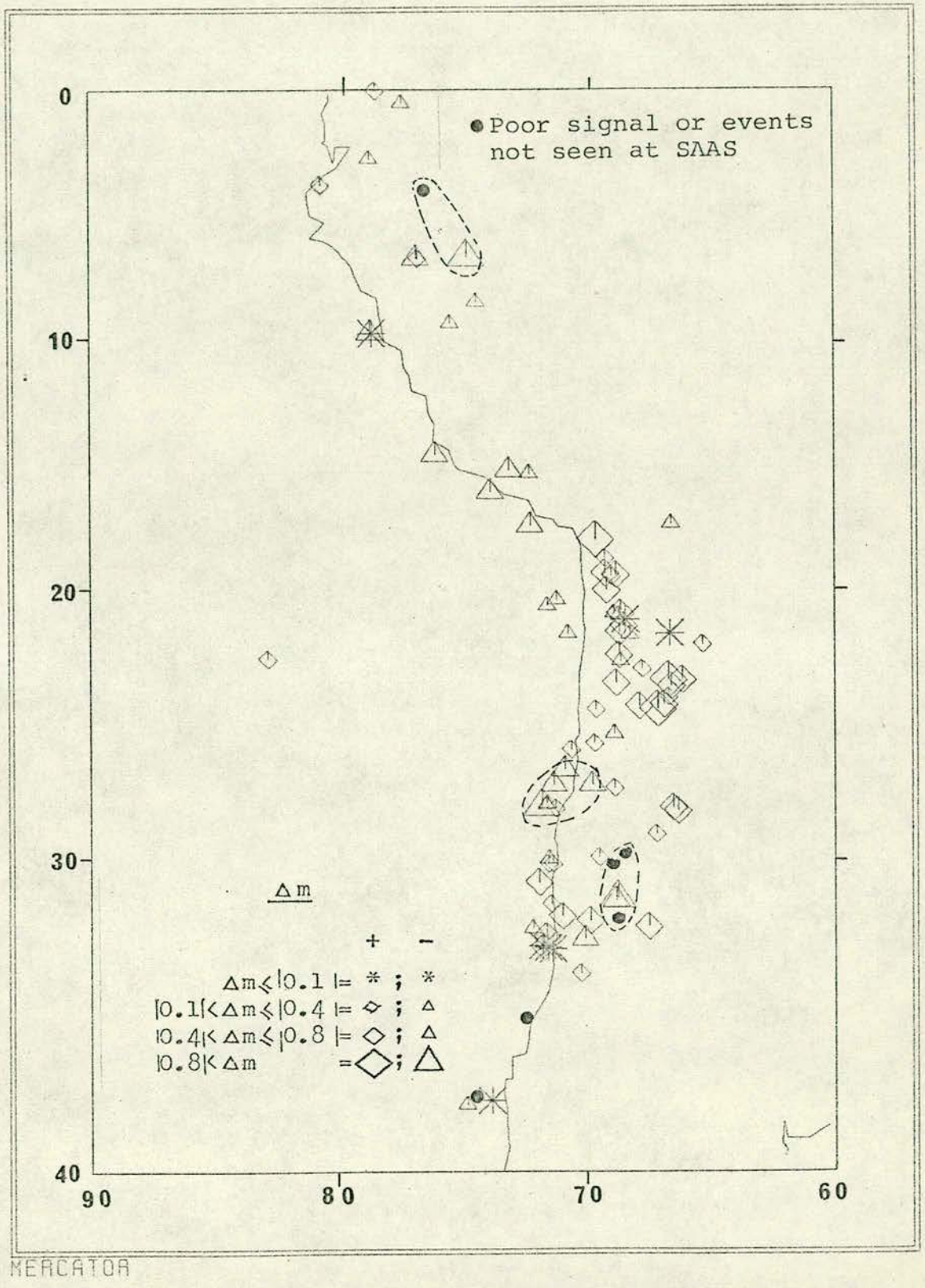

Figure 21.- DISTRIBUTION OF Δm IN WESTERN SOUTH AMERICA

- Andean Region between 17° and 25° South latitude. See Figure 21.
- Western Chile between 29° and 34° South latitude. See Figure 21.
- Catamarca and Mendoza Provinces, Argentina. See Figure 21.

4.5.4 Discussion

The distribution of Δm values observed at SAAS on Figures 18, 19, 20 and 21, shows some peculiarities which can be summarized as follows:

- In the range up to $\Delta = 95^{\circ}$, SAAS records more events with smaller amplitudes than expected, resulting in a greater number of Δm with negative values (see also Figure 22).
- No events reported by NOAA $m_b \leq 5.0^{\circ}$ have been detected in SAAS records in the range 90° to 95°, excepting some events in the East Europe and Middle East region that are in this range of distance. This poor detection rate agrees with the sharp minimum value of amplitudes at this sort of distance found by Carpenter et al (1967).
- Most events reported by NOAA $m_b \leq 4.9$ in the range between 80° and 90°, were not detected on SAAS records or were detected mostly with smaller amplitudes than expected.
- All events, reported by NOAA, which occurred in the central and southern Pacific Ocean and in the central and southern Atlantic Ocean were recorded by SAAS; more events with Δm having positive values were observed from the Pacific Ocean than from the Atlantic Ocean.
- There are four regions from which the events recorded by SAAS produced Δm with mainly positive values; these

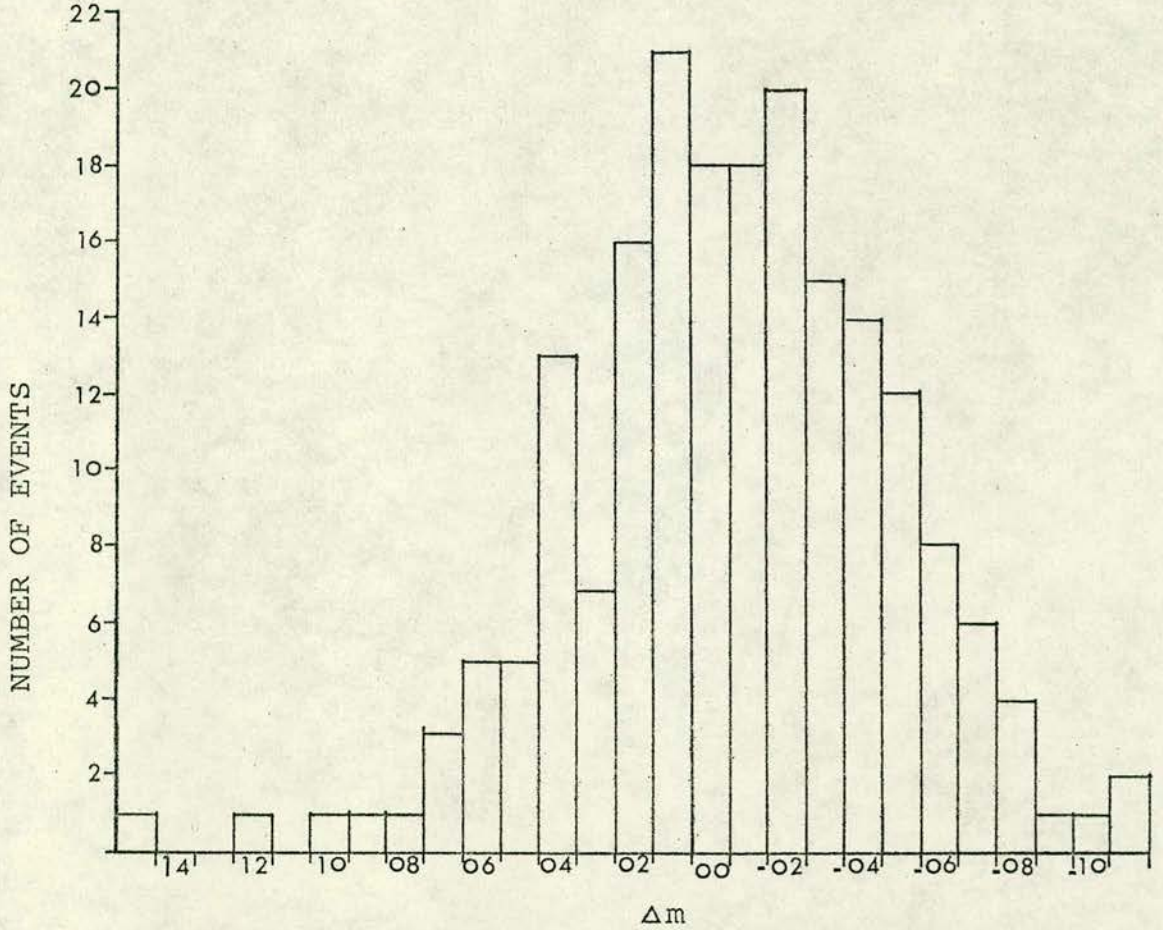

Figure 22.- HISTOGRAM OF THE FREQUENCY OF OCCURRENCE OF Δm

regions are:

the Western side of Mexico and part of Central America, Santander Province in Colombia (relatively positive only), Eastern Pacific Ocean in front of Peru and some parts of the Andes below latitude 17°S.

- Many events which occurred in the region North of South America between 30° and 40° of epicentral distance were not detected (or poorly detected) on SAAS records. The other events of this region have Δm with large negative values (except the deep events, like the ones occurred in Santander Province in Colombia).
- Events occurred in Southern Africa and in the San Juan Province of Argentina were also poorly recorded at SAAS.

The general tendency of SAAS to record smaller amplitudes than expected from the magnitude-distance relation could suggest an area with low Q under the station. There appears to be a correlation between ΔTT and Δm values observed at SAAS (compare Figures 11 and 18). Areas with events which have Δm with mainly positive values (larger amplitude) have ΔTT with mainly negative values (early arrivals) and vice versa, as found by Romney et al (1962).

Some small areas with events that have Δm with different values from the events of the same region (e.g. Santander in Colombia and San Juan in Argentina) may indicate a source radiation pattern effect with respect to SAAS. In general, deeper events have Δm with positive values and ΔTT with negative values (except for the events in the Peru-Brazil border, the area of San Juan in

Argentina and Santander Province in Colombia). See Figure 23.

It appears also that the events with Δm having a positive value have relatively simple large signals and the ones with a negative value have complex signals (see Figure 24) as was pointed out by Gupta and Rastogi (1972) and Douglas et al (1971, 1973).

It is evident that by analysing the distribution ΔTT and Δm observed at SAAS, it is possible to define some areas with very distinct characteristics inducing peculiarities in the structure under these areas or in the path that the seismic waves followed before reaching the station. The importance of these areas in the interpretation of some features of South American tectonics is discussed in Chapter 6 where the azimuth and apparent velocity residuals observed at SAAS are also interpreted.

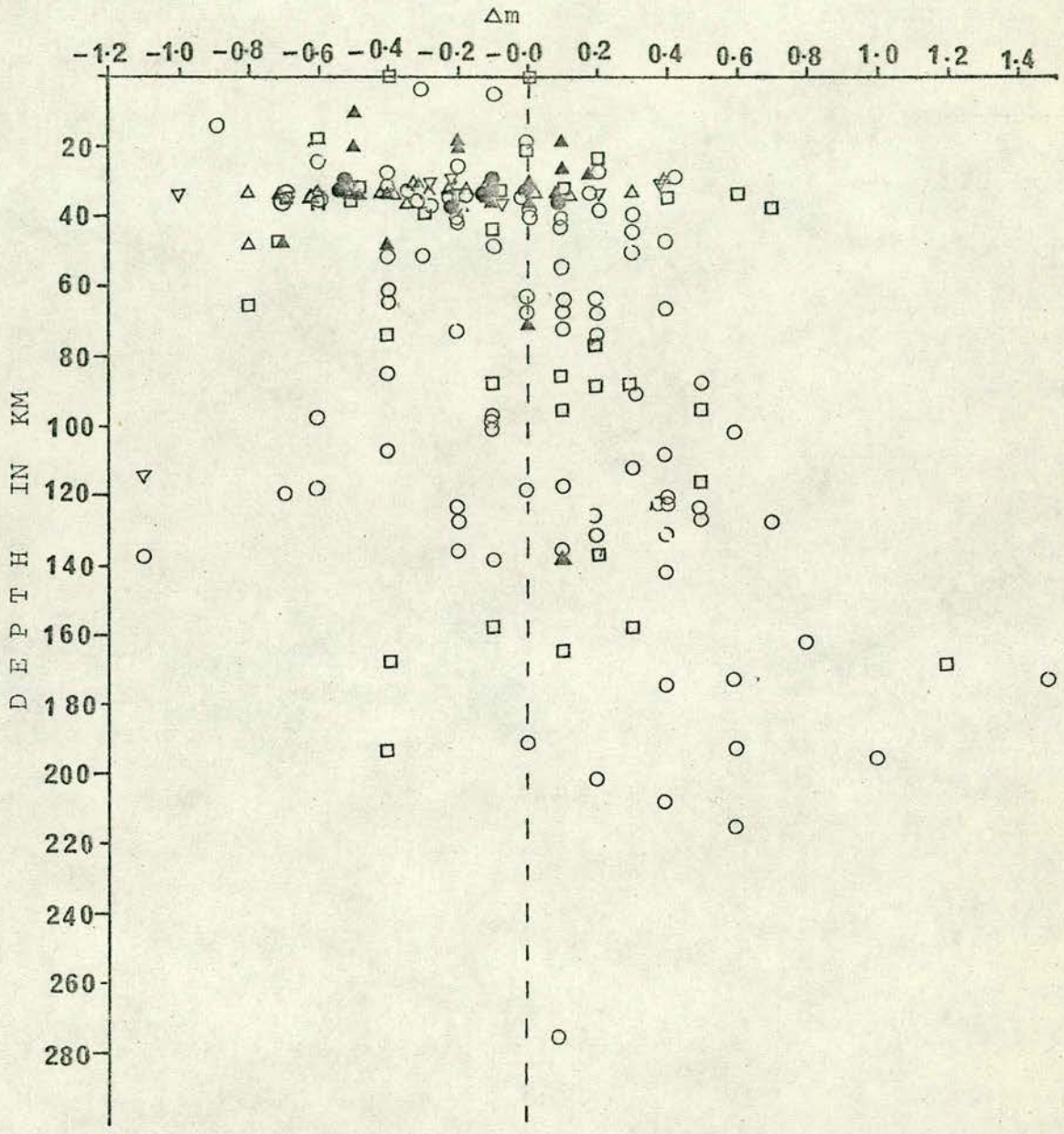

▲East Europe and Middle East (including African events)
△Atlantic Ocean and Mid Atlantic Ridge
▽South Sandwich Island Region
●East Pacific Ocean
○Western South America
□Northern Latin America

Figure 23.- DISTRIBUTION OF Δm WITH DEPTH

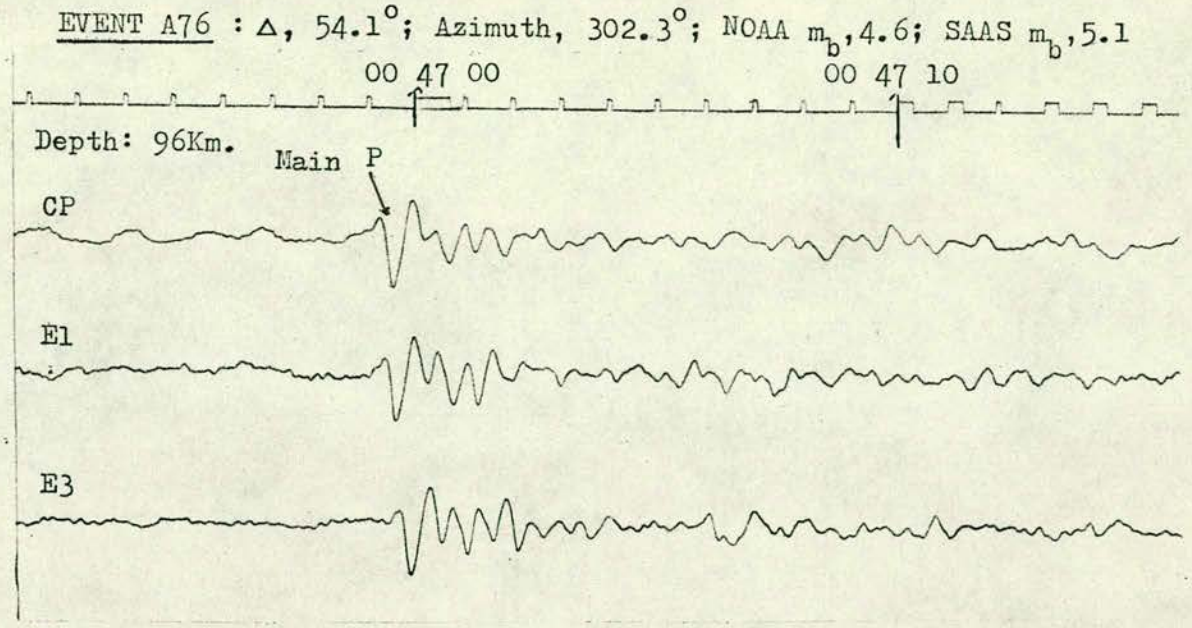

SIMPLE SIGNAL EVENT RECORDED AT SAAS

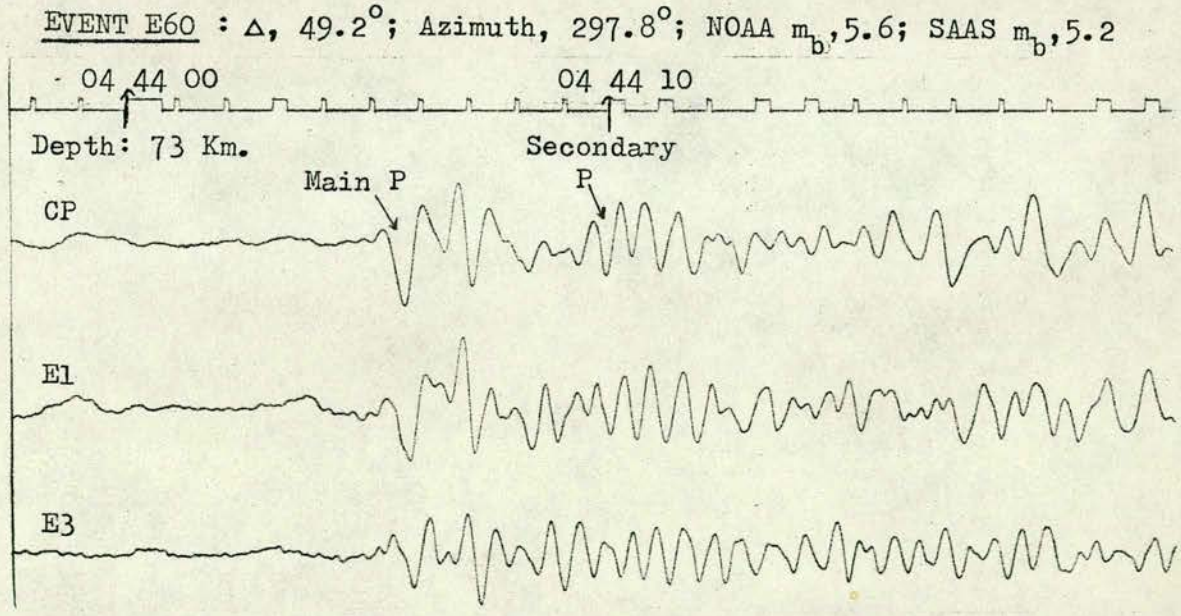

COMPLEX SIGNAL EVENT RECORDED AT SAAS

Figure 24.- SEISMOGRAMS SHOWING A SIMPLE AND A COMPLEX EVENTS RECORDED AT SAAS

CHAPTER 5

AZIMUTH AND APPARENT VELOCITY FROM SAAS DATA

5.1 Introduction

The ability of arrays to determine the azimuth and apparent velocity of seismic waves, is a most useful tool in studying the Earth's interior and also in the locations of epicentres from a single station. To do this, two assumptions regarding the geometry of the array are usually made:

a) For each seismic wave the azimuth and apparent velocity ($dT/d\Delta$) remain constant across the array.

b) The area occupied by the array is a plane surface, disregarding any effect of the Earth's curvature.

These conditions are more likely to be fulfilled in arrays with their apertures not exceeding 0.5° and with all their points being within 200 metres in altitude. Larger aperture arrays or larger departures in altitude between points of an array will produce noticeable effects in the calculation of azimuth and apparent velocity if only the assumptions mentioned above are taken into consideration.

Structural conditions under the array could cause large departures in the observed values of azimuth and apparent velocity. Otzuka (1966) made use of these departures (azimuth departures up to 10° and $dT/d\Delta$ departures up to 1 sec/degree) observed at the University of California array in the Coast Ranges of central California to study the structure of the upper mantle under this array. Niazi (1966) used azimuth deviations of more than 20°,

observed at TFSO array to infer a dipping of the Mohorovicic discontinuity under TFSO. Chinnery and Toksoz (1967) tried to compensate for the effects of the structure under LASA to study the $dT/d\Delta$ of some natural events by comparing a derived travel time curve with data from the Longshot nuclear explosion. Cleary et al (1968) tried to correlate the deviations of azimuth and $dT/d\Delta$ observed at WRA (Warramunga array) with the structure under the array by using Niazi's (1966) equations. Later in this chapter a method is presented to assess the structure under SAAS and obtain time corrections for SAAS points by using seismic waves arriving almost perpendicular to the surface (from $\Delta > 160^{\circ}$).

To calculate the azimuth and the apparent velocity (or $dT/d\Delta$) from array data one uses the relative time delays at each point of the array and their relative positions with respect to a reference point. There are two ways of obtaining the solutions:

a) By successive approximations or beamforming; different sets of delays are inferred which correspond to preset values of azimuth and/or apparent velocity. The delayed signals are then summed, correlograms may be formed, and the amplitude of the signal output gives an indication of the best solution.

b) By least squares fitting of the true delays observed at each point of the array.

Other methods of finding azimuth and apparent velocity from array data are mostly concerned with obtaining quick visual solutions for preliminary analysis of events. Nomograms and tables

which coincide with graphical observations of the relative arrival times can be used, but they give approximate solutions only.

The beamforming method is used in on-line array routines for epicentral locations. It has some computing advantages over the least squares method and can be fully automated to analyse all phases of an event detected by arrays. On the other hand, the least squares method gives more accurate solutions and allows one to separate, for each point of the array, the time errors caused by the local structure underlying the array from the time error caused by discontinuities encountered by the seismic waves in their journey from the source to the station. This in turn permits the insertion of proper individual site corrections. For these reasons, the least squares method is used in this research.

Some versions of these methods developed at the Global Seismology Unit of IGS in Edinburgh are briefly described in this chapter. The equipment to execute these array processing techniques is also described.

More than 120 events recorded by SAAS have been processed for this research, belonging to two different periods of the operation of SAAS. Details of the data used and of the results which have been obtained are included at the end of this chapter.

5.2 Digital Processing Facilities at Edinburgh

The seismic recording systems attached to IGS, including SAAS, use multichannel magnetic tape to record the seismic data as frequency modulated carrier waveforms. To process this data, the Geophysical Laboratories of IGS in Edinburgh are equipped with complete analogue playback facilities and have an extensive on-line digital processing system installed at the Edinburgh Regional Computing Centre (ERCC). A description of this equipment is given by Houliston (1973); a brief description of the digital processing system only is given here.

The digital processing system at ERCC comprises a Racal-Thermionic T8100 analogue replay unit, provided with 24 analogue frequency filters and a 16 channels ink jet-pen recorder, which are linked to a PDP15 digital computer through a programming board.

The analogue tapes are replayed at 8 or 16 times the recording speed (15/128 inches/second) in the analogue replay unit; the analogue outputs are connected to the programming board which enables the outputs to be connected to the jet-pens, the analogue filters, or to the multiplexer and analogue to digital converter of the PDP15 computer as required (see Figure 25). Normally the analogue signals are filtered before they reach the computer.

The maximum word length of the converter is 12 bits for 10 volts input. The fastest sampling rate at this word length is 29,000 samples/second. The core storage of the computer can store up to 24,000 (18 bit) words of information.

The data processed by the computer can be written on to a digital tape, written on a disc, punched on paper tape, printed

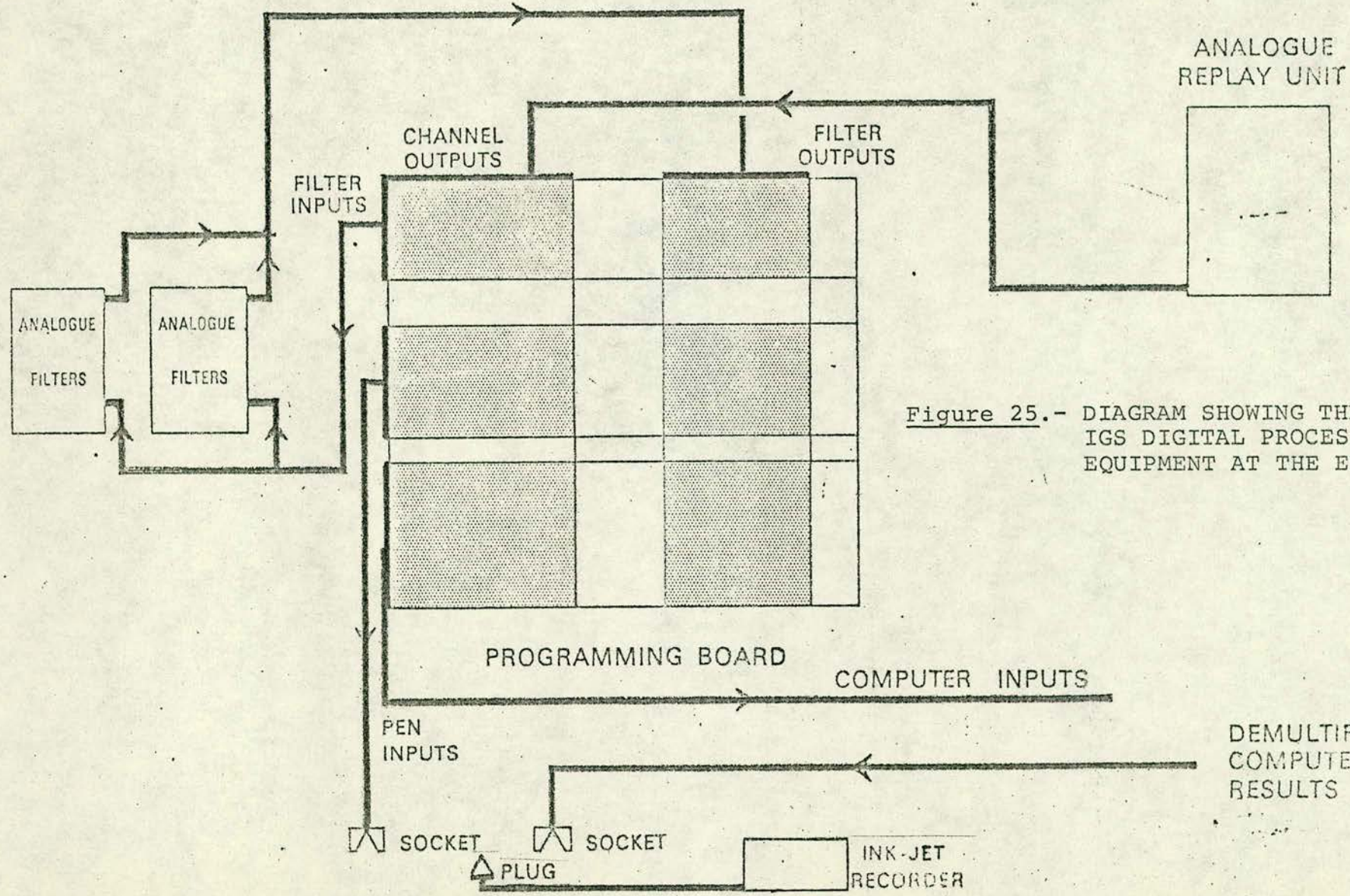

Figure 25.- DIAGRAM SHOWING THE IGS DIGITAL PROCESSING EQUIPMENT AT THE ERCC

by teletype, or converted to analogue form to be displayed directly on the jet-pen recorder. The digital tape deck is IBM compatible, enabling the digitized data to be processed on the IBM 370 or ICL 4/75 of the ERCC. The demultiplexer converts up to sixteen digital outputs to analogue form to be displayed on the jet-pen recorder. See Figure 26 for an example of demultiplexed records.

An improved system of sampling command has been developed (Houliston, 1973) which derives the sampling rate (100,50 or 25 samples/sec) from the carrier frequency of the flutter compensation channel of the analogue data and may also, if desired, compensate for drop-outs on the analogue tape.

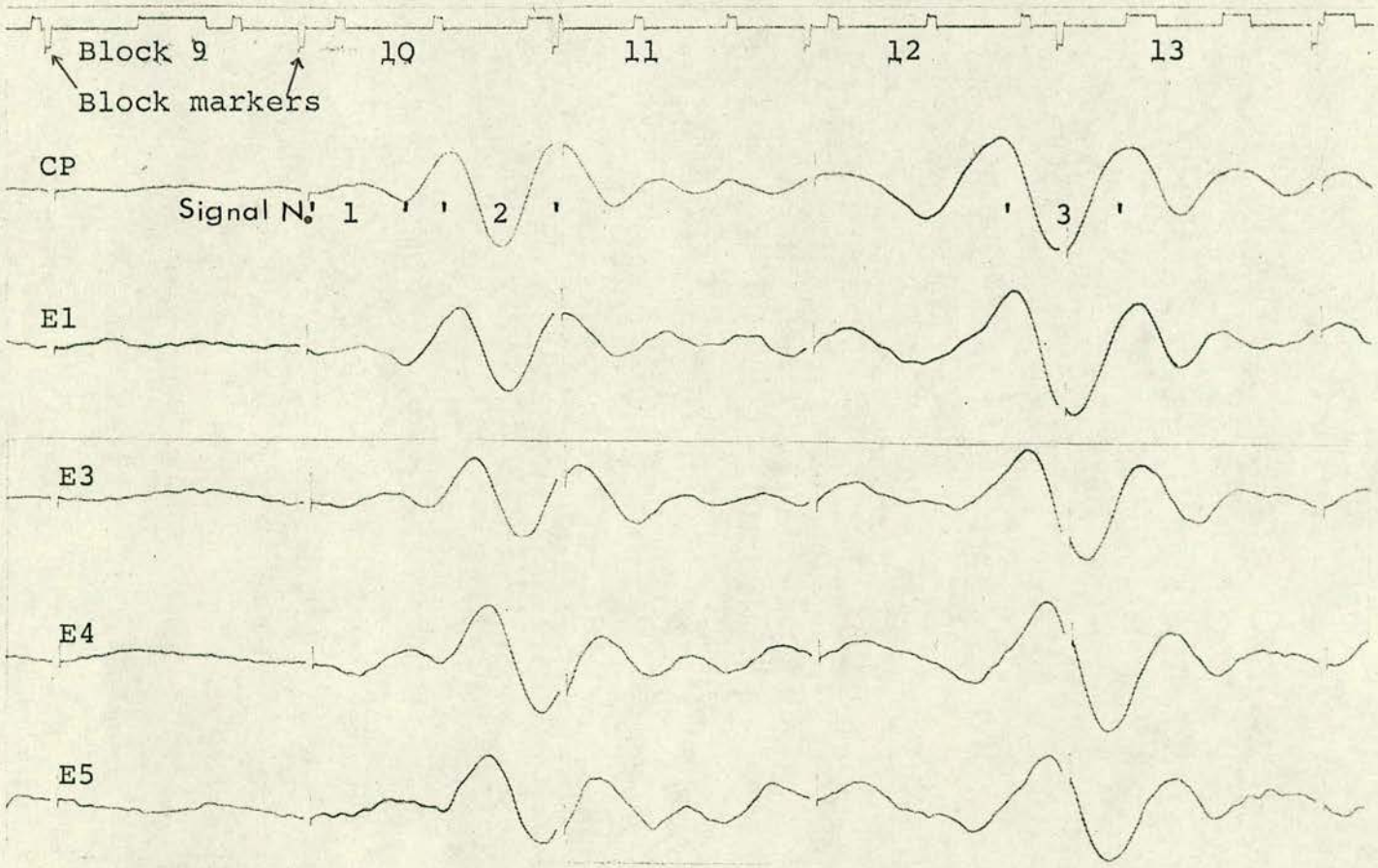

Figure 26.- SEISMOGRAM SHOWING A VISUAL PLAY-OUT OF A TYPICAL SIGNAL WHICW WAS DIGITIZED AND THEN RETURNED TO ANALOGUE FORM

5.3 Array Processing Techniques Available at Edinburgh

5.3.1 Beamforming Techniques

There are two beamforming techniques available at the Global Seismology Unit of IGS in Edinburgh. Both techniques use the same principle of summing the signals of the points of a seismic array with varying lags (calculated from preset azimuths and apparent velocities), until the optimum solution is found which corresponds to the best estimate of azimuth and apparent velocity observed at the array.

The differences between these techniques are in the ways of inputing and processing the data, and obtaining the solutions. One of the techniques uses the program AZANDT (Lilwall, 1973). This program and the digitized data are run in a relatively large computer (i.e. an IBM 370), and only a small chosen portion of the signal is processed at a time.[1] The sums for different preset conditions (lags corresponding to different azimuths and apparent velocities) are displayed in the form of a matrix with the maximum value normalised to 1 which indicates the optimum values of observed azimuth and apparent velocity. This process can be repeated by reducing the gaps between the preset azimuths and apparent velocities, around the optimum values found in the preceding run, until resolution is no longer improved. Further details of this program are given in Appendix 2-A, where an example of a typical matrix output is also presented.

The other beamforming technique available at Edinburgh uses a program written for a PDP15 computer (Fyfe, 1973) which operates

---

(1) See Figure 26

by using the digital processing equipment set up at the ERCC, directly on analogue tapes recorded at the stations. There is no limit to the portion of signal which can be processed by this method, the preset azimuths and apparent velocities can be changed with more flexibility than in the AZANDT program, and appropriate frequency band pass filters can be changed as required. The program can operate in two modes:

- Normal beamforming: all channels are summed together and the resulting signal is displayed on the ink jet-pen recorder. Up to 15 different combinations of azimuths and apparent velocities can be processed each time. See Figure 27.
- Cross multiplication: the network is split into two arms which are summed separately and the results multiplied together; a running sum over a specified window is computed on the cross multiplication and the output is displayed as a correlogram on the ink jet-pen recorder, together with the multiplication result and the sums of the arm of the array. Only 3 combinations of azimuths and apparent velocities can be processed each time. See Figure 28.

5.3.2 Least Squares Technique

This method of calculating azimuth and apparent velocity from array data uses the relative onset times of arrivals recorded at the points of an array. These relative arrival times or delays can be obtained from analogue magnetic tape records in two ways:

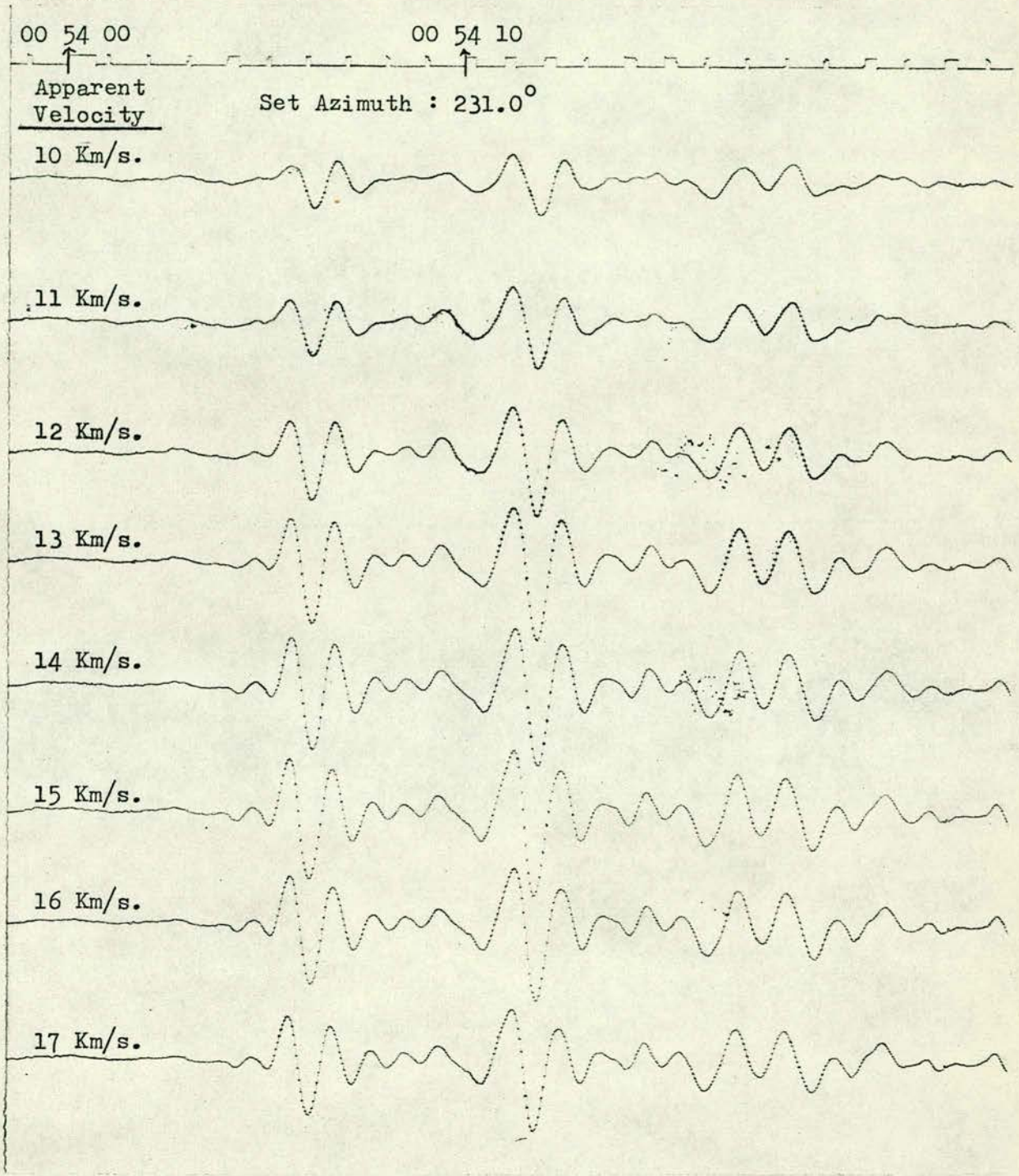

Figure 27.- OUTPUT OF A NORMAL BEAMFORMING TECHNIQUE, SHOWING THE RESULTS OF SEVERAL COMBINATIONS OF AZIMUTH AND APPARENT VELOCITY

EVENT E 1 : Set Azimuth, 231°; Set App. Vel., 15.0 Km/s.

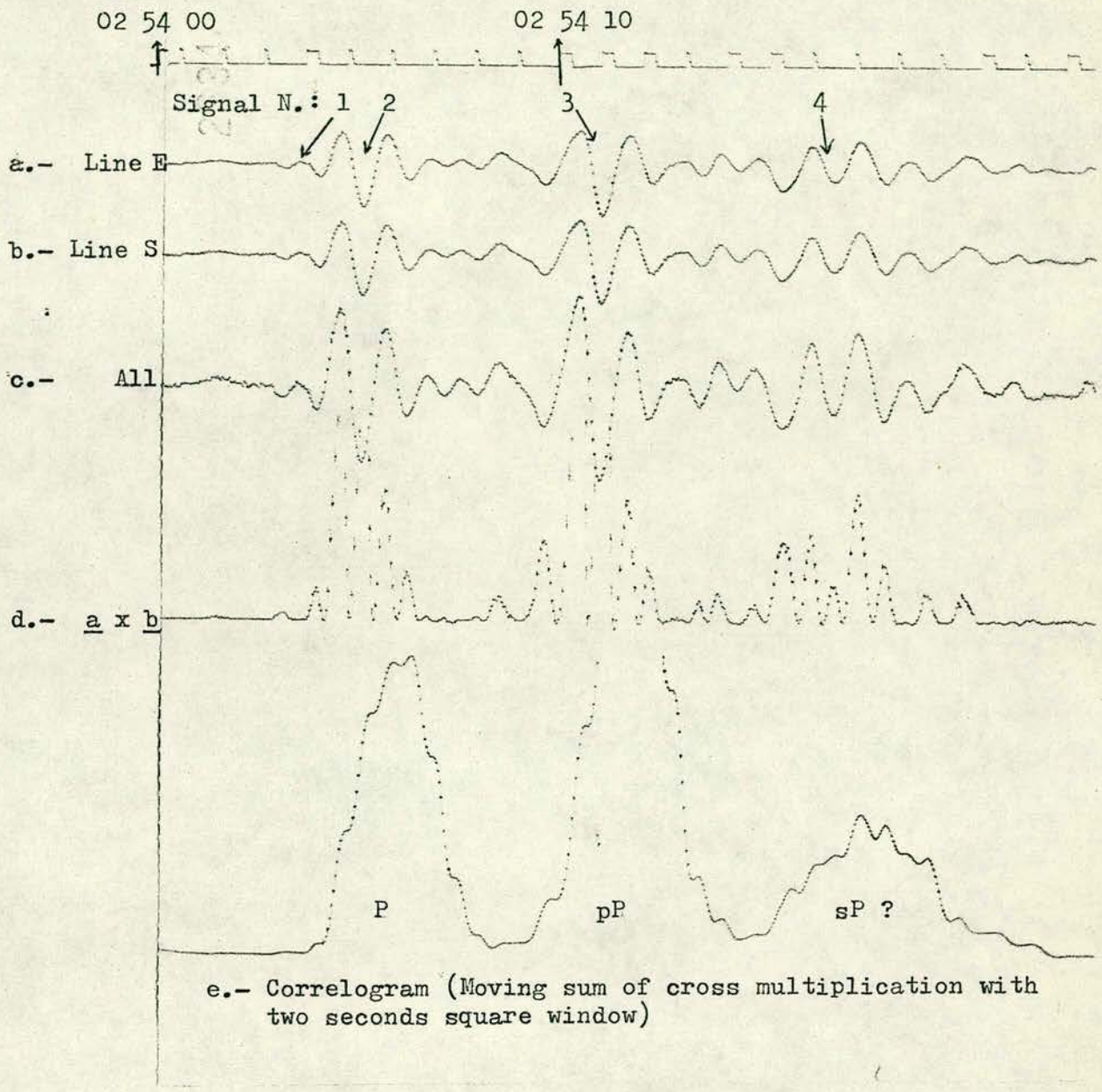

Figure 28 (a).- CORRELOGRAMS OF A CLEAR AND A POOR SIGNAL EVENTS: CLEAR SIGNAL EVENT

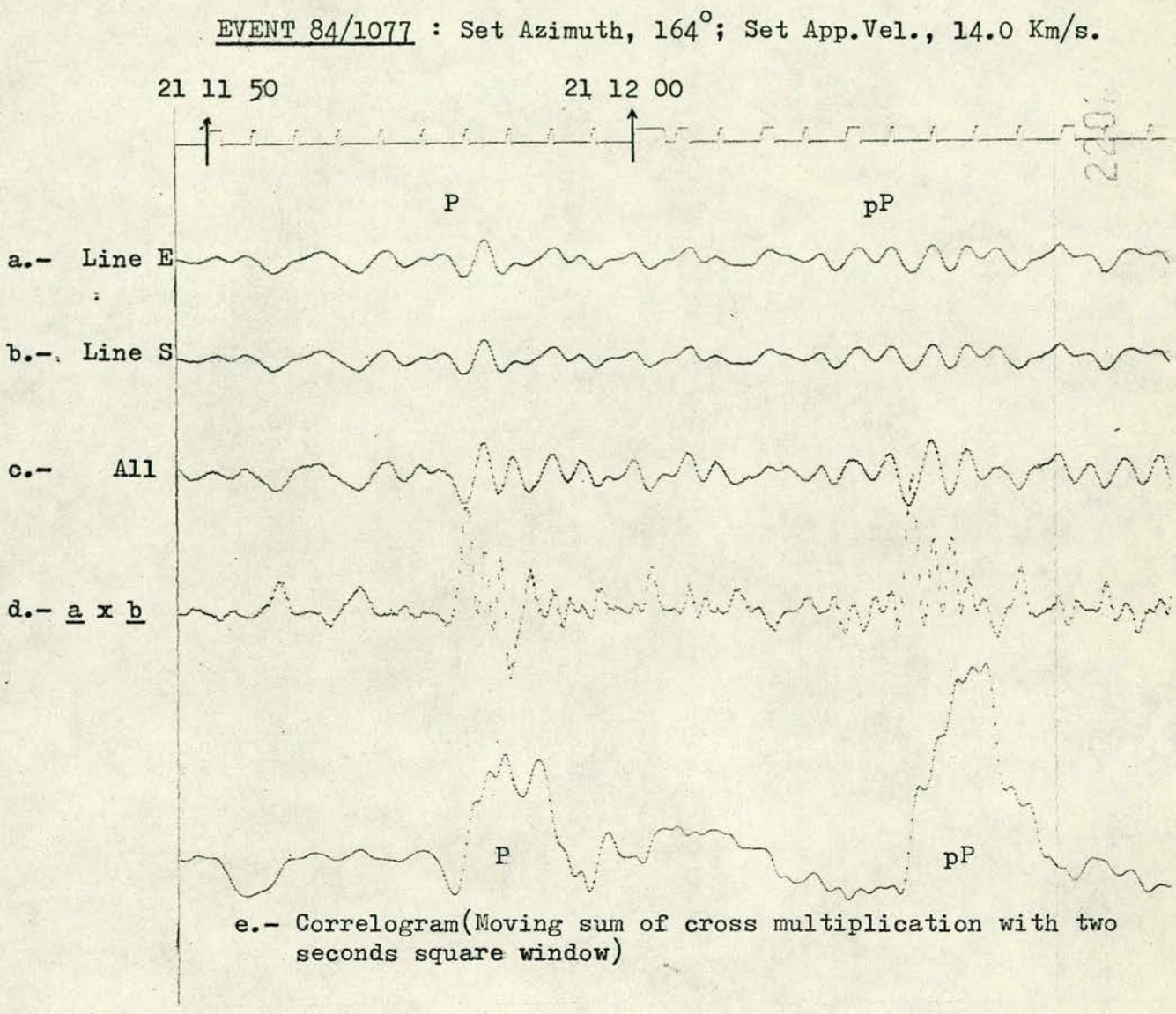

Figure 28 (b).- CORRELOGRAMS OF A CLEAR AND A POOR SIGNAL EVENTS: POOR SIGNAL EVENT

- Manually, from paper playouts. The readings can be done by using scaled magnifiers or by using a semi automatic digitizer (i.e. D'Mac digitizer).
- Automatically, from digitized data by using digital computers.

In the manual method of analysis conspicuous points of the signal being processed (peaks or valleys), are normally chosen to find the relative arrival times, which should be easily identified in all channels. A component is chosen (normally CP in the case of SAAS records), to which the time readings of the other array components are referred. Sometimes, portions of the signal are manually matched, between a reference trace and the traces recorded by the other components of the array, in order to find the relative time arrivals (Cleary et al, 1968). Reading accuracy in the manual method can be up to 1/100 sec. The disadvantages of the manual method of analysis are the existence of several sources of error (alignment of pens on paper record, misreadings, false identification of signals) and the time and effort implied in the whole analysis and manipulation of the data.

The automatic method of obtaining the relative arrival times at each point of an array available at Edinburgh, which has been used in the present research, is based in the program called DELAYS (Lilwall, 1973). This program correlates, by pairs, a small portion of the signal between a master trace and the trace of each other point of the array (see Figure 26). The DELAYS program uses digitized seismic signal as input data and produces the required delays in seconds. This program is explained in more detail in

Appendix 2-B where an example of an output listing is shown.

The observed azimuth and apparent velocity are calculated in this research by using the program AVTS. Figure 29 illustrates the geometrical representation of the fundamental equation which is solved by the least squares method (see Berrocal, 1968). This program uses as input data the delays obtained from the DELAYS program and the output includes the observed azimuth and apparent velocity, and for each point of the array: the expected arrival time (calculated from the expected azimuth and apparent velocity), the relative travel time residuals and the residual for the best fitting of the least squares solution. A further explanation of this program and its listing is given in Appendix 2-C, together with some examples of input data and output printouts.

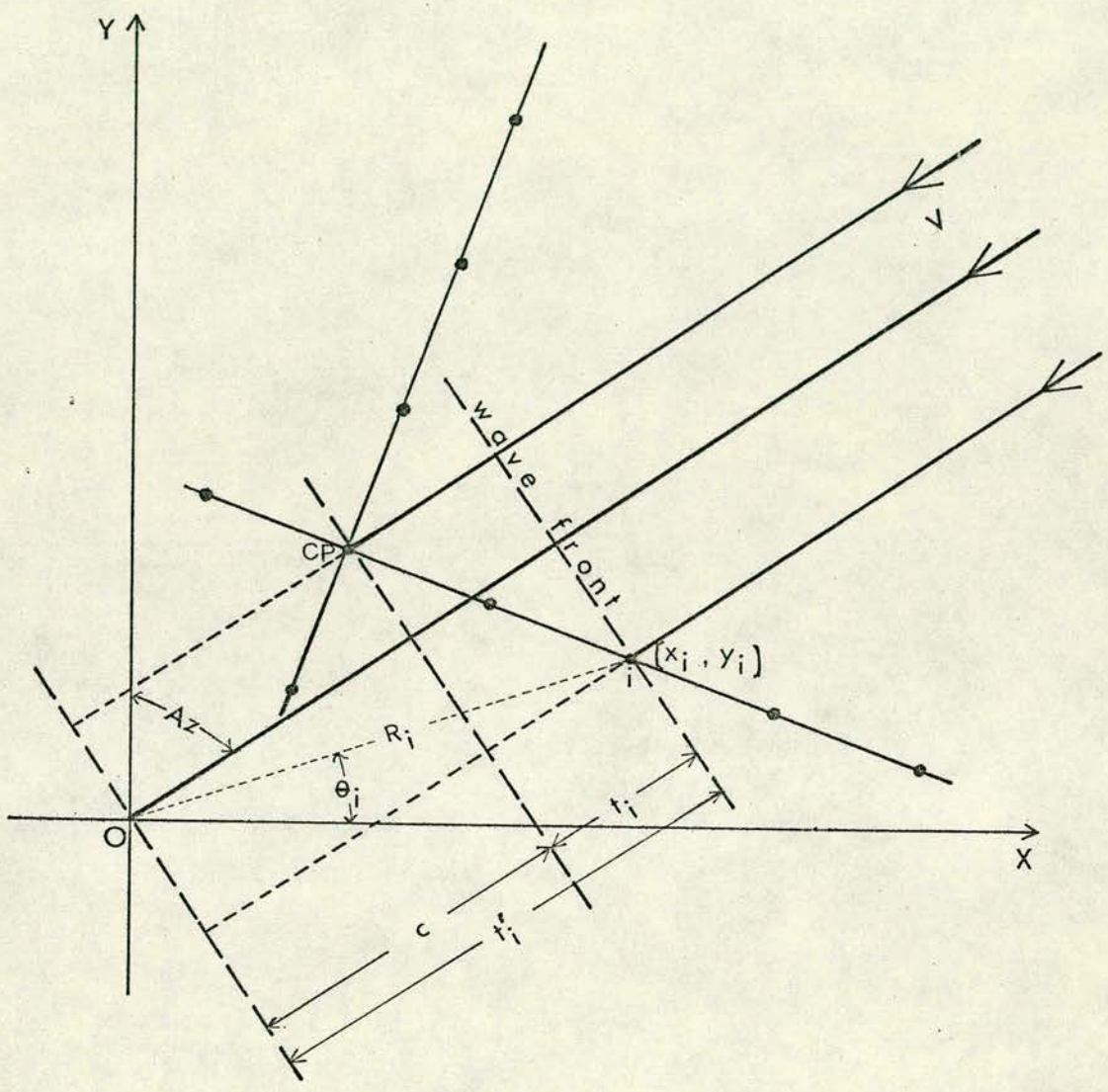

$$Az = \arctan(a/b)$$

$$V = (a^2 + b^2)^{-\frac{1}{2}}$$

a and b are found in the least squares solution of

$$ax_i + by_i + t_i + c = 0 \quad , \quad i = 1,2,\ldots n \quad (n=\text{number of points}) \qquad (14)$$

FIG. 29 AZIMUTH (Az) AND APPARENT VELOCITY (V) FROM ARRAY DATA

5.4 Data Used in the Present Study

The events used to study the azimuth and apparent velocity observed at SAAS were chosen from the events used in the analysis of travel-times and magnitude residuals (Chapter 4) which are listed in Appendix 1. From these events, only 122 were suitable for the correlation-by-pairs analysis (with the DELAYS program) to find the true relative delays. These 122 events are identified in Appendix 1 (column EVENT no.) by numbers preceded by a letter A or E. The letter A events belong to a period when SAAS was operating with only 9 points (CP, E1, E3, E4, E5, S1, S3, S4 and S5), and the letter E events to a period when SAAS operated with 14 points (E2, EE, SE, W2, and WE and the 9 points mentioned above). For the E events only 9 out of the 14 points were considered, to make the data compatible with the data used in the A events, and also because the coordinates of the extreme points, which were not used, are provisional only. Signals from E2 were not used because they showed anomalous early arrivals on the visual playouts.

The quality of the signal of the 122 events was compared and this permitted to separate 82 events with very clear signal; the remaining events have weak signal but still permitted fairly reliable time delays to be obtained. Other events that were originally chosen to be processed but had poor digitized signal were left aside (Events marked A or E ... missing in Appendix 1).

Every event was reproduced in a visual analogue playout to see the quality of the signal at each point of the array. Then the chosen events were digitized- the analogue tape was played back at 15/16 inces/second (8 times the recording speed) and the

signals were passed through frequency filters set at 0.1 to 5.0 Hz before being digitized. The maximum sample rate possible for more than 8 channels was 50 samples/second recording time. Normally 2 recorded minutes of signal were digitized for each event, taking care to start the digitization some 30 recorded seconds before the onset of the event.

Subsequently, a visual record of the digitized data was obtained, after being converted back into the analogue form and displayed on the ink jet-pen recorder. In this print-out, block markers are inserted which allow one to locate the portions of signal required to be processed (see Figure 26). The beginning of the portions of signal to be processed are referred to the preceding block markers, by measuring the separation and length of the portion in millimetres. The length of each recorded second of the time encoder signal is also measured in millimetres.

These values from the visual playouts, identification for each event and their parameters involved in the calculations were punched on cards and submitted together with the digitized tape and the DELAYS program, to be processed in a 370 IBM computer of the ERCC. The time delays punched on cards as output of the DELAYS program were used as input of the AVTS program, and processed in a ICL 4-75 computer through an EMAS terminal (Edinburgh Multi-Access System) set at the Geophysical Laboratories of IGS.

5.5 Original Results

The azimuth and apparent velocity observed at SAAS for the 122 events used in this study (most of them with several phases analysed) and obtained without considering any correction in the calculations, are listed in Appendix 3-A. These events have been grouped according to their epicentral region. The following regions have been considered:

- Eastern Europe and Middle East
- Atlantic Ocean and Ridge
- South Sandwich Islands Region
- East Pacific Ocean facing South America
- Northern Latin America (0^{o} - 30^{o}N)
- Southern Latin America (0^{o} - 40^{o}S)

Large departures (from the expected values calculated from NOAA epicentral determinations) in azimuth and apparent velocity for the P phase were observed from the original results. These departures are considered in this work to be mainly caused by discontinuities in the seismic paths or by tectonic features near the source, and are named in this study as "azimuth residual" (ΔAZ) and "apparent velocity residual" (ΔAV) and are calculated by subtracting the expected values from the observed ones. The distribution of these residuals is shown in Figures 30 and 31 respectively.

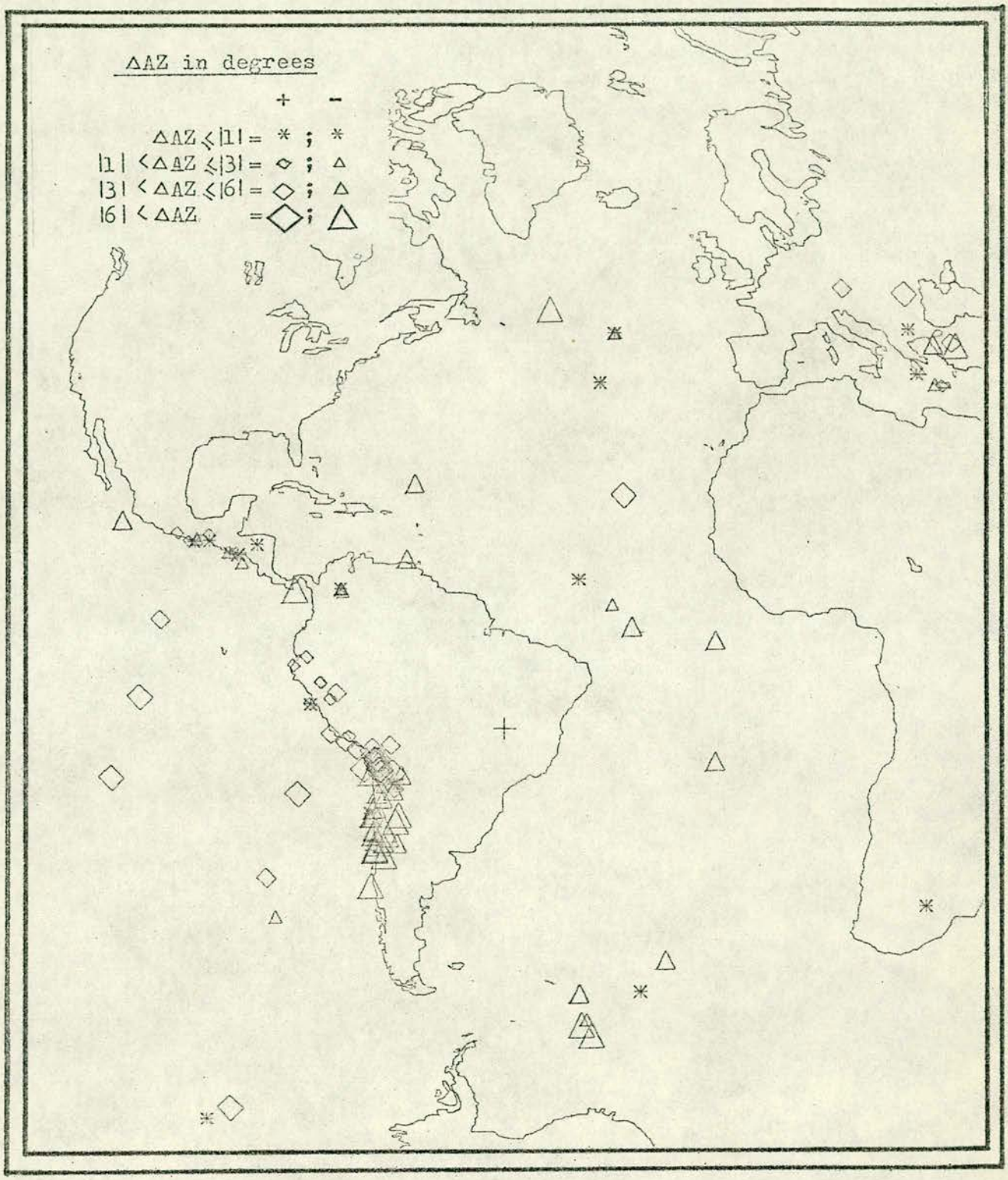

Figure 30.- DISTRIBUTION OF ΔAZ, FOR ALL EVENTS USED IN THIS STUDY, PROCESSED WITHOUT THE CORRECTIONS DUE TO STRUCTURE UNDER SAAS

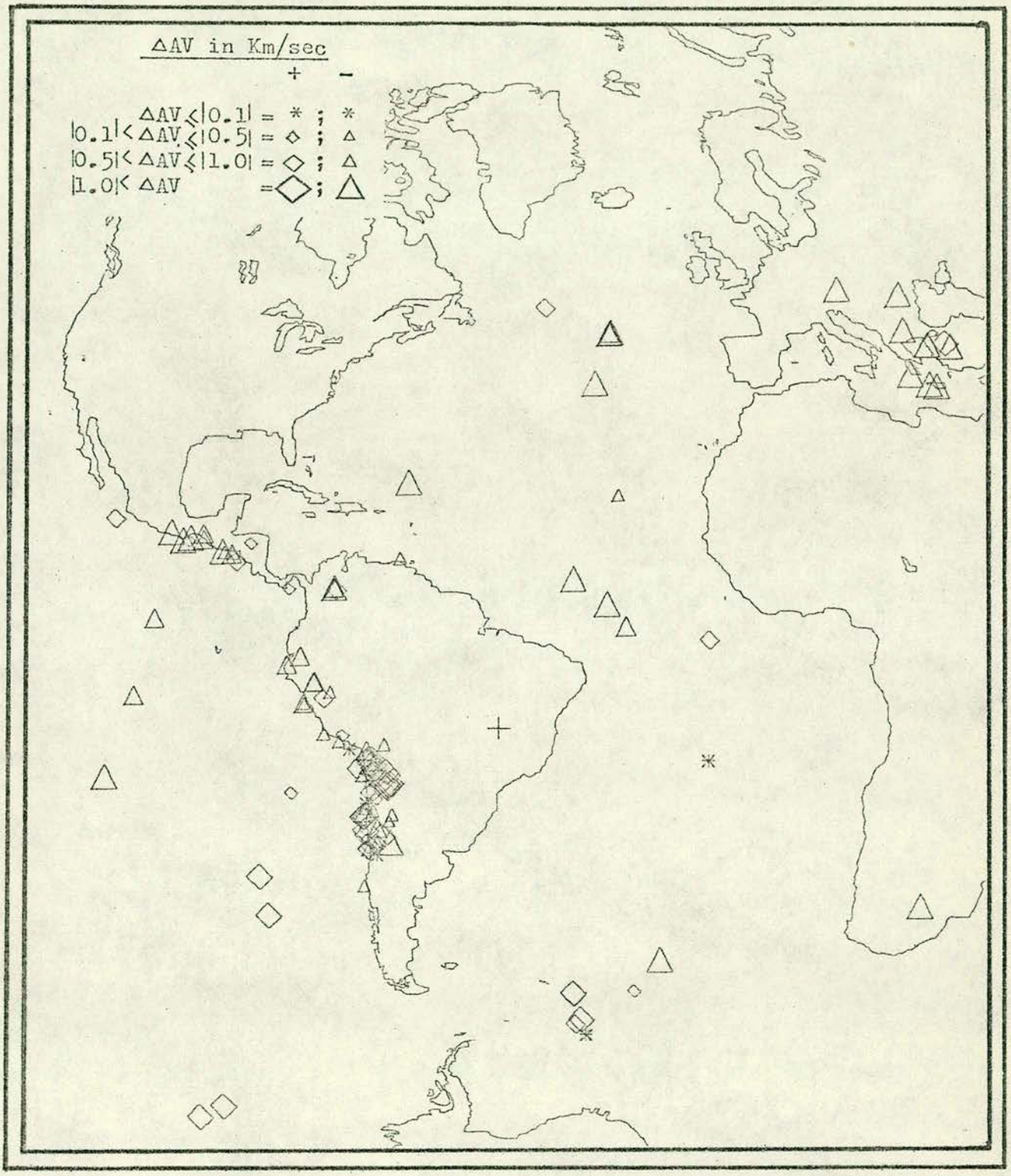

Figure 31.- DISTRIBUTION OF ΔAV, FOR ALL EVENTS USED IN THIS STUDY, PROCESSED WITHOUT THE CORRECTIONS DUE TO STRUCTURE UNDER SAAS

It can be observed that ΔAZ and ΔAV tended to have similar values for the events within the regions mentioned above or within areas inside these regions. Before doing any analysis of the distribution of ΔAz and ΔAV, it is necessary to consider any effect that the structure under SAAS could have had in the calculation of the observed azimuth and apparent velocity.

5.6 Effect of Structure under SAAS

The observed azimuth and apparent velocity of seismic events calculated from array data can have considerable departures from their expected values. These differences, as mentioned before, may be caused by the following:

a) Complexity of the structure at the source (or near the source).
b) Lateral and horizontal discontinuities in the seismic paths.
c) Structure under the recording array.
d) Errors during the analysis of records.

The analysis and interpretation of the first two sources of departure, from the expected values, are the objective of this study; the fourth source has been minimized by the use of automatic ways of processing the data, therefore it is necessary to find out what effect the structure under SAAS could have in the computation of azimuth and apparent velocity.

The following considerations have to be borne in mind when considering the structure under SAAS.

- SAAS is located in the central area of the Brazilian shield, therefore it is likely that the crust under SAAS has a relatively simple structure with the Moho almost horizontal.
- The surface structure is different in the two lines of the array. From CP to E5 the sites are located on two prominent outcrops of quartzite, E2 being near the boundary of the outcrops. Frpm CP to S5 the sites

are located mostly on top of thick sediments which form an almost plane surface, with an average altitude of 100 metres below CP altitude (see Figure 32).

At present, there has been no opportunity of carrying out any seismic refraction experiment to determine in detail the structure under SAAS.

The method used in this research to assess the effect of the structure in the travel-time of seismic waves under each component of SAAS was based on the assumption that the PKIKP phases with $\Delta > 160^{\circ}$, should arrive almost simultaneously at every point of the array, regardless of any effect of the source structure or mislocation of the epicentre. If the structure under every point of the array were similar, if the Moho were horizontal, and if the altitude of the points were the same, then the observed arrival times should be similar to the expected ones (i.e. almost simultaneous, with small allowances for the azimuth and distance of the epicentre). Departures of the observed arrival times from the expected arrival times, represent differences in the structure under the array.

In Table 7 are listed the events used to study the structure under SAAS, and in Figure 32 are presented the relative travel-time residuals (departures from the expected values which were obtained by using the DELAYS and AVTS programs referred to CP); the cross sections for the two lines of SAAS deduced from these relative residuals and from the known surface structure are also shown in Figure 32.

The two events with azimuth 329° and 14° have similar relative residuals which is also the case for the other two events which have

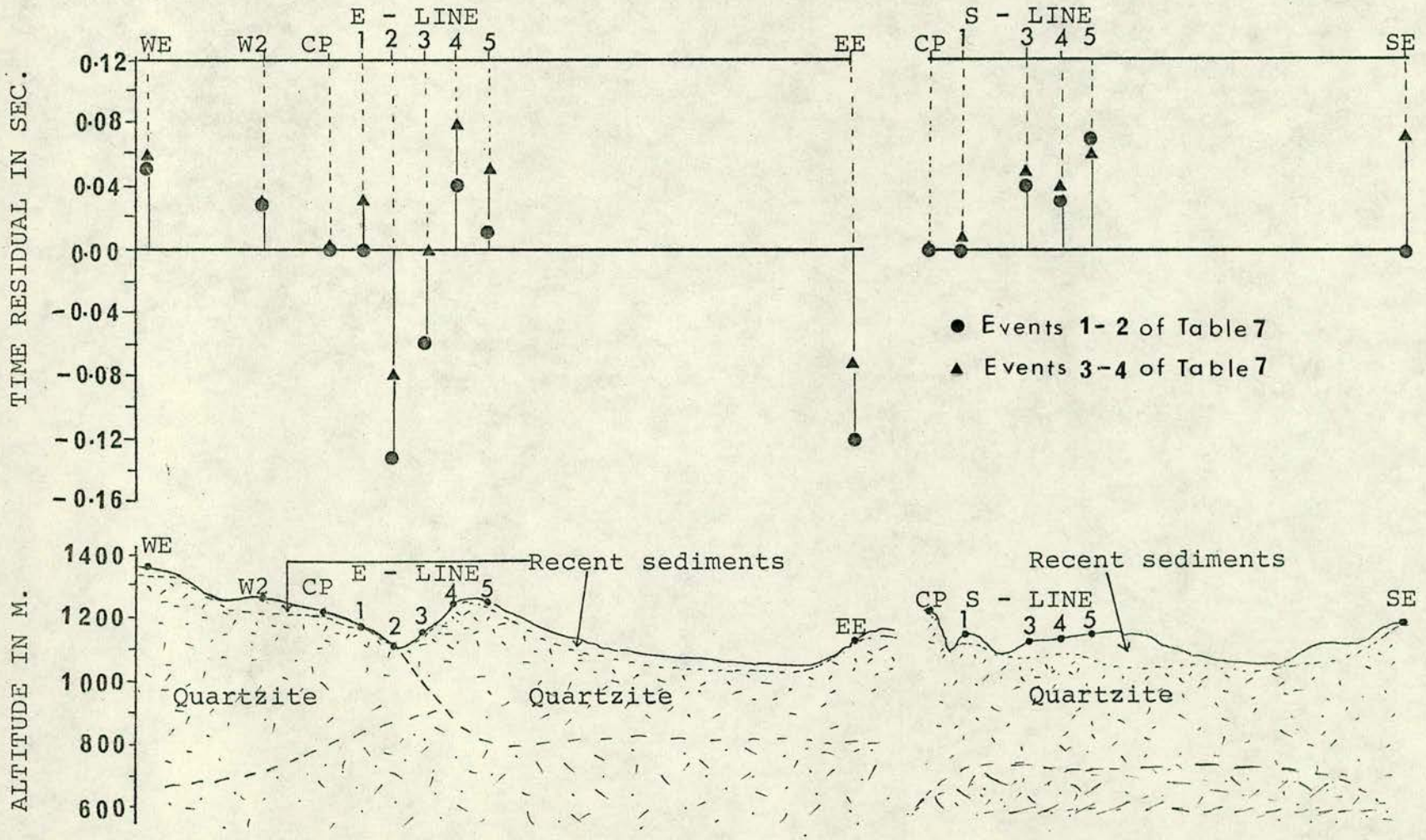

Figure 32.- DIAGRAM SHOWING THE CORRELATION BETWEEN THE OBSERVED PKIKP DELAYS AND THE TOPOGRAPHY OF SAAS LINES, WITH A SURFACE STRUCTURE INFERED FROM THE SURFACE GEOLOGY OF THE AREA

TABLE 7

EVENTS USED TO OBTAIN TIME CORRECTIONS DUE TO STRUCTURE UNDER SAAS

	DATE	H	m_b	h	REGION	Δ^O	TV	TA
1	25 OCT 72	170503.7	6.0	47	Ryukyu Islands	167.8	158.7	14.7
2	13 NOV 72	081148.8	5.5	372	Bonin Islands R.	165.7	138.9	329.8
3	02 DEC 72	001947.2	6.3	33	Mindano, Phi.Is.	169.5	185.2	149.3
4	02 DEC 72	014047.8	5.9	54	Mindano, Phi.Is.	169.5	185.2	149.4

H : Origin Time
h : Depth in Km
Δ : Epicentral Distance in Degrees
TV: Expected Apparent Velocity
TA: Expected Azimuth

TABLE 8

TIME CORRECTIONS DUE TO STRUCTURE UNDER SAAS, DEDUCED FROM PKIKP EVENTS

POINT	CORRECTION	POINT	CORRECTION
CP	0.00 sec.	S1	-0.01 sec.
E1	-0.01	S3	-0.05
E2	0.10	S4	-0.04
E3	0.02	S5	-0.06
E4	-0.06	SE*	-0.04
E5	-0.03	W2	-0.03
EE*	0.06	WE	-0.04

* Provisional values only

almost opposing azimuths to the first ones. All four events have at each point of SAAS nearly the same value of relative residuals, except at the extreme points (EE and SE) which may be due to the uncertainty of the positions of these points; although small delays can be seen in most sites, for the events coming from the SW with respect to the relative residuals of the other events, the PKIKP relative residuals can be considered to be constant at each point of SAAS and therefore be a result of the structural differences under SAAS.

There is a correspondence between the relative travel-time residuals and the topography of the W-E line, a phenomenon that is not observed in the N-S line where the relatively late arrivals do not correspond to the relatively lower altitudes. The overlapping structure suggested in Figure 32 could explain, in part, the distribution of the relative residuals of the W-E line, especially if one considers the observed permeability of these formations which could cause a reduction in the velocity of the seismic waves.

For instance, between CP and E2 there is a relative delay of $\approx$0.1 sec (the signal arriving earlier at E2), and the altitude of CP is $\approx$ 100 metres above that of E2. This alone would represent a P velocity of 1 km/sec for the quartzite formation where the two points are installed; this velocity is too low for a metamorphic rock, according to Birch (1942), who suggested velocities between 4.0 and 5.6 km/sec for this type of rock. Even if the rock was saturated by water, due to their observed permeability, the velocity would not reach values as low as 1 km/sec, but it could in extreme

conditions be between 3 and 4 km/sec. This would represent a difference in level between CP and E2 of 300 to 400 metres, to account for the observed 0.1 sec relative residual. As the superficial difference in level is only 100 metres, the other 200 or 300 metres have to be explained as a difference in the thickness of the quartzite formation, the true dimension of which would depend on the P velocity distribution of the layers involved (see Figure 32). The relative residuals of the W-E line did not suggest any dipping structure under that part of SAAS.

The relatively late arrivals of the N-S line with reference to CP, contrast with the topography of this line (see Figure 32). Part of the positive delays could be due to the thick sediments underlying more of the N-S sites, while CP is on a metamorphic formation, but the large value of these relative residuals, increasing to the South, could suggest a dipping structure (perhaps the Moho) in that direction. See also Table 8.

The relative travel-time residuals of some events recorded at SAAS with a good signal, representing the regions of concentration of the events being studied (mentioned in 5.3), are plotted in Figure 33. In this case only the 9 internal points of SAAS which were used in the calculations are considered. The distribution of the relative residuals of some of these representative events could suggest the existence of a structure dipping to the South-West, if the total value of the relative residual were assumed to be caused by the structure under SAAS. If this assumption were correct, the distribution of the relative residuals for all opposite azimuth events should be proportionally similar, but this is not so.

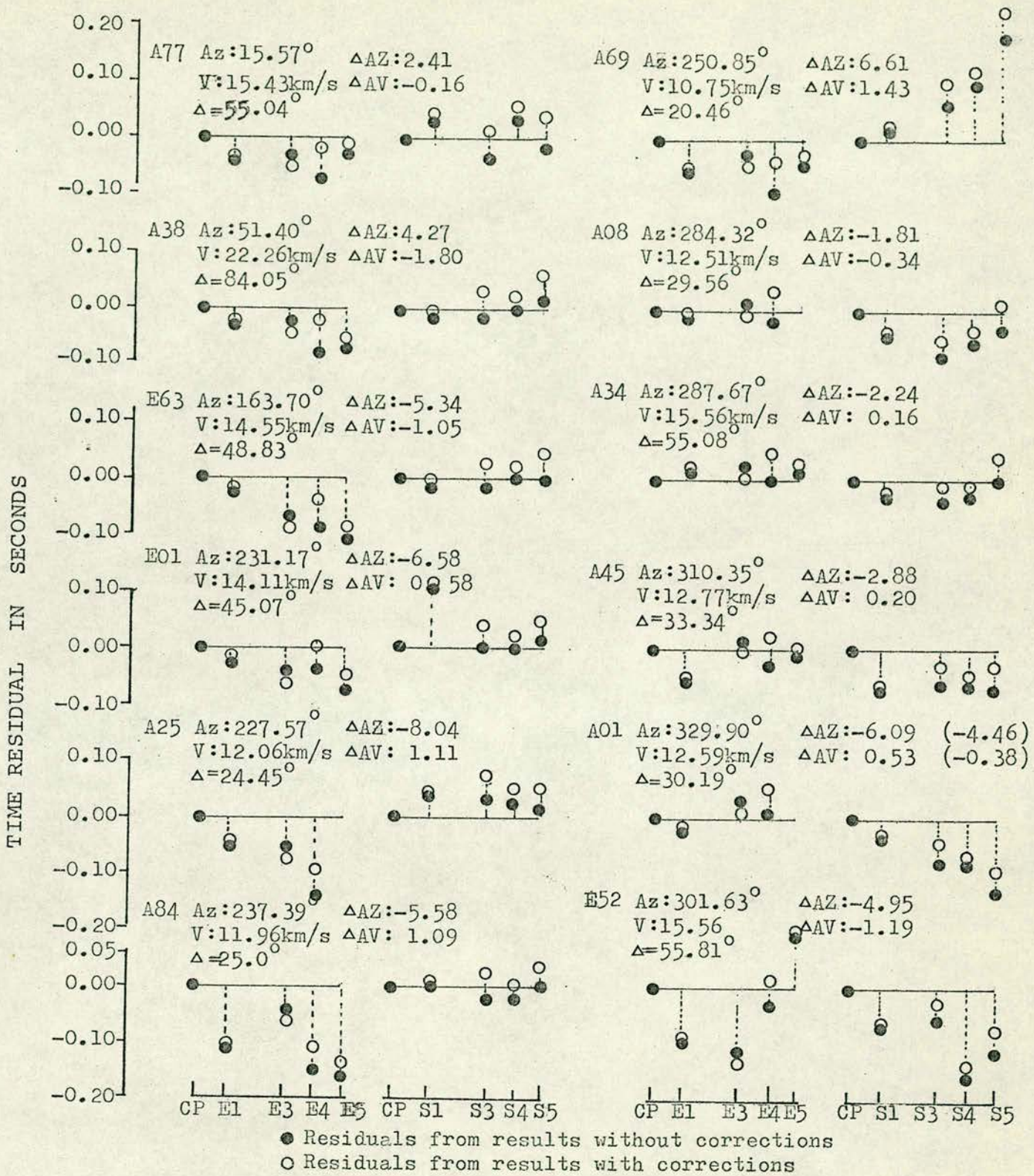

Figure 33.- RELATIVE TRAVEL-TIME RESIDUALS AT EACH POINT OF SAAS FOR TYPICAL EVENTS, OBTAINED WITH AND WITHOUT APPLYING TIME CORRECTIONS DUE TO STRUCTURE UNDER SAAS

For instance, the relative residuals of event A 38 and E 01 could match a SW dipping structure (even if the value of all the relative residuals do not completely agree with this), but the relative residuals from events E 63 and A 01 show completely opposite behaviour.

Another argument which could support the non existence of the effect of a dipping structure under SAAS, when using the corrected data, can be obtained by comparing the distribution of ΔAZ and ΔAV in Figures 34 and 35 respectively with the distribution suggested by Otsuka (1966, Fig. 4, page 663) which shows a cyclic distribution with opposite effect for ΔAZ and ΔAV caused by a dipping structure under the array when the residuals are distributed against the expected azimuth. This distribution is not observed for the residuals obtained at SAAS.

For these reasons, and because the PKIKP events did not show a SW dipping structure it was assumed that most of the value of the relative residuals, for the events in the P range of SAAS, was due to effects away from the station and that the time corrections due to the structure under SAAS deduced from the PKIKP events were the proper ones to use in this study. It is, however, understood that these corrections will take away, only partially, the effect of the structure when events with smaller angles of incidence are considered, (i.e. events with smaller epicentral distance), therefore the final results of ΔAZ and ΔAV, after applying the PKIKP corrections, should still be slightly affected by differences of structure under SAAS.

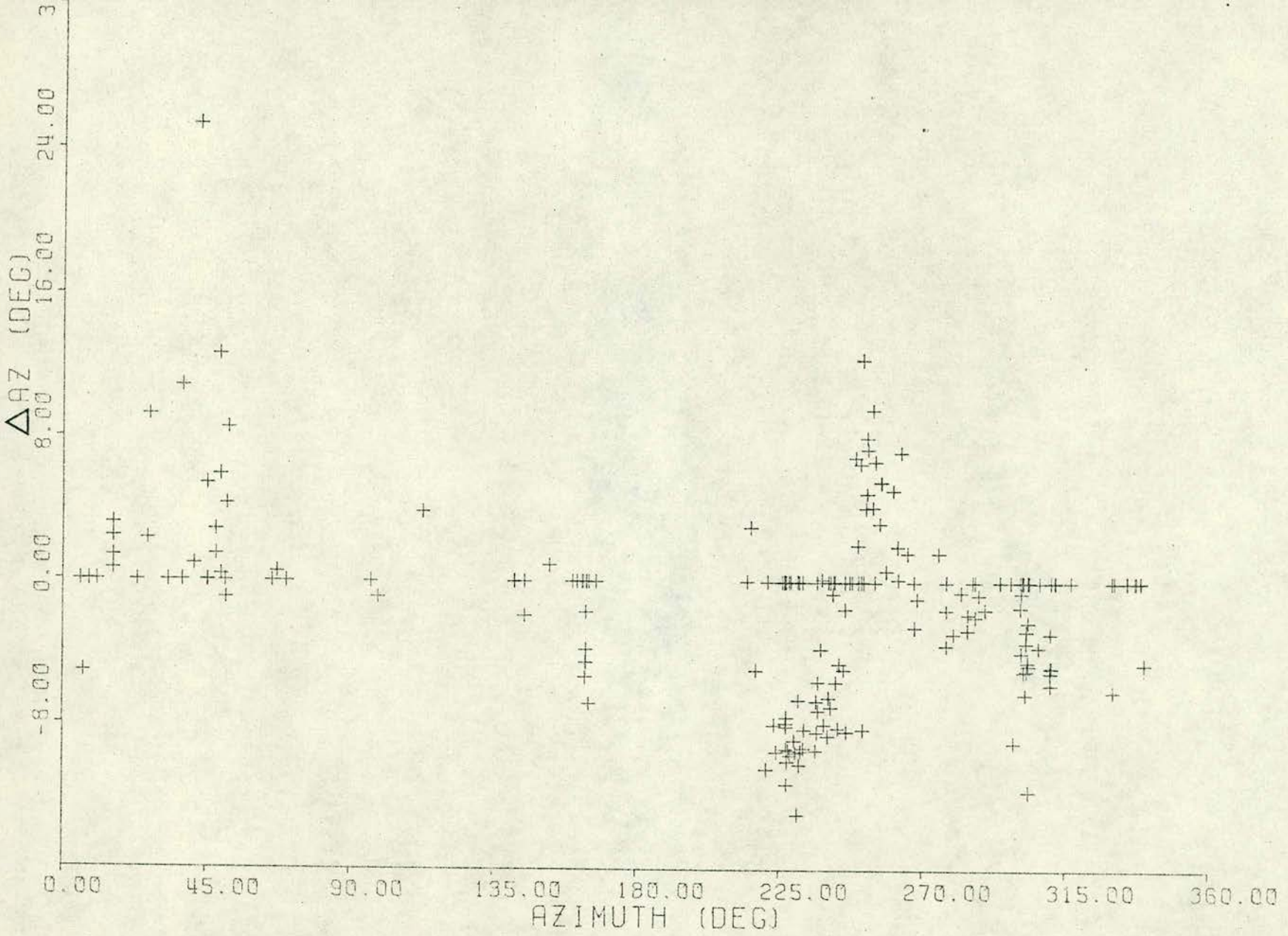

Figure 34.- DISTRIBUTION OF ΔAV FROM CORRECTED RESULTS, AGAINST AZIMUTH

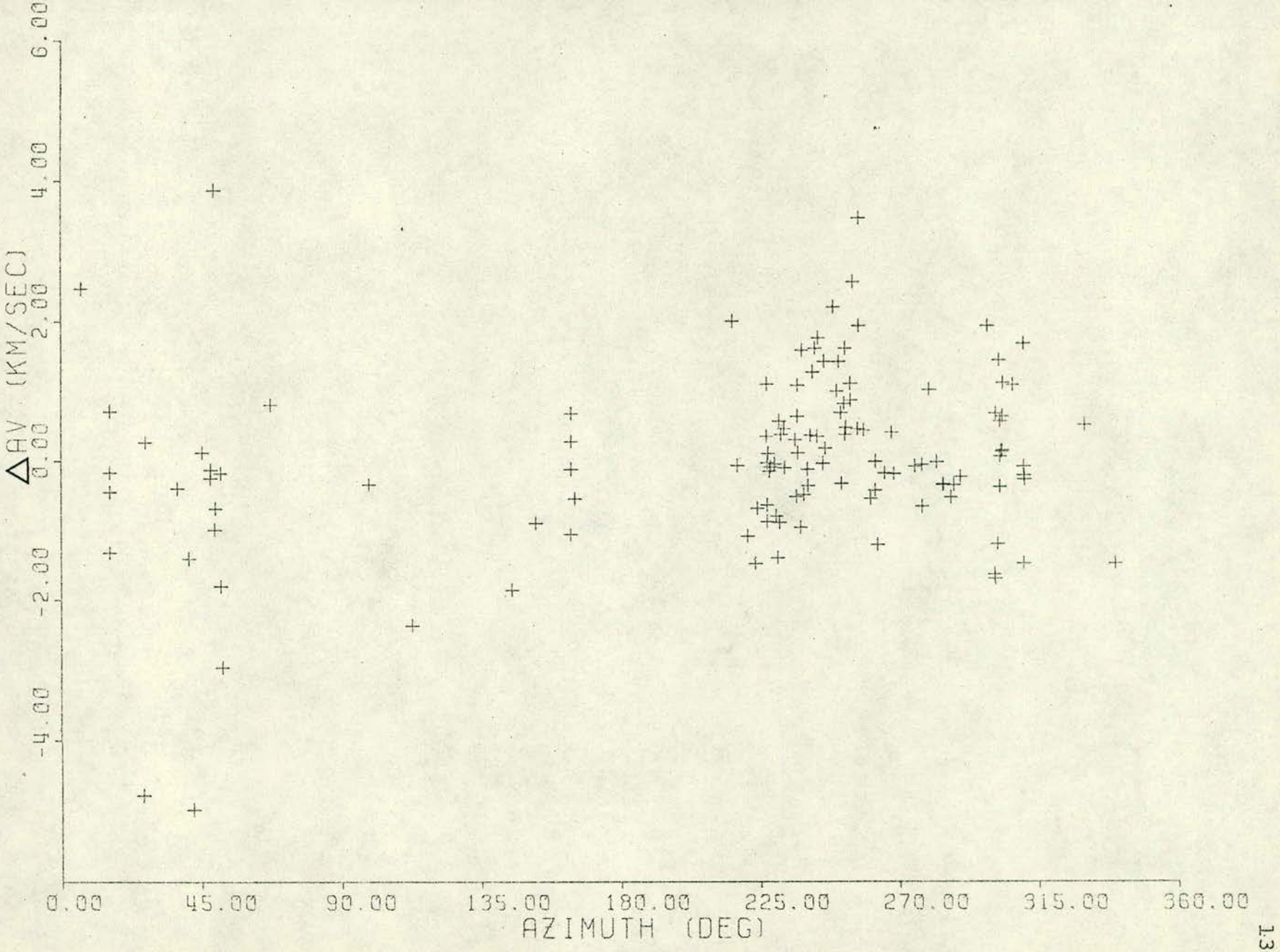

Figure 35.- DISTRIBUTION OF ΔAV FROM CORRECTED RESULTS, AGAINST AZIMUTH

The residuals obtained after applying the structure corrections, for the same representative events considered before, are also plotted in Figure 31. In general it appears that there has been a relative improvement in the N-S line (except for the events coming from the NW), but the same cannot be claimed for the W-E line.

It is considered therefore that it is better to use the observed azimuth and apparent velocity, modified by the PKIKP corrections for the effect of structure under SAAS, to study the Earth's interior under South America, than the original uncorrected results.

5.7 Corrected Results

5.7.1 General Considerations

The time corrections due to the structure under SAAS, obtained with the PKIKP events, were applied to the arrival times of the 122 events studied. The corrected values of azimuth and apparent velocity are listed in Appendix 3-B; ΔAZ from the corrected events are presented in Figures 36 and 37 and ΔAV in Figures 38 and 39; Figures 36 and 38 are the residuals belonging to events with good signal, the other two figures include all 122 residuals.

In Appendix 3-B the events are grouped in the same regions as for the original results listed in Appendix 3-A. In each event all the phases that were clearly identified in the majority of SAAS components and within the first 90 seconds of the signal, were processed. To calculate ΔAZ and ΔAV, the observed parameters of the first P onset of each event were used. In some events it is possible to identify a small phase (generally with higher frequency), preceding the main P phase by less than 2 seconds; in these cases the values of azimuth and apparent velocity of the main P phase were considered to obtain ΔAZ and ΔAV.

The distribution of ΔAZ and ΔAV with respect to the epicentral region of the events being studied, and their relationship with the main tectonic features of South America are the prin cipal objectives of this research. An analysis of the observed azimuth and apparent velocity of all phases which were processed, and that may present some relationship with some tectonic features, or interesting signal patterns which could lead to some speculation about the structure under South America, has also been carried out.

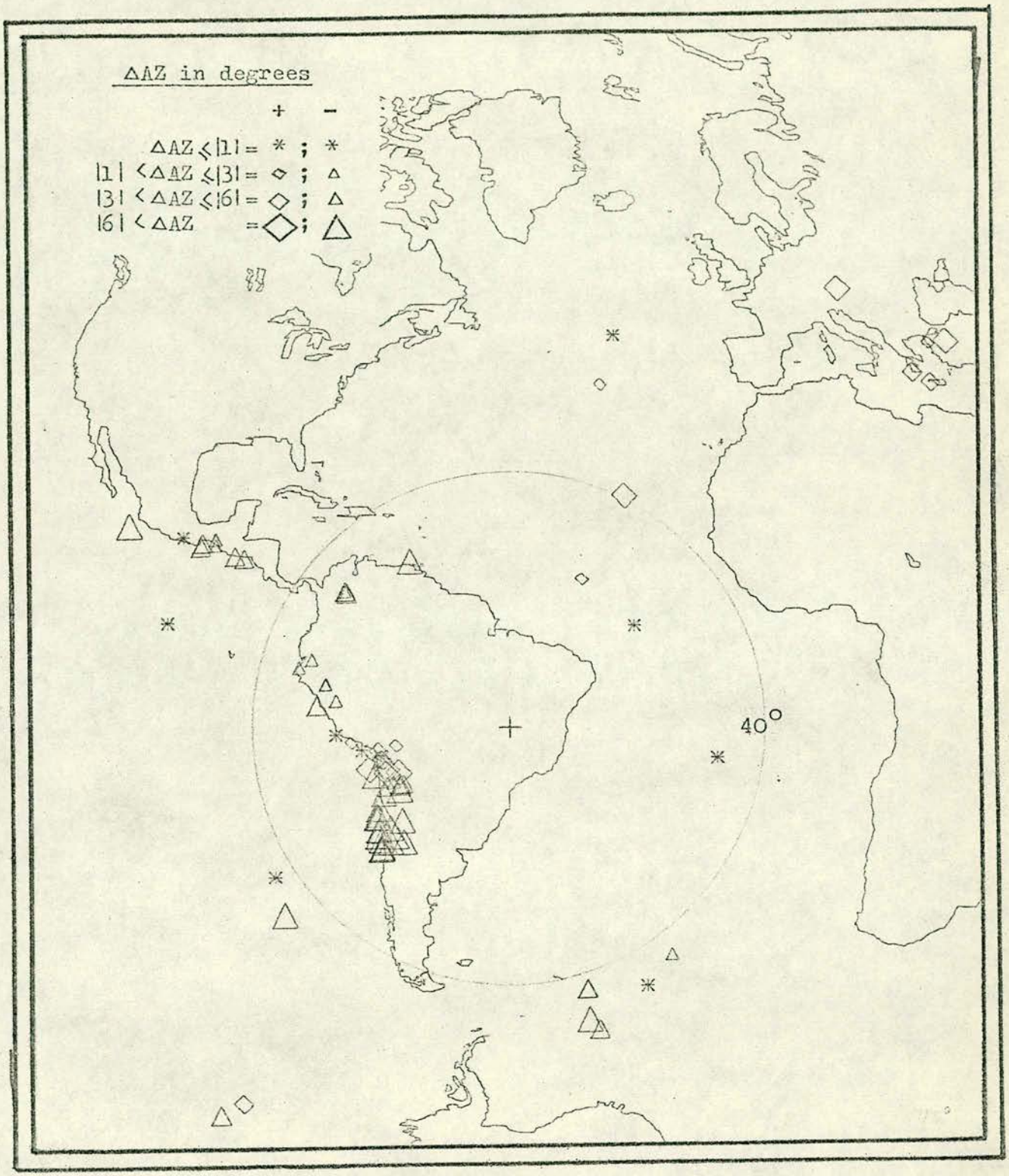

Figure 36.- AZIMUTHAL DISTRIBUTION OF ΔAZ FROM GOOD SIGNAL EVENTS, AFTER APPLYING TIME CORRECTIONS DUE TO THE STRUCTURE UNDER SAAS

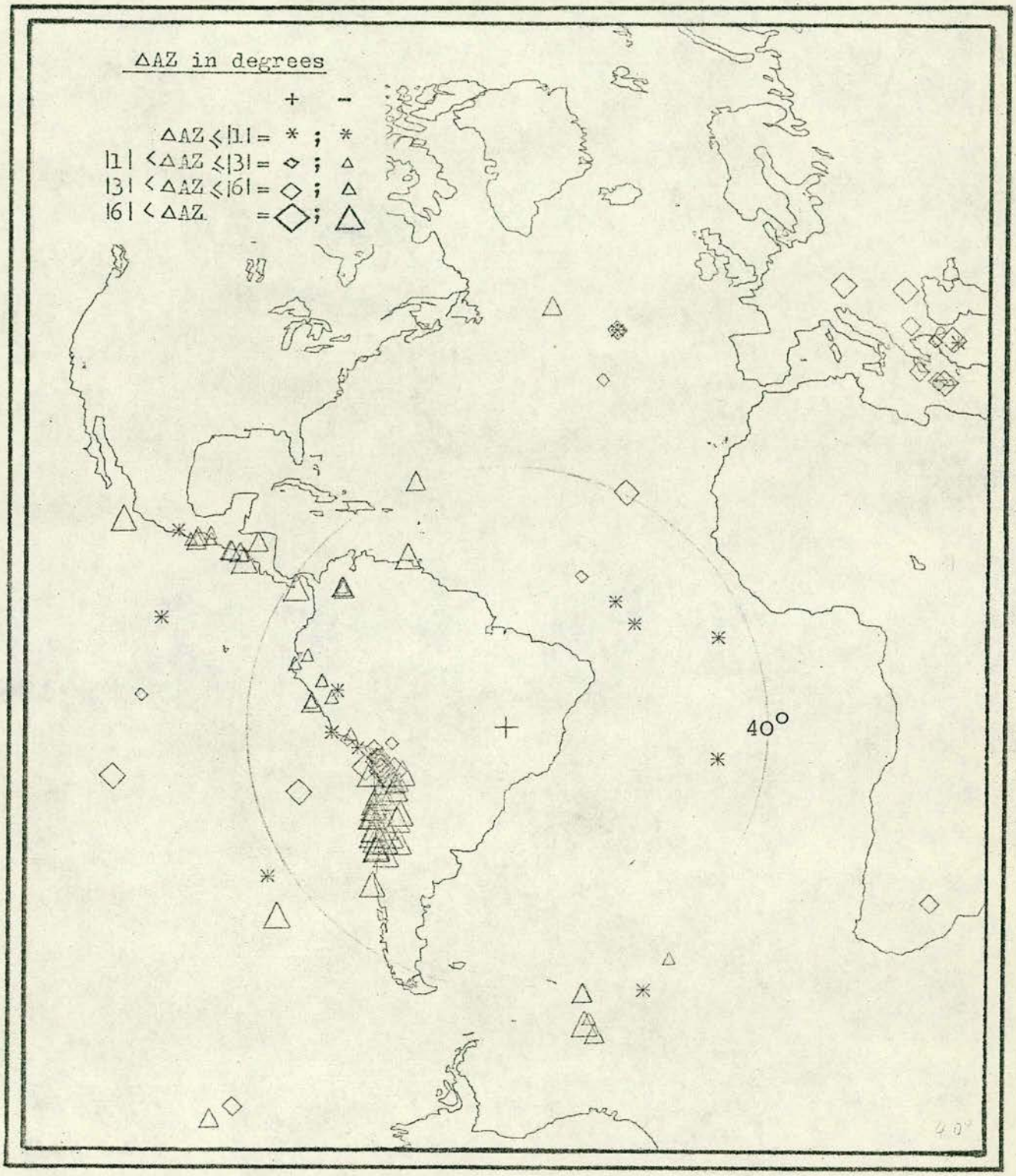

Figure 37.- AZIMUTHAL DISTRIBUTION OF ΔAZ FROM ALL EVENTS STUDIED, AFTER APPLYING TIME CORRECTIONS DUE TO THE STRUCTURE UNDER SAAS

The interpretation of the distribution of these residuals and their relationship with South American tectonics is carried out in Chapter 6. The analysis of secondary and some refracted phases is only briefly presented here, without further interpretation; they represent other potential sources of future research on South American tectonics.

5.7.2 Distribution of ΔAZ and ΔAV

By inspecting the distribution of ΔAZ and ΔAV in Figures 34 to 39, it can be seen that most of the results obtained from the weak signal events agree with the results of the good signal events.

In general terms (see Figure 34), it could be said that the events coming from azimuths between 6° and 152° have their ΔAZ mainly positive, showing the maximum values at around 45°. The events from around 164° azimuth (South Sandwich Islands) present their ΔAZ of around -5°. Another concentration of ΔAZ with large negative values (larger than -10°) appears between azimuth 220° and 250° (Andean region between 22° and 40° of South latitude) which systematically get less negative as the azimuth approaches the 250° value. At 250° azimuth (Chile-Bolivia border) a very distinct change in the behaviour of ΔAZ occurs, where it reaches large positive values (over 6°) which get smaller (less positive) as the azimuth increases again up to 290° (Peru-Ecuador border) where ΔAZ -2°. From 300° up to 320° of azimuth (Northern region of Latin America) ΔAZ is mainly negative, with values of up to -6°.

The distribution of ΔAV is less distinctive, showing a dispersion of values, with large, perhaps anomalous, values for the residuals of the events recorded at SAAS with a poor signal.

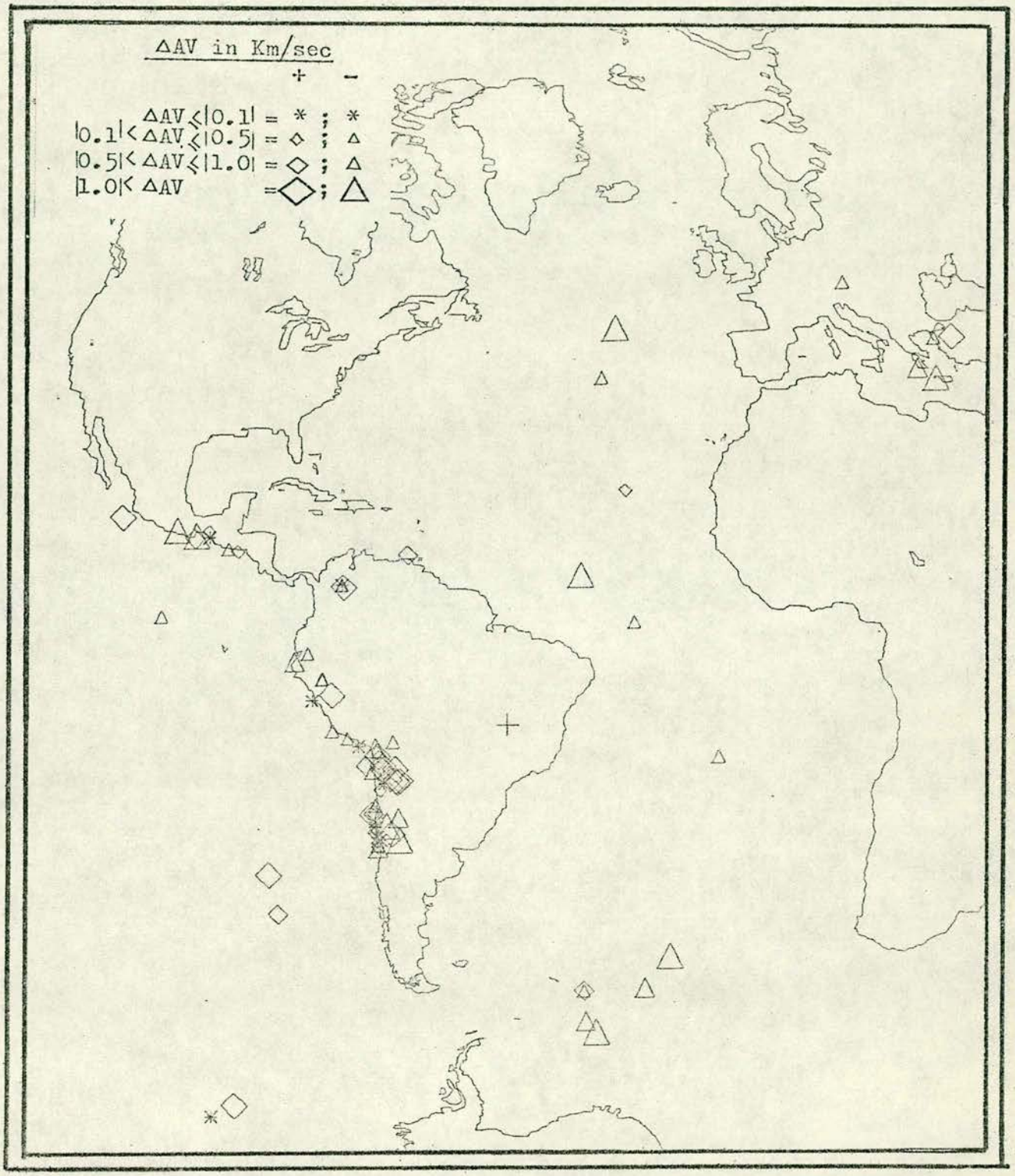

Figure 38.- AZIMUTHAL DISTRIBUTION OF ΔAV FROM GOOD SIGNAL EVENTS, AFTER APPLYING TIME CORRECTIONS DUE TO THE STRUCTURE UNDER SAAS

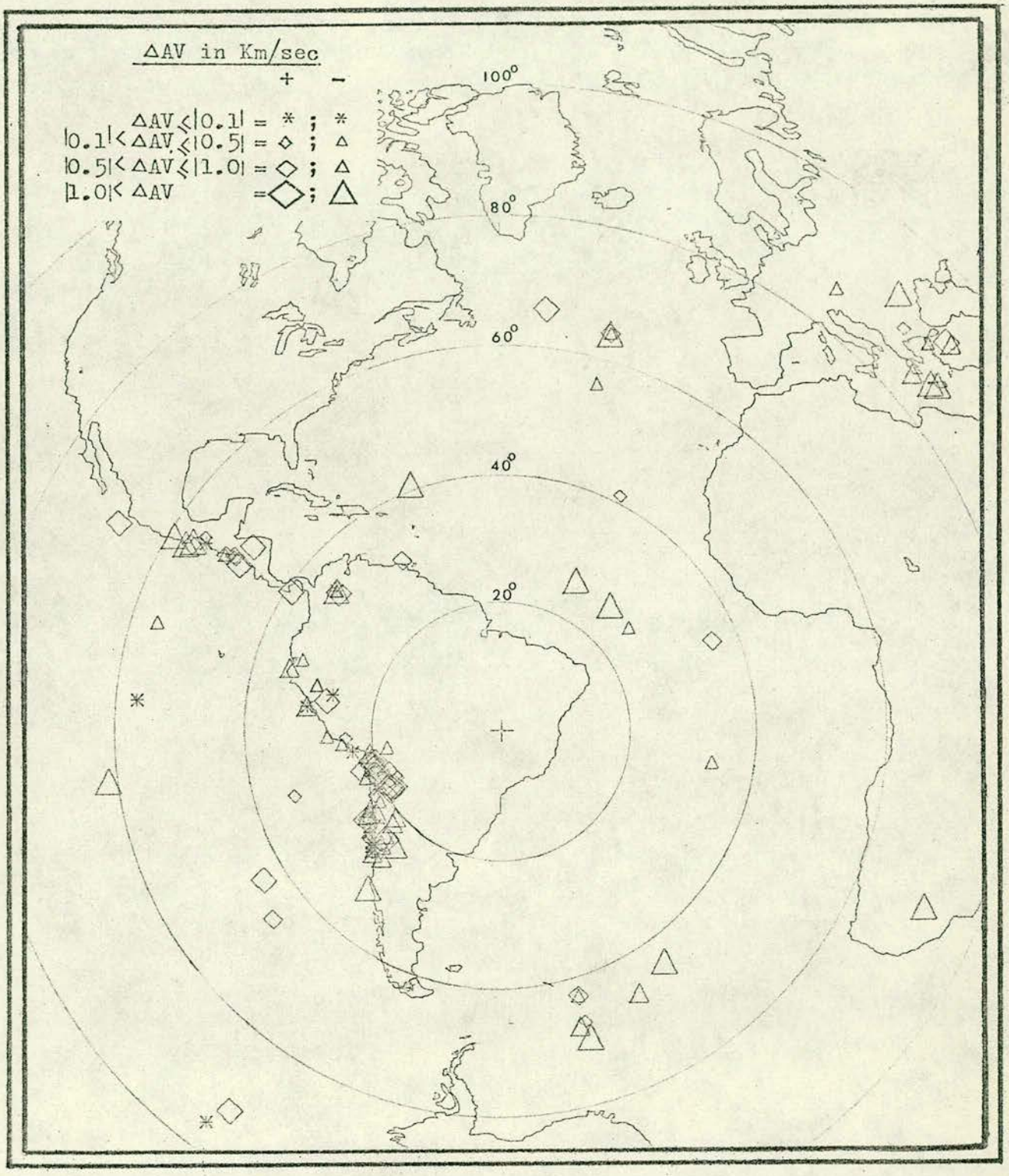

Figure 39.- AZIMUTHAL DISTRIBUTION OF ΔAV FROM ALL EVENTS STUDIED, AFTER APPLYING TIME CORRECTIONS DUE TO STRUCTURE UNDER SAAS

Still, it can be seen (see Figure 35) that most of the events coming from 0^{o} to 164^{o} of azimuth have negative or small positive values of ΔAV.

The events from the southern part of the Andes have negative values of ΔAV (larger than -1.0 km/sec), which appears to become less negative and reach large positive values of ΔAV (larger than 2.0 km/sec) at the Chile-Bolivia border region. Beyond 260^{o} of azimuth and up to 330^{o}, ΔAV presents dispersed values between +2.0 and -1.7 km/sec.

For a better interpretation of the distribution of ΔAZ and ΔAV and because the main subject of this research is based on the study of these residuals, it is necessary to analyse in more detail their distribution with reference to the epicentral regions of the events being studied. These regions, as mentioned before are:

- Eastern Europe and the Middle East (see Figures 40 and 41)
  On the whole the events of this region recorded at SAAS presented positive values of ΔAZ and negative values of ΔAV observed at SAAS. The smaller departures for both residuals, considering the good signal events only, are for the two events in the Aegean Sea near the coast of Turkey; the events which occurred on the eastern side of this region present a large ΔAZ (over $+9^{o}$), one of these (event N A 05) which occurred in Turkey (39.28^{o}N, 29.42E) has a very anomalous ΔAV(+3.87 km/sec) considering the other events of this region; at the western side of

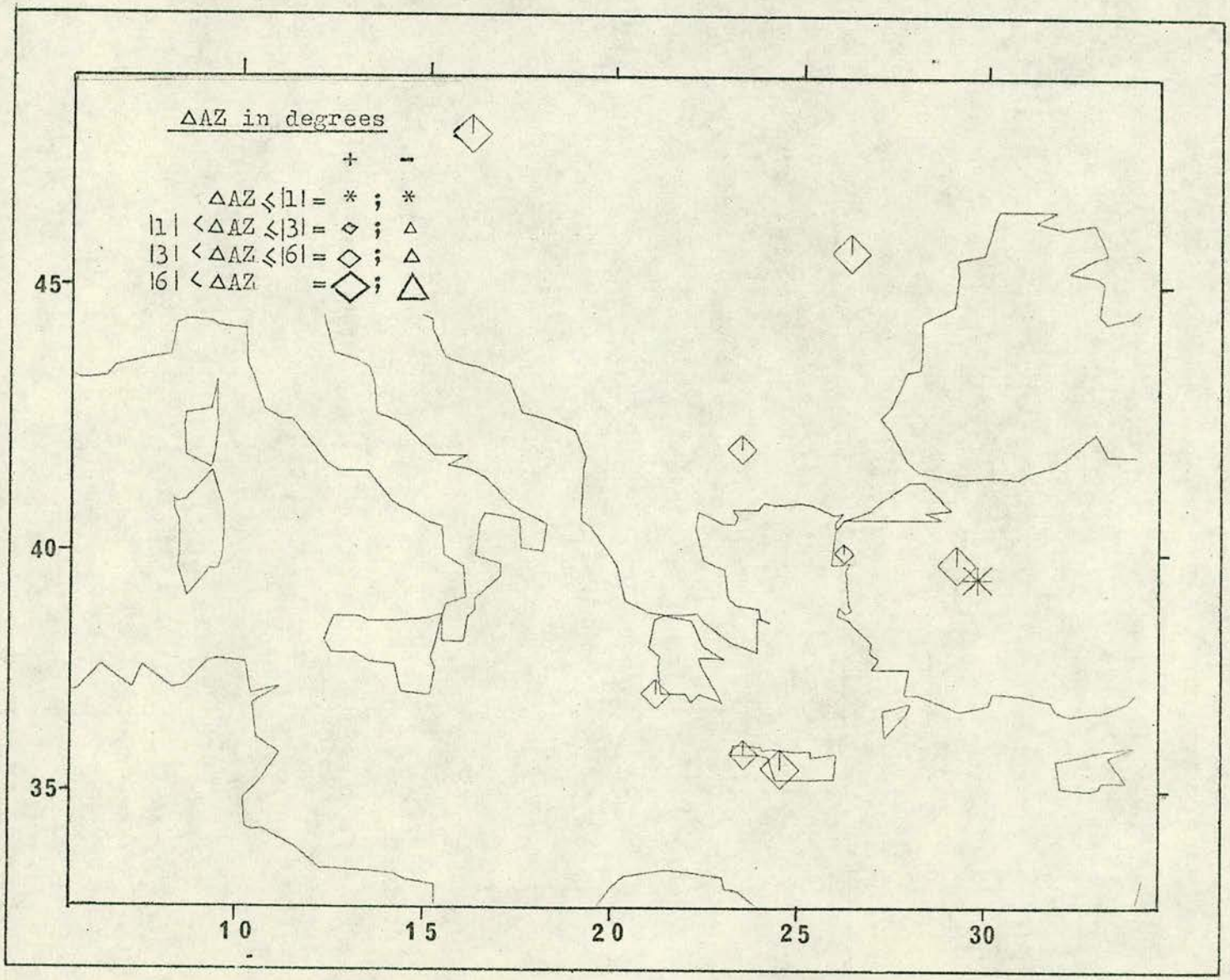

Figure 40.- DISTRIBUTION OF CORRECTED RESULTS OF ΔAZ IN THE EAST EUROPE - MIDDLE EAST REGION

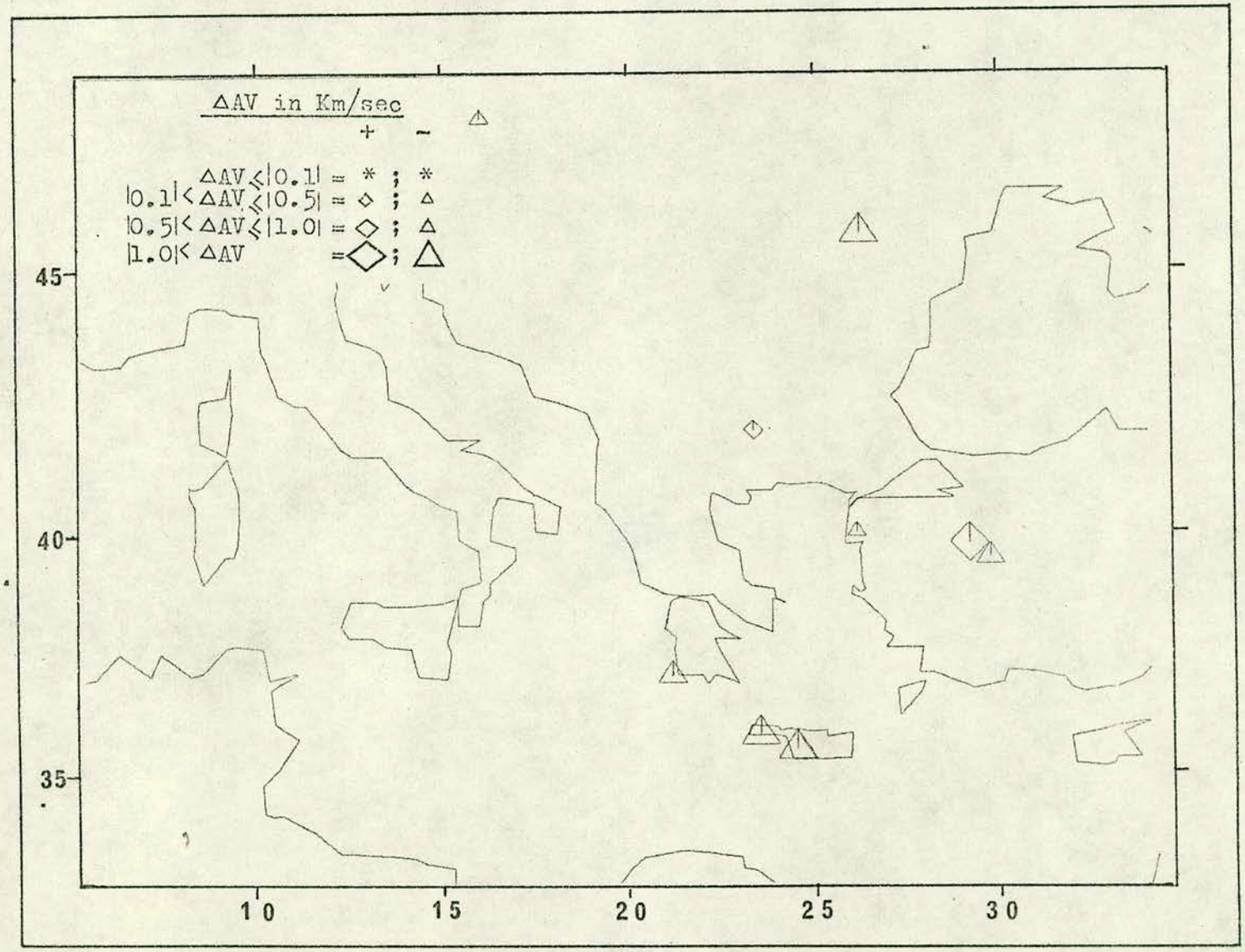

Figure 41.- DISTRIBUTION OF CORRECTED RESULTS OF ΔAV IN THE EAST EUROPE-MIDDLE EAST REGION

this region the two observed events have medium positive values (around 5^{o}) for ΔAZ and relatively large negative values for ΔAV (-0.98 and -1.80 km/sec). The residuals for the weak signal events, although they agree with the general behaviour of the residuals obtained from the good signal events, do not often agree with the detailed analysis made above.

- Atlantic Ocean and Mid-Atlantic Ridge (see Figures 36 to 39)
Most events in this region showed a very small positive value of ΔAZ (the larger departure being 2^{o} considering the good signal events only) except for an event which occurred NW of the Cape Verde Islands which had a very large value of ΔAZ (around $+9^{o}$). It may be observed that ΔAV has also relatively small value, mainly negative, with a very anomalous large negative value (-4.77 km/sec) for an event which occurred on the western side of the central Mid-Atlantic Ridge. Most of the residuals belonging to the poor signal events also agree with the general distribution of the residuals in this region as analysed above.
- South Sandwich Island Region (see Figures 36 to 39)
All events around the Scotia Arc have negative values of ΔAZ (between -3.8^{o} and -6.8^{o}). One event, having ΔAZ -1.7^{o}, gave a poor signal at SAAS. Two events to the East of the Scotia Arc, near and in the southern part of the Atlantic Ridge respectively, have very small value of ΔAZ ($+0.90^{o}$ and -1.94^{o} respectively). ΔAV has values between +0.69 and -1.05 km/sec for the events in the Scotia Arc, having more negative values for the events in

the souther part of the Arc; ΔAV for the events in the southern part of the Atlantic Ridge is large and negative (-0.89 and -1.85 km/sec).

- Southern East Pacific Ocean (see Figures 36 to 39)
  There were only five widely dispersed events, located in the bast area of this region, that were recorded with a good signal at SAAS during the period of study, and only three with a weak signal. Perhaps the only noticeable pattern worthy of note is the positive values of ΔAZ of the events located in front of Peru, but these events were recorded with a poor signal at SAAS therefore there is no great certainty as to the observed values.
- Northern Latin America (0° -30°N) (see Figures 42 and 43)
  Most of the events from this region have values of ΔAZ between -2° and -7° with the exceptions of the event E 14 (18.78°N, 106.73°W) which had a larger negative value (-8.94°), and the event E 53 (16.60°N, 97.98°W) which had a smaller negative value (-0.62°). The events recorded at SAAS with a poor signal, but which were considered in this analysis show values of ΔAZ similar to those of the events with clear signals. It is important to notice that these events are concentrated towards the southern part of the region, with the exception of the Santander Province (Colombia) events. The distribution of ΔAV for the events recorded in this region show dominant positive values, mostly in the southern part of Central America.

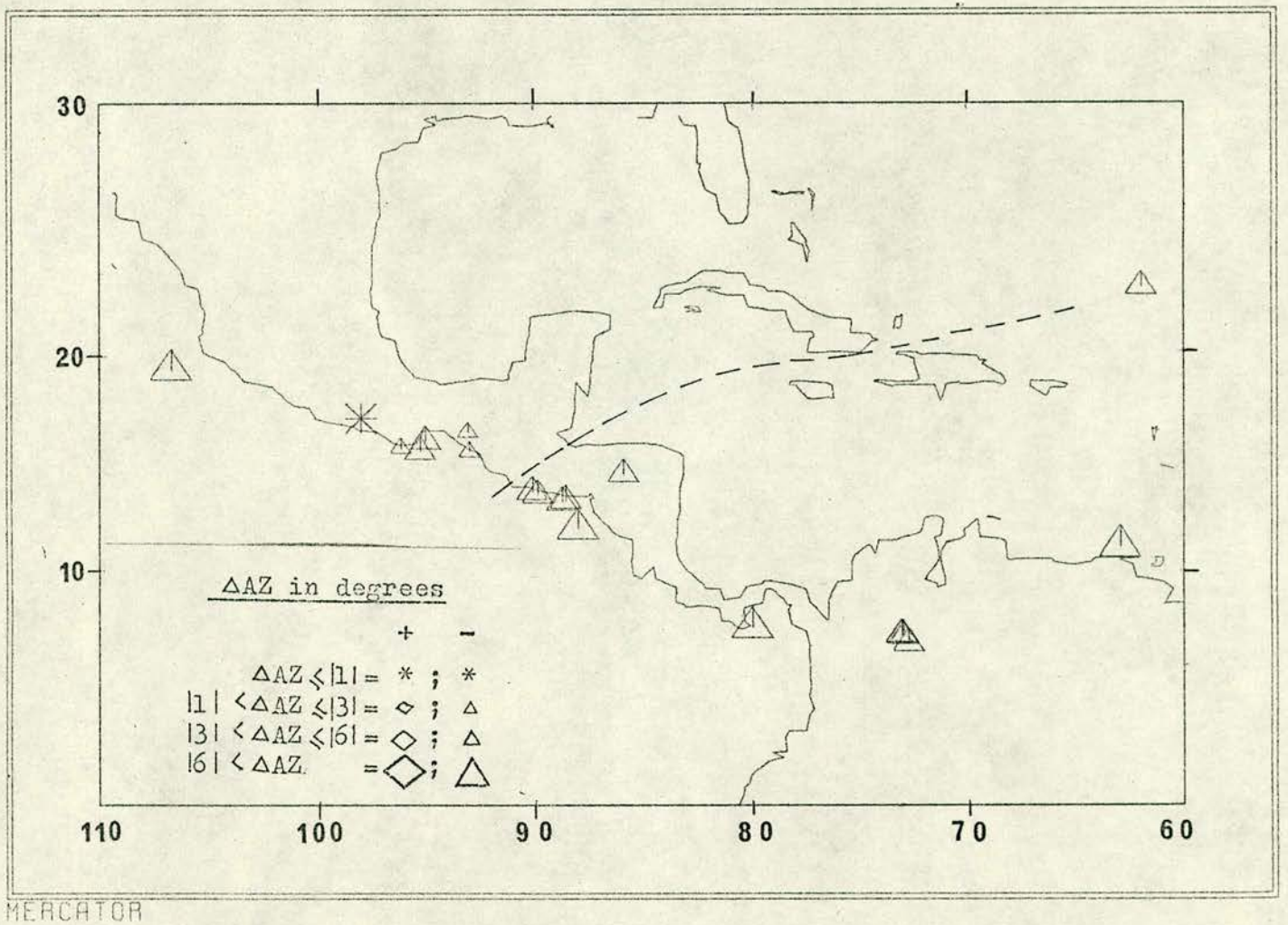

Figure 42.- DISTRIBUTION OF CORRECTED RESULTS OF ΔAZ IN THE NORTHERN LATIN AMERICAN REGION

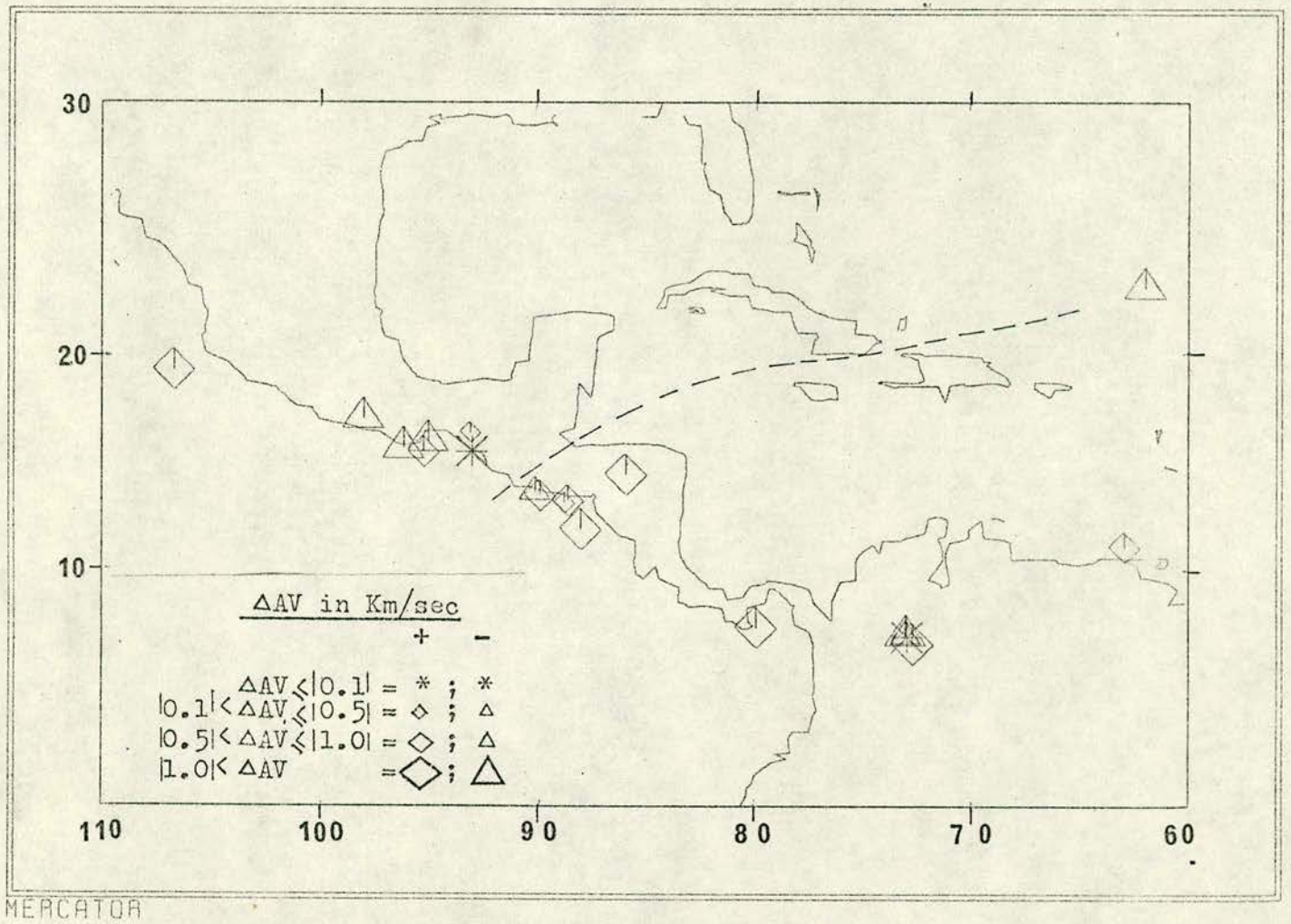

Figure 43.- DISTRIBUTION OF CORRECTED RESULTS OF ΔAV IN THE NORTHERN LATIN AMERICAN REGION

Negative values of ΔAV are observed at around 16°N latitude (especially for the shallower events of this area), and at some of the Santander Province (Colombia) events.

- Southern Latin America (0° -40°S)

The events of this region have their ΔAZ distributed very clearly in three areas (see Figure 44).

1. From 0° to 16°S: Mainly small negative values of ΔAZ (smaller than -4°).
2. From 16°S to 22°S: ΔAZ is increasingly positive up to values larger than 8°.
3. From 22°S to 40°S: All ΔAZ values are increasingly negative with values mainly between -3° and -12°.

The ΔAV of the events of this region can be grouped as follows (see Figure 45):

1. From 0° to 18°S: ΔAV mainly negative with values smaller than -0.52 km/sec, except for the event A 02 (9.42°S, 75.49°W) with ΔAV = 1.03 km/sec, and E 06 (15.21°S, 73.11°W) with ΔAV = 0.42 km/sec but with a poor signal at SAAS.
2. From 18°S to 25°S: ΔAV mainly positive with values up to 2.21 km/sec.
3. From 25°S to 30°S: ΔAV mainly negative with increasing values up to -1.39 km/sec, except for the events near the coastal line below 27.7°.
4. Coastal line from 27.7°S to 30.5°S: ΔAV with mainly small positive values (less than 0.5 km/sec).
5. Coastal line from 31°S to 33°S: ΔAV with mainly very small negative values close to 0.

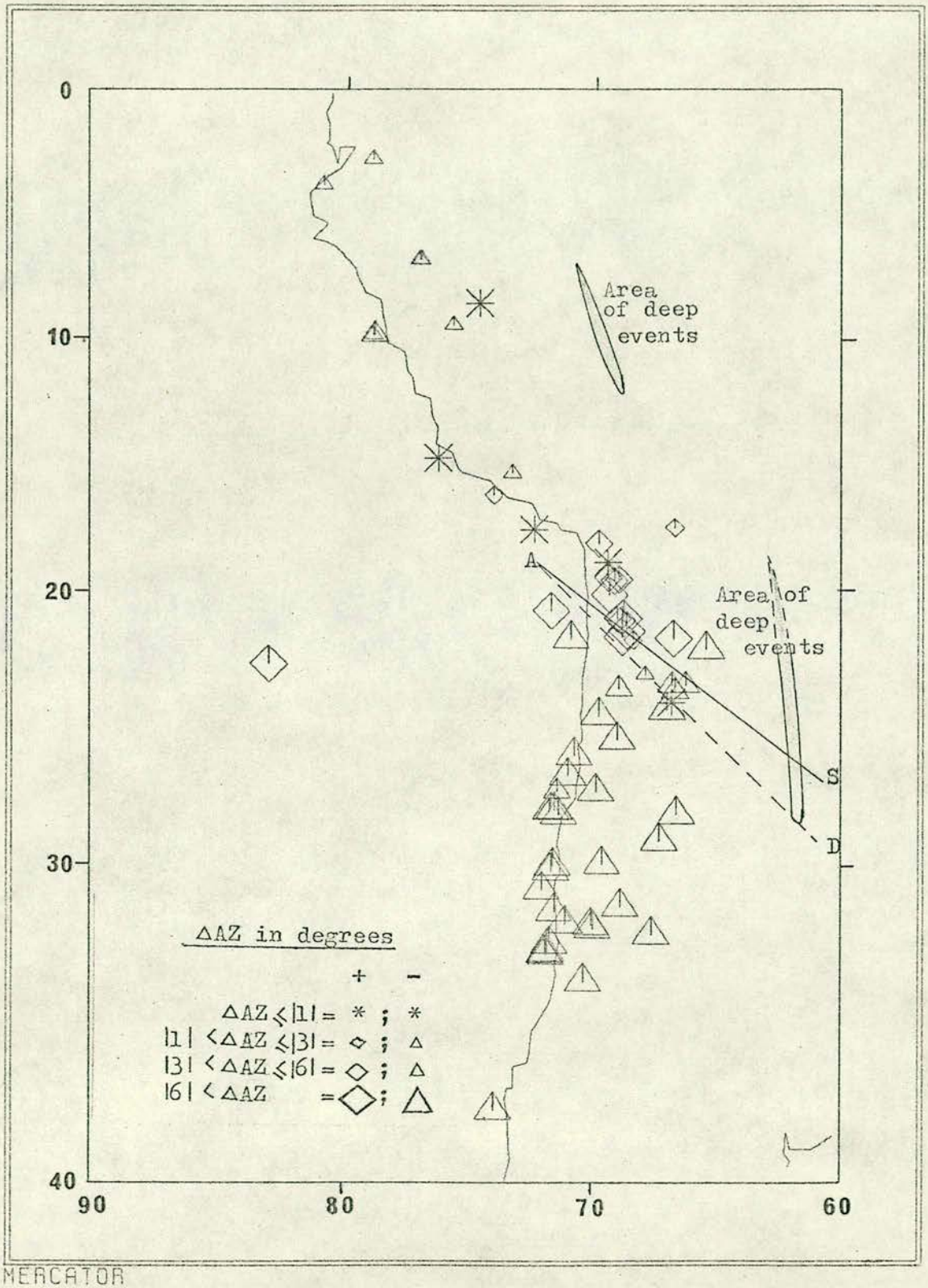

Figure 44.- DISTRIBUTION OF CORRECTED RESULTS OF ΔAZ IN THE WESTERN SOUTH AMERICA REGION

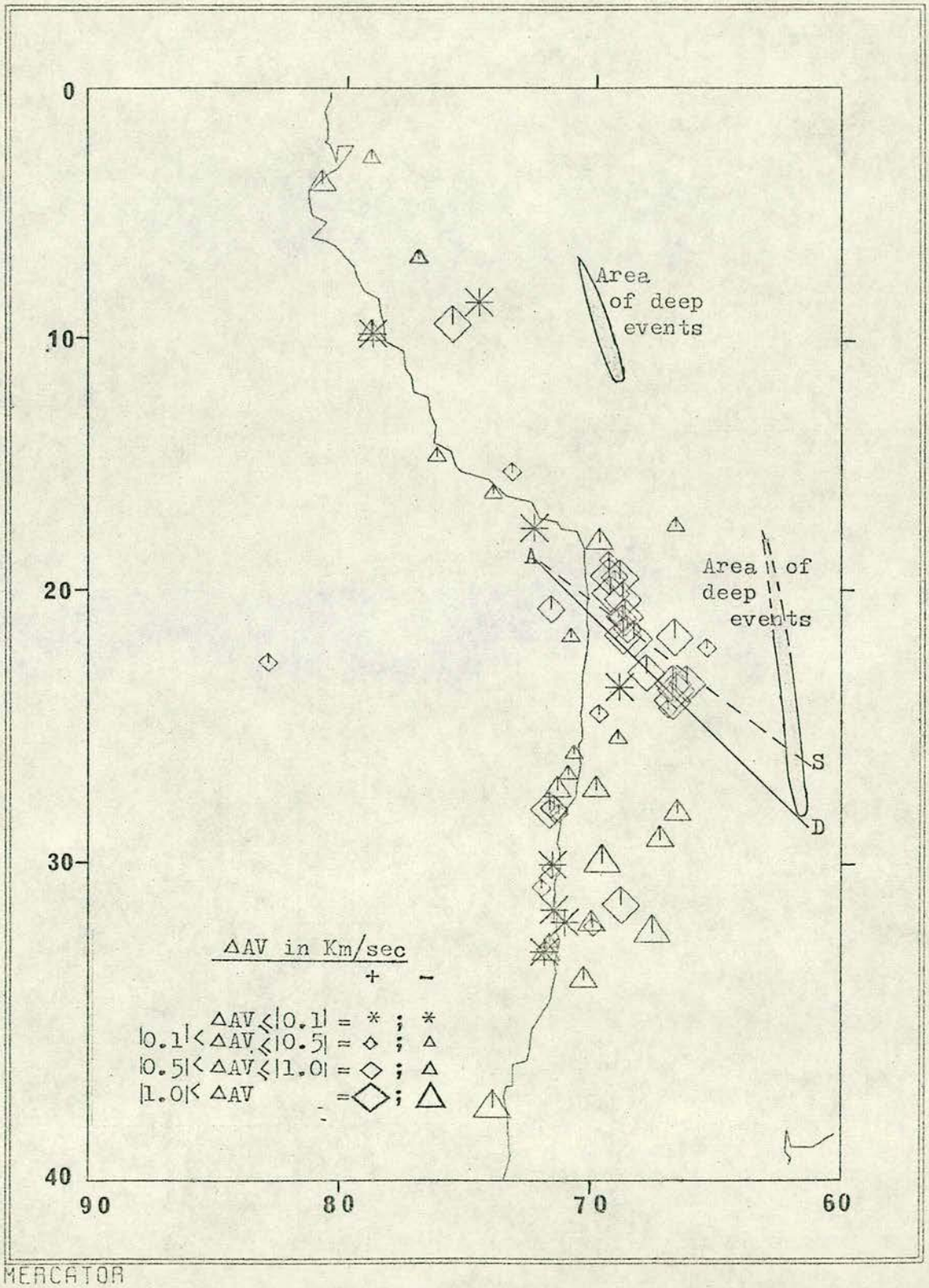

Figure 45.- DISTRIBUTION OF CORRECTED RESULTS OF ΔAV IN THE WESTERN SOUTH AMERICA REGION

6. San Juan Province, Argentina (around 32°S and 69°W): ΔAV with positive values.
7. Mendonza Province, Argentina (32°S, 67°W): presents one event with large negative ΔAV (-1.47 km/sec).
8. From 33° to 40°: only two events with a poor signal detected at SAAS occurred in this area, but both have negative values of ΔAV (-0.68 and -1.08 km/sec).

5.7.3 Azimuth and Apparent Velocity of Secondary P Phases

Every clear phase arriving between the main P and the PP phase, usually during the first 60 seconds after the onset is defined in this research as a "secondary P phase". This definition includes some high frequency-low amplitude phases that precede the main P phase in some events (see Figure 47), but excludes the reflected phases pP, sP, PP and PcP.

The observed azimuth and apparent velocity computed for the secondary P phases are included in Appendix 3-A and 3-B (without and with corrections applied respectively),together with the same parameters obtained for the main P phase and for the reflected P phases, in some events.

It was not possible to obtain a correlation between most of the observed secondary P phases, but it is possible that their existence may be due to discontinuities within the Earth's mantle, as was suggested by Niazi and Anderson (1965), Johnson (1967), Kanamori (1967), Simpson (1973), etc.. The observed secondary phases that show some correlation are the following:

1 sec

EVENT E17: Δ,17.6°; h,275 km; m_b,3.8; Exp. Az,246.8; Exp.App.V,10.7 Km/s.

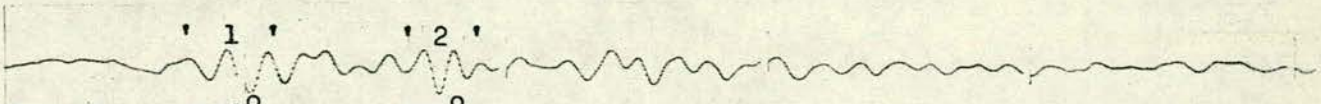

Obs.Az, 238° 251°
Obs.App.V, 10.5 Km/s. 14.0 Km/s.

EVENT A51: Δ,17.9°; h,119 km; m_b,4.0; Exp.Az,251.8; Exp.App.V,10.8 Km/s.

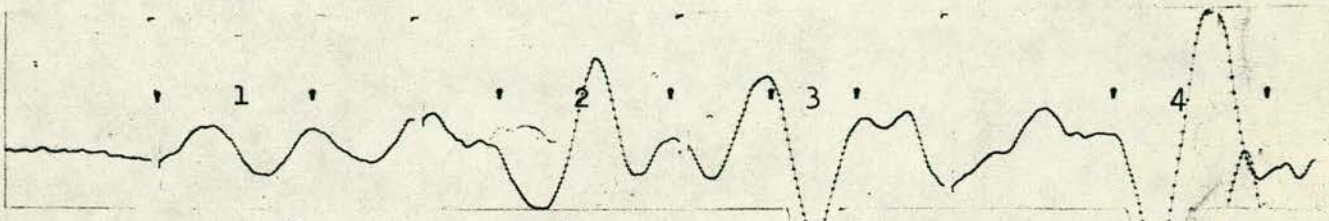

Obs.Az, 264° 267° 244° 265°
Obs.App.V, 8.7 Km/s. 9.5 Km/s. 9.5 Km/s. 10.6 Km/s.

EVENT A41: Δ,18.7°; h,215; m_b,4.5; Exp.Az,243.6°; Exp.App.V,10.8 km/s.

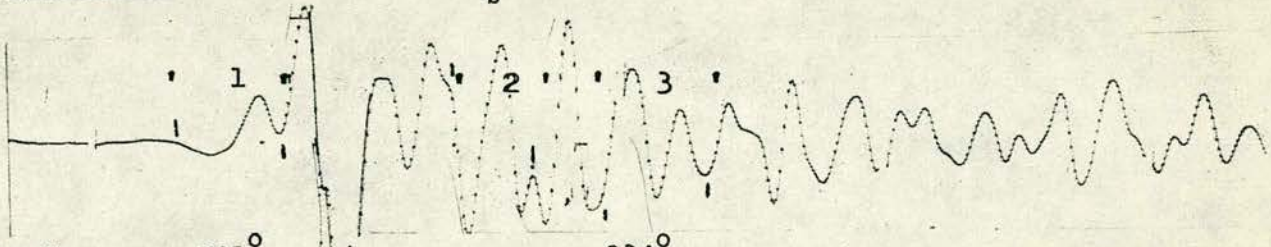

Obs.Az, 240° 234°
Obs.App.V, 11.46 Km/s. 9.2 Km/s.

EVENT E55: Δ,20.3°; h,131 Km; m_b,4.8; Exp.Az,251.2; Exp.App.V,10.9 Km/s.

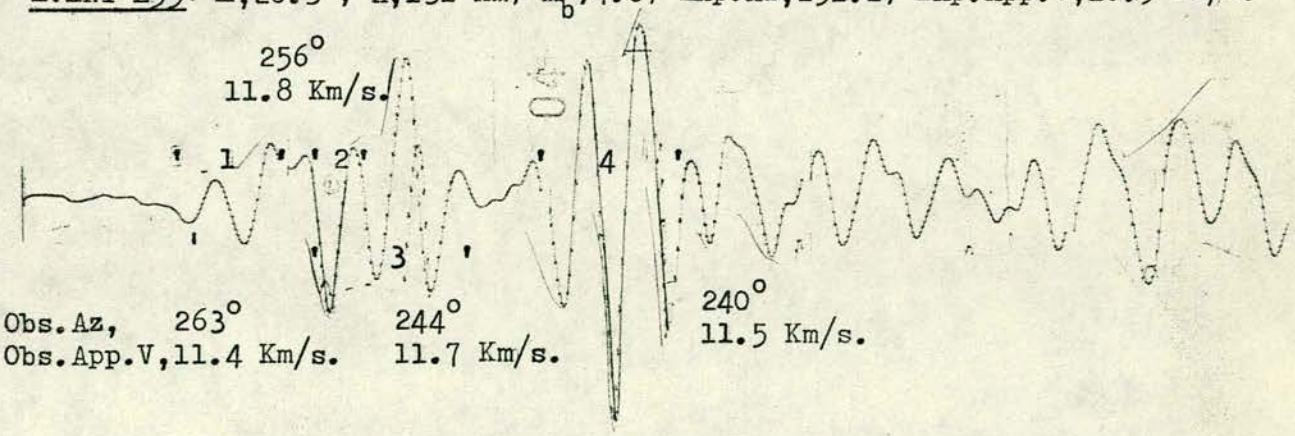

Obs.Az, 263° 244° 240°
Obs.App.V, 11.4 Km/s. 11.7 Km/s. 11.5 Km/s.

Figure 46.- SEISMOGRAMS OF SOME EVENTS RECORDED AT SAAS FROM 20°. (Signals analysed are marked as ' 3 ')

EVENT A69: Δ,20.5°;h, 121; m_b,4.5; Exp.Az,250.7°; Exp.App.V,11.0 Km/s.

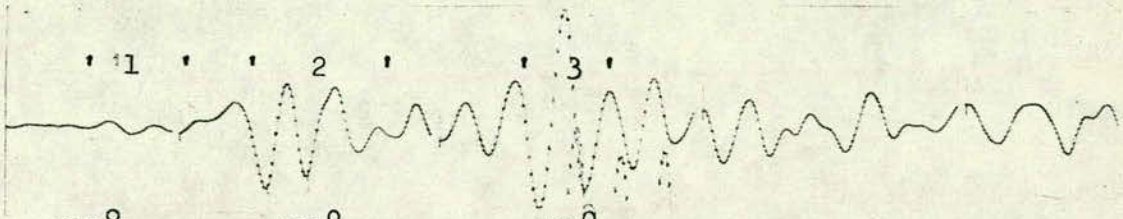

Obs.Az, 257° 257° 257°
Obs.App.V, 12.5 Km/s. 12.2 Km/s. 13.8 Km/s.

EVENT A70: Δ,20.6°; h,132; m_b,5.2; Exp.Az,258.8°; Exp.App.V,11.0 Km/s.

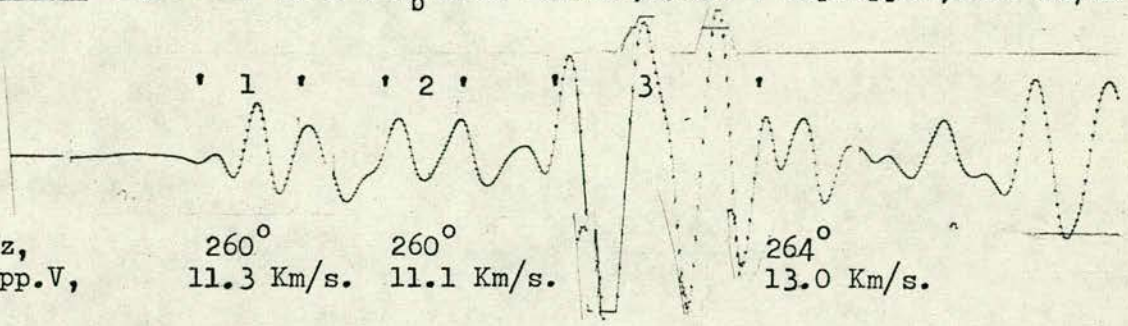

Obs.Az, 260° 260° 264°
Obs.App.V, 11.3 Km/s. 11.1 Km/s. 13.0 Km/s.

EVENT A48: Δ,20.7°; h,127; m_b,4.0; Exp.Az,257.1°; Exp.App.V,11.0 Km/s.

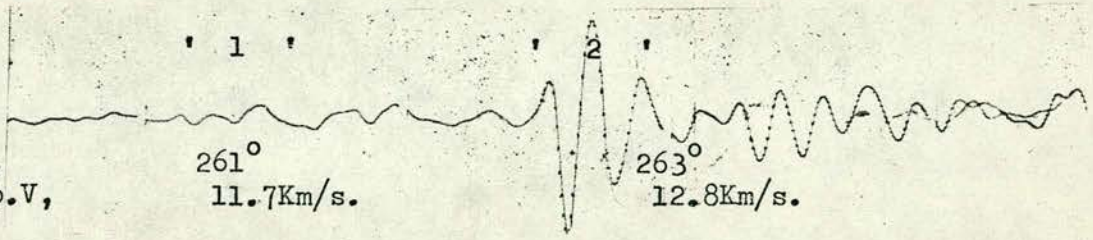

Obs.Az, 261° 263°
Obs.App.V, 11.7Km/s. 12.8Km/s.

EVENT A12: Δ,20.9°; h,162; m_b,3.6; Exp.Az, 260.9°; Exp.App.V,11.2 Km/s.

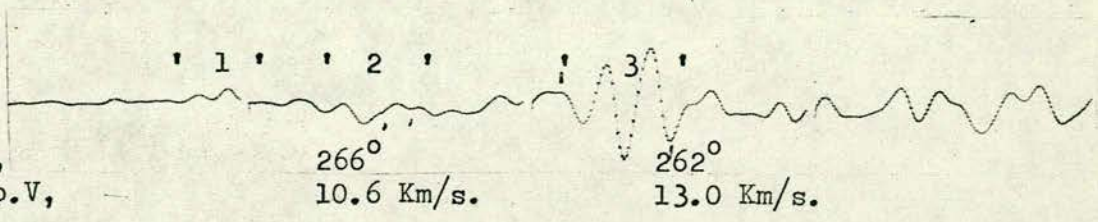

Obs.Az, 266° 262°
Obs.App.V, 10.6 Km/s. 13.0 Km/s.

Figure 46 (Cont.)

- Multiple phases from events of Δ around 20°: several events from the Northwest of Argentina, North of Chile, Chile-Bolivia border, Bolivia and Peru-Bolivia border are included in this range of distance (Δ between 17.6° and 22.3°). Some of these events, including the observed azimuth and apparent velocity of the P phases that were analysed, are shown in Figure 46. Most of these events have depths greater than 100 km, and most of the observed apparent velocities are larger than expected, especially in the case of the large amplitude secondary phase observed in events E41, A69, A70 and A48 of Figure 46.
- Precursor to main P phases: some events show a small phase, which arrives just before the main P (within a second or two) and that usually has higher frequency than the other P phases (main, secondary and reflected). Some examples of these precursor phases are illustrated in Figure 47. The main characteristic of most of the observed precursor phases is their value of apparent velocity which is larger than the value of this parameter observed for the main P phase.
- Multiple phases from shallow events with Δ larger than 40°: These events needed a longer trace to be processed, therefore up to 4 minutes of recorded data were digitized. The observed azimuth and apparent velocity of the phases which were analysed are included in Appendix 3. The relative arrival time of the phases that show some important results are presented in Table 9.

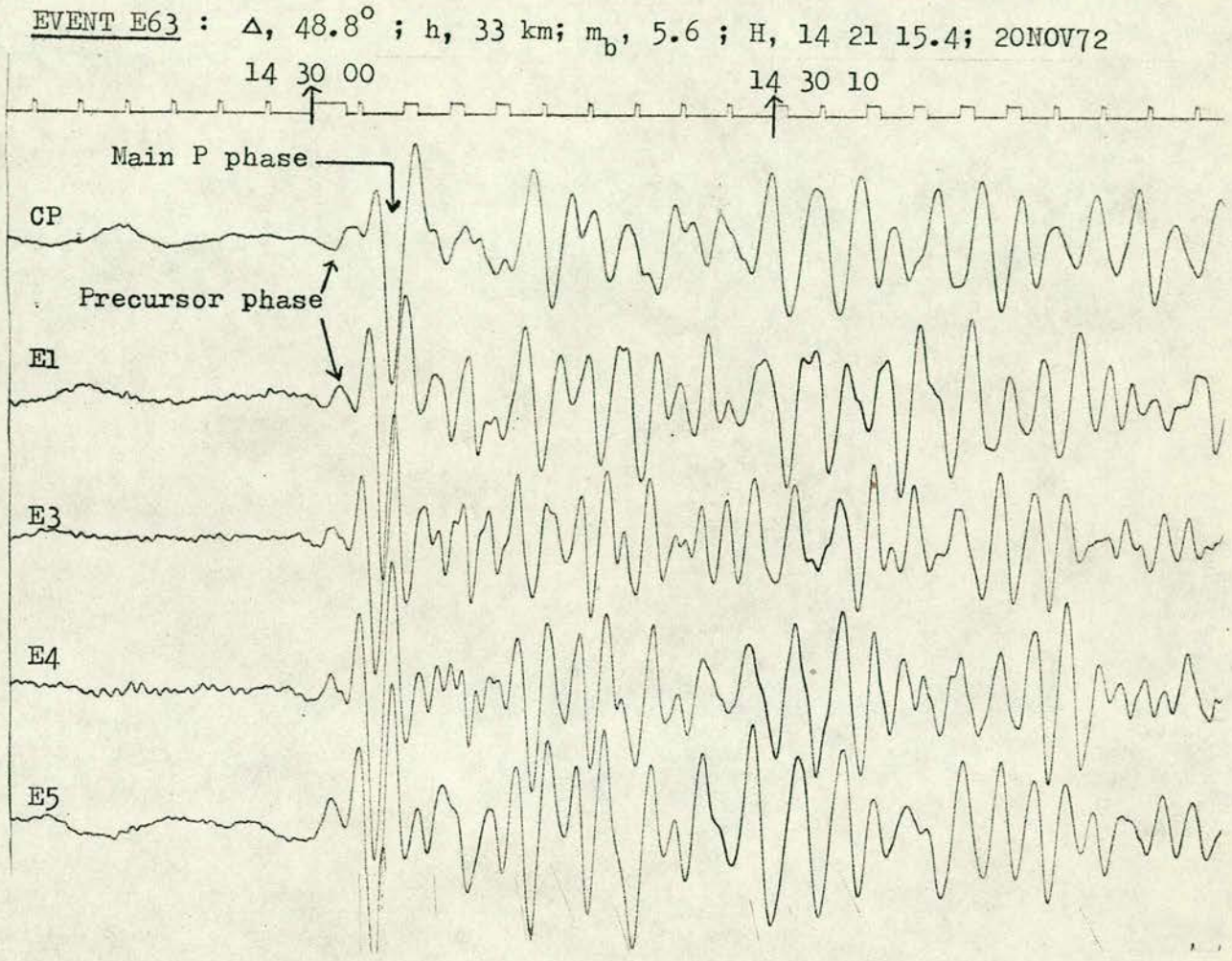

Figure 47.- SEISMOGRAM SHOWING A TYPICAL HIGH FREQUENCY PRECURSOR PHASE

TABLE 9

SIGNAL NO.	EVENTS N.		
	E1	E13	E14
1	PRE	PRE ?	PRE
2	P	P	P
3	pP	4	2
4	11*	8	6
5	19	14	9
6		18	19
7		22	25
8		28	36
9		31	39
10		37	42
11		42	49
12		55	52
13		65	60
14		69	63
15		77	69
16		85	77
17		92	91
18		-	101
19		-	108
20		114	117
21		123	125

* Number of seconds after onset

PRE: Precursor phase

5.7.4 Azimuth and Apparent Velocity of Reflected Phases

In some events, it has been possible to identify some reflected phases such as pP, PP and PcP. Appendix 3-B includes the reflected phases which were possible to identify by their apparent velocity value observed at SAAS.

CHAPTER 6

INTERPRETATION OF THE RESULTS

6.1 Introduction

The means and the methods of obtaining certain seismic observations for events which occurred in several regions of the Earth, within 95° of SAAS, have already been described in the first chapters of this thesis. These have led to four different kinds of residuals, as follows: travel time and magnitude residuals analysed in Chapter 4, and azimuth and apparent velocity residuals analysed in Chapter 5.

The objective of this chapter is to correlate these residuals, observed at SAAS, with the main tectonic features of the regions being studied, with special attention to some regions of South America.

The tectonic models discussed in this work are based on the concepts of the new plate tectonics theory. For this reason, the most important postulates of this theory, which could be relevant to the present research, are presented in this chapter, as well as the most important results of some studies of South American tectonics (including the tectonics of the Caribbean region).

The fundamental argument of this research, as mentioned before, is based on the relationship that the observed residuals could have with possible refractions that lateral and horizontal discontinuities of the Earth's interior could introduce to the seismic rays travelling from the source to the recording station. For this reason, the results of refractions, obeying Snell's laws, at different sets of

possible boundaries in the upper mantle under western South America, are presented. The distribution of velocities at the boundaries have been taken from previous tectonic studies.

6.2 Plate Tectonics Theory

The original concepts of the plate tectonics theory were proposed almost simultaneously by McKenzie and Parker (1967) and by Morgan (1968). They based their hypotheses on the concepts of ocean-floor spreading and the formation of oceanic crust suggested by Dietz (1961) and by Hess (1962), and on the transform faults study made by Wilson (1965). The theory of plate tectonics provides a mechanism for continental drift which was proposed originally by A. Wegener in 1912, and it also provides a means of correlating the observed seismicity of a region with its tectonic structures or to attempt some explanation of certain seismic anomalies observed at some stations, such as the residuals observed at SAAS and presented in chapters 4 and 5 of this thesis.

The basic idea of the plate tectonics theory is that the outermost shell of the solid Earth, called the lithosphere, is divided in several rigid plates which grow along relatively narrow linear belts (ridges), are transported on a less rigid shell called the asthenosphere and are consumed or destroyed at the compression boundaries (where the crust is shortened by thickening in young folded mountain ranges, or where there are ocean trenches).

The basic concepts and more important features of plate tectonics as visualised by Dietz and Holden (1970) are summarised in Figure 48, in the following way:

A. The process begins when a spreading rift develops under a continent (e.g. the original South America-Africa continent) that is resting on a single crustal plate (lithosphere). Molten basalt from the asthenosphere spills out.

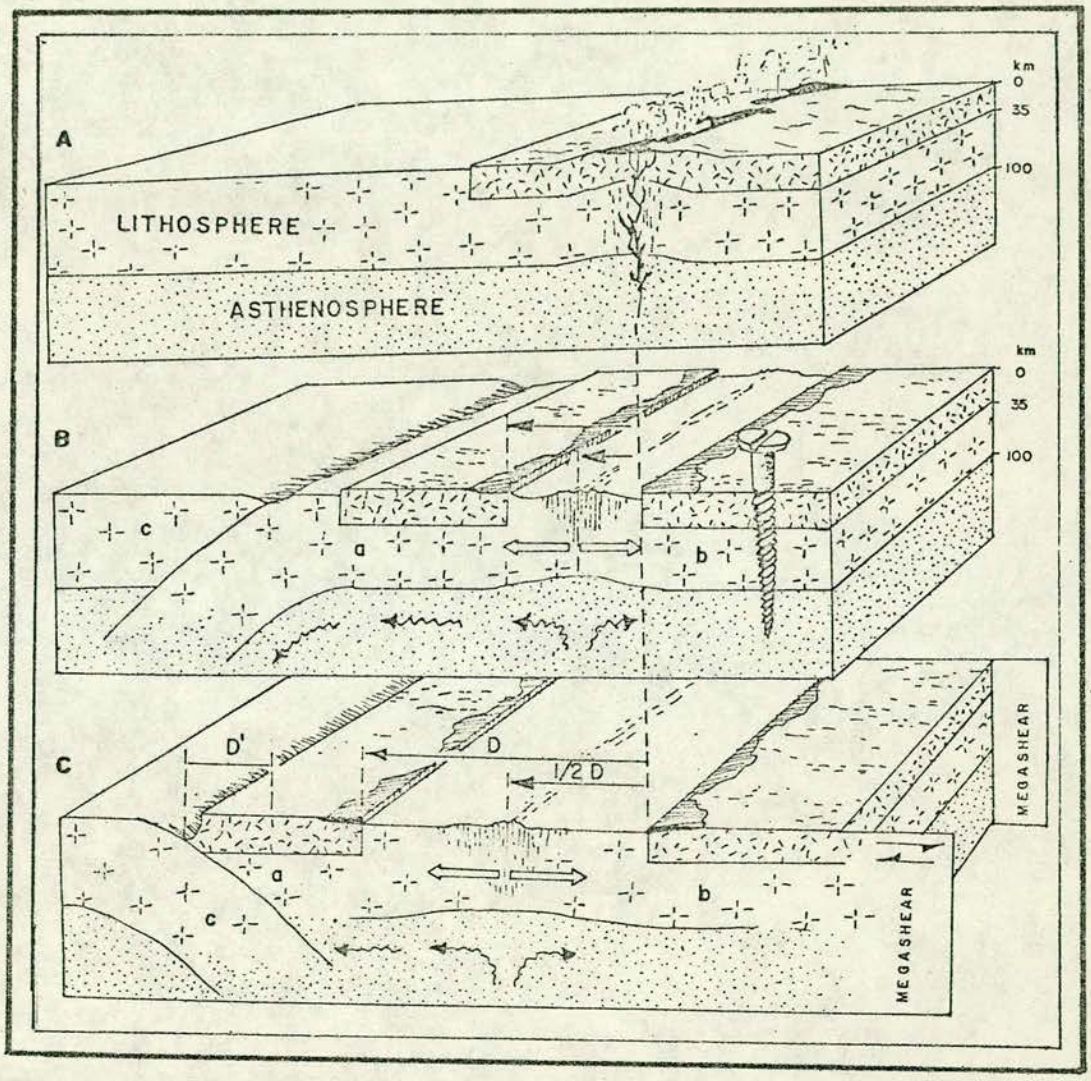

Figure 48.- BASIC CONCEPTS OF THE PLATE TECTONICS THEORY

After Dietz and Holden (1970).

B. A zone of subduction, or trench (e.g. Peru-Chile trench), is formed into which oceanic crust of the new moving plate (a) is pulled and "consumed". As the new continent (e.g. South America) carried by plate (a) is rafted to the left, a new ocean basin (e.g. Mid-Atlantic Ridge) is created between the two land masses, preserving the rift in its central part.

C. In the third stage, the continent on plate (a), which has a low density (e.g. South America) encounters and overrides the trench for some distance (D'). As a consequence orogenic processes are activated (e.g. Andes), and eventually the lithosphere slab reverses, or flips, its directions from west-dipping to east-dipping. Plate (b) (i.e. African plate) remains arbitrarily fixed for illustration purposes only.

The idea of the "flip" of the slab's direction suggested by Dietz and Holden (1970) is a discussible argument, which is not generally accepted, but for which there exists some possible evidence (i.e. in the Caribbean region).

These are the principles of this new theory, but it must be borne in mind that the tectonic processes explained in Figure 48 must be more complicated and differ from region to region. There are some conflicting evidences and some unsolved problem which are the subject of continuous research; some of these problems which chiefly concerns seismologists as pointed out by Isacks et al (1968), are regarding the characteristic pattern of island arcs and ocean ridges, and the shape and size of the down-going slabs. It is also

not clear what exactly happens near the trenches to the lithosphere of the colliding plate that is not consumed. These points are relevant in the discussion of this work.

Le Pichon (1968) divided the lithosphere into six principal plates and calculated the rates and directions of underthursting at the subduction zones (see Figure 49). He suggested, from his calculations, that the Pacific plate is reducing its size, the American, Eurasian and African plates are increasing their sizes, and that the Indian and Antarctic plates are not changing greatly in size.

One of the most convincing pieces of evidence in favour of continental drift, even before Wegner's postulations, is the good agreement between opposite coastlines across the Atlantic ocean. The Pangaea suggested by Wegner, as the single Palaeozoic continent, that broke into fragments which tended to separate, has been reconstructed by Dietz and Holden (1970) since the Permian to the present. Geological and paleomagnetic evidences have been used in this reconstruction, which has led to the conclusion that there is an overall north-western drift of South America. A clear indication of the north-western drift of South America (and of the north-eastern drift of Africa) are the two chains in the Southern Atlantic (see Figure 50) called Rio Grande (cc') and Walvis (cc"), which form a V shape, and which originated about 135 million years ago from the "thermal centre" Walvis(c).

The time scale for the current episode of sea-floor spreading and continental drift is still a matter of argument. The geomagnetic

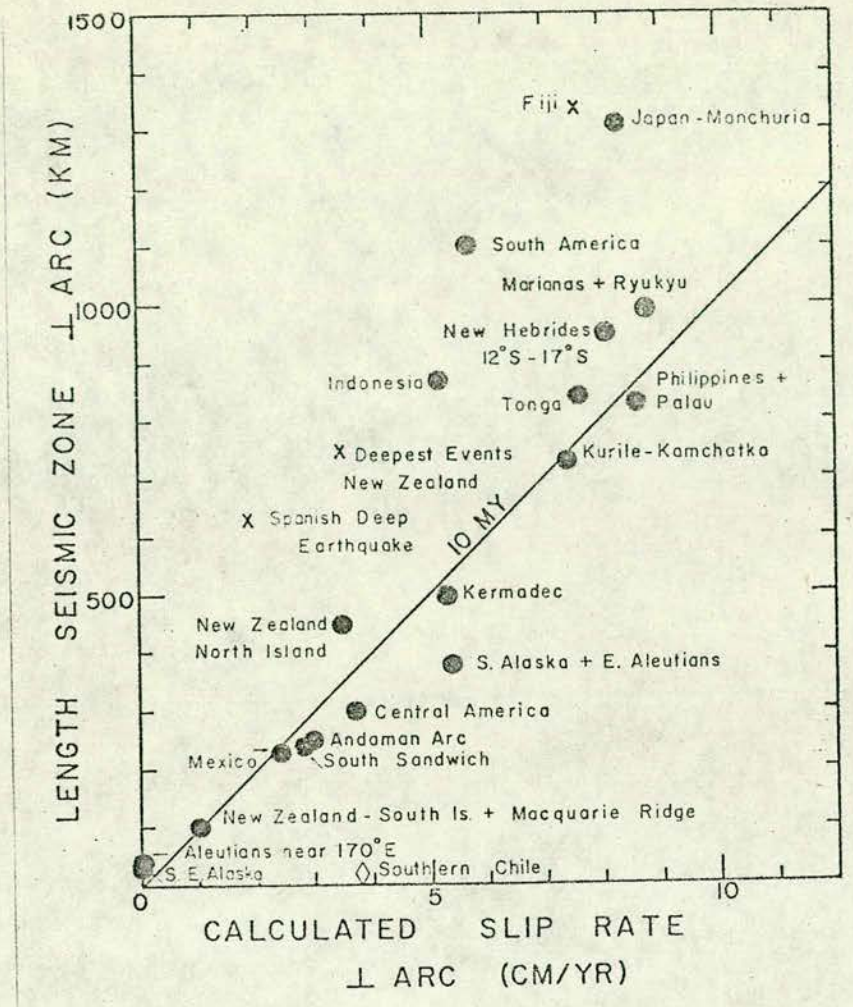

Figure 49.- LE PICHON'S (1968) CALCULATED RATES OF CONVECTION AND LENGTH OF SEISMIC ZONE FOR VARIOUS ISLAND ARCS AND ARC-LIKE FEATURES. After Isacks et al (1968).

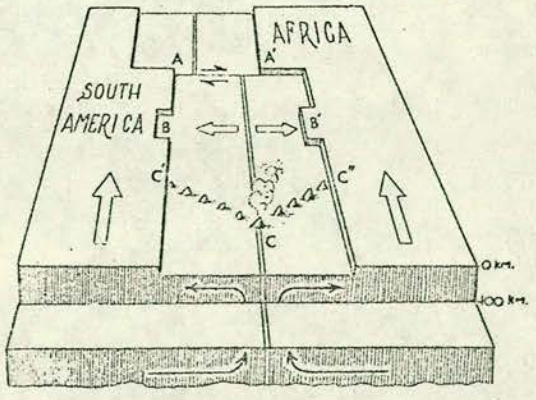

Figure 50.- DIAGRAM SHOWING WILSON'S (1965) IDEA OF TRANSCURRENT FAULTS AND THE N-W DRIFT OF SOUTH AMERICA. After Dietz and Holden (1970).

time-scale based on a uniform spreading rate in the South Atlantic ocean (Heirtzler, 1968)[1] indicates that it started in the late Mesozoic era (79 Million years ago). Ewing and Ewing (1967) indicates that the most recent episode of spreading began about 10 million years ago, after a break in spreading and continental drift which lasted 30 to 40 million years. Bott (1971) presents some results of the Deep Sea Drilling Project on the South Atlantic ocean, published by A.E. Maxwell et al, 1970. These results confirmed the predictions of the Vine-Matthews hypothesis (the past history of the Earth's magnetic field reversals may be fossilized as oceanic magnetic anomalies) and also confirm the theory of ocean-floor spreading, and the timing obtained by Heirtzler (1968)[1] for the same area. The continuity of the sea-floor spreading process in the last 70 million years was also established by the drilling programme results, which do/es not agree with the break in the continental drift process, suggested by Ewing and Ewing (1967). It is important to have a good assessment of the time involved in the drifting process of South America, and consequently of the time involved in the formation of the Andes and of its down-going slab, to be able to figure the structural conditions under the seismic regions of South America.

The interconnection between Seismology and the plate tectonics theory was thoroughly analysed by Isacks et al (1968). By studying some well located events in the Tonga Islands area, they were able to prove the existence of a down-going slab of the lithosphere in that area. They suggested that the thickness of the seismic zone

---

(1) Should read (Heirtzler et al, 1968)

in the slab could vary between 20 and 100 km. They pointed out that the termination of a seismic arc could be in the form of an abrupt or gradual transition to a transform fault, by a decrease in the rate of convergence to zero, or by some combinations of these. Some of the characteristics found for the Tonga arc slab have been found by other researchers under the Andean region of South America, as is shown in the next section.

Regions of high attenuation associated with down-going slabs were detected by Oliver and Isacks (1967) and by Barazangi and Isacks (1971) in the Tonga arc. A region of extremely low Q was observed in the concave side of the Tonga arc. See Figure 51. High Q value for the lithosphere (and slab) and for the mesosphere and low Q value for the asthenosphere were also indicated by the authors mentioned above.

The development of mountain belts based on the plate tectonics theory was presented by Dewey and Bird (1970). Cordilleran-type mountain belts (like the Andes) developed by the underthrusting of a continent by an oceanic plate are illustrated in Figure 52 as presented by Dewey and Bird (1970).

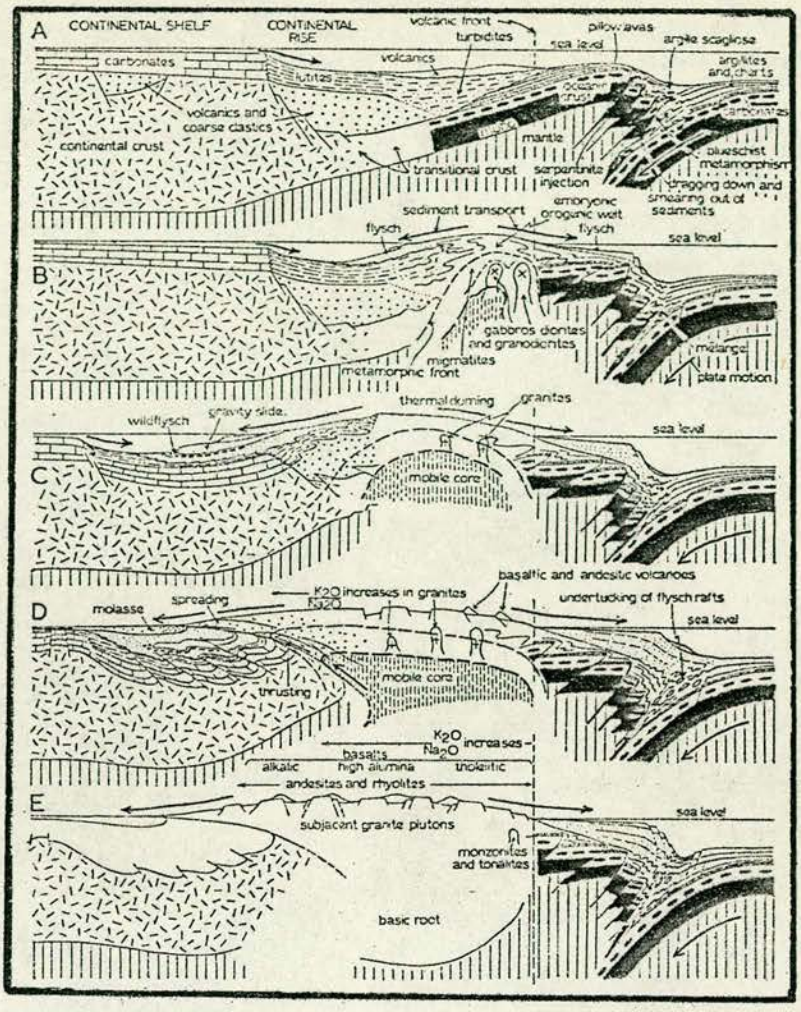

Figure 52.- EVOLUTION OF A CORDILLERAN-TYPE MOUNTAIN BELT. After Dewey and Bird (1970).

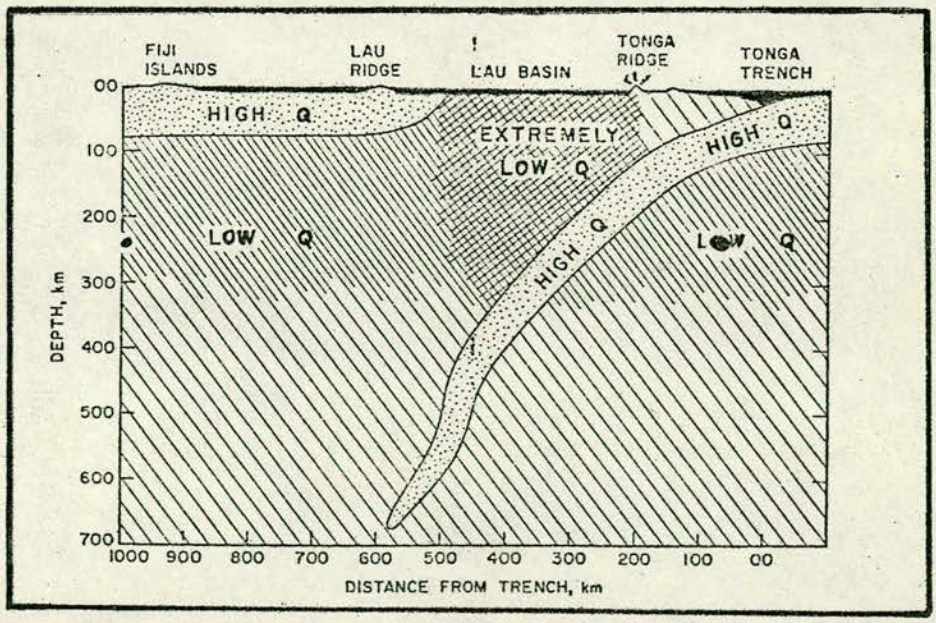

Figure 51.- HIGH AND LOW-ATTENUATION ZONES UNDER THE TONGA ARC. After Barazangi and Isacks (1971).

6.3 Review of Some Studies on South American Tectonics

Several gravity surveys have been carried out in most of the Andean countries of South America with the purpose of studying the internal constitution of the Andes, especially in its southern part. Since the 1950's the Carnegie Institution of Washington, through its Department of Terrestrial Magnetism, has been involved in several Geophysical projects in cooperation with South American institutions, especially in the branches of Seismology, Terrestrial Magnetism and Electrical Conductivity.

Aldrich et al (1958) by using seismic refraction data reported the Andean root to reach a depth of 70 km in the Chile-Peru-Bolivia border region, and suggested a two layer model for the crust. Using gravity data, Lomnitz (1962) arrived at similar conclusions regarding the Andean root under the Chile-Peru-Bolivia border region (18^{o}S), and suggested a reduction of the thickness of the root of the Andes towards the South, beginning at 23^{o}S, reaching values as low as 50 km at 35^{o}S, which may get smaller still in the lower latitudes. Dragicevic (1970) arrived at similar conclusions to those of Lomnitz(1962) for the Chilean Andes structure, determining the densities for the crust (2.84 gr/cm^3) and for the lithosphere (3.27 gr/cm^3). These studies show a correlation between the topography and the deep structure of the Andean root, but the most important observation that concerns the present study is the change in the thickness of the Andes found by Lomnitz which begins at around 23^{o}S.

Woollard (1960) re-examined the refraction data obtained by the Carnegie group in 1956-1957 and, using secondary arrivals, obtained

the following distributions of P velocities under the Andes: Surface layers, 5.3 km/sec; up to 25 km of depth, 6.2 km/sec; from 25 to 48 km, 6.7 km/sec; and 8.0 km/sec down to 70 km.

Fisher and Raitt (1962) carried out some offshore explosion studies of the Peru-Chile trench, in front of the Peruvian coast, finding an oceanic crust of 11 km (including 4 km of water) which increases to about 17 km under the trench. James (1971) by using phase and group velocities of both Rayleigh and Love waves obtained models of the crust and upper mantle for the west-central South America region. The results of these two investigations are shown in Figure 53. From gravity data, James (1971), also reached results which agree with those obtained from his and other seismic studies. He concluded that the maximum crustal thickness in other parts of the Andes not associated with the "altiplano" (Lake Titicaca plateau) where it is over 70 km, may be of the order of 55-60 km.

Some seismic studies in the Chile Central area, between 30^{o}S and 35^{o}S, agree with the results obtained from the gravity data (Chuaqui, 1973) and suggested a P velocity of 6.1 km/sec in the crust and of 8.1 km/sec in the lithosphere. This last value is different to that found by Olea (1966) for the northern region of Chile, where it is assumed to be 7-8 km/sec. Chuaqui's crustal velocity is lower than that suggested by Woollard (1960).

The tectonic implications of the large Chilean earthquake of May 1960 (around 38^{o}S) were studied by Plafker (1972). He suggested the fault strike to be N 10^{o}E, a fault dip of 35^{o} to the East (down-dip width of 120 km), and that the dip slip displacements

derived for the megathrust showed a convergence azimuth of around N80°E which was different from the convergence azimuth derived from the earthquake-related displacements (N94°E). Le Pichon (1968) and Isack's et al (1968 convergence azimuths for this area (Southern Chile) were N79°E and N70°E respectively. For the northern part of the Andes (Peru), Le Pichon (1968) assumes almost the same convergence azimuth as for the southern Andes, while Isacks et al (1968) found an eastward convergence azimuth derived from nodal plane solutions of earthquakes.

The rate of crustal convergence in western South America from paleomagnetic data is assumed to vary from 7 to 12 cm/year, as discussed in Plafker (1972). At the latitude of southern Chile it is assumed that the East Pacific rise and the Mid-Atlantic ridge have half-spreading rates of 5 and 2 cm/year respectively. To explain the maximum convergence rate, the East Pacific plate must be migrating, eastward relative to the trench, at 10 cm/year, and the Americas plate be migrating, westward relative to the trench, at 2 cm/year. Morgan et al (1969), from magnetic anomalies on the Chile rise, gives an average half-spreading rate of 10 cm/year, during the last 25 million years, and a rate of about 4.6 cm/year between 25 and 55 million years ago. Herron and Hayes (1969) suggested that this change in rate occurred during the last 10 million years. Plafker (1972) finds these convergence rates too low, by a factor of 2 or 3, to explain the 20 metres of thrust observed after the may 1960 Chilean event.

There appears to be a difference on the behaviour of the down-going slab under the northern and southern parts of western

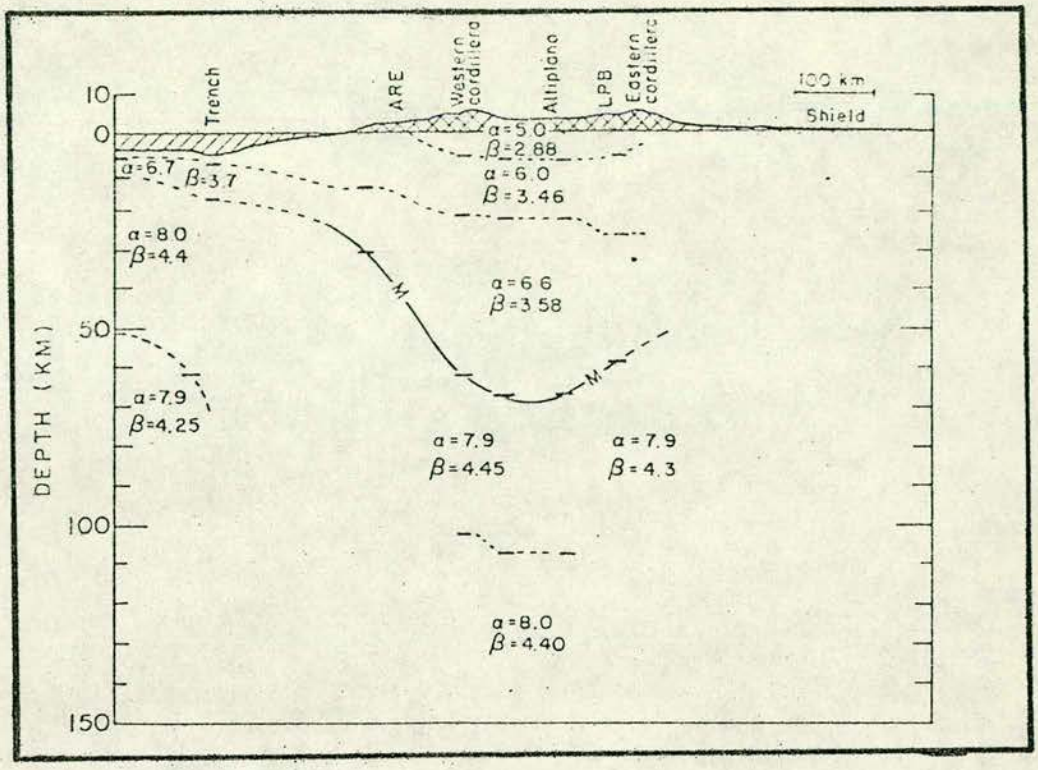

Figure 53.- CROSS SECTION OF CRUSTAL AND UPPER MANTLE STRUCTURE, ACROSS SOUTHERN PERU, AS INFERRED FROM SURFACE WAVES RESULTS. After James (1971).

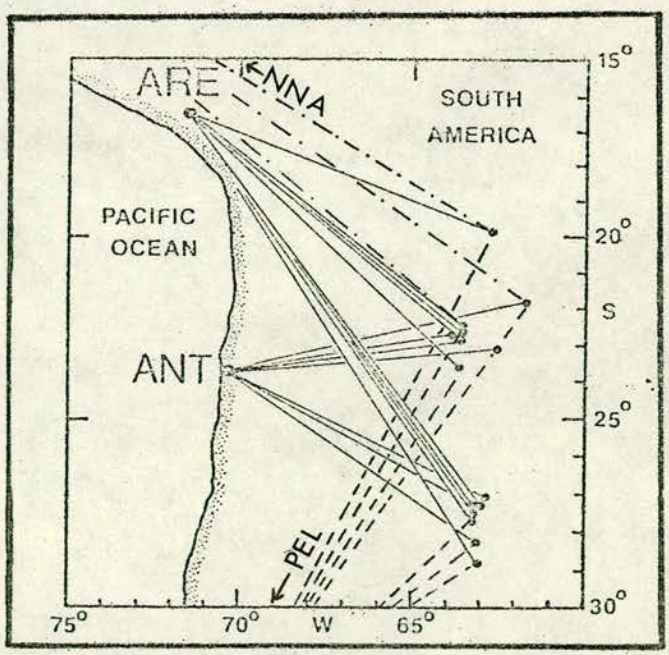

Figure 54.- PATHS FROM DEEP EVENTS OF NORTHERN ARGENTINA TO PERUVIAN AND CHILEAN STATIONS. After Isacks and Barazangi (1973).

South America. The azimuth of convergence seems to be slightly different, and the lack of deep events in the southern part of South America suggests a smaller protrusion of the slab into the Earth, which could be a consequence of different rates of convergence. This in turn could be caused by differences on the relative drift of the East Pacific and Americas plates, at different latitudes of South America.

Lateral variations in the attenuation of Sn phases (S phase travelling in the uppermost part of the mantle), were studied by Molnar and Oliver (1969) for different regions of the Earth. For the Andean region of western South America they found a similar distribution of Q values to those observed in the Fiji-Tonga region (see Figure 51).

Isacks and Barazangi (1973) carried out a study of high frequency shear waves arriving after the S phase from deep South American earthquakes (North Argentina-South Bolivia), as recorded at Nana (NNA), Arequipa (ARE), Antofagasta (ANT) and Peldehue (PEL). See Figure 54. They defined these high frequency shear waves as waves guided by the descending lithosphere and because they looked like the S waves of near events, in frequency and velocity, they were named as Sn phases. These Sn phases were well observed at NNA and ARE and probably at ANT, but not at PEL. The observations at ANT were masked by the P signals in the case of large earthquakes and were not reliable (poor location) in the case of small ones. Nevertheless, the clear waves of a few well located deep events in the Argentina-Bolivia border did not show at ANT characteristics of waves guided by the slab.

The lack of observation of Sn phases at PEL and the attenuation observed at this station for S phases originated at the deep events of the Argentina-Bolivia border, brought Isacks and Barazangi (1973) to the following conclusion: "These observations plus other data on Sn and Lg propagation along the west coast of Chile suggest the existence of a major structural feature near latitudes 28^{o}-33^{o}S that affects the propagation of high frequency shear waves between the zone of deep events and PEL. For example, the descending slab may be torn into two separate segments". ANT observations could also be explained by this form of reasoning, assuming that the proposed division of the slab is to the North of ANT, as is postulated in the present research.

The transmission of the high frequency shear waves studied by Isacks and Barazangi (1973), as guided waves in the descending lithosphere suggests the continuity of the slab, at least between the deep events of the Argentina-Bolivia border and the Peruvian coast between Nana and Arequipa. Some deep events from the Peru-Brazil border studied by Molnar and Oliver (1969) and recorded at NNA and ARE, also suggest the continuity in that part of the slab. The continuity of the slab under the Peruvian Andes, is also supported by this research.

The late arrival time of S phases from the deep Argentina-Bolivia border events, recorded at NNA and ARE between 13^{o} and 16^{o} of distance, suggested to Isack and Barazangi a rapid increase in velocity near 650-700 km as compared with the Jeffreys-Bullen velocity distribution model. In the present research some evidence of this

high velocity anomaly has also been detected and will be discussed later on.

Geological, petrochemical and geochronological studies in the Andean region between 26°S and 29°S were carried out by Clark et al (1973). They concluded that the Eastern Pacific plate has been continuously consumed under the Americas plate, during the development of the Andean orogen from the late Triassic to the present. Most of the ore deposits in this region, according to Clark et al (1973), were derived largely from subducted oceanic sediments and basalts. In contrast, they noticed a 2000 x 200 km belt of economic tin mineralization ranging in age from Lower Paleozoic to Neogene, which is extended from northwestern Argentina to southern Peru, giving a "persuasive evidence for the existence of a zone anomalously rich in that metal in the mantle." It is necessary to mention that the belt of tin mineralization reported by Clark et al (1973) coincides with a major tectonic feature suggested in the present study.

Another suggestion which favours the existence of an anomaly in the descending slab under the Chilean Andes, is mentioned by Clark et al (1973), "The Neogene-Pleistocene development of E-W-trending linear arrays of volcanoes and of qualitatively differing geomorphological regimes around 27°S, coinciding with abrupt changes in the present depth of the Peru-Chile trench and distribution of earthquake foci, suggest the existence there of a significant discontinuity in the descending plate, perhaps initiated during the Mio-Pliocene "break-out".

Another region of interest to the present research is the northern part of South America, the Caribbean Sea, Central America and Mexico.

Due to the complexity of its structure there are different points of view regarding the tectonic history of this region.

Freeland and Dietz (1971) suggested the development of this region in seven time sequence reconstructions, from the Palaeozoic to the present. They related its evolution to plate junctions between North America, South America and Africa, before the separation started, and to strike-slip, extensional and compressional motions as the two American plates moved westward. They suggested three microcontinents filling the Pangaea gap between North America, South America and Africa (Yucatan, Nicaragua - Honduras and Bahamas). Another craton, Oaxaca, was placed along western Mexico. The Isthmus of Panama and the Antilles, according to Freeland and Dietz, are new-cratons created in Mesozoic-Caenozoic time. When the South American plate started drifting westward from Africa, at the end of the Jurassic (135 million years ago) the Caribbean Sea was created.

During the end of the Lower Cretaceous (100 million years ago), according to Freeland and Dietz, the South American plate shifted to a more northerly drift, initiating a subduction region and the orogeny existent along northern Venezuela. (This change in the direction of the South American drift is one of the arguments that is strongly supported in the present research.) After this, the Caribbean Sea attained its modern aspect.

The origin of the Greater Antilles, was explained by Freeland and Dietz (1971) by the split of the Jurassic sediments of the Gulf of Honduras and East coast of Nicaracua, during the Lower

Cretaceous. The two parts which resulted from the split, drifted north eastward with respect to North America forming the nucleus of proto-Cuba and the proto-Hispaniola. Later, the proto-Hispaniola nucleus was subdivided into various blocks forming Jamaica, Puerto Rico, the Virgin Islands, etc.. The Lesser Antillas arc, according to Freeland and Dietz (1971) was initiated as a subduction zone, 250 km to the West of its present position which later migrated to the East. Freeland and Dietz suggest that throughout the Tertiary, interaction continued between the Caribbean blocks, and that the North American plate drifted faster (westward) than the South American plate (northwestward) slightly closing the Caribbean Region.

The Caribbean area according to Freeland and Dietz, is a subplate attached to the South American plate, "with little or no movement between them at this time". The Cayman-Puerto Rico megashear separates the Caribbean-South American plate from the North American plate which includes the Gulf of Mexico, Yucatan, Cuba and the Bahamas. The East and West limits of the Caribbean are occupied by subduction areas with inward slabs (see Figure 55).

Mattson (1972) suggested that the idea of activation and collision types of plate convergence at continental margins, applied to oceanic crusts, offers a partial solution to the differing development of the Yucatan-Cuba and the Nicaragua-Hispaniola areas.

a)

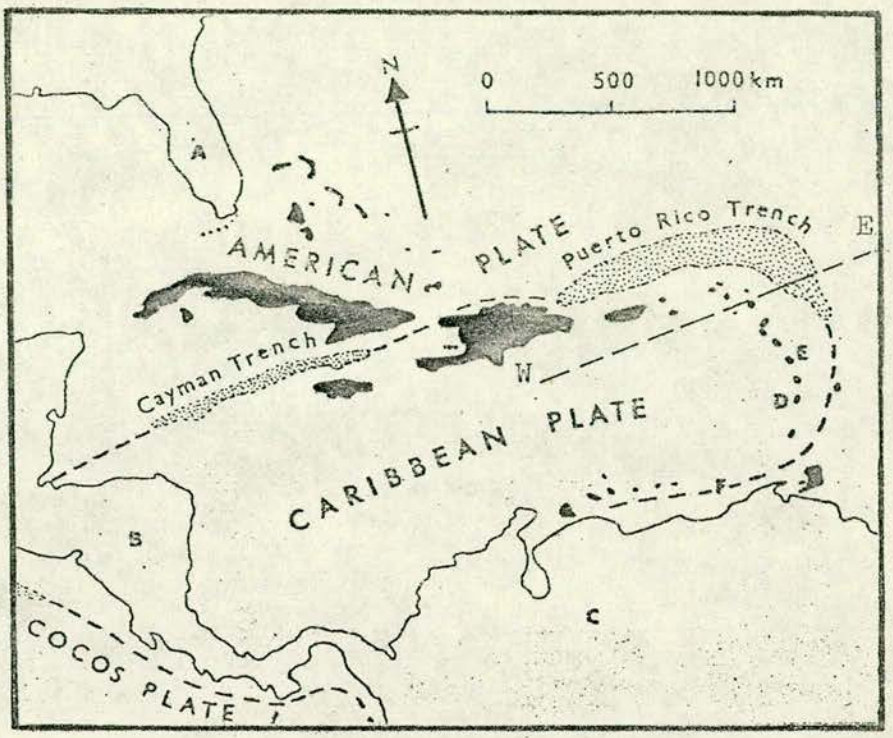

A, Florida; B, Central America; C, South America; D, Martinique; E, St Vincent; F, boundary between the American Plate and the Caribbean Plate.

b)

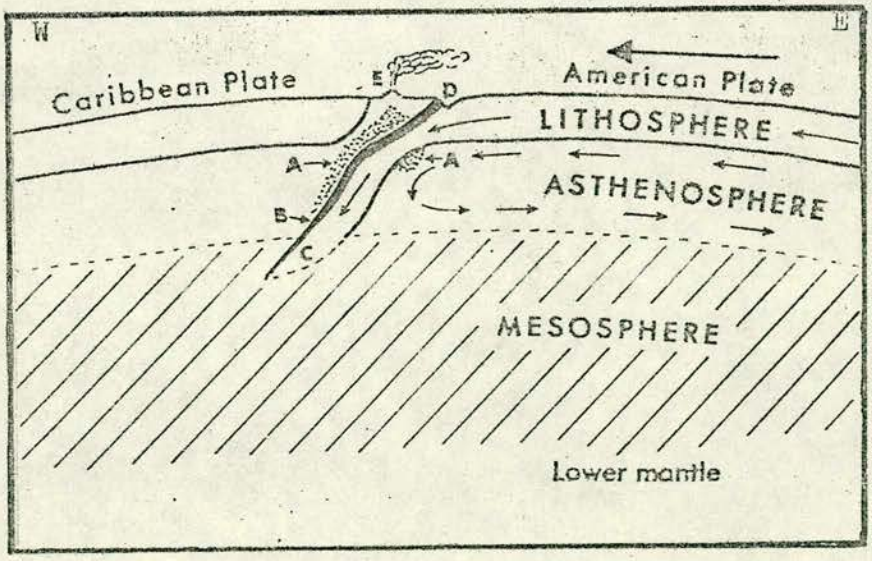

A, Zones of stress heating; B, seismic zone; C, zone of plate destruction; D, Island Arc Trench; E, volcanoes on active plate margin.

Figure 55.- Map and section (W-E) showing main features of the Caribbean tectonics. After Booth (1973).

6.4 Refraction of a Seismic Ray at a Dipping Discontinuity

Let us assume a dipping discontinuity separating two media having different seismic waves velocities, as shown in Figure 56, and let us follow the analysis made by Otsuka (1966): $\vec{S}_i$ is the incident ray at the point O on the discontinuity which yields a refracted ray $\vec{S}_r$. The vector $\vec{n}$ is normal to the plane of the dipping discontinuity, and i and r are the angles of incidence and of refraction with respect to $\vec{n}$. From Snell's law of refraction, the following relationship is obtained:

$$|\vec{S}_r| \sin(r) = |\vec{S}_i| \sin(i) \tag{15}$$

or

$$|\vec{S}_r| \cos(r) - |\vec{S}_i| \cos(i) = f(i) \tag{16}$$

Considering the plane formed by $\vec{n}$ and $\vec{S}_i$, the vector $\vec{S}_r$ can be separated as follows:

$$\vec{S}_r = \vec{OA} + \vec{OB} \tag{17}$$

where $\vec{OA}$ is parallel and $\vec{OB}$ is perpendicular to $\vec{n}$. Therefore,

$$\vec{S}_r = \left[\vec{S}_r \cdot \vec{n}\right]\vec{n} + \left[\vec{n} \times \vec{S}_i\right] \times \vec{n} \tag{18}$$

$$\vec{S}_r = \left[\vec{S}_r \cdot \vec{n}\right]\vec{n} + \vec{S}_i - \left[\vec{S}_i \cdot \vec{n}\right]\vec{n}$$

$$\vec{S}_r = \vec{S}_i + \left\{\left[\vec{S}_r \cdot \vec{n}\right] - \left[\vec{S}_i \cdot \vec{n}\right]\right\}\vec{n}$$

$$\vec{S}_r = \vec{S}_i + \left\{|\vec{S}_r| \cos(r) - |\vec{S}_i| \cos(i)\right\}\vec{n}$$

from the relation between $\vec{S}_r$ and $\vec{S}_i$ in equation (16), equation (18) becomes:

$$\vec{S}_r = \vec{S}_i + f(i)\vec{n} \tag{19}$$

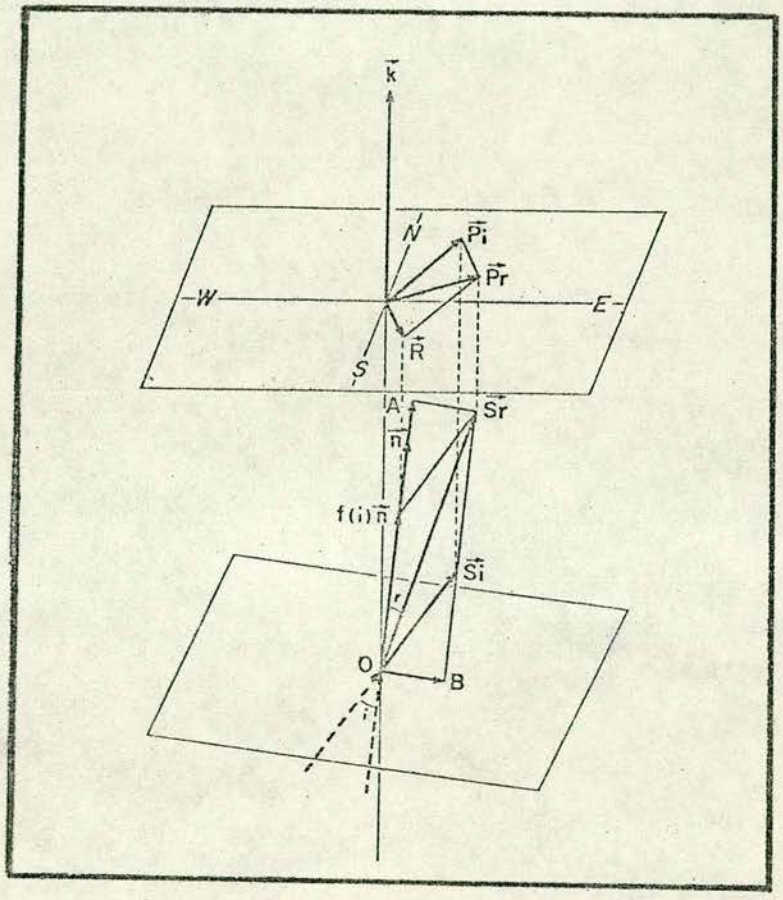

Figure 56.- Geometry of a seismic ray Si, incident on dipping interface at O yelding refracted ray s_r and their projection in the horizontal plane.
After Otsuka (1966).

Projecting the vectors $\vec{S}_i, \vec{S}_r$ and $f(i)\vec{n}$ onto the horizontal plane, the vectors $\vec{P}_i, \vec{P}_r$ and $\vec{R}$ are respectively obtained; $\vec{k}$ in Figure 56 is a vertical vector, $\vec{P}_i$ and $\vec{P}_r$ are apparent slowness vectors, which from equation (19) are related as follows:

$$\vec{P}_r = \vec{P}_i + \vec{R} \tag{20}$$

where $\vec{R}$ is the anomaly vector. Finally, it can be concluded that:

$$\text{slowness anomaly} = |\vec{P}_r| - |\vec{P}_i| \tag{21}$$

and

$$\text{azimuth anomaly} = \text{angle}\ (P_i P_r) \tag{22}$$

Equations (21) and (22) are the deviations in slowness (1/apparent velocity) and in azimuth caused by a dipping discontinuity interfering with the seismic ray somewhere in its path. These deviations will cause the seismic ray to separate from its theoretical path, in such a way that the ray which reaches the recording station would have started along another different path, which in normal conditions would not have reached the station, as illustrated in Figure 58. Horizontal discontinuities affect mostly the apparent velocity observed at the surface. Lateral discontinuities affect mostly the azimuth of the seismic ray's path, but the overall effect of a discontinuity on the apparent velocity or in the azimuth depends on the angle of incidence that the seismic ray has at the discontinuity.

The residual in azimuth (ΔAZ) observed at an array, means the difference between the azimuth of the observed deflected path

and the azimuth of the path that the seismic ray should have followed if there had not been an interfering discontinuity.

The residual in apparent velocity (ΔAV) observed at an array means the difference between the apparent velocity of the observed deflected path and the apparent velocity of the theoretical path. ΔAV is composed of the combination of the deflexion caused by the dipping discontinuity and the deflexions caused by horizontal discontinuities.

From the arguments discussed above, it may be concluded that lateral (and dipping) discontinuities are better traced by studying the residuals in azimuth, and that horizontal discontinuities are better detected by analysing residuals in apparent velocity (1/slowness).

In order to simplify the concept of the effect caused by a dipping discontinuity on the observed azimuth and apparent velocity at an array, it is better to consider a two dimensional medium and only the horizontal or the vertical components of the seismic ray, at a time. Figure 57 shows the effect of a discontinuity to the horizontal (or vertical) component of a seismic ray, in two different boundary conditions.

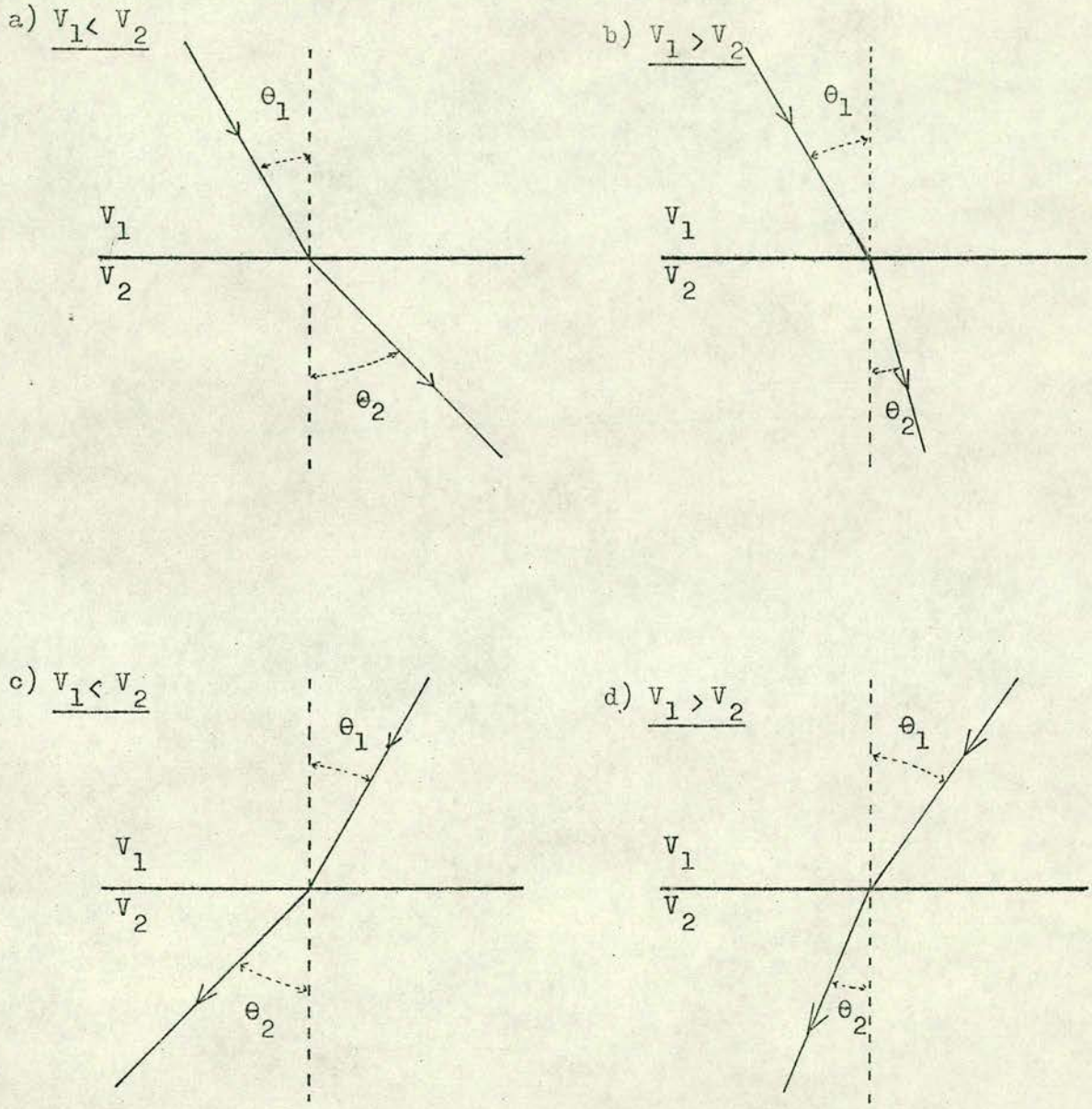

Figure 57.- TWO DIMENSIONAL DEFLECTION OF A SEISMIC RAY CAUSED BY A DISCONTINUITY

6.5 Deviations due to Refraction in Typical Discontinuities

Figure 58 illustrates the possible behaviour of a seismic ray from a typical shallow event of epicentre E, occurring near a subduction zone, with the slab dipping approximately in the direction of the recording station (S). It is assumed that the section of Figure 58-a is perpendicular to the extension of the slab. The theoretical path in Figure 58-a leaves the hypocentre (H) and follows through the slab up to the point T where it penetrates the asthenosphere and continues up to the station (S). The horizontal projection (ETS) of the seismic ray travelling from H to S is shown in Figure 58-b, where the projection of the boundary between the lithosphere (slab) and the asthenosphere has been marked through the projection of the point T on the surface. Depending on the seismic ray velocities at the slab and at the asthenosphere, the horizontal component of the seismic ray will be deflected to the North or to the South of the theoretical path, and the vertical component of the seismic ray will get deeper or shallower with respect to its theoretical path. The case in which the seismic velocity at the slab is higher than the velocity at the asthenosphere is shown in Figure 58; the horizontal component of the suggested real path (ERS) is drawn in Figure 58-b, but the vertical component of the observed path is just indicated up to the refraction point (R) at the discontinuity in Figure 58-a, because it may be affected by horizontal discontinuities before reaching the station.

The longitudinal wave velocities for a model suggested by Isacks and Barazangi (1973) for the central part of western

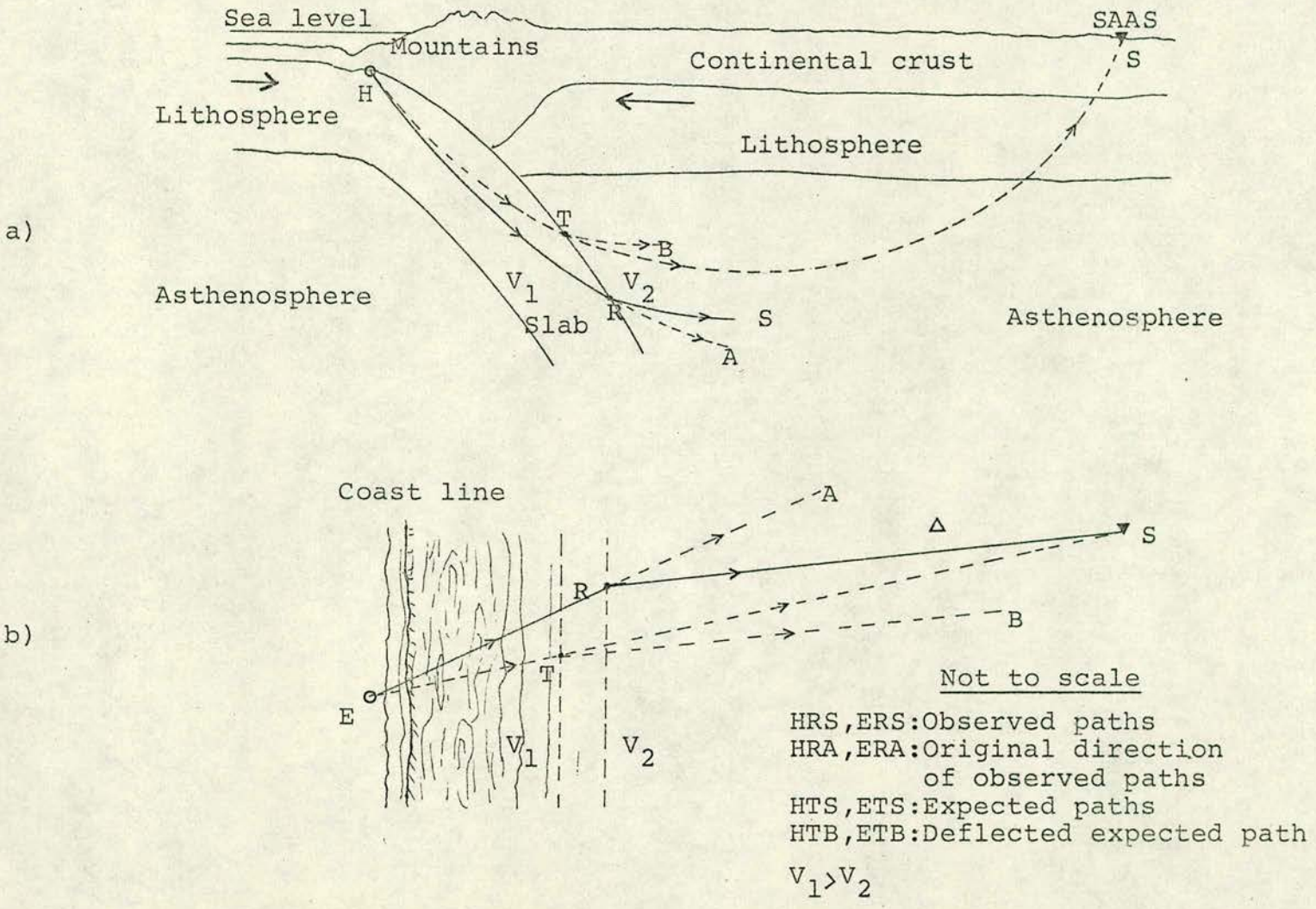

Figure 58.- DEVIATIONS DUE TO REFRACTION ON A TYPICAL DISCONTINUITY

South America, are shown in Figure 59, which is taken as a reference model for further discussions during this study.

The angle of refraction (θ_2) from snell's law is:

$$\theta_2 = \text{arc sin}(V_2/V_1 \sin(\theta_1)) \qquad (23)$$

where θ_1 is the angle of incidence, and V_1 and V_2 are the seismic ray velocities in the two sides of the discontinuity (see Figure 57); consequently, in the case of both, the horizontal and the vertical components of the path, the deviation ($\Delta\theta$) caused by the discontinuity is:

$$\Delta\theta = \theta_1 - \theta_2 \qquad (24)$$

The values of V_2/V_1 for different possible discontinuities of the model shown in Figure 59 are presented in Table 10. In Figure 60 the values of $\Delta\theta$, calculated for the different values of V_2/V_1 of Table 10, are plotted against the angle of incidence (θ_1).

TABLE 10

DIRECTION OF RAY	V_2	V_1	V_2/V_1
Crust→Lithosphere	8.14 km/sec	6.1 km/sec	1.3344
Lithosphere→Crust	6.1	8.14	0.7494
Slab→Asthenosphere	8.0	9.4	0.8511
Asthenosphere→Slab	9.4	8.0	1.1750

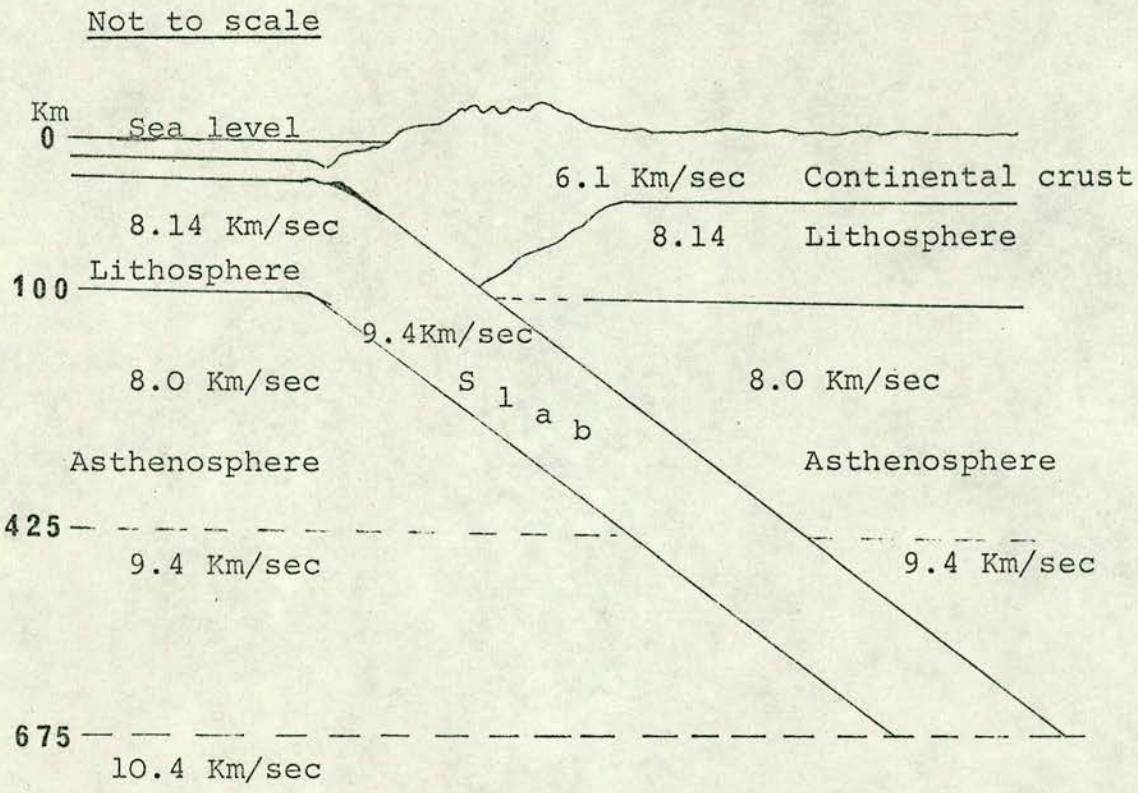

Figure 59.- EARTH MODEL UNDER SOUTHERN PERU

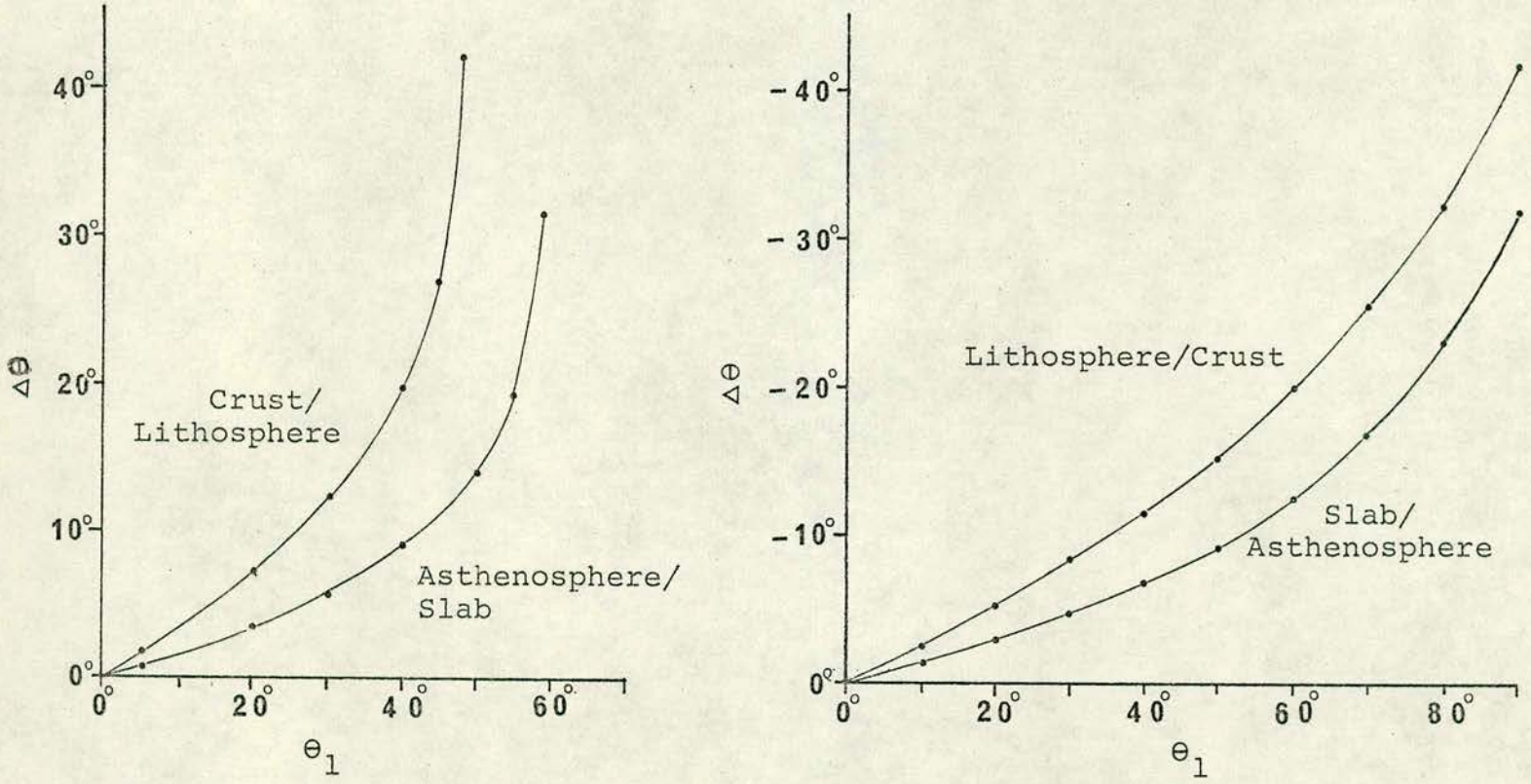

Figure 60.- DEFLECTIONS ($\Delta\theta$) CAUSED BY TYPICAL DISCONTINUITIES, AT DIFFERENT ANGLES OF INCIDENCE (θ_1)

It is necessary to mention once more, that $\Delta\Theta$ represents the deflection caused by the discontinuity to the theoretical path, in the horizontal or in the vertical plane, which deviates the seismic ray to another direction away from the recording station, but $\Delta\Theta$ also represents the deflection of another path in the same discontinuity, which brings a different seismic ray to the recording station.

Some paths followed by rays arriving at the recording station may have been affected by one or more discontinuities, therefore large departures from the theoretical values of azimuth and apparent velocity can occur if the deflections add in a given sense or some small departures can result if the deflections tend to cancel.

6.6 Interpretation of the Residuals Observed at SAAS

6.6.1 General Pattern

The distribution of the residuals observed at SAAS are shown in Figures 11 (ΔTT), 18 (Δm), 37 (ΔAZ) and 39 (ΔAV). Although the main purpose of this research is concerned with the South American region, some events from other regions within 95^{o} from SAAS have also been studied for comparison.

It has been seen in Chapter 4 that the distribution of ΔTT suggests an effect of the regional tectonic features on the travel time of seismic waves, because events from the same region present the same sort of ΔTT when recorded at SAAS. Similarly, the distribution of Δm, and of the areas for which SAAS has a poor detection capability (Figure 18), analysed also in Chapter 4, show a regional pattern which could be correlated with the one observed from the ΔTT distribution (Figure 11) in the following way:

- The regions with events having a positive value of ΔTT (observed late arrivals) were identified in Chapter 4 as regions of poor detection capability at SAAS (large negative values of Δm, events detected at SAAS with poor signal, or events not detected at all on SAAS records). Examples of these regions are the Eastern Europe-Middle East region, the Caribbean region and the South Sandwich Islands region. Southern Africa and the western United States regions could be included in this category. It should be noted that some events of the Eastern Europe-Middle East region with m_b compatible with that of some

events of the same region, not detected on SAAS records or detected with poor signal, were clearly seen on SAAS records. This suggests a possible effect of the source structure on the transmission of seismic waves in this region; the events which occurred in the area extending from the Adriatic Sea, crossing Greece and up to the Dodecanese Islands are very poorly detected at SAAS, but this does not occur with the events of the same region but which occurred on both sides of the area mentioned above (see Figure 19). It should be noticed also, that this region presents the consumption of a continental plate under a similar one (Le Pichon, 1968), and that the Caribbean region (Mattson, 1972) and the South Sandwich Islands region (Ewing et al 1971), also both have the characteristics of oceanic plates consumed by oceanic plates.

- The regions with events having a negative value of ΔTT (observed early arrivals) usually, as seen in Chapter 4, are regions for which SAAS recordings give a positive value of Δm. These regions are western Mexico, Central East Pacific Ocean, and some areas of western South America. The interesting feature is that these regions are included between 220^{o} and 310^{o} of azimuth (see Figure 18), suggesting a low attenuation anomaly in the mantle under the western part of South America. This could also be explained by structural conditions near the source, such that the seismic rays are not interfered with during their journey to SAAS

(which, in some cases, is supported by the observed ΔAZ), or are favoured by low attenuation structures existing near the source.

- The Mid Atlantic Ridge region shows events with mainly small values of ΔTT and of Δm, which is also the case of some events of the southern part of the Easter Island Cordillera. This agrees with what one expects from the structures of these regions, which are less complicated than at the other end of the plates, therefore their seismic parameters are observed, at most azimuths from the epicentres, without large departures from the expected values.

The general distribution of ΔAZ and ΔAV, analysed in Chapter 5 also shows that events of any given region have similar characteristics as observed at SAAS, regarding the azimuth and apparent velocity of the recorded signals. From Appendix 6 it can be seen that effects of timing errors (dt) on the measurements of the delays increase with the epicentral distance and that these effects are also dependent on the aperture of the array, therefore, the values of azimuth and apparent velocity for events with large epicentral distance are less precise than for the events nearer to SAAS.

Despite the considerations mentioned above, some general peculiarities can be seen in the distribution of ΔAZ (Figure 37) and ΔAV (Figure 39) of all the events studied, including the ones at large epicentral distances from SAAS, which are noteworthy:

- Regions where consumption of plates occurs (Andes, East Europe-Middle East, Caribbean and South Sandwich Island regions) contain events with relatively large value of ΔAZ.
- Oceanic Ridge regions (Mid Atlantic Ridge, and Easter Island Cordillera) contain events with relatively small values of ΔAZ.
- The fact that events from any given region have similar values of ΔAZ and ΔAV (East Europe-Middle East, Atlantic Ridge, South Sandwich Island, Western Mexico, some areas of the Andes, etc.) suggests a similar effect of the tectonic structure of these regions on the ray paths of events originating in these regions.
- Considering the aperture of the array used in this study (12.5 km), it may be seen from Appendix 6 that SAAS measurements of azimuth and apparent velocity, for typical values of observed $dt (\approx |0.02|$ sec), are within $|1.8\%| \pm 0.6^{\circ}$ and $|1.8\%| \pm 0.3\%$ of accuracy, respectively, for events with $\Delta = 40^{\circ}$. Beyond this distance the resolution power of the array is increasingly smaller, therefore it may be considered that the values of ΔAZ and ΔAV are quite reliable within $\Delta = 40^{\circ}$. Being so, the observed difference between the values of ΔAZ belonging to the events with $\Delta \leqslant 40^{\circ}$, coming from both sides of the meridian on which SAAS lies, is very significant (see Figure 37): the Atlantic Ridge events have small values of ΔAZ, inferring an uninterrupted path from the sources to the station, whilst the Andean events present

large values of ΔAZ implying a highly disturbed path.

- The distribution of ΔAV does not show the characteristic observed for ΔAZ. It appears to suggest a relationship with epicentral distance (see Figures 39 and 61) as follows: mainly positive values of ΔAV at around $\Delta = 20^{\circ}$, between $\Delta = 38^{\circ}$ and 45° (except for the South Sandwich Island Region), and between $\Delta = 64^{\circ}$ and 80°. Because the resolution power of SAAS decreases with epicentral distance, as mentioned before, the values of ΔAV beyond $\Delta = 40^{\circ}$ have less significance in the present interpretation. The positive values of ΔAV at around $\Delta = 20^{\circ}$ suggest a high velocity horizontal discontinuity at around 650 km of depth, and the ones at Δ between 38° and 45° suggest another high velocity horizontal region below 800 km of depth.

6.6.2 Residuals from the Northern part of Latin America

This region contains the Caribbean Area, the northern part of South America and the western part of Mexico.

By considering the distribution of ΔTT (see Figure 17) it is possible to divide this region in two parts by a line going through the Cayman Trench and the South of Guatemala. The northern part of this region (western Mexico) contains events with mainly negative values of ΔTT, whereas the events which occurred in the southern part of this region (Caribbean area and northern South America), have mainly positive values of ΔTT. These positive values of ΔTT are observed for events occurring down to 0° of latitude (see Figure 15). The distribution of Δm (Figure 20) and of ΔAV (Figure 43) also

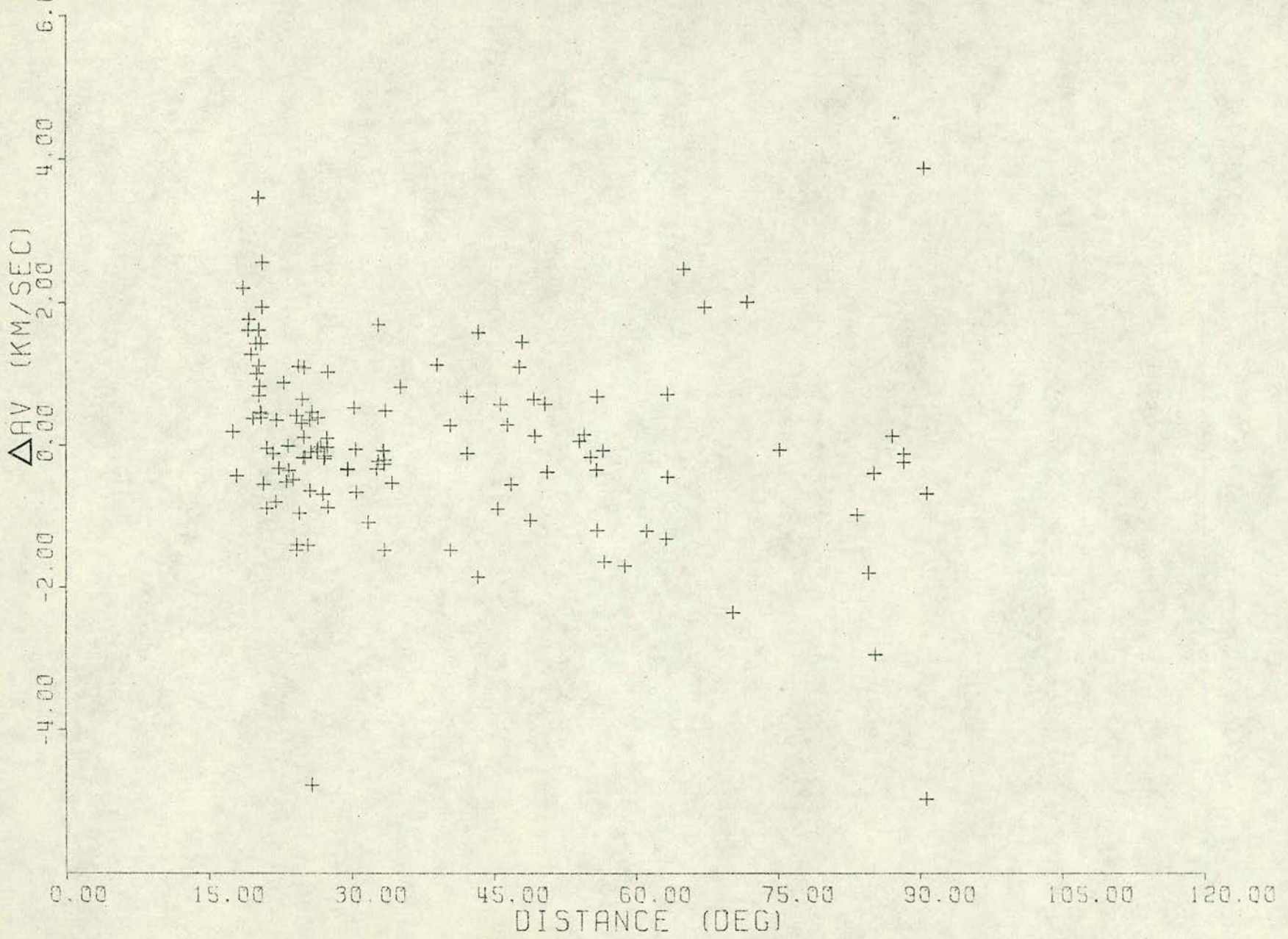

Figure 61.- DISTRIBUTION OF ΔAV AGAINST EPICENTRAL DISTANCE

agrees with the division suggested by the distribution of ΔTT: the northern part of this region shows events with mainly positive values of Δm and negative values of ΔAV, whilst its southern part has events with mainly negative values of Δm and positive values of ΔAV. All events from this region have a negative value of ΔAZ (see Figure 42).

The distribution of these residuals (except ΔAZ) indicates a difference in the behaviour of the seismic waves produced by events in this region which coincides with the different tectonic structures that exist on both sides of the Cayman Trench-South of Guatemala line, as it was seen in 6.3. Perhaps the distribution of ΔAV is associated with the epicentral distance (Δ around 40^{o}) as suggested in 6.5.1. But the distribution of ΔTT and Δm suggest that the seismic rays of events occurring at the northern part of this region travel along paths which are anomalous in respect of both the amplitude and the travel time, when recorded at SAAS. Some intermediate depth events ($h \approx 180$ km) in the southern part of this region, such as the ones occurred in Santander Province (Colombia) or in the western side of the Caribbean area, show opposite values of ΔTT or/and of Δm than the other events of this area.

In an earlier paper (Berrocal et al, 1972) the negative values of Δm of the Caribbean events, were explained as amplitude attenuation occurred at a lateral discontinuity under the Amazon Basin (see Figure 62). The fact that some intermediate depth events occurred in this area, do not present this anomaly,

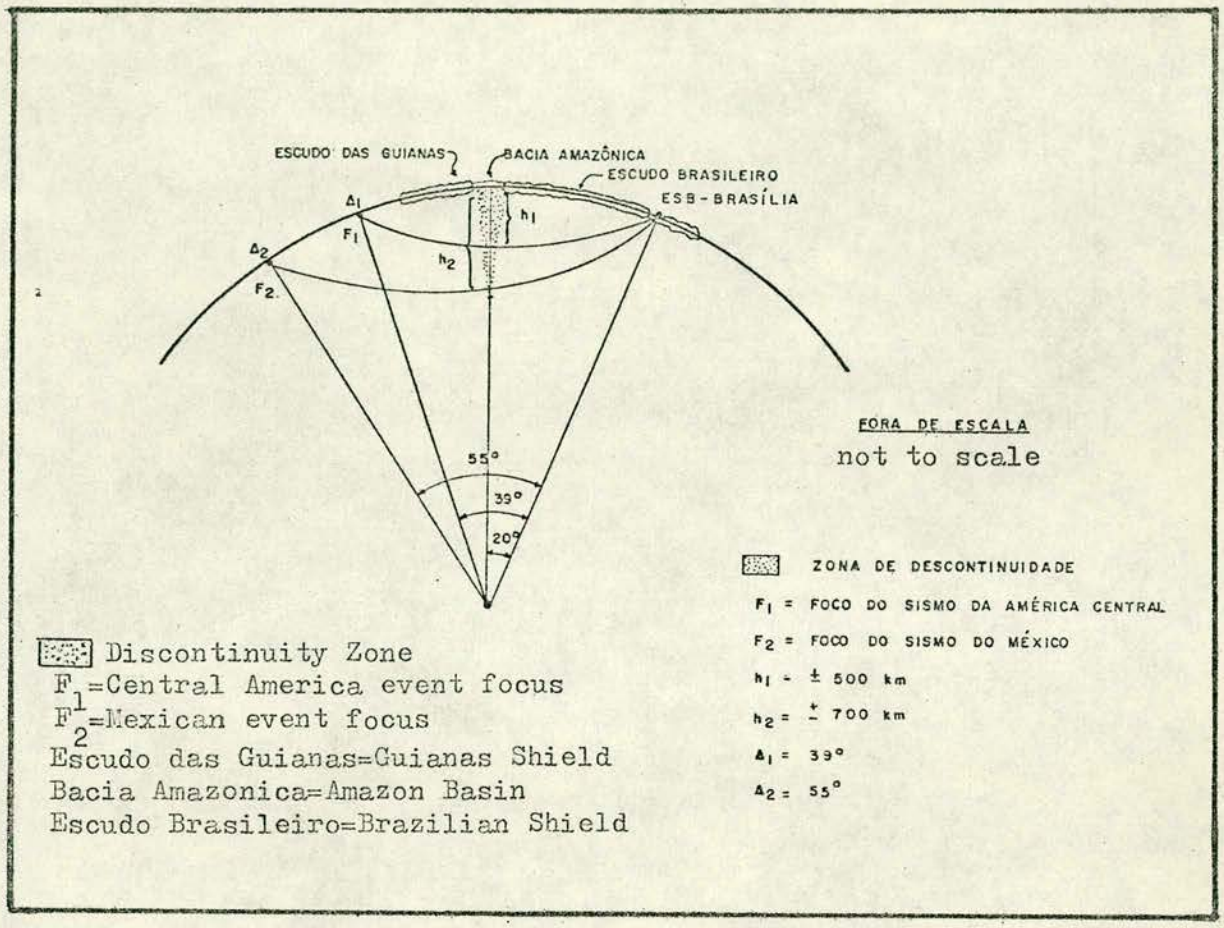

Figure 62.- LATERAL DISCONTINUITY UNDER THE AMAZON BASIN
After Berrocal et al (1972).

as found in the present study, do not agree with the theory of a lateral discontinuity under the Amazon Basin to explain the attenuation observed for the shallower events of the Caribbean-northern South America area.

On the other hand, the anomaly observed at SAAS for the events which occurred in the southern part of this region is not observed at USA stations, but it is observed at other South American stations below 10^{o}S. This observation could support the existence of a lateral discontinuity between the southern part of this region and SAAS. The main superficial structural features of the area between the sources of these anomalous events and the South American stations below 10^{o}S are the northeastern part of the Andes (northern Venezuela) and the Amazon Basin. The lithospheric slab under this part of the Andes does not reach depths lower than a few hundreds of Km., therefore it could not affect the path of events which occurred in the northern limit of the southern part of this region. It could be argued that the slabs around the Caribbean area could affect the amplitude and the travel time of the events of this area, but this would explain neither the case of the events located at the West and East extremes of the area, nor the same anomaly observed for events of northwestern South America (see Figure 20).

If a lateral discontinuity would be the cause of the anomaly observed at SAAS, for the Caribbean and northwestern South America events, then the more probable one would be a discontinuity under the Amazon Basin as suggested by Berrocal *et al* (1972) in Figure 62. They based their assumption in the following facts: the large positive

gravity anomaly observed in the central area of the Amazon Basin and the existence of small, infrequent, seismic events all along this basin. These facts suggest a physical separation of the Guyana and Brazilian shields which could be a consequence of internal conditions in the Earth's mantles that constitute a lateral discontinuity under the Amazon basin. The absence of deep events to the north of the Amazon Basin is another argument in favour of a possible lateral discontinuity to explain the anomalous amplitude and travel time observed at SAAS for the events occurred in the Caribbean area and in the northwestern part of South America. A lateral discontinuity under the Amazon Basin could explain also the negative values of ΔAZ observed in this region, assuming a higher velocity in the southern part of the discontinuity, therefore, following a refraction model of Figure 57-a.

Freeland and Dietz (1971) indicate that the northern and southern limits of the Caribbean "plate" are areas of shear movements, with the Caribbean plate moving to the East, with respect to the Americas plate. This could suggest a given source radiation pattern effect as the cause of the anomaly of the Caribbean events when observed at SAAS. But if this is so, the USA stations, located opposite to SAAS with respect to the areas of the shear movements, would present the same effect, which is not the case. Furthermore, this shear movement would not explain the case of the anomaly observed also for the events occurring at the West and East extreme of the Caribbean area.

Therefore, it seems that the most probable theory to explain

the attenuation of amplitude and travel time that the Caribbean and northern of South America events present when observed at SAAS, is a lateral discontinuity. It is difficult to explain the existence of a lateral discontinuity like the one suggested under the Amazon Basin, specially being extended up to several hundred Km. into the mantle. The existence of large transcurrent faults systems at either end of the suggested discontinuity (see Figure 63) could have some relationship with its origin. The proper existence of the Amazon Basin can be regarded as a superficial evidence of a significant discontinuity in the internal structure of the area occupied by the basin.

Despite any possible explanation to account for the observed anomalous residuals at SAAS, for events occurring in the Caribbean area and northern South America, it can be concluded that the internal structure under the northern part of South America (to the North of the Amazon Basin) shows a high attenuation anomaly.

6.6.3 Residuals from the Western Part of South America

This region is mainly occupied by the portion of the Andes from 0^{o} to $35^{o}S$, and represents part of the area of subduction between the East Pacific and the South American plates.

The distribution of ΔTT (Figure 15) and Δm (Figure 21) of the events which occurred in this region shows that, in general, the whole region offers favourable conditions for the transmission of seismic waves: most values of ΔTT observed at SAAS are negative (early arrivals) and most values of Δm are positive (larger amplitude than expected), near zero or small negative.

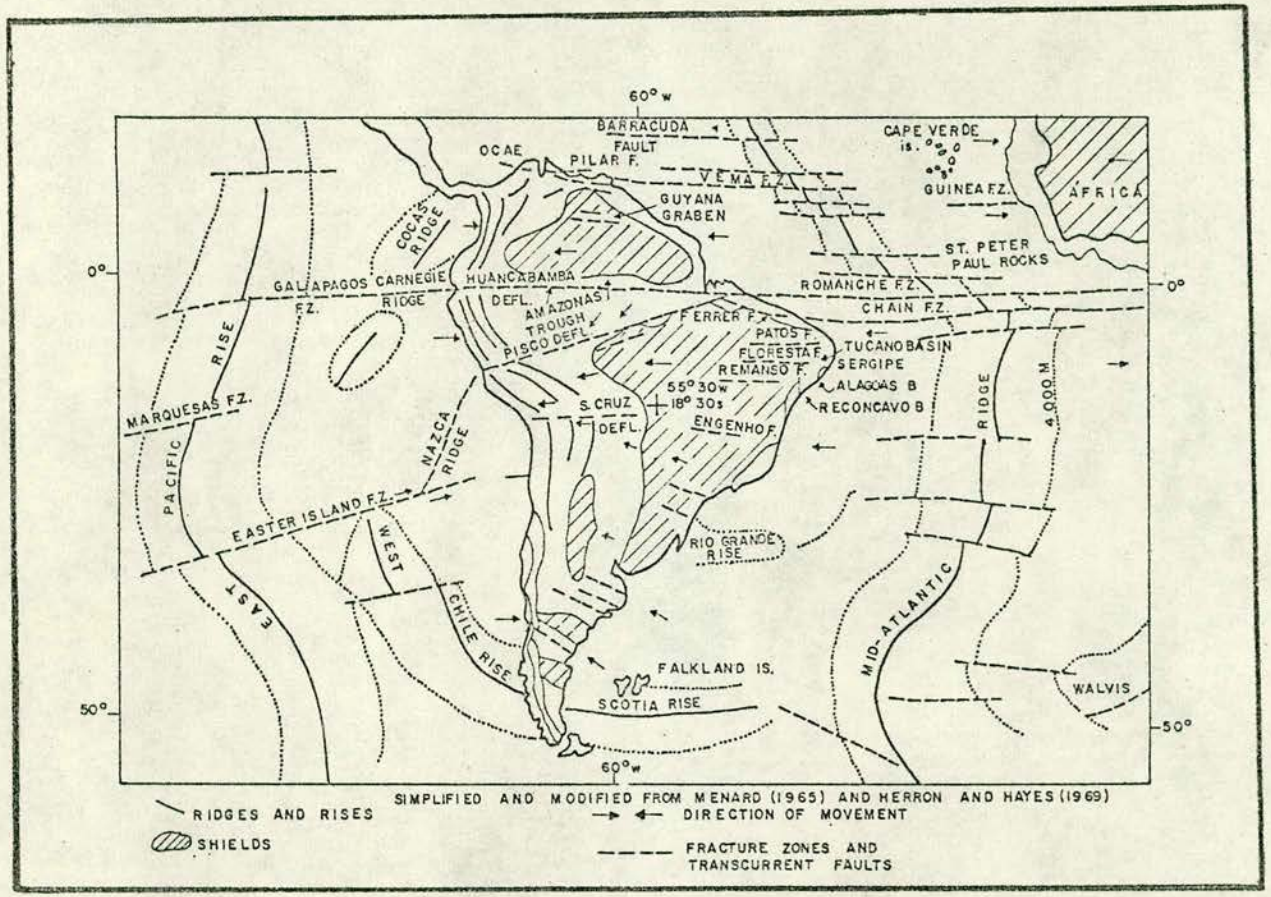

Figure 63.- GENERALIZED DIAGRAM OF PRINCIPAL TRANSCURRENT FAULTS IN SOUTH AMERICA. After Loczy (1970).

This suggests the existence of low attenuation internal structures under the area comprised between this region and SAAS. The few small areas which do not follow this general pattern are shown in Figures 15 and 21.

As it was presented in Chapter 4, the two places within this region for which SAAS has a low detection capability (events recorded with a poor signal) are the northeastern part of Peru (around 5^{o}S, 76^{o}W) and the San Juan Province Argentina (around 31^{o}S, 74^{o}W). Another area which can be considered in this category, is located around 27^{o}S and 71^{o}W. Some events which occurred within these areas have also a positive value of ΔTT, confirming the relationship between travel time and amplitude discussed before. The important feature to observe about these "anomalous" areas (Figure 21) is that they are located in the northern and southern extremes of the region being studied.

The distribution of ΔAV (Figure 45) shows a more defined pattern which suggests the existence of some velocity anomalies, especially in the case of the events which occurred below 20^{o}S. The pattern observed in Figure 45 could be explained by assuming the existence of a high velocity horizontal discontinuity at around 650 km of depth which would account for the large positive values of ΔAV observed between 18^{o}S and 24^{o}S. This high velocity anomaly should have produced positive ΔAV for most events within this region in the range between 20^{o} and 30^{o} of epicentral distance, as it can be observed at some Peruvian events and also at some Chilean events below 28^{o}S. Being so, the negative (and small

positive) values of ΔAV observed between $21^{o}S$ and $32^{o}S$ suggest a lateral discontinuity under the boundary between the areas of large positive and negative value of ΔAV, defined by the line A-D in Figure 45.

To produce a negative value of ΔAV, the velocities on the two sides of the discontinuity have to be distributed in such a way that the side nearest to the station has the lower velocity value (following the model shown in Figure 57-d).

To explain the positive values of ΔAV observed for the events at the southern part of the region being studied, given the probable existence of a lateral discontinuity in their path, two situations are possible:

a) The lateral discontinuity does not reach depths larger than 250 km., which is the depth of the path of the event with large positive ΔAV, nearest to the discontinuity, when it passes under the projection of the discontinuity on the surface (line A-D in Figure 45), or

b) The orientation of the discontinuity is such that the inclination of the ray does not change when it passes through the discontinuity, even if the azimuth does change. The condition for this to be possible is that the line of intersection, between the refractor and the vertical plane through the seismic ray, must be at right angles with the ray.

The second possibility seems more plausible, especially because it also explains the negative value of ΔAZ of the events which

occurred to the South of the discontinuity as it will be discussed later. This implies that the discontinuity would have to reach depths greater than 600 km to deflect the rays of the events which occur in the southern extreme of this region. The line A-D in Figure 45 also passes through the South extreme of the epicentral area of the deep events occurring in northern Argentina (depths greater than 600 km), which could have some relationship with the suggested lateral discontinuity, and gives in this way an argument in favour of the vertical extension of the discontinuity down to over 600 km.

The distribution of ΔAZ (Figure 44) shows still a more defined pattern than the one obtained in the case of ΔAV. The distribution of ΔAZ in this region, as presented in Chapter 5, allows the events to be grouped in three areas: from 0^{o} to $16^{o}S$ (near zero or small negative values of ΔAZ), from $16^{o}S$ to $22^{o}S$ (mainly positive values of ΔAZ), and from $22^{o}S$ to 40^{o} (mainly large negative values of ΔAZ). The boundary at around $22^{o}S$ between the areas of positive and negative values of ΔAZ suggests also the existence of a lateral discontinuity. The line A-S in Figure 44 (and Figure 45) represents the horizontal projection of the lateral discontinuity as deduced from the ΔAZ distribution, which has been extended up to cross the epicentral area of the deep events occurring in northern Argentina.

A lateral discontinuity deepening down to more than 600 km would also, as mentioned before, explain the negative values of ΔAZ shown by the events which occurred in the South side of the discontinuity, assuming that the velocity in the side nearest to the station is

lower than the velocity in the other side of the discontinuity (refraction type d of Figure 57).

In summary, the following arguments support the existence of a lateral discontinuity in the central area of western South America:

a) The suggested discontinuity separates areas of contrasting values of ΔAV and ΔAZ deduced from SAAS observations. The angle DAS (see Figures 44 or 45) formed by the horizontal projections of the discontinuity as deduced from each residual distribution, may imply a southwestern dipping of the discontinuity, which will be discussed later.

b) The depth required for the discontinuity to explain the values of ΔAV and ΔAZ, for events of the southern part of the discontinuity, must exceed 600 km, which coincides with the depth of the deep events of northern Argentina. This, together with the fact that the superficial projection of the discontinuity coincides with the epicentral area of these deep events, suggests a relationship between the suggested lateral discontinuity and the presence of the deep earthquakes of this area.

c) To explain both the observed negative values of ΔAZ and the observed positive values of ΔAV for events at the south side of the discontinuity, it is required that the velocity in the station side of the discontinuity should be lower than in the opposite side, following a refraction model illustrated in Figure 57-d.

The distribution of ΔAZ for the events between $16^{o}S$ and $22^{o}S$ can be further subdivided into two small areas:

a) A southern area which has events with mainly larger positive values of ΔAZ (greater than $+3^{o}$) which is extended from $22^{o}S$ up to around $19^{o}S$.

b) A northern area which has events with mainly small values of ΔAZ having its southern limit at around $19^{o}S$ and can be extended up to at least $14^{o}S$. The values of ΔAZ in this case are between $\pm$ 2.5^{o} only.

To explain the larger positive values of the area between $22^{o}S$ and $19^{o}S$ two possibilities can be contemplated (see Figure 64):

a) A refractor (boundary between slab and asthenosphere) orientated in the NW-SE direction, following a refraction model of Figure 57-c, assuming the higher velocity in the side of the station (asthenosphere).

b) A refractor (slab-asthenosphere) orientated almost in the N-S direction following a refraction model of Figure 58 and Figure 57-b, assuming the higher velocity in the side of the event (slab).

The first possibility does not agree with the velocity distribution model presented in Figure 59 or with the refraction models of the other areas of this region with similar refractor (slab-asthenosphere), as it will be seen later. On the other hand, this area must have a highly disturbed internal structure that may change the characteristics which are observed in the other areas of this region. Another

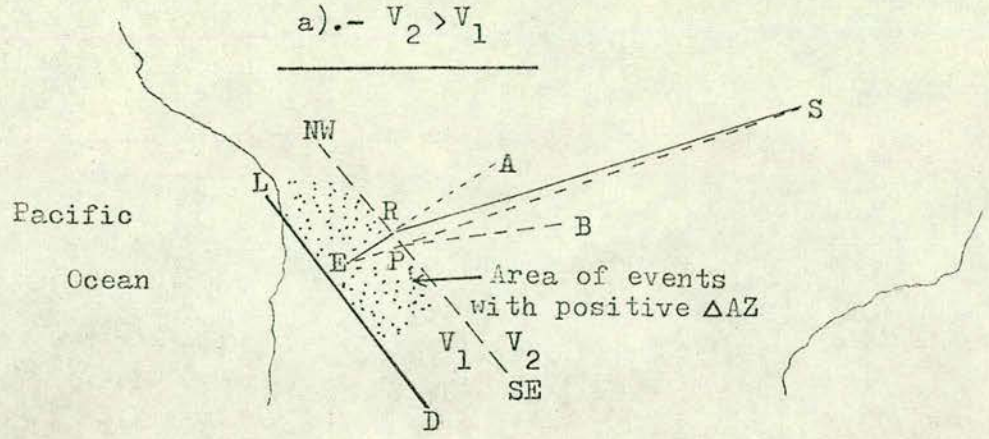

E R A : original direction of observed path
E R S : observed path
E P S : theoretical path
E P B : deflected theoretical path
L D : lateral discontinuity
NW-SE and N-S : slab-asthenosphere refractors

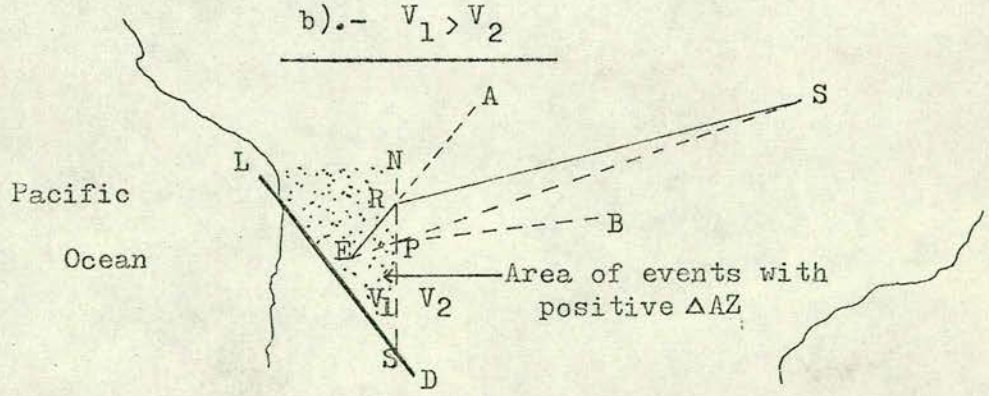

Figure 64.- TWO REFRACTION MODELS TO EXPLAIN THE POSITIVE VALUES OF ΔAZ FOR EVENTS FROM THE CHILE-BOLIVIA BORDER REGION

argument which can be conclusive is the orientation of the refractor: from surface evidences it appears to follow the N-S direction assumed in the second possibility, but the suggested lateral discontinuity just to the south of this area, may create conditions for a NW-SE refractor.

The small values of ΔAZ for the events of the area between $19^{o}S$ and $14^{o}S$, could be due to the fact that this area is extended around the station's latitude, but this implies a refractor (slab-asthenosphere) not interfering with the horizontal componenent of the seismic ray (incidence angle near 90^{o}). Apparently, from surface evidence, the refractor in this area follows a NW-SE direction which means that the angle of incidence of the horizontal component of the seismic rays produced by the events of this area, is different than 90^{o}. To explain these small values of ΔAZ under the presence of a NW-SE refractor, a very gentle deviation between the expected and observed paths, caused by the slab-asthenosphere boundary, must be assumed.

This last argument could be applied also to the small negative values of ΔAZ of the events which occurred between $14^{o}S$ and the equator.

Summarising, the effects of the possible refractors mentioned above (see Figure 65) on the distribution of ΔAZ in the western South America region, are as follows:

a) A gentle deviation of the horizontal component of the seismic rays caused by the slab-asthenosphere refractor, which produces a positive value of ΔAZ when the theoretical path, of events located to the South of SAAS, is bent southwards following the models of Figure 57-b and Figure 58

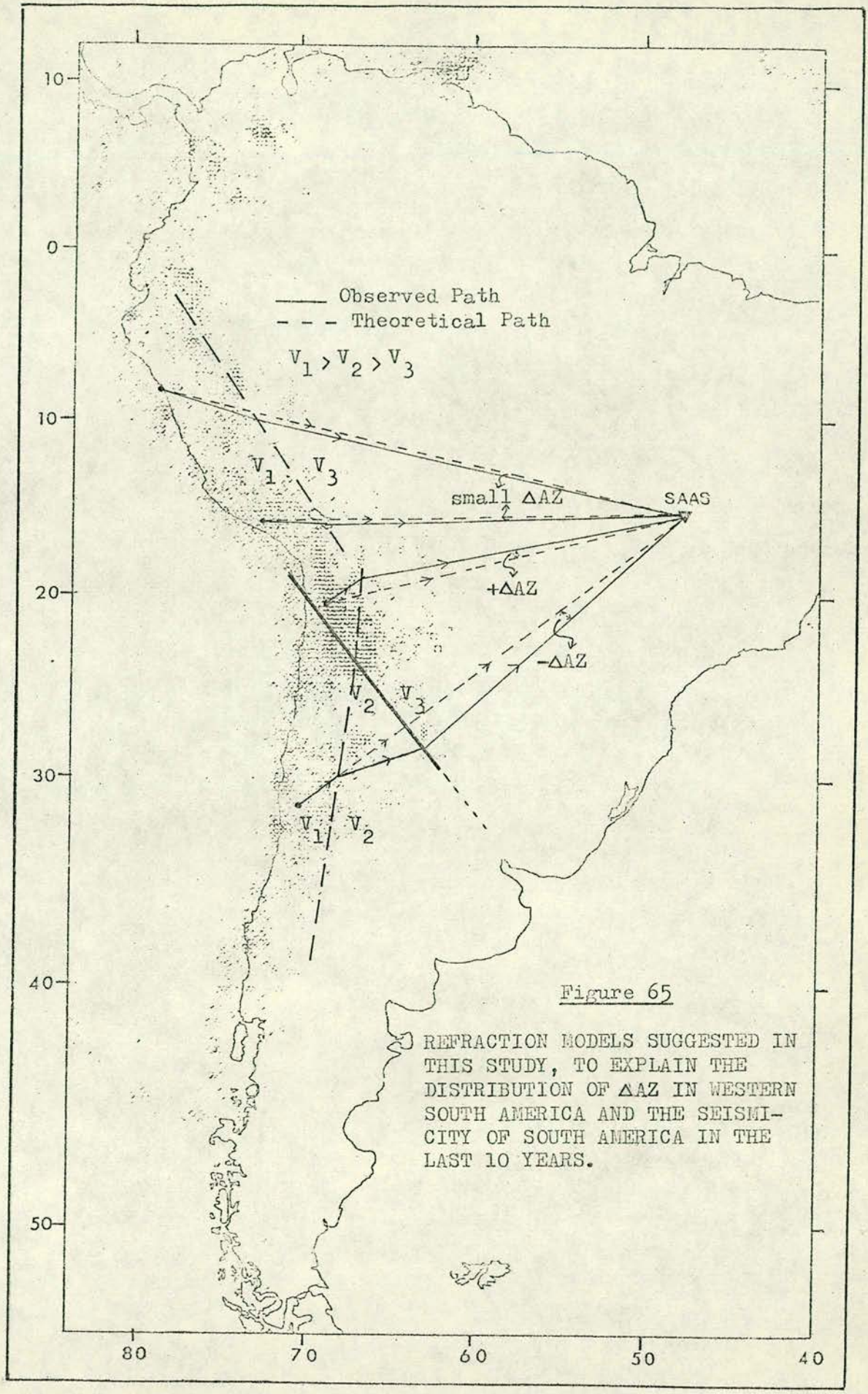

Figure 65

REFRACTION MODELS SUGGESTED IN THIS STUDY, TO EXPLAIN THE DISTRIBUTION OF ΔAZ IN WESTERN SOUTH AMERICA AND THE SEISMICITY OF SOUTH AMERICA IN THE LAST 10 YEARS.

(the case when the refractor is almost N-S) or a negative value of ΔAZ when the expected path, of events located to the North of SAAS, is bent northwards following the model of Figure 57-d (the case when the refractor is almost NW-SE).

b) A change on the value of ΔAZ, which otherwise should have been positive, for the events below $22^{o}S$, caused by a suggested lateral discontinuity following the model of Figure 57-d, which together with the deflection caused by the slab-asthenosphere refractor produces a large negative value of ΔAZ.

6.6.4 Main Tectonic Features of South America

By interpreting the distribution of the residuals of four seismic parameters, from SAAS data, which have been analysed in the present research, it has been possible to infer the presence of some discontinuities, of regional significance, and to find evidence which supports other main features of South American tectonics. The following are the main results obtained in this research:

First of all, the entire discussion is based on the postulates of the plate tectonic theory, which offers a means to explain the distribution of the residuals observed at SAAS. Therefore the results reached in this study are consistent with the basic structure suggested fo South America by the plate tectonic theory.

A horizontal discontinuity at over 600 km of depth, having a high velocity property, has been suggested in this research, to explain the dominant early arrivals and positive values of ΔAV observed at SAAS for events within 40^{o} of epicentral distance. Some events from the northern region of Latin America, and from a

few small areas in western South Americ, show positive travel-time residuals (observed late arrivals), suggesting the existence of a regional anomaly in the case of events from the northern region of Latin America, and of local anomalous structures under the small areas of western South America. Isacks and Barazangi (1973) suggested the existence of a high velocity discontinuity at 675 km of depth (see Figure 59), from the arrival time and the observed multiplicity of the S phase originating from deep events of northern Argentina when recorded at some stations in western South America. Several other seismic studies in other regions have suggested an increase in the velocity gradient at depths between 600 and 700 Km, notably those of Niazi and Anderson (1965), Johnson (1967), Green and Hales (1968), Archambeau et al (1969), Helmberger and Wiggins (1971), Wiggins and Helmberger (1972), Jordan (1973) and Simpson (1973).

From the analysis of the magnitude residuals it has been possible to conclude that either the northern part of South America has an internal structure showing a high amplitude attenuation anomaly (low Q) or that there is a lateral discontinuity down to over 600 km of depth, under the Amazon Basin showing this anomaly (see Figures 62 and 66). From this same analysis it is suggested that the western region of South America has an internal structure with low attenuation characteristics (high Q), except for some small areas in the northern and southern extremes which may have localised anomalous internal structures with low Q values.

A lateral discontinuity under the Amazon Basin could also, as mentioned before, explain the negative values of ΔAZ observed for

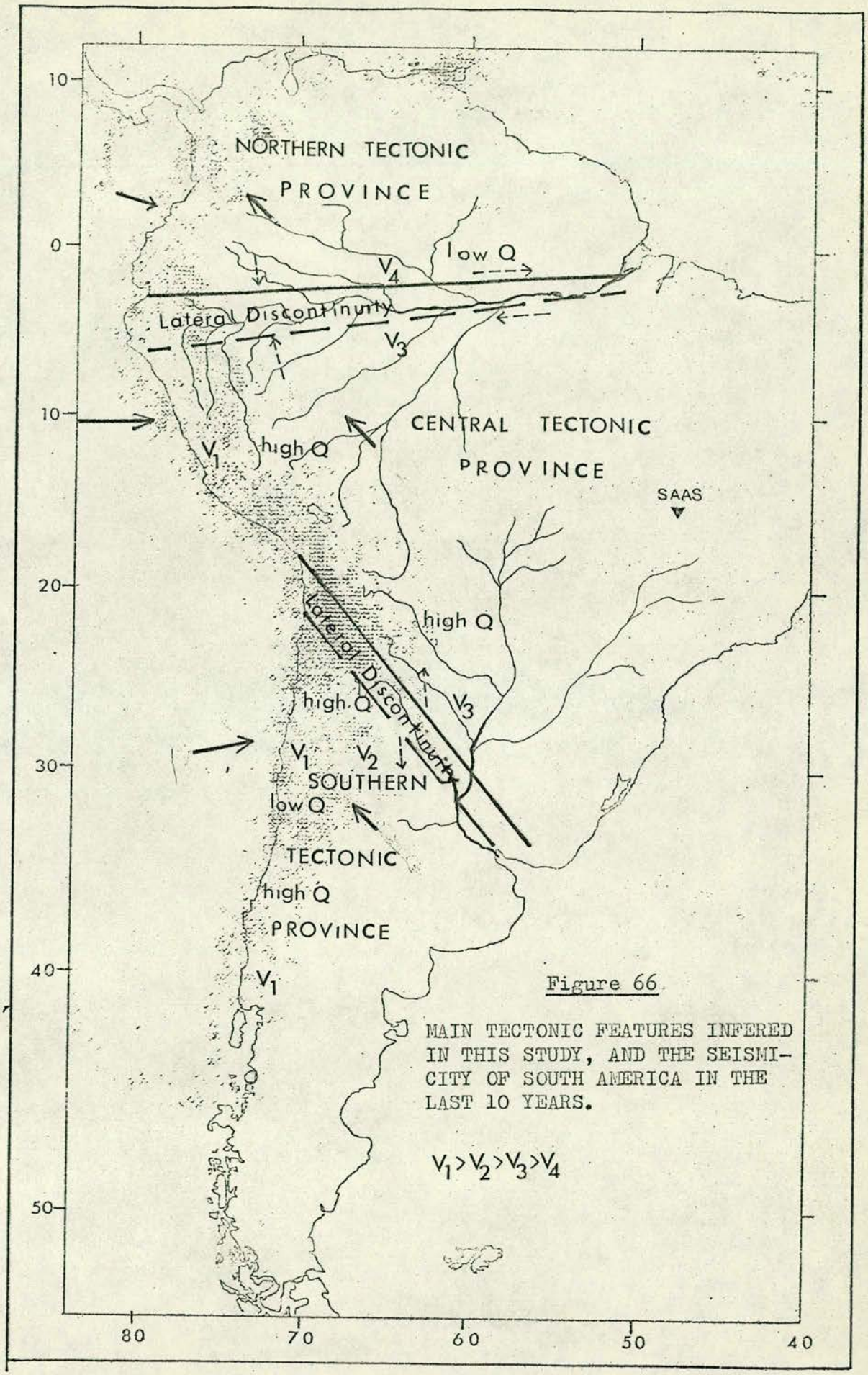

Figure 66

MAIN TECTONIC FEATURES INFERED IN THIS STUDY, AND THE SEISMICITY OF SOUTH AMERICA IN THE LAST 10 YEARS.

$V_1 > V_2 > V_3 > V_4$

the events which occurred in the northern region of Latin America, and agrees with the transcurrent fault systems of the region, show in Figure 63. Due to these observations and to what was discussed in 6.6.3, the theory which postulates a lateral discontinuity under the Amazon Basin is favoured in this research. Nevertheless, the possibility of this lateral discontinuity being just the boundary between the northern region, with probable high attenuation characteristic and the southern low attenuation region, must also be considered.

A second lateral discontinuity, the discontinuity under the central part of western South America having a NW-SE orientation, has been suggested in this study to explain the distribution of ΔAZ and ΔAV observed at SAAS as shown in Figure 66. Apart from the arguments discussed in the last section (6.6.3), the following observations from other studies of South American tectonics support this theory:

a) The change in the present depth of the Andean "root" which begins at around $23^{o}S$ (thicker to the North), as found by Lomnitz (1962).

b) The observation of a guided Sn phase, from deep Argentinean events recorded at some Peruvian stations, and the lack of detection of this phase at Chilean stations (see Figure 54). This lead Isacks and Barazangi (1973) to suspect the separation of the slab into "two sections at around $28^{o}S$ to $33^{o}S$".

c) A 2,000 x 200 km belt of tin mineralization ranging in age from Lower Paleozoic to Neogene, which was not derived from

subducted oceanic sediments and basalts, being extended from northwestern Argentina to southern Peru (Clark et al, 1973), and representing an anomalous source of ore deposits in that region.

d) The E-W trending linear arrays of volcanoes and of qualitatively-differing geomorphological regimes observed by Clark et al (1973) at around 27°S, suggesting a discontinuity of the down-going slab, in that orientation.

e) The difference in the convergence rate between the East Pacific and the Americas plates observed in southern Chile (≈7cm/year) and in the northern part of western South America (Peruvian latitudes) (≈12 cm/year as discussed by Plafker (1972).

CHAPTER 7

FURTHER EVIDENCES FOR THE RESULTS OBTAINED IN THIS RESEARCH

7.1 Introduction

The main tectonic features of South America suggested in this study, which were inferred from the analysis of SAAS data, have been discussed in Chapter 6, where some evidences obtained from other tectonic studies supporting these features, were presented.

In this Chapter, some data from other sources which support the results discussed in Chapter 6 will be analysed. These sources are: the vertical distribution of the South American seismicity, the main physiographic features of the region and a time-space correlation between the deep events of this continent.

An intent to assess the origin of the suggested lateral discontinuities, is made when analysing the possible origin of the physiographic features.

7.2 Vertical Distribution of South American Seismicity

An evidence which supports the theory of lateral discontinuities under the central part of western South America, and the Amazon Basin, can be found in the sections shown in Figures 68 to 76. These sections represent the horizontal projection of all events (from 01 JAN 1964 to 30 APR 1973), which occurred in the areas shown in Figure 67, into a vertical plane passing through the middle of each area, and orientated to be perpendicular to the surface features which suggest the orientation of the subduction line.

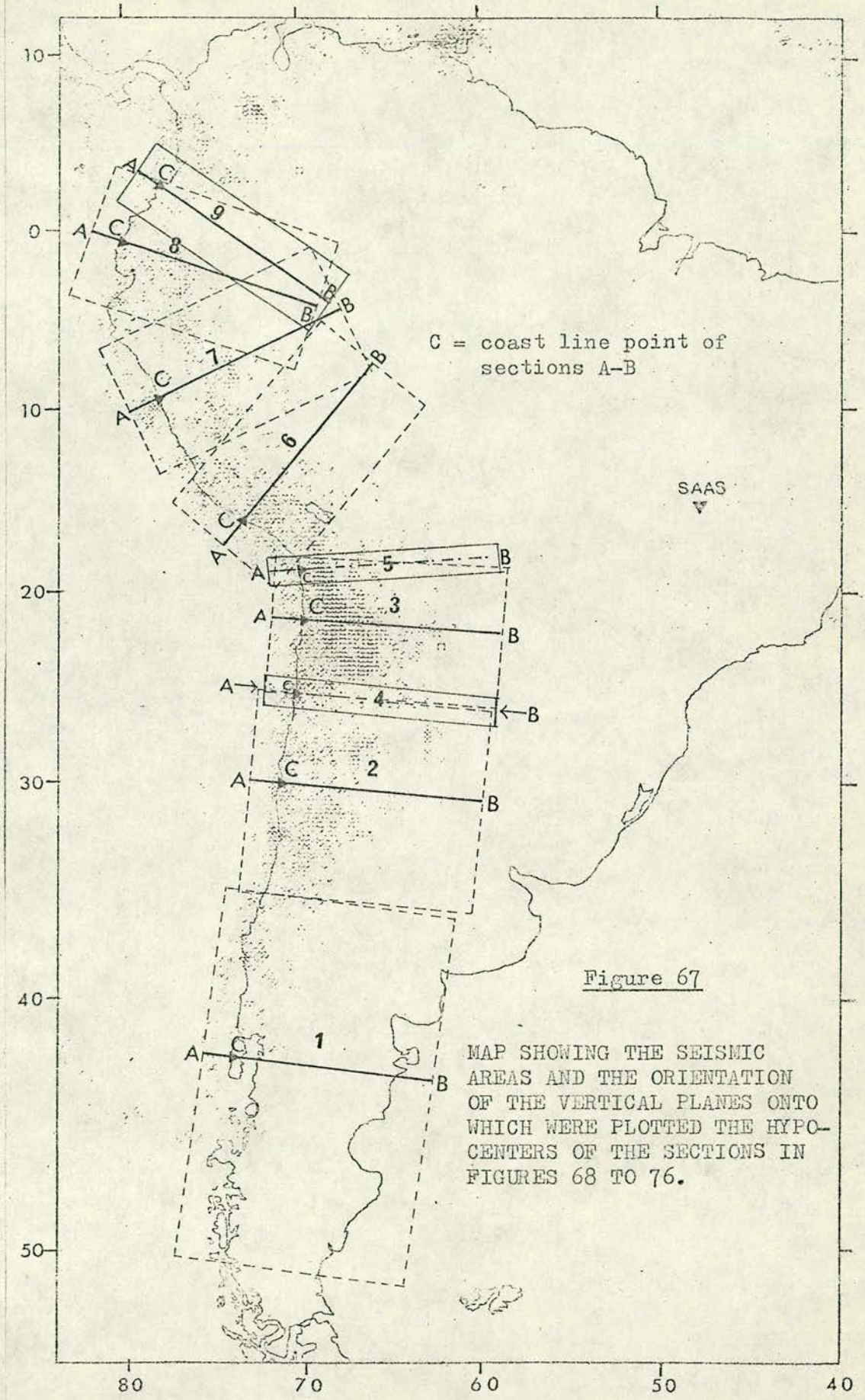

Figure 67

MAP SHOWING THE SEISMIC AREAS AND THE ORIENTATION OF THE VERTICAL PLANES ONTO WHICH WERE PLOTTED THE HYPO-CENTERS OF THE SECTIONS IN FIGURES 68 TO 76.

From Figure 68, it may be seen that the angle of eastwards dip of the slab, is equal to 38^{o}, which agrees with the angle suggested for this area by Plafker, 1972 ($\approx 35^{o}$). In Figure 69, the same angle is again suggested, but its projection does not reach the deep events ($h \approx 625$ km) shown in that section, inferring that these events are in a different plane (slab). Figure 70 shows a very interesting pattern: the events down to about 300 km of depth suggest two planes, one dipping at 38^{o} and the other at 47^{o}, both with eastwards dipping; the plane with a dipping angle of 47^{o} passes through the deep events of the section whilst the other does not. Because the angle of dipping is similar to thos observed in the previous sections, the plane which does not reach the deep events is assumed to belong to a continuous down-going slab coming from 50^{o}S up to somewhere between 18^{o}S and 25^{o}S, which are the North and South limits of the area considered in plotting the section of Figure 70. As suggested in Chapter 6, this area is crossed diagonally by the NW-SE surface projection of a lateral discontinuity, therefore the section of Figure 70 shows physical differences of two slabs separated by the suggested lateral discontinuity: the southern slab with a dipping angle of 38^{o} and maximum depth of around 300 km, and the northern slab with a dipping angle of 47^{o} and a maximum depth of over 600 km. This is supported by the sections of Figures 71 (to the South of the discontinuity) and of Figures 72 and 73 (to the North of the discontinuity).

The sections of Figures 74, 75 and 76 suggest the existence

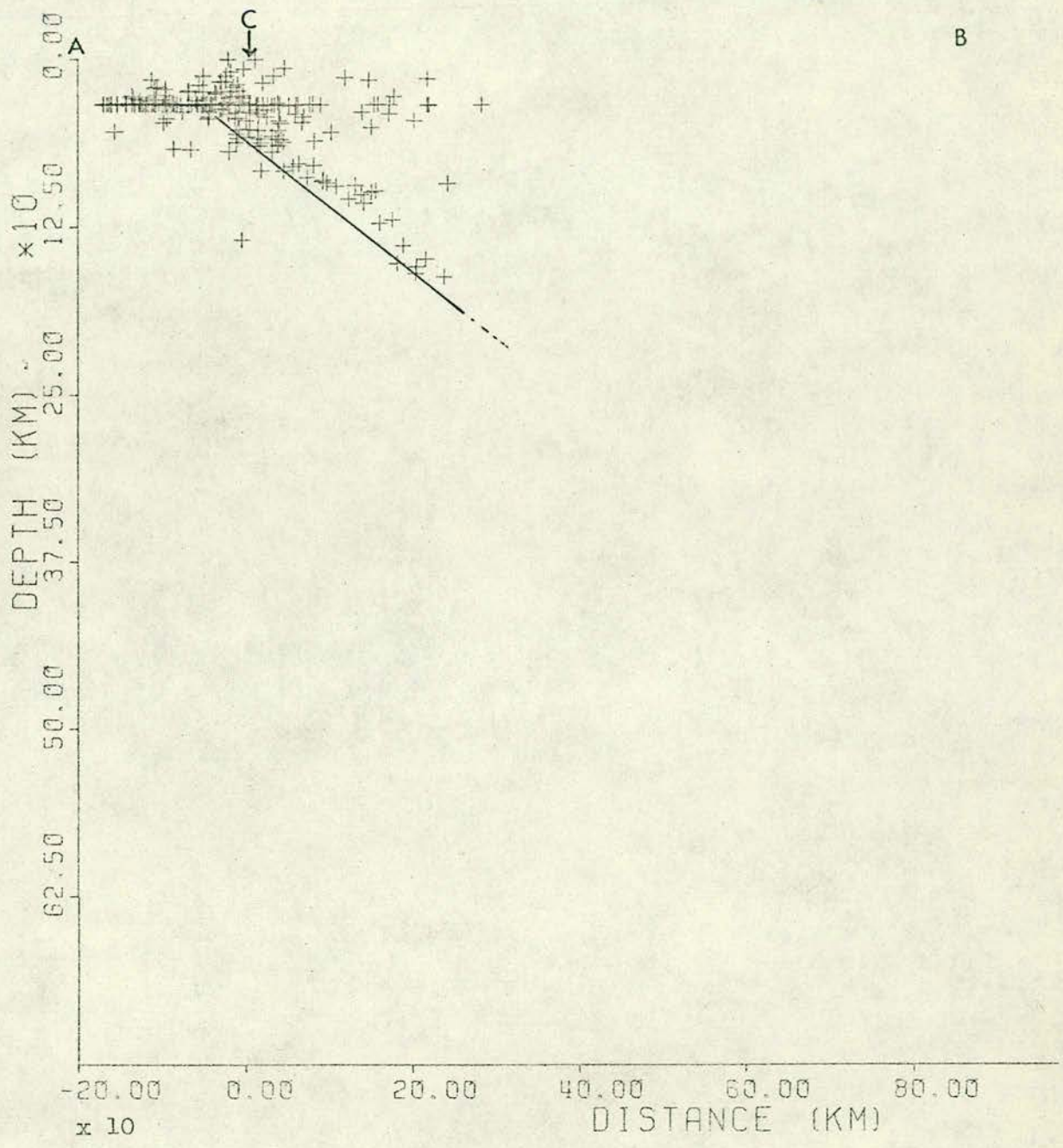

Figure 68.- SECTION A-B OF AREA 1 OF FIGURE 67

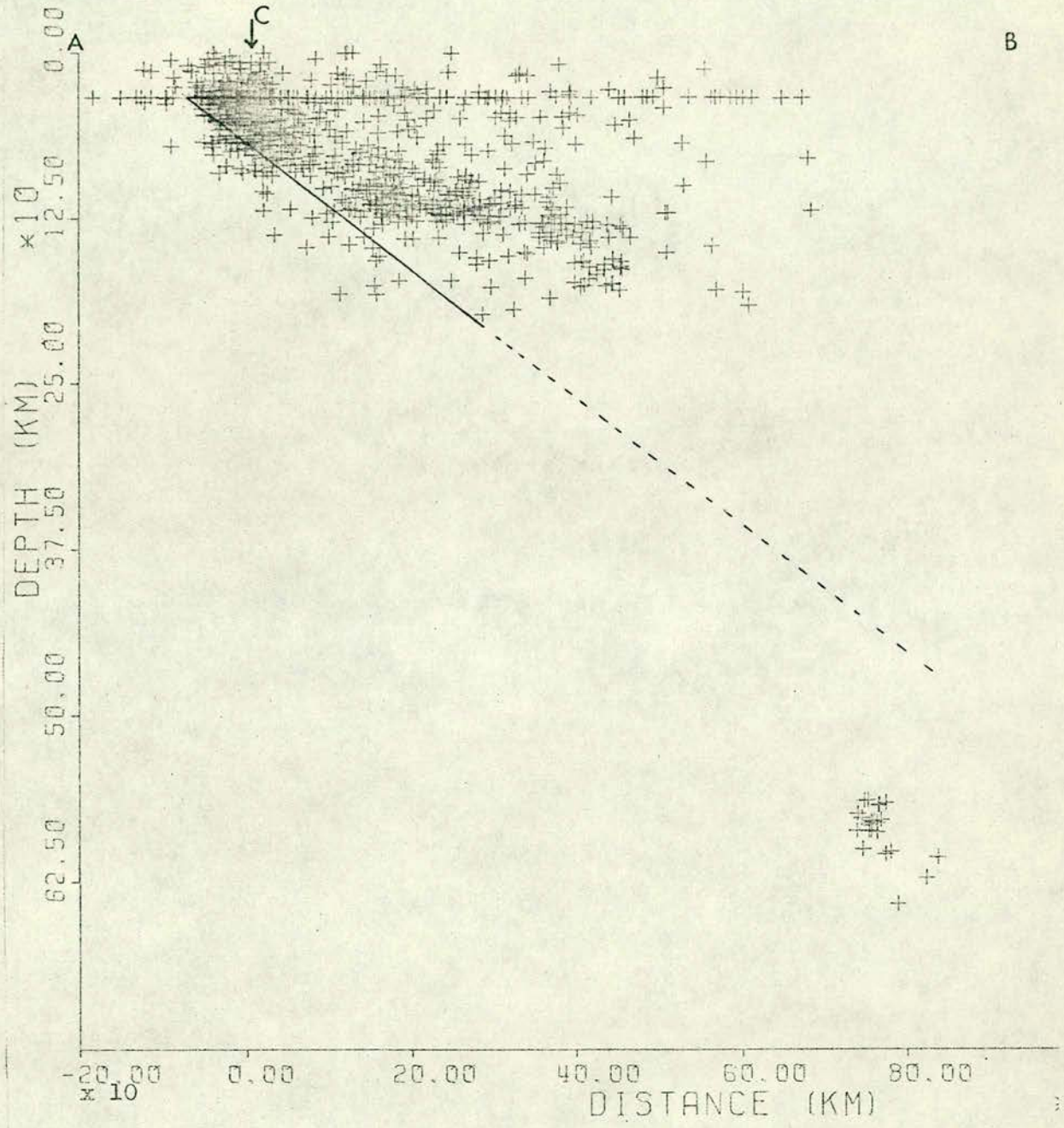

Figure 69.- SECTION A-B OF AREA 2 OF FIGURE 67

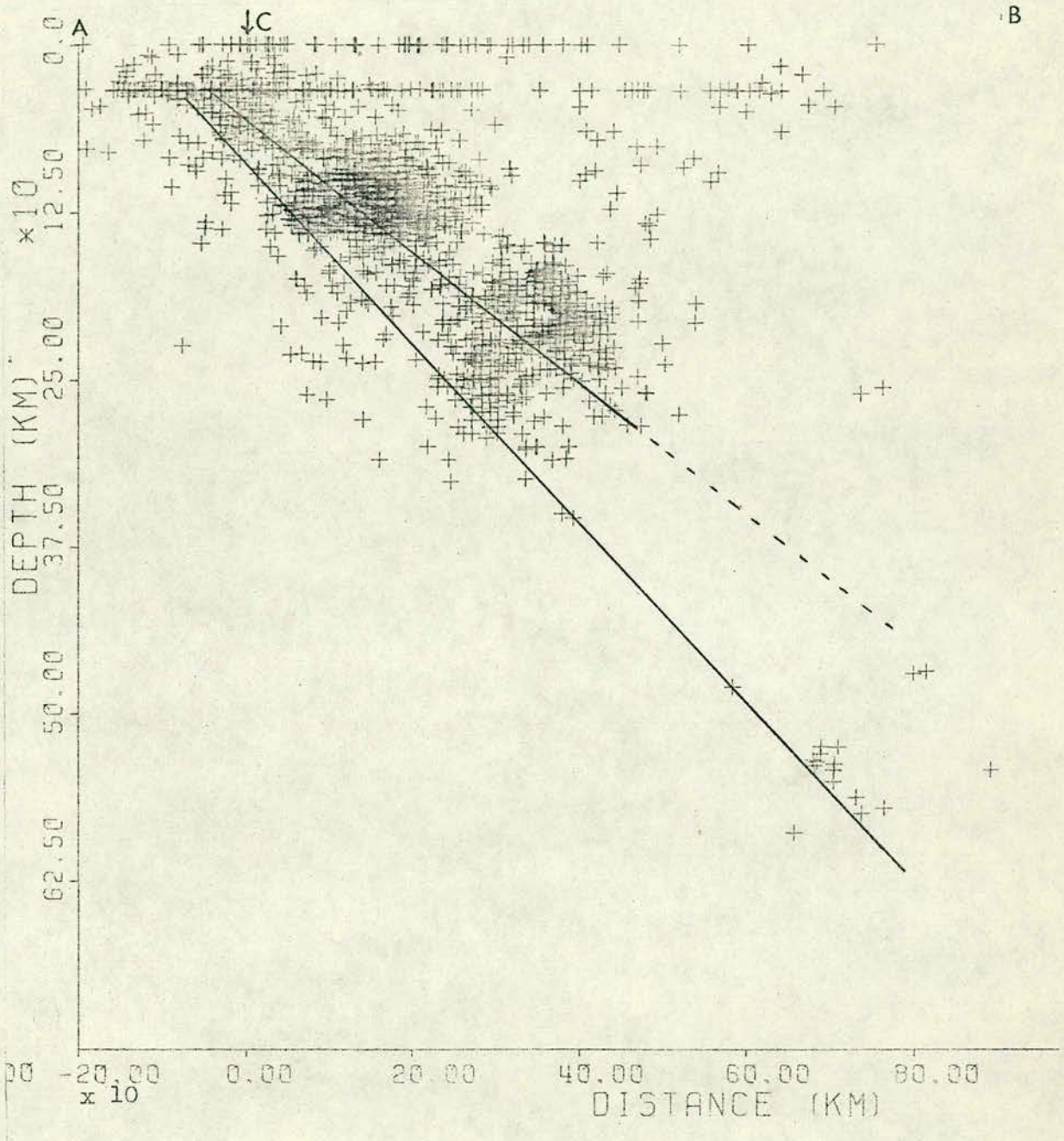

Figure 70.- SECTION A-B OF AREA 3 OF FIGURE 67

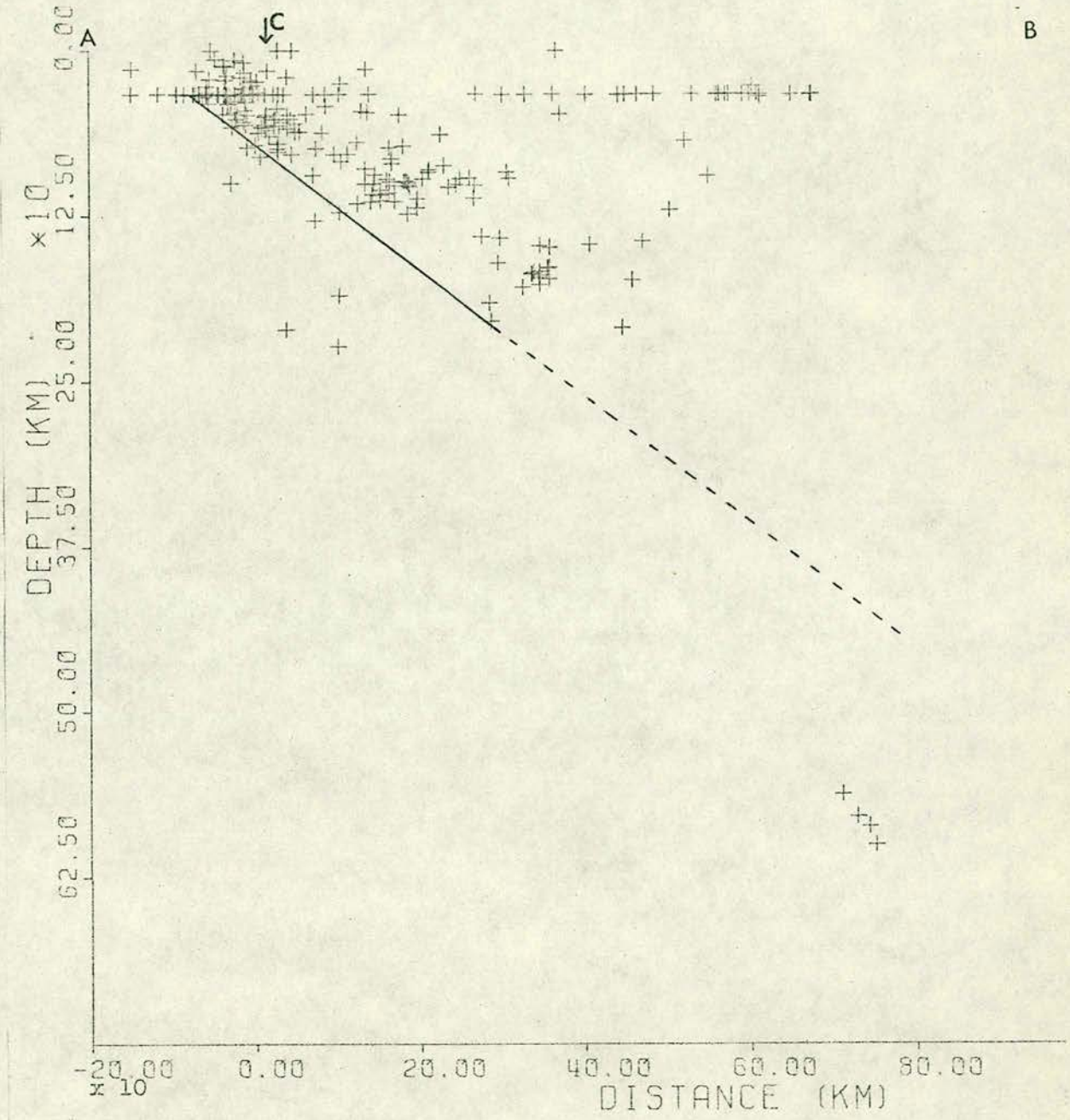

Figure 71.- SECTION A-B OF AREA 4 OF FIGURE 67

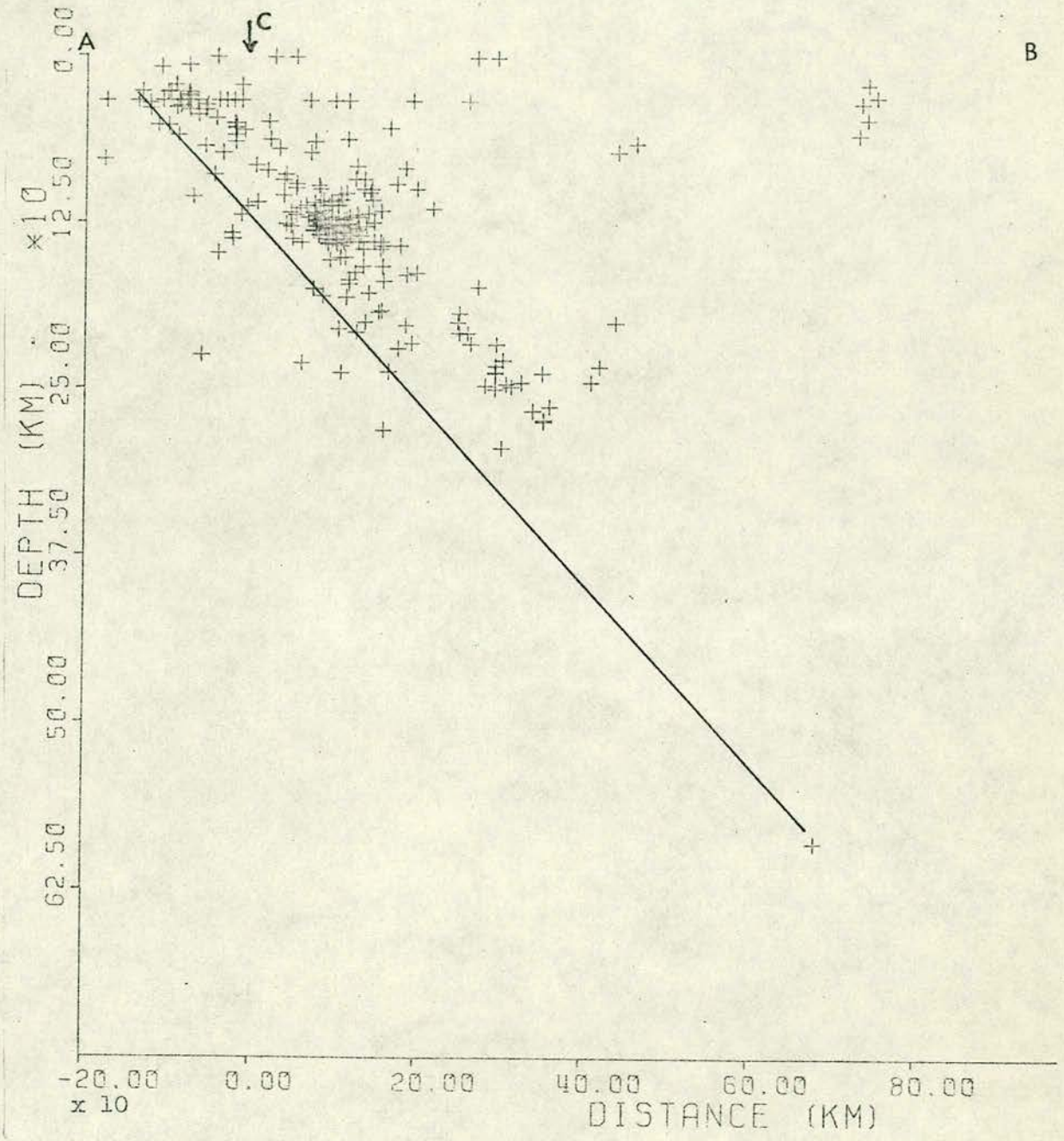

Figure 72.- SECTION A-B OF AREA 5 OF FIGURE 67

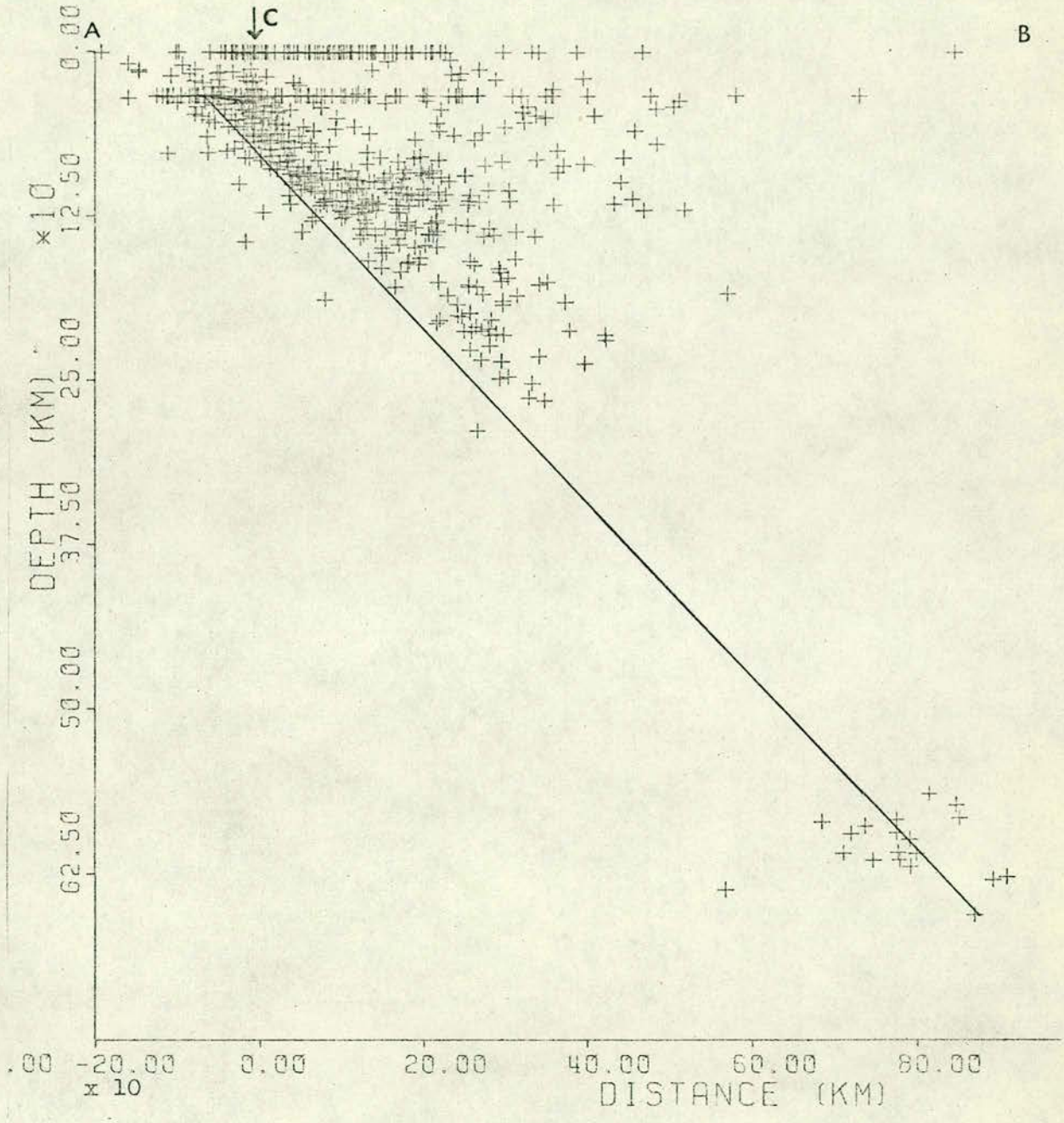

Figure 73.- SECTION A-B OF AREA 6 OF FIGURE 67

of another anomaly in the configuration of the descending slab under the Peru-Ecuador border region, although less clearly than the case discussed above. In Figure 74, the slab still presents a dipping angle of 47° and maximum depth of over 600 km. In Figure 75, the distribution of the projected hypocentres, suggests a dipping angle of the slab, in a southeastwards direction, of around 43° and a maximum depth of around 300 km for the majority of the events. Three events suggest a maximum depth of around 400 km, and one of around 650 km. This last deep event, which was a very unusual phenomenon, occurred on 31 JUL 1970 (01.4S, 72.5 W h = 651 km, m_b = 7.1). It seems to be associated with the mechanism which produces the deep events of the Peru-Brazil border (between 10°S and 6°S), rather than with a slab of 650 km depth, dipping southeastwards from the Colombian Pacific coast. The section of Figure 76 shows a reduction in the maximum depth of the slab in the northernmost of the areas shown in Figure 67, supporting the assumption of a slab with 300 km maximum depth for the previous section. Therefore, there appears to be some indication of the existence of a lateral discontinuity around the Peru-Ecuador border region, which may be related to the discontinuity suggested under the Amazon Basin.

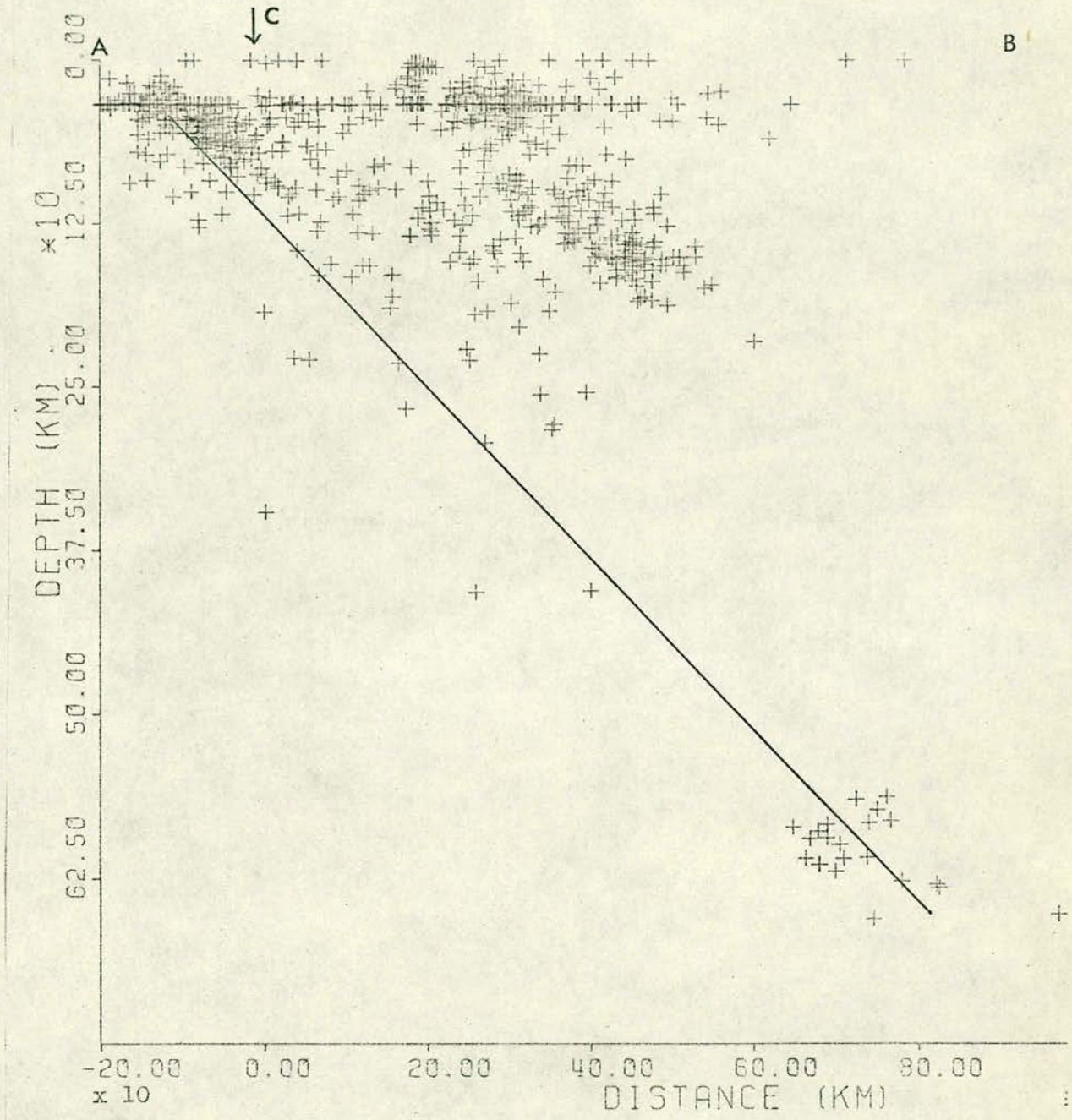

Figure 74.- SECTION A-B OF AREA 7 OF FIGURE 67

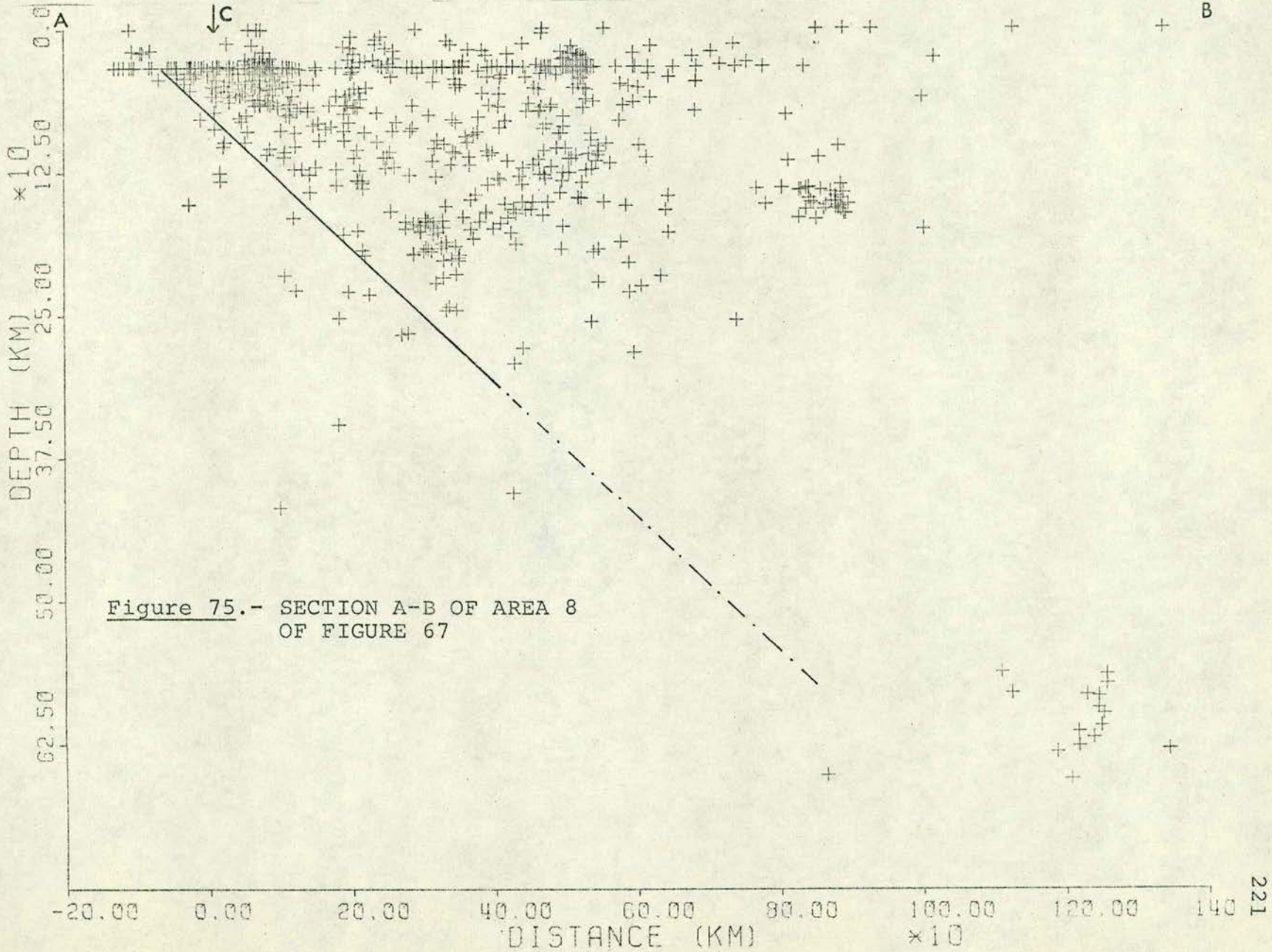

Figure 75.- SECTION A-B OF AREA 8 OF FIGURE 67

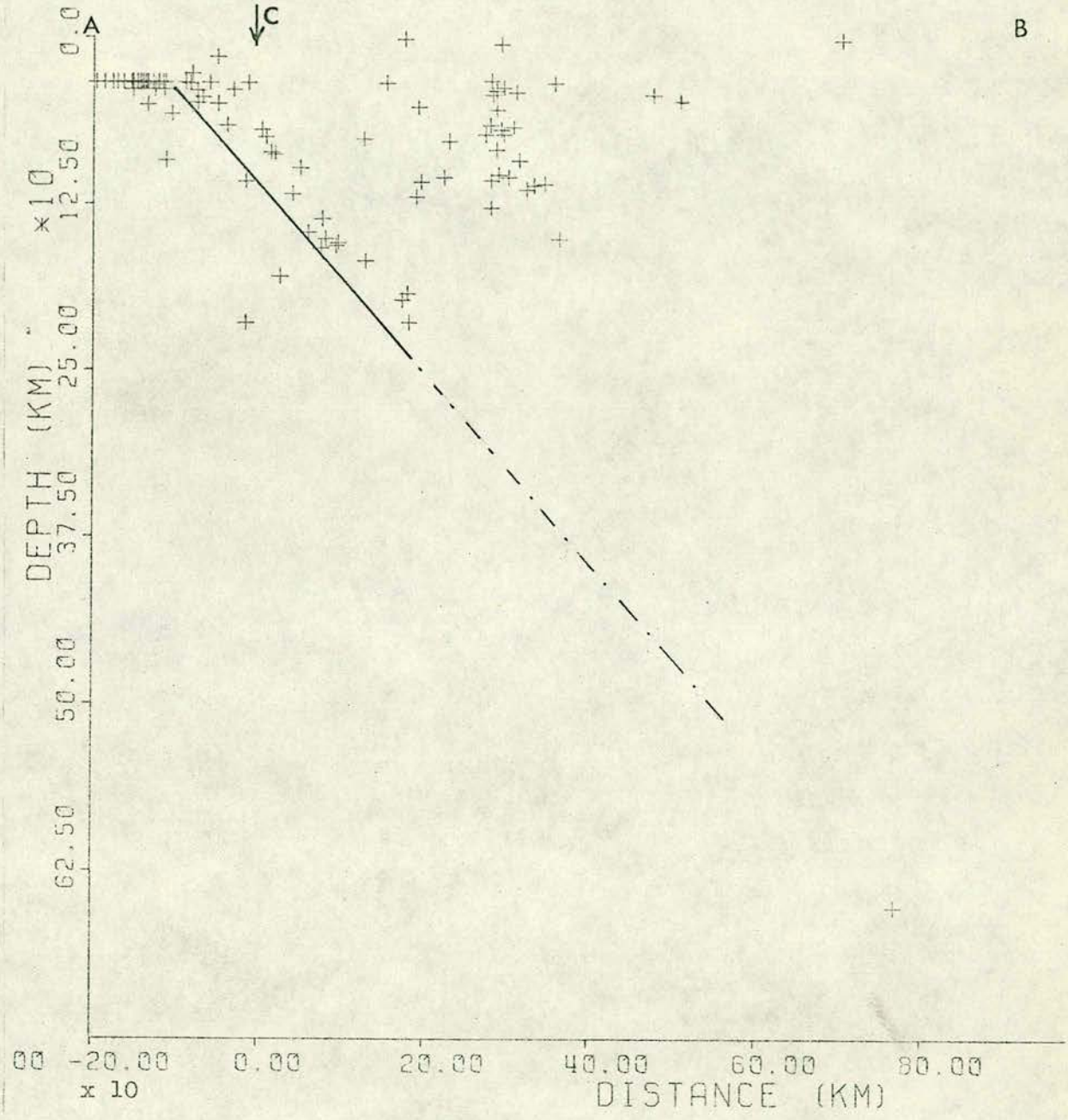

Figure 76.- SECTION A-B OF AREA 9 OF FIGURE 67

7.3 South American Physiographic Features Related to the Suggested Discontinuities

An explanation for the development of the suggested lateral discontinuities under the central part of western South America, and under the Amazon Basin, may be inferred from the probable origin of present physiographic features and from the history of the drift of this continent, as follows: (see Figure 66).

The surface projection of the discontinuity suggested in the central part of western South America coincides with the marked change in orientation of the Pacific coast line of this continent and of the Peru-Chile trench, from an almost N-S to a NN-SE direction. If the discontinuity projection line at the surface is continued to the SE, it will pass through the epicentral area of the deep events of northern Argentina, follow the hidrographic system of the Salado-Parana rivers and finally will reach the River Plate estuary. The suggested lateral discontinuity in the central part of western South America, can be considered as a boundary between two tectonic provinces of this continent, the southern and the central tectonic provinces, having different tectonic characteristics.

The existence of historically active volcanoes from 15^{o}S to 27^{o}S may also be related to the suggested lateral discontinuity; no historically active volcanoes are found to the North between 15^{o}S and 2^{o}S, and to the South between 27^{o} and 38^{o}S (which suggests other discontinuities at around 2^{o}S, as will be seen later, and at 38^{o}S, but with no seismic evidences, obtained in this study, for the latter).

It is suspected that these physiographic features have been

caused by the combination of the different convergence rate (at the southern and central tectonic provinces) and the overall change of drifting direction from westwards to northwestwards of the South American plate during the Lower Cretaceous (Freeland and Dietz, 1971). It could be that before this change in the drift direction, the bend of the Pacific coast line at around 18°S, which may have been more gentle, was at the same latitude as that of the present epicentral area of the deep Argentinean events. Perhaps since the beginning of the South American drift (end of Jurassic), the rates of convergence of the southern and central tectonic provinces were different in the same proportion as they are at present. This alone would have created favourable conditions for the origin of a lateral discontinuity, and the geometry of the slabs under the two provinces was always governed by the different convection rate. Under these conditions, before the Lower Cretaceous, there may have been two geometrically different slabs under western South America, the smaller one being under the southern province, which were divided by a lateral, perhaps vertical, discontinuity, which had a dominantly E-W direction, and at a latitude corresponding to the actual area of deep Argentinean events.

After the change in the drifting direction of South America during the Lower Cretaceous, and under the continuous convection rate difference between the southern and central tectonic provinces, the lateral discontinuity started to change its E-W orientation to a NW-SE one; from being vertical it became a southwestwards dipping plane, at least below the lithosphere. As South America drifted to the NW, the southernmost and deepest corner of the slab

under the ancient central tectonic province was left behind at its original latitude (or near it), but its corresponding point on the Pacific coast line (the bend of the coast line at around 18°S) was shifted to the N-W of its original position. This would explain the angle DAS formed by the surface projection of the discontinuity as deduced from the analysis of ΔAV and ΔAZ, in the following way: the events within the angle DAS showing positive values of ΔAV (Figure 45) and negative values of ΔAZ (Figure 44), have depths of around 200 km and are in the southern tectonic province, but very close to the lateral discontinuity which is dipping southwestwards; the seismic ray of these events must have an angle very near to normal with the intersection of a vertical plane passing through the seismic ray and the plane of the lateral discontinuity, therefore its inclination does not change even if its azimuth is affected by the discontinuity. Being so, the value of ΔAV must show the regional behaviour, which is a tendency to produce positive values of ΔAV at SAAS, and the values of ΔAZ must be similar to that of the events of the southern tectonic province, which is also correct. Therefore, the line AS, in Figure 44 and 45, represents the surface projection of the intersection of the lateral discontinuity with a vertical plane passing through point A and a point just to the North of the events within angle DAS, and the line AD is a projection at the surface of the intersection between the discontinuity and a vertical plane containing the line AD, which finds the discontinuity at a depth over 200 km at a latitude just to the South of the events which occurred within

the angle DAS, and coincides with the surface intersection of the lateral discontinuity at the point A. Therefore, the intersection between the lateral discontinuity and the surface must be at a line passing through A and rotated anticlockwise with reference to the lines AD and AS, as shown in Figure 66, but just a small angle, because the lateral discontinuity must be vertical at the lithosphere and crust.

The surface projection of the discontinuity under the Amazon Basin, is orientated almost in the E-W direction. Its intersection with the surface coincides with the proper river. It coincides in the East end with the Amazon river estuary, which is located at a marked change in the orientation of the northeastern Atlantic coast line of South America. At the West end and at around 4^{o}S, it coincides with another change in the orientation of the Pacific coast line of South America (from NW-SE to a NE-SW direction). It must be noticed that at around this point there is also a change in the surface characteristics of the Andes: a change in direction similar to that of the coast line, a sudden reduction on the width of the mountain range from around 300 km to less than 150 km., and the reappearance of historically active volcanoes which are extended up to the northern end of the Andes.

All the above considerations, and the earlier discussions of Chapter 6 suggest that the region North of the discontinuities under the Amazon Basin should be regarded as a separate tectonic province which has different tectonic characteristics than the central and southern provinces, as indicated in Figure 66.

Following the discussion of the lateral discontinuity separating the Southern and central tectonic provinces of South America, the suggested discontinuity under the Amazon Basin must have been originated by a probable difference in the subduction rates, between the central and northern provinces, as suggested by the depth of their respective slabs inferred from the sections of Figures 74, 75 and 76. It could be that the northern province was slowed down from its originally westwards drift rate by the Caribbean sub-plate drifting eastwards, creating a favourable condition for a lateral vertical discontinuity, which also was inclinated in a southwards direction, below the lithosphere, after the change in the drifting direction of South America during the Lower Cretaceous.

As observed in the case of the discontinuity separating the southern and central tectonic provinces, the point at around $4^{o}S$, where the Pacific coast line of South America changes its direction, was situated before the Lower Cretaceous at the same latitude as the actual epicentral area of deep events at the Peru-Brazil border region ($10^{o}S$-$6^{o}S$). The ancient northernmost and deepest end of the slab was also left behind after South America changed from westward to northwestwards drifting direction.

7.4 Time-Space Correlation of Deep South American Events

Finally, the suggestion of a continuous 600 km depth, slab under the central tectonic province, limited by the two lateral discontinuities inferred in this study, is supported by an apparent relationship between the deep events which occur at the southern and northern deep ends of this slab.

In Figure 77 have been plotted in a time-space dimension, all reported deep events which occurred in South America in the last 10 years. The southern end of the slab presents larger number of small occurrences, never larger than $M_S = 6.4$, whilst the northern end presents fewer shocks but with magnitudes mainly larger than $M_S = 6.4$.

It appears that, because the present northwestwards drift of South America, the slab tend to follow the movement of the lithosphere overlying it, creating compressional and extensional strains at the deepest ends of the slab. The extensional strains are more easily, and therefore, more frequently released, than the compressional ones, as can be observed in Figure 66, and Figure 77.

Their relationship in time is also quite clear. During the first years of the period studied, the northern deep events occurred at intervals of more or less one year, following a sequence of events in the southern end which appear to migrate northwards until the release of energy at the northern end of the slab. This sequence can last several months or just a few weeks. From March, 1967 up to February, 1968 only three small events ($M_S \approx 5.0$) occurred at the northern end of the slab and since then there was

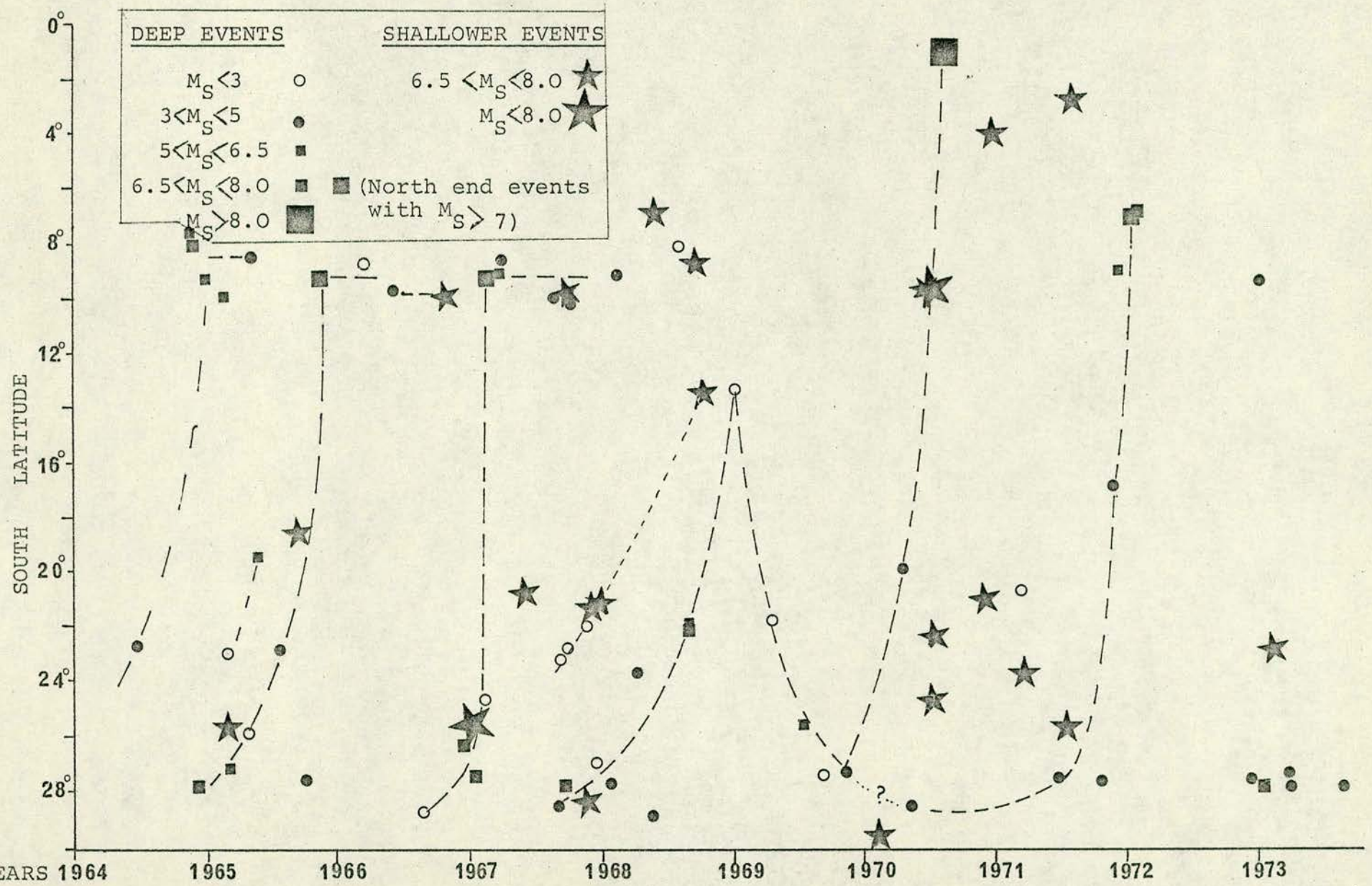

Figure 77.- TIME SPACE RELATION BETWEEN DEEP EVENTS FROM SOUTH AMERICA. SHALLOWER EVENTS FOLLOW THE PATTERN OF THE DEEP ONES.

not any reported earthquake up to July, 1970. During all that period in the southern end there was a great activity with two events having M_s= 6.4 following a northwards migration, which in January, 1969, reached an unusual latitude of 13°S. After this, the events at the South end appear to migrate southwards up to November, 1969 when they again recover their usual northwards migration, on this occasion going much further North than usual until the occurrence of an event with M_S = 9.1 at a latitude of 1.4°S, this being on a Northern extension of the axis of the usual northern deep events. At the end of May, 1970 a large disastrous event took place at the Peruvian northern coast (around 10°S). Therefore, these large unusual shocks, followed unusually great activity at the southern end of the slab, which was not followed by the yearly energy release rate at the northern end. If this is so, the observation of the seismic activity at the deep ends of the slab under the central tectonic province of South America, could offer a means for the prediction of some large disastrous earthquakes in this continent.

ACKNOWLEDGEMENTS

I sincerely wish to thank Dr. P.L. Willmore, Director of the Global Seismology Unit of the British Institute of Geological Sciences, for his guidance throughout this research and for allowing the use of the methods and equipment of his Unit. I am very grateful to Ing. Alberto Giesecke, Director of the Instituto Geofisico del Peru and of CERESIS, for his support and encouragement to complete this study.

I also wish to thank Dr. S. Crampin and Dr. R. Lilwall for their constructive critisism and useful comments during the preparation of the text and for their assistance in the computer programs used in this work. The basic data and many illustrations were obtained with Dr. Lilwall's programs.

I have to thank Mr. A. Miller for his contribution in Chapter 2 and and for his effort during the installation of SAAS. I am also indebted to Mr. G. Neilson for his help in the revision of the manuscript and useful comments, to C. Fyfe for his assistance with the digital equipment at ERCC, and to Mr. D. Houliston for his assistance with the analogue equipment used in this research. I also wish to thank Mrs. G. Hall for her effort made during the typing of the final text.

Many thanks also to the University of Brasilia staff envolved

with SAAS and to the colegues of the Grupo de Geofisica of the Department de Geociencias of the UnB who were involved with different aspects of this research.

I am especially grateful to my dear wife who besides her continuous encouragement through this study, helped in the typing of the final scratch of this thesis and in the preparation of the illustrations, and who together with my dear doughter, made many sacrifices,which able me to finish this work.

The final stage of this research was completed under a fellowship granted by UNESCO, for which I thank Dr. F. d'Albe, and under a fellowship granted by the Carnegie Institution of Washington for which I am grateful to Dr. L.T. Aldrich.

BIBLIOGRAPHY

Aldrich, L.T., H.E. Tatel, M.A. Tuve and G.W. Wetherill, 1958.The Earth's crust, Carnegie Inst. Wash. Year Book, 57, 104-111.

Archambeau, C.B., E.A. Flinn and D.G. Lambert, 1969. Fine structure of the upper mantle, J. Geophys. Res., 74, 5825-5865.

Asbel, I. Ja., V.I. Keilis-Borok and T.B. Yanovskaja, 1966. A technique of a joint interpretation of travel-time and amplitude-distance curves in the upper mantle studies, Geophys. J.R. astr. Soc., 11, 25-55.

Barazangi, M. and B. Isacks, 1971. Lateral variations of seismic-wave attenuation in the upper mantle above the inclined earthquake zone of the Tonga Island arc: deep anomaly in the upper mantle[1], J. Geophys. Res., 76, 8493-8516.

Berrocal, J., 1968. The aplication of seismograph arrays to the study of regional seismicity,M. Ss. thesis, University of Edinburgh.

Berrocal, J., E.A. Ladeira, A. Faria, J. Barros,R.B. de Oliveira, S.A.B. Vieira, 1972. Aspectos tectonicos da America do Sul obtidos atraves da Estacao Sismologica de Brasilia, Boletim no.12, SICEG, Universidade Federal de Ouro Preto, M.G. - Brazil.

Birch, F. (Edit.), 1942. "Handbook of Physical Constants", Geol. Soc. America Spec., paper 36.

Bolt, B.A. and O.W. Nuttli, 1966. P wave residuals as a function of azimuth, J. Geophys. Res., 71, 5977-5985.

Booth, B., 1973. Pyroclastic paoxysms, New Scientist, 59, 697.

Bott, A., 1971. The interior of the Earth, Edward Arnold (Publishers) Ltd, London U.K.

Bune, V.I., N.A. Vvedenskaya, I.V. Gorbunova, N.V. Kondorskaya, N.S. Landyreva and I.V. Fedorova, 1970. Correlation of M_{lh} and m_{pv} by data of the network of seismic stations of the U.S.S.R., Geophys. J.R. astr. Soc., 19, 533-542.

Bungum, H., E.S. Husebye and F. Ringdal, 1971. The NORSAR array and preliminary results of data analysis, Geophys. J.R. astr. Soc., 25, 115-126.

Carpenter, E.W., P.D. Marshall and A. Douglas, 1967. The amplitude-distance curve for short period teleseismic P-waves, Geophys. J.R. astr. Soc., 13, 61-70.

Chinnery, M.A. and M.N. Toksoz, 1967. P-wave velocities in the mantle below 700 km, Bull. Seism. Soc. Am., 57, 199-226.

Chuaqui, L., 1973. A simple model of the crust and upper mantle in central Chile, Bull. Seism. Soc. Am., 63, 819-825.

Clark, A.H., E. Farrar, J.C. Caelles, S.J. Haynes, R. Lortie, S. McBride, S. Quirt, and M. Zentilli, 1973. The magmatic, tectonic and metallogenetic evolution of the central andean mobile belt between latitudes 26^{o} and 29^{o} south: an investigation of one transect of the 'andean-type' consuming plate margin environment, SUMMARY presented at the Session of the Geodynamics Conference, IASPEI, Lima, August 22nd.-28th.

Cleary, J.R. and A.L. Hales, 1966. An analysis of the travel times of P waves to North American stations, in the distance range 32^{o} to 100^{o}, Bull. Seism. Soc. Amer., 56, 467-489.

Cleary, J.R., C. Wright and K.J. Muirhead, 1968. The effects of local structure upon measurements of the travel time gradient at the Warramunga seismic array, Geophys. J.R. astr. Soc., 16, 21-29.

Crampin, S. and S.N. Morgan, 1971. The response of the racal-thermionic seismic recording system, Report no.5, Institute of Geological Sciences Geophysical Division, Edinburgh.

Crampin, S., C.J. Fyfe and D.J. Houliston, 1973. Automatic analysis of tape-recorded seismic signals, Report, Institute of Geological Sciences Geophysical Division, Edinburgh.

Dewey, J.F. and J.M. Bird, 1970. Mountain belts and the new global tectonics, J. Geophys. Res., 75, 2625-2647.

Dietz, R.S., 1961. Continent and ocean basin evolution by spreading of the sea floor, Nature, Lond., 190, 854-857.

Dietz, R.S. and J.C. Holden, 1970. Reconstruction of Pangaea: breakup and dispersion of continente, Permian to Present, J. Geophys. Res., 75,

Douglas, A., P.D. Marshall and D.J. Corbishley, 1971. Absorption and complexity of P signals, Nature phys. Sci., 233, 50-51.

Douglas, A., P.D. Marshall, P.G. Gibbs, J.B. Young and C. Blamey, 1973. P. signal complexity re-examined, Geophys. J.R. astr. Soc., 33, 195-221.

Dragicevic, M., 1970. Carta gravimetrica de los Andes meridionales e interpretacion de las anomalias de gravedad de Chile central, Publicacion N. 93, University of Chile, Editorial Universitaria, S.A., Santiago-Chile.

Duda, S.J., 1965. Secular seismic energy release in the circum-Pacific belt, Tectonophysics, 2, 409-1965.

Ewing, J. and M. Ewing, 1967, Sediment distribution on the mid-ocean ridges with respect to spreading of the sea floor. Science, N.Y., 156, 1590- 1592.

Ewing, J.I., W.J. Ludwing, M. Ewing and S.L. Eittreim, 1971, Structure of the Scotia Sea and Falkland, J. Geophys. Res., 76, Plateau 7118-7137.

Fisher, R.L., and R.W. Raitt, 1962. Topography and structure of the Peru-Chile trench. Deep-sea Research. Vol.9.

Freeland, G.L. and R.S. Dietz, 1971. Plate tectonic evolution of Caribbean-Gulf of Mexico region, Nature, 232, 20-23.

Fyfe, C.F., 1973. (Personal comunication), IGS report in preparation.

Green, R.W.E. and A.L. Hales, 1968. The travel times of P waves to 30° in the central United States and upper mantle structure, Bull. Seism. Soc. Amer., 58, 267-289.

Gupta, H.K. and B.K. Rastogi, 1972. Earthquake m_b vsM_s relations and source multiplicity, Geophys. J.R. astr. Soc., 28, 65-89.

Gutenberg, B. and C.F. Richter, 1956. Magnitude and energy of earthquakes, Ann. Geofis. 9, 1-15.

Hales, A.L., J.R. Cleary, H.A. Doyle, R.Green and J. Roberts, 1968. P-wave station anomalies and the structure of the upper mantle, J.Geophys. Res., 73, 3885-3896.

Heirtzler, J.R., G.O. Dickson, E.M. Herron, W.C. Pitman, 1968. Marine magnetic anomalies, geomagnetic field reversals, and motions of the ocean floor and continents, J. Geophys. Res., 73, 2119-2136.

Helmberger, D. and R.A. Wiggins, 1971. Upper mantle structure of midwestern United States, J. Geophys. Res., 76, 3229-3245.

Herrin, E., 1968. Introduction to the 1968 seismological tables for P phases, Bull. Seism. Soc. Am., 58, 1193-1195.

Herrin, E. and J. Taggart, 1962. Regional variations in Pn velocity and their effect on the location of epicenters, Bull. Seism. Soc. Am., 52, 1037-1046.

Herrin, E. and J. Taggart, 1968. Regional variations in P travel times, Bull. Seism. Soc. Am., 58, 1325-1337.

Herrin, E., W. Tucker, J. N. Taggart, D. W. Gordon and J.L. Lobdell. 1968. Estimation of surface-focus P travel times, in 1968 Seismological Tables for P Phases, (chairman, E. Herrin).

Herron, E.M. and D.E. Hayes, 1969. A geophysical study of the Chile ridge, Earth Planet. Sci. Lett., 6, 77.

Hess, H.H., 1962. History of ocean basins. In Petrologic studies: a volume in honor of A.F. Buddington, 620, Geological Society of America.

Houliston, D., 1973. The seismic data processing systems of the Institute of Geological Sciences in Edinburgh, IGS Bulletin 2 (in press).

Husebye, E.S., R. Kanestrom and R. Rud, 1971. Observations of vertical and lateral P-velocity anomalies in the Earth's mantle using the Fennoscandian continental array, Geophys. J.R. astr. Soc., 25, 3-16.

Isacks, B.L. and M. Barazangi, 1973. High frequency shear waves guided by a continuous lithosphere descending beneath western South America, Geophys. J.R. astr. Soc., 33, 129-139.

Isacks, B., J. Oliver and L. Sykes, 1968. Seismology and the new global tectonics, J. Geophys. Res., 73, 5885-5899.

Jacob, A.W.B. and P.L. Willmore, 1972. Teleseismic P waves from a 10 ton explosion, Report no. 16, Institute of Geological Sciences Geophysical Division, Edinburgh.

James, D.E., 1971. Andean crustal and upper mantle structure, J. Geophys. Res., 76, 3246-3271.

Jeffreys, H. and K.E. Bullen, 1940. Seismological Tables, Brit. Assoc. Adv. Sci., Gray-Milne Trust.

Johnson, L.R., 1966. Measurements of mantle velocities of P waves with a large array, Ph.D. thesis, Calif. Inst. Tech., Pasadena.

Johnson, L.R., 1967. Array measurements of P velocities in the upper mantle, J. Geophys. Res., 72, 6309-6325.

Johnson, L.R., 1969. Array measurements of P velocities in the lower mantle, Bull. Seism. Soc. Amer., 59, 973-1008.

Jordan, T.H., 1973. Estimation of the radial variation of seismic velocities and density in the Earth, Ph.D. thesis, California Institute of Technology, Pasadena.

Jordan, J.N. and R.N. Hunter, 1972. A comparison of NOS and USSR magnitudes, Geophys. J.R. astr. Soc., 27, 23-28.

Julian, B.R. and D.L. Anderson, 1968. Travel times, apparent velocities and amplitudes of body waves, Bull. Seism. Soc. Amer., 58, 339-366.

Kanamori, H., 1967. Upper mantle structure from apparent velocities of P waves recorded at Wakayama micro-earthquake observatory, Bull. Earthquake Res. Inst. Tokyo, 45, 657-678.

Key, F.A., 1968. Some observations and analyses of signal generated noise, Geophys. J.R. astr. Soc., 15, 377-392.

Le Pichon,. 1968. Sea-floor spreading and continental drift, J. Geophys. Res., 73, 3661-3697.

Lilwall,, R.C., 1973. Array processing programs to find, a) relative arrival times and b) azimuth and dT/dΔ from a digitised recording, Report no.34 Institute of Geological Sciences Gophysical Division, Edinburgh.

Lilwall, R.C. and A. Douglas, 1970. Estimation of P-wave travel times using the Joint Epicentre Method, Geophys. J.R. astr. Soc., 19, 165-181.

Loczy, L., 1970. Role of transcurrent faulting in South America tectonic framework, American Association of Petroleum Geologist Bull, 54, 11.

Lomnitz, C., 1962. On Andean structure. J. Geophys. Res., 67, 351-364.

Lomnitz, C., 1971. Travel-time errors in the laterally inhomogeneous earth, Bull. Seism. Soc. Amer., 61, 1639-1654.

Lomnitz, C. and A. Vargas. 1969. Estimacion de tiempos de recorrido de ondas sismicas, Ann. Inst. Geofis., (Mexico) 14, 71-73.

Mattson, P.H., 1972. Plate tectonics in the Caribbean, Nature, 235, 155.

McGinley, J.R. and Don L. Anderson, 1969. Relative amplitudes of P and S waves as a mantle reconnaissance tool, Bull. Seism. Soc. Am., 59, 1189-1200.

McKenzie, D.P. and R.L. Parker, 1967. The north Pacific: an example of tectonics on a sphere, Nature, Lond., 216, 1276-1280.

Miller, A., 1973. (Personal comunication), IGS report in preparation.

Molnar, P. and J. Oliver, 1969. Lateral variations of attenuation in the upper mantle and discontinuities in the lithosphere, J. Geophys. Res., 74, 2648-2682.

Morgan, W.J., 1968. Rises trenches, great faults, and crustal blocks, J. Geophys. Res., 73, 1959-1982.

Morgan, W.J., P.R. Vogt, and D.F. Falls, 1969. Magnetic anomalies and sea floor spreading on the Chile rise, Nature, 222, 137.

Niazi, M., 1966. Corredtions to apparent azimuths and travel time gradients for a dipping Mohorovicic discontinuity, Bull. Seism. Soc. Amer., 56, 491-509.

Niazi, M. and Don L. Anderson, 1965. Upper mantle structure of western North America from apparent velocities of P waves, J. Geophys. Res., 70, 4640-4653.

Nuttli, O.W., 1972. The amplitudes of teleseismic P waves, Bull. Seism. Soc. Amer., 62, 343-356.

Olea, R., 1966. Determinacion de hipocentros y su aplicacion al estudio del Norte de Chile. Publ. 43, Santiago.

Oliver, J. and B. Isacks, 1967. Deep earthquake zones anomalous structures in the upper mantle, and the lithosphere, J. Geophys. Res., 72, 4259-4275.

Otsuka, M., 1966. Azimuth and slowness anomalies of seismic waves measured on the central California seismographic array. Part II: Interpretation, Bull. Seism. Soc. Amer., 56, 655-675.

Plafker, G., 1972. Alaskan eathquake of 1964 and Chilean earthquake of 1960: implications for arc tectonics, J. Geophys. Res., 77, 901-925.

Richter, C.F., 1935. An instrumental earthquake magnitude scale, Bull. Seism. Soc. Am., 25, 1-32.

Romney, C., B.G. Brooks, R.H. Mansfield, D.S. Carder, J.N. Jordan and D.W. Gordon, 1962. Travel times and amplitudes of principal body phases recorded from Gnome, Bull. Seism. Soc. Am., 52, 1057-1074.

Simpson, D.W., 1973. P wave velocity structure of the upper mantle in the Australian region, P.h.D. thesis Australian National University.

Wiggins, R.A. and D.V. Helmberger, 1972. Upper mantle structure of Western United States, preprint.

Willmore, P.L., 1972. Discussions on 10-ton explosions for teleseismic observations, Proceedings from the seminar on seismology and seismic arrays, Oslo, 22-25 November 1971, 43-47.

Wilson, J.T. 1965. A new class of faults and their bearing on continental drift, Nature, 207, 343.

Woollard, G.P., 1960. Seismic crustal studies during the IGY, 2, Continental program (IGY Bulletin 34), Trans. AGV, 41, 351-355.

APPENDICES

APPENDIX 1

RELATION AND ANALYSIS OF EVENTS USED IN THE PRESENT STUDY

NOAA EPICENTRAL DATA					SAAS READINGS			
DATE	ORIG.TIME	MB	DEP.	REGION	OBS.TIME	MB	EVENT N.	
10MAR72	061428.3	4.2	33	N.ATLANTIC RIDGE	E 062258.3	4.5	18A/0351	
10MAR72	102503.4	5.2	128	NEAR C.OF VENEZUELA	I 103105.2	5.4	A01	
11MAR72	003831.7	4.9	33	PERU	I 004417.7	4.7	A02	
11MAR72	014133.1	3.9	157	EL SALVADOR	E 015016.9	4.2	A03	
11MAR72	035045.9	5.1	85	NEAR C.OF GUATEMALA	I 035939.1	5.2	A04	
13MAR72	173515.0	5.0	35	NEAR C.OF N.PERU	E 174127.8	4.4	18B/1621	
13MAR72	140545.8	5.4	33	TURKEY	E 141847.3	5.4	A05	
16MAR72	020909.1	4.4	25	OFF C.OF C.CHILE	E 021453.1	4.2	19B/0220	
16MAR72	090701.4	4.6	28	NEAR C.OF C.CHILE	I 091246.1	5.0	A06	
19MAR72	220848.3	4.9	40	NEAR C.OF C.CHILE	E 221429.7	5.2	A07	
20MAR72	073349.6	6.1	64	N.PERU	I 073949.1	6.2	A08	
20MAR72	165027.1	5.4	33	N.PERU	I 165631.1	5.3	A09	
20MAR72	170246.5	5.4	33	EASTER I.CORDILLERA	E 171315.9	4.9	20B/0690	
20MAR72	201222.3	5.0	33	OFF C.OF C.CHILE	E 201852.5	4.8	20B/0800	
22MAR72	033156.0	3.6	162	PERU-BOLIVIA B.R.	E 033626.0	4.4	A12	
23MAR72	092359.6	4.9	33	S.SANDWICH I.R.	I 093223.7	4.7	A13	
27MAR72	081447.7	5.1	33	S.ATLANTIC RIDGE	E 082118.6	4.7	A14	
27MAR72	083125.2	4.2	95	OAXACA MEXICO	E 084058.7	4.3	22A/1269	
27MAR72	085204.0	4.3	33	C.MID.ATLANTIC RIDGE	I 085727.2	4.6	A15	
27MAR72	120941.2	5.2	63	NEAR C.OF PERU	I 121520.6	4.8	A16	
27MAR72	203212.6	0.0	33	OFF C.OF C.CHILE	E 203756.3	4.1	22B/0001	
28MAR72	080850.1	4.1	69	NEAR C.OF C.CHILE	I 081429.0	4.1	22B/0416	
30MAR7I	110020.1	5.6	72	NEAR C.OF C.CHILE	I 110546.2	5.7	23A/0400	
31MAR72	025802.4	4.7	33	S.GREECE	I 031029.0	4.8	A17	
31MAR72	081352.8	4.7	66	NEAR C.OF C.CHILE	I 081919.4	4.9	A18	
31MAR72	105439.4	4.3	164	N.COLOMBIA	I 110104.6	4.4	A19	
31MAR72	121956.3	4.7	49	NEAR C.OF C.CHILE	E 122449.2	4.6	A20	
31MAR72	153653.5	5.5	33	S.SANDWICH I.R.	I 154444.6	5.4	A21	
31MAR72	203200.9	4.5	18	DODECANESE I.	E 204450.5	4.6	23A/1600	
15APR72	094227.8	4.4	99	NORTHERN CHILE	I 094702.4	4.3	27A/0428	
16APR72	000331.7	4.6	136	RUMANIA	E 001620.5	4.7	A22	
16APR72	101003.6	4.9	18	AUSTRIA	I 102240.8	4.7	A23	
16APR72	110444.3	4.4	19	AUSTRIA	E 111721.9	4.2	27A/1339	
17APR72	192559.7	4.3	88	EL SALVADOR	E 193450.7	4.2	27B/0770	
18APR72	055152.8	4.7	33	N.ATLANTIC OCEAN	E 060213.7	4.8	27B/1144	
18APR72	081411.8	5.1	33	OFF C.OF N.CHILE	E 081914.3	4.8	A24	
19APR72	105732.1	4.4	33	ECUADOR	E 110405.4	4.1	28A/0470	
19APR72	121847.9	5.3	104	S.JUAN PROV.ARGENT.	I 122359.1	4.6	A25	
20APR72	024923.8	4.8	33	EASTER I.CORDILLERA	E 025959.5	4.6	28A/1038	
22APR72	022250.7	5.2	33	S.W.ATLANTIC OCEAN	I 023107.2	5.0	28B/1023	
23APR72	032218.2	4.3	175	CATAMARCA PROV.ARGEN.	E 032650.2	4.7	29A/0192	
23APR72	184504.7	4.7	33	S.OF AFRICA	E 185600.6	4.7	29A/0744	
24APR72	012048.2	5.8	33	EASTER I. REGION	I 013048.8	5.7	29A/0980	
25APR72	005949.8	4.7	33	TANGANYICA	E 011159.5	4.2	29B/0144	

NOAA EPICENTRAL DATA					SAAS READINGS			
DATE	ORIG.TIME	MB	DEP.	REGION	OBS.	TIME	MB	EVENT N.
26APR72	053520.3	4.2	44	OAXACA,MEXICO	E	054457.9	4.1	29B/1113
26APR72	063023.9	5.0	26	TURKEY	I	064315.4	5.1	A28
26APR72	155945.0	4.8	28	TURKEY	I	161236.0	5.0	A29
28APR72	162638.6	4.6	119	S.JUAN PROV.ARGEN.	E	163148.4	4.0	30A/1587
29APR72	182938.3	5.1	47	CRETE	E	184212.4	4.7	A30
30APR72	003048.0	5.0	88	NEAR C.OF C.CHILE	I	003617.7	5.5	A31
30APR72	105519.5	4.4	77	OFF C.OF C.AMERICA	E	110403.6	4.6	A32
01MAY72	223235.0	4.4	18	OFF C.OF COSTA RICA	E	224044.8	3.8	31A/0921
02MAY72	065623.4	5.8	33	E.CENT.PACIFIC OCEAN	I	070558.2	5.9	A34
02MAY72	110634.8	4.6	33	CARIBBEAN SEA	E	111434.0	4.5	31A/1369
02MAY72	191501.8	5.0	20	S.NEVADA	E	192729.2	5.0	31A/1663
04MAY72	060543.7	3.9	172	CHILE-ARGENTINA B.R.	I	061002.7	5.4	31B/1215
04MAY72	062640.5	5.1	115	CHIAPAS,MEXICO	I	063557.4	5.6	A36
04MAY72	214000.9	5.9	46	CRETE	I	215221.3	5.2	A38
05MAY72	171439.9	0.0	121	S.JUAN PROV.ARGENT.	E	171958.5	4.1	A39
05MAY72	193833.4	5.3	33	S.SANDWICH I.R.	E	194624.6	5.0	A40
07MAY72	165240.3	4.9	33	N.ATLANTIC RIDGE	I	165841.3	4.2	32B/0748
06MAY72	114030.5	4.5	215	JUYJUY PROV.ARGENT.	I	114437.6	5.1	A41
07MAY72	113148.5	4.6	50	NEAR C.OF PERU	E	112652.1	4.2	A42
07MAY72	220630.1	5.4	33	S.PACIFIC CORDILLERA	E	221809.6	4.9	A44
08MAY72	061800.7	0.0	50	N.COLOMBIA	E	062426.0	4.2	A45
08MAY72	092054.5	5.0	10	GREECE-BULGARIA B.R.	E	093343.8	4.5	A46
08MAY72	134031.0	4.8	168	N.COLOMBIA	E	134656.7	4.0	32B/1490
10MAY72	103156.8	4.0	127	N.CHILE	E	103627.6	4.7	A48
10MAY72	173035.0	5.4	89	ECUADOR	I	173702.8	5.2	A49
12MAY72	134841.1	4.0	119	CHILE-BOLIVIA B.R.	E	135309.0	4.0	33B/1182
12MAY72	171635.9	5.0	102	BOLIVIA	I	172032.9	4.9	A51
13MAY72	102914.6	4.5	112	CHILE-ARGENTINA B.R.	I	103445.9	4.8	A52
13MAY72	140221.5	4.8	33	N.ATLANTIC OCEAN	E	141329.6	4.5	34A/0590
13MAY72	142424.7	4.9	40	PERU-ECUADOR B.R.	I	143108.6	5.0	A53
13MAY72	150638.2	4.8	33	N.ATLANTIC RIDGE	I	151704.5	4.6	A54
13MAY72	151935.9	5.7	38	NEAR C.OF C.CHILE	I	152518.1	5.7	34A/0632
13MAY72	163713.3	4.8	33	N.ATLANTIC RIDGE	E	164739.4	4.6	A55
13MAY72	164022.0	5.0	33	N.ATLANTIC RIDGE	E	165047.2	5.0	A56
13MAY72	214456.0	5.4	40	NEAR C.OF C.CHILE	I	215038.5	5.4	A57
15MAY72	091255.4	4.9	51	NEAR C.OF C.CHILE	I	091821.2	4.6	A58
15MAY72	100940.0	5.6	39	CHILE-ARGENTINA B.R.	I	101454.6	5.8	A59
15MAY72	112129.3	5.0	33	S.PACIFIC CORDILLERA	I	113250.8	4.9	A60
15MAY72	121243.3	4.7	33	C.MID-ATLANTIC RIDGE	E	121808.9	4.4	A61
15MAY72	220731.0	4.5	33	S.GEORGIA I.R.	E	221512.7	4.3	34B/0858
16MAY72	104514.0	4.2	120	CHILE-ARGENTINA B.R.	E	105037.5	3.5	34A/1307
16MAY72	163127.0	0.0	33	PANAMA-COLOMBIA B.R.	E	163840.5	4.3	35A/0730
17MAY72	210902.1	4.6	193	N.COLOMBIA	E	211528.7	4.2	A63
18MAY72	155244.1	4.5	209	JUYJUY PROV.ARGENT.	I	155654.0	4.9	A64
18MAY72	173720.6	4.8	195	JUYJUY PROV.ARGENT.	I	174131.5	5.8	A65
19MAY72	011343.5	4.4	50	TUNISIA	E	012517.9	4.4	35B/0163
19MAY72	050104.7	4.9	40	NEAR C.OF C.CHILE	I	050638.8	5.2	A66
19MAY72	110109.1	4.2	33	NEAR C.OF OAXACA MX.	E	111044.8	4.2	35B/0511
19MAY72	134009.0	4.2	33	OFF C.OF N.CHILE	E	134504.6	3.9	35B/0603
19MAY72	155822.9	4.6	129	MENDOZA PROV.ARGENT.	I	160329.2	5.3	A67

NOAA EPICENTRAL DATA					SAAS READINGS			
DATE	ORIG.TIME	MB	DEP.	REGION		OBS.TIME	MB	EVENT N.
19MAY72	170000.0	4.9	0	S.NEVADA	E	171228.3	4.5	A
19MAY72	170000.0	4.9	0	S.NEVADA	E	171228.3	4.5	35B/0728
20MAY72	052746.2	4.5	121	CHILE-BOLIVIA B.R.	E	053215.1	4.9	A69
20MAY72	054035.8	4.7	48	PANAMA	E	054805.7	4.0	35B/1175
21MAY72	012407.9	5.2	132	N.CHILE	I	012837.5	5.4	A70
21MAY72	035030.9	5.4	85	NEAR C.OF PERU	I	035548.4	5.0	A71
21MAY72	075148.4	4.7	128	CHILE-BOLIVIA B.R.	E	075613.6	4.5	A72
21MAY72	105529.7	3.9	126	CHILE-BOLIVIA B.R.	I	105956.9	4.4	A73
22MAY72	124827.7	5.2	34	NEAR C.OF N.CHILE	E	125339.8	4.5	A75
23MAY72	003745.2	4.6	96	NEAR C.OF CHIAPAS,MX	I	004701.1	5.1	A76
23MAY72	100444.1	5.0	33	AZORES I.R.	E	101415.2	4.9	A77
23MAY72	164230.0	4.7	106	N.CHILE	E	164706.0	5.1	A78
25MAY72	064253.9	4.6	33	N.EASTER I.CORDILL.	E	065236.9	4.8	A79
25MAY72	132237.5	4.8	33	S.W.ATLANTIC OCEAN	E	133121.8	4.5	37A/0600
25MAY72	141214.7	4.8	74	N.CHILE	E	141700.8	5.0	A80
25MAY72	141752.4	4.2	129	S.PERU	E	142251.6	4.1	37A/0630
26MAY72	104852.2	4.9	33	S.ATLANTIC RIDGE	E	105650.7	4.3	37A/1361
26MAY72	174154.3	4.8	33	S.ATLANTIC RIDGE	E	174954.1	4.6	A81
27MAY72	050558.3	0.0	33	NEAR C.OF N.CHILE	E	051120.3	4.4	A83
27MAY72	101256.8	5.0	4	NEAR C.OF N.CHILE	E	101822.7	4.9	A84
27MAY72	114537.4	4.8	118	CHILE-BOLIVIA B.R.	E	115002.6	4.9	A85
28MAY72	030217.9	4.8	33	HONDURAS	E	031056.6	4.3	A86
28MAY72	031436.3	4.7	33	TURKEY	E	032738.7	4.7	A87
28MAY72	072814.3	4.8	53	NEAR C.OF C.CHILE	E	073332.6	4.9	A88
28MAY72	083851.5	5.0	33	S.E.CENT.PACIFIC O.	I	084652.0	4.5	A89
28MAY72	094614.5	4.9	4	NEAR C.OF N.CHILE	E	095139.4	4.6	A90
08OCT72	024541.6	5.4	33	WEST CHILE RISE	I	025401.5	5.3	E 1
08OCT72	080143.0	4.1	173	CATAMARCA PROV.ARGEN.	E	080614.7	4.7	E 2
08OCT72	143851.7	4.7	73	CHILE-ARGENTINA B.R.	E	144339.8	4.5	E 3
08OCT72	184046.8	4.9	33	S.SANDWICH I.R.	E	184914.8	4.6	84/0993
08OCT72	210325.1	0.0	33	S.SANDWICH I.R.	E	211154.3	4.4	84/1077
09OCT72	161718.1	4.9	98	S.PERU	E	162228.4	4.3	E 6
10OCT72	092605.1	4.6	138	PERU-BRAZIL B.R.	E	093144.6	3.5	85/0653
10OCT72	121823.2	4.9	33	SOUTH OF PANAMA	E	122550.3	4.7	E 8
10OCT72	224218.5	5.5	127	CHILE-BOLIVIA B.R.	I	224645.2		85/1125
13OCT72	160505.4	3.5	168	NORTHERN COLOMBIA	I	161130.7	4.7	E10
14OCT72	052241.3	4.8	42	N.C.OF OXACA MEXICO	I	053223.0	4.6	E11
16OCT72	034951.7	5.0	65	LEEWARD 2.	E	035622.7	4.2	88/0240
19OCT72	203154.2	4.4	33	S.E.CENT.PACIFIC O.	I	203834.2	4.6	E12
20OCT72	043348.9	5.7	33	N.ATLANTIC OCEAN	I	044124.4		E13
20OCT72	081748.6	5.7	38	OFF C.OF JALISCO MX.	E	082840.6	6.4	E14
21OCT72	082746.6	3.6	121	NORTHERN CHILE	E	083218.9	4.0	90/1226
21OCT72	125002.7	4.1	123	S.JUAN PROV.ARGENT.	E	125521.9	4.5	E16
22OCT72	024311.4	3.8	275	SOUTHERN BOLIVIA	E	024705.7	3.9	E17
22OCT72	082210.6	5.2	62	N.C. OF N. PERU	E	082818.8	5.2	E18
23OCT72	054718.8	4.5	24	NORTHERN CHILE	E	055233.9	3.9	E19
23OCT72	114111.1	3.6	63	CHILE-ARGENTINA B.R.	E	114619.7	3.8	91/1396
26OCT72	231555.9	4.7	124	CHILE-BOLIVIA B.R.	E	232029.3	4.5	E21
27OCT72	152252.9	4.6	137	PERU-BRAZIL B.R.	E	152821.6	4.4	E22
29OCT72	030924.5	4.9	33	C.MID ATLANTIC RIDGE	E	031452.8	4.5	94/0960

NOAA EPICENTRAL DATA					SAAS READINGS			
DATE	ORIG.TIME	MB	DEP.	REGION	OBS.TIME	MB	EVENT N.	
29OCT7	165511.2	0.0	33	S.SANDWICH I.R.	E 170338.5	4.9	E26	
29OCT72	190830.6	5.1	114	S.SANDWICH I.R.	E 191623.1	4.0	94/1532	
30OCT72	015040.7	4.9	33	N.ATLANTIC OCEAN	E 015817.9	4.1	E28	
31OCT72	215631.6	4.1	67	N.C.OF C.CHILE	E 220207.9	4.5	E29	
01NOV72	010226.5	4.6	19	N.C.OF C.CHILE	E 010851.1	4.6	E30	
01NOV72	100552.9	3.4	123	NORTHERN CHILE	E 101020.8	3.9	96/0532	
02NOV72	144342.0	5.2	20	REP.OF SOUTH AFRICA	I 145457.1	4.7	E33	
02NOV72	182445.9	4.6	24	NEAR C.OF NICARAGUA	E 183331.9	4.8	E34	
02NOV72	194850.3	5.0	33	S.SANDWICH I.R.	E 195641.9	4.0	96/1736	
03NOV72	035720.8	4.4	201	JUJUY PROV.ARGENTINA	E 040132.4	4.6	97/0221	
03NOV72	073804.0	4.4	159	NORTHERN COLOMBIA	E 074430.1	4.3	E37	
03NOV72	161342.0	5.1	33	NEAR EASTER I.CORD.	I 162356.1	6.0	E39	
03NOV72	235755.3	5.3	127	NORTHERN CHILE	I 000223.1	5.5	E41	
03NOV72	013337.3	4.6	35	LEEWARD I.	E 014031.7	4.3	97/0994	
03NOV72	013838.2	4.7	37	LEEWARD I.	E 014532.6	4.1	97/0997	
05NOV72	215620.5	5.0	61	NEAR C. OF N.PERU	E 220229.3	4.6	E44	
07NOV72	053521.2	5.5	137	LA RIOJA PROV.ARGENT.	I 054004.7	5.6	E45	
07NOV72	120513.8	5.2	33	N.ATLANTIC OCEAN	E 121552.1	4.7	E46	
08NOV72	124028.3	4.0	141	CHILE-BOLIVIA B.R.	E 124454.5	4.4	E47	
09NOV72	022700.5	4.9	14	NEAR C.OF N. CHILE	E 023225.4	4.0	100/0180	
09NOV72	064838.4	5.3	32	S.SANDWICH I.R.	E 065707.6	4.8	100/0337	
09NOV72	083120.9	3.7	101	CHILE-ARGENTINA B.R.	E 083553.6	4.3	100/0396	
11NOV72	212759.1	4.8	33	EASTER I.R.	E 213807.9	4.8	101/0009	
13NOV72	044345.2	5.5	33	N.C.OF OXACA MEXICO	I 045319.3	5.0	E52	
13NOV72	062127.0	4.7	33	N.C.OF GUERRERO MX.	I 063123.9	4.6	E53	
13NOV72	084944.2	4.6	33	N.C. OF OAXACA MX.	E 085917.4	4.6	101/1267	
13NOV72	230636.4	4.8	131	CHILE BOLIVIA B.R.	E 231101.5	5.2	E55	
15NOV72	043710.6	4.7	193	SALTA PROV.ARGENTINA	I 044126.6	5.3	E56	
15NOV72	045222.3	4.7	191	SOUTHERN BOLIVIA	I 045629.3	4.7	E57	
15NOV72	112741.6	4.2	40	NEAR C.OF VENEZUELA	E 113349.3	3.9	102/1325	
16NOV72	165945.9	4.6	33	S.OF PANAMA	E 170715.8	3.9	103/0712	
19NOV72	043524.1	5.6	73	EL SALVADOR	E 044407.0	5.2	E60	
19NOV72	233150.7	4.6	100	CHILE BOLIVIA B.R.	E 233622.3	4.5	E61	
20NOV72	034251.5	4.3	42	NORTHERN CHILE	E 034751.7	4.4	105/0273	
20NOV72	142115.4	5.6	33	S.SANDWICH I. R.	I 142959.8	5.8	E63	
20NOV72	211059.4	4.9	47	OFF C.OF C.CHILE	E 211632.1	5.3	E64	
21NOV72	040453.6	4.5	33	N.C.OF OXACA MEXICO	I 041429.9	4.9	E65	
21NOV72	055645.6	4.6	27	NEAR C.OF N.CHILE	E 060203.9	4.2	E66	
22NOV72	104458.8	5.0	42	COLOMBIA	E 105130.3	4.8	106/0490	
22NOV72	232953.1	4.6	33	NEAR C.OF N.CHILE	E 233500.5	4.7	E68	
23NOV72	010704.9	4.9	33	N.OF ASCENCION I.	E 011355.0	4.4	E69	

APPENDIX 2

SOME ARRAY PROCESSING METHODS AVAILABLE AT EDINBURGH

A) AZANDT Program (Lilwall, 1973)

This program finds the azimuth and $dT/d\Delta$ (or the apparent velocity) of seismic signals recorded by arrays in analogue form. The data is digitized using the equipment described in 5.2 and the MTDIG program (Fyfe, 1973) into 12 bit integer words and written onto 1/2" magnetic tape in blocks of 2048 (16 bit) integer words. The array channels are digitized as a series of frames and sequentially written onto the 1/2" tape. The number of frames digitized per second corresponds then to the number of samples per second on the individual channels. Within each frame there is a delay of about 450 micro seconds (analogue recording time) between each successive sample, leading to a time difference between the first and last samples in a frame of about 7 milliseconds when 16 channels are being digitized. This difference is ignored. AZANDT works by summing with lags a section of the trace for a range of preset azimuths and $dT/d\Delta$. The sum of squares for each sum with lags is determined and normalised so that the largest value is equal to 1. The normalised values for the range of azimuths and $dT/d\Delta$ considered, are printed out in the form of a matrix, and the values of azimuth and $dT/d\Delta$ corresponding to 1 are taken as the optimum solutions. The starting azimuth and $dT/d\Delta$ are calculated from the epicentre data of the event and from the P wave curve for distances up

to 100°. Alternatively a separate $dT/d\Delta$ value can be fed in. The program forms the first matrix with these values of azimuth and $dT/d\Delta$ and preset increments in either direction; further matrices are then formed, centred on the maxima of the previous and smaller preset increments, until resolution is no longer improved. Details of each event and of the array coordinates are fed into the computer on punched cards. The location and definition of the signal to be processed are obtained from a visual analogue print out of the digital data. This print out is obtained with the MTREAD program (Fyfe, 1973); an example of such a print out is shown in Figure 26 with some details of the signal to be processed. For explanation of the input cards see Lilwall (1973). An example of the output (final matrix only) is presented in this appendix.

AZANDDT PROGRAM: FINAL MATRIX (EVENT E 1 2)

TAPE POSITIONED AT BEGINNING OF BLOCK 6

MAX SUM OF SQUARES = 154171440

	6.900	6.950	7.000	7.050	7.100	7.150	7.200	7.250
228.50	0.9797	0.9811	0.9848	0.9722	0.9723	0.9714	0.9761	0.9781
228.75	0.9789	0.9811	0.9848	0.9848	0.9716	0.9767	0.9761	0.9774
229.00	0.9789	0.9811	0.9848	0.9844	0.9772	0.9767	0.9755	0.9834
229.25	0.9789	0.9811	0.9810	0.9903	0.9772	0.9771	0.9823	0.9815
229.50	0.9789	0.9790	0.9870	0.9903	1.0000	0.9830	0.9823	0.9815
229.75	0.9782	0.9854	0.9870	1.0000	0.9963	0.9830	0.9823	0.9823
230.00	0.9849	0.9950	0.9967	0.9932	0.9963	0.9830	0.9830	0.9823
230.25	0.9945	0.9950	0.9918	0.9932	0.9963	0.9963	0.9830	0.9805

BEST DTDD= 7.05000 SEC/DEGREE
BEST VELOCITY= 15.74469 KM/SEC
BEST AZIMUTH= 229.75000 DEGREES

END OF EVENT

B) DELAYS program (Lilwall, 1973)

This program finds the true relative onset times of arrivals recorded at each point of a seismic array. This is done by measuring the time delay needed in each trace to align it with a chosen master trace. The alignment is obtained by cross-correlating a small section of the master trace with each one of the other traces, which are inserted with varying time delays to find the maximum correlations. The crosscorrelation function (C) as defined by Lilwall (1973) is:

$$C = \frac{\sum M_i T_{i+t}}{\left(\left(\sum M_i^2\right)\left(\sum T_{i+t}^2\right)\right)^{\frac{1}{2}}} \qquad (i = A, A+1, \ldots\ldots B-1, B) \qquad (A2\text{-}1)$$

Where M_i, T_i are the time series for the master and second trace respectively. A and B define the section of the trace to be correlated and t is the time delay successively inserted in the second trace. Several sections of the signal can be processed. The first approximate delay to be used is calculated from the azimuth and apparent velocity deduced from the epicentral coordinates (Δ up to 100°) of the event or from a $dT/d\Delta$ inserted separately. The apparent velocity is computed in this program with reference to the Herrins (1968) tables; this apparent velocity and the computed azimuth constitute the expected values of these parameters for a given station. Once the sections of the master trace and the second trace to be correlated are approximately aligned, then the program only performs the crosscorrelation within a small time window of the approximate

delay, changing the delays by one sample interval. The sample rate of the digitized data gives an estimate of the time accuracy obtained with this method. The input data for this program is similar to that used for the program AZANDT. An example of the input data and the output print out of the DELAYS program is also presented in this appendix.

DELAYS PROGRAM INPUT DATA

```
08OCT72 024541.6 5.4  33 WEST CHILE RISE      E 1  1


 NUMBER OF CHANNELS          =   16
 BLOCK NUMBER                =   10
 MASTER TRACE                =    2
 SAMPLES PER SECOND          =   50.00
 START OF PROCESSED TRACE=       0.11
 LENGTH OF TRACE             =    0.85
 TIME WINDOW OF DELAYS       =    0.35
 EVENT LATITUDE              =  -38.42
 EVENT LONGITUDE             =  -93.29
 EVENT DEPTH                 =   33.00
 EVENT AZIMUTH               =  231.168
 EVENT DIST                  =   45.73
 EVENT EXTENDED DIST         =   45.81
 HERRINS DTDD VALUE          =    7.87


 STATION   2 USED AS REFERENCE
 LAGS FORMED FOR EVENT CO-ORDS
 LAT     -38.42   LONG     -93.29
```

DELAYS PROGRAM: TYPICAL CORRELATION (EVENT E 1 1)

TRACE NO 6 E4
****
DELAY = 3 SAMPLES OR 0.060 SECS TRUE DELAY= 0.42 SECS

MAX CORRELATION = 0.598

MAXIMUM VALUE IS 0.5981

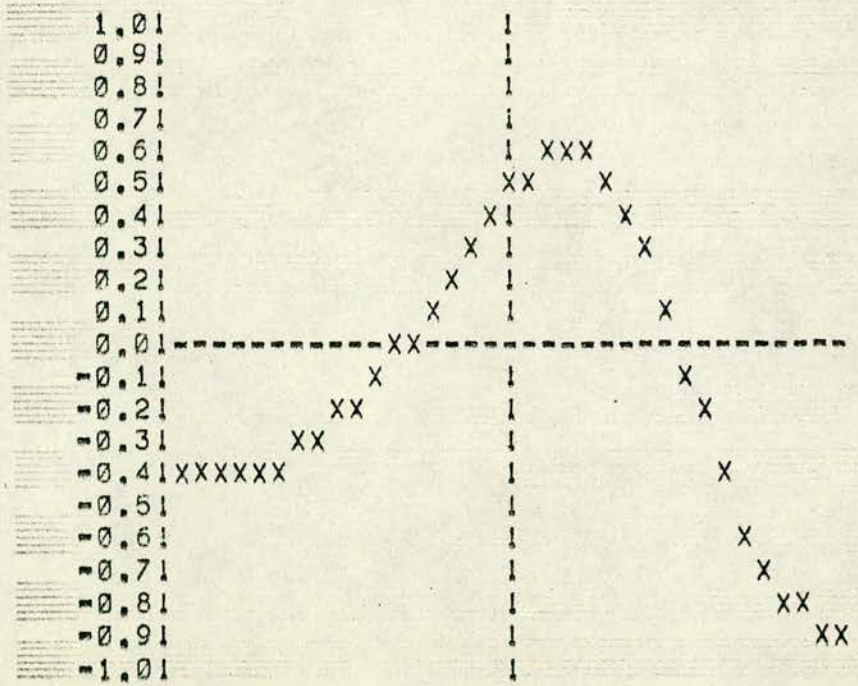

DELAYS PROGRAM OUTPUT (EVENT E 1 1)

SUMMARY OF RESULTS

SITE	DELAY	MAX CORRELATION	
CP	0.00	0.00	1.0000
E1	0.06	0.06	0.8129
E2	0.06	0.06	0.8073
E3	0.30	0.30	0.9496
E4	0.42	0.42	0.5981
E5	0.44	0.44	0.8607
EE	1.62	1.62	0.6740
S1	-0.04	-0.04	0.9388
S3	-0.32	-0.32	0.9827
S4	-0.44	-0.44	0.6680
S5	-0.68	-0.68	0.9720
SE	-1.96	-1.96	0.9549
W1			
W2	-0.10	-0.10	0.7008
WE	-0.38	-0.38	0.9006

C) ATVS program

This program calculates the observed azimuth and apparent velocity from the relative time delays (in seconds) of the components of an array, (the AZAV version of this program accepts the time delays measured in length units). Figure 29 illustrates the geometrical representation of the fundamental equation which is solved by the least squares method (see Berrocal, 1968). This program also finds the expected arrival times for each member of the array, deduced from the expected azimuth and apparent velocity which in turn are calculated, separately from this program, from the reported epicentral parameters, the geographical coordinates and appropriate seismic travel-time tables. In the present research, the input data for AVTS was provided by the punched cards output from the DELAYS program, therefore the expected apparent velocity is referred to the Herrin (1968) tables. The print out of AVTS contains the values of the observed and expected azimuth and apparent velocity, and two time residuals for each point of the array (used in the calculations). The time residuals considered are the "least squares residual" (observed time-best fitting) and the "travel time-residual" (observed time-expected time). The variance and the mean square root of the squared least squares residuals are also shown in the print out. The listing of AVTS and an example of the input data and output print out are included in this appendix.

AVTS PROGRAM LISTING

```
%BEGIN
SELECT INPUT(1)
SELECT OUTPUT(2)
%REAL TA,TV,TC,TS,X1,Y1,T1,X2,Y2,T2,XY,XT,YT,A,B,C,D,E,AF,BF,CF,W, %C
      AZ,AV,DIST,REP,RSM
%INTEGER N,I,J,M
%BYTEINTEGER PN1,PN2,SYM,SYN,SYP
%REALARRAY X,Y,TT,RT,ELS,CA,CORR(1:18)
%BYTEINTEGERARRAY ET(1:52),R,P,AP,AM(1:18)
!N IS THE NUMBER OF POINTS OF THE ARRAY BEING USED
READ(N)
!READING COORDINATES OF THE N POINTS OF THE ARRAY
%CYCLE I=1,1,N
   11:SYM=NEXT SYMBOL
   ->16 %UNLESS SYM=' ' %OR SYM=NL
   SKIP SYMBOL; ->11
   16:READ SYMBOL(R(I));READ SYMBOL(P(I))
   READ(X(I));READ(Y(I))
READ(CORR(I))
%REPEAT
NEWLINES(6);SPACES(16)
%PRINTTEXT'AZIMUTH AND APPARENT VELOCITY FROM SAAS DATA'
NEWLINES(2);SPACES(9)
%PRINTTEXT'RELATIVE TIME ARRIVALS IN SECONDS FROM CROSS CORRELATION O/P'

NEWLINES(4);SPACES(6)
%PRINTTEXT 'COORDINATES OF USED POINTS'
NEWLINES(2);SPACES(25)
%PRINTTEXT'POINT      X(I)      Y(I) '
NEWLINES(2)
%CYCLE I=1,1,N
   SPACES(26)
   PRINT SYMBOL(R(I));PRINT SYMBOL(P(I));SPACES(6)
   PRINT(X(I),2,3);SPACES(3)
   PRINT(Y(I),2,3);NEWLINE
%REPEAT;NEWPAGE
!READING AND PRINTING THE EVENT TITLE
20:SYN=NEXT SYMBOL
->21 %UNLESS SYN=' ' %OR SYN=NL
SKIP SYMBOL; ->20
21:%CYCLE I=1,1,52
   READ SYMBOL(ET(I))
   %IF ET(I)='*' %THEN %STOP
%REPEAT
NEWLINES(6);SPACES(6)
%PRINTTEXT 'EVENT DATA'
NEWLINES(2);SPACES(7)
%PRINTTEXT'DATE    O.TIME   M  DEP.       REGION          SIGNAL  DIST.'

READ(DIST)
NEWLINES(2);SPACES(6)
%CYCLE I=1,1,52
```

(AVTS PROGRAM LISTING-CONT.)

```
   PRINT SYMBOL(ET(I))
%REPEAT
PRINT(DIST,3,2)
READ(TA);READ(TV)
!TA AND TV ARE THE EXPECTED AZIMUTH AND APPARENT VELOCITY
TS=SIN(TA*(Π/180))/TV
TC=COS(TA*(Π/180))/TV
!TT(I) ARE THE EXPECTED TIME ARRIVALS TO EACH POINT OF THE ARRAY
%CYCLE I=1,1,N
   TT(I)=-(X(I)*TS+Y(I)*TC)
%REPEAT
!READING TIME DELAYS AND RATIOS FOUND IN THE CROSS CORRELATION
%CYCLE I=1,1,N
   19:SYP=NEXT SYMBOL
   ->17 %UNLESS SYP=' ' %OR SYP=NL
SKIP SYMBOL; ->19
   17:READ SYMBOL (AP(I)); READ SYMBOL (AM(I))
   READ (RT(I));READ(CA(I))
   %IF (RT(I))=-10.00 %THEN ->100
   RT(I)=RT(I)+CORR(I)
100:%REPEAT
!CALCULATING OBSERVED AZIMUTH(AZ) AND APPARENT VELOCITY(AV)
X1=0;Y1=0;T1=0;X2=0;Y2=0;T2=0;XY=0;XT=0;YT=0;M=0;REP=0;RSM=0
%CYCLE I=1,1,N
   ->12 %IF RT(I)=-10
   ->12 %IF CA(I)<0.4
      4:X1=X1+X(I);Y1=Y1+Y(I);T1=T1+RT(I)
   X2=X2+X(I)**2;Y2=Y2+Y(I)**2;T2=T2+RT(I)**2
   XY =XY+X(I)*Y(I);XT=XT+X(I)*RT(I);YT=YT+Y(I)*RT(I)
   M=M+1
   REP=REP+CA(I)
12:%REPEAT
      A=XY*M-X1*Y1;B=X2*M-(X1)**2;C=Y2*M-(Y1)**2
      D=X1*T1-XT*M;E=Y1*T1-YT*M
      AF=(E*A-C*D)/(A**2-C*B)
      BF=(D-B*AF)/A
      CF=-(X1*AF+Y1*BF+T1)/M
      W=(M-3)/(AF**2*X2+BF**2*Y2+2*AF*BF*XY+2*AF*XT+2*BF*YT+2*AF*CF*X1%C
        +2*BF*CF*Y1+T2+2*CF+M*CF**2)
      AZ=ARCTAN(BF,AF)
      AV=1/RADIUS(AF,BF)
      %CYCLE I=1,1,N
         %IF RT(I)=-10.00 %THEN->13
         ELS(I)=AF*X(I)+BF*Y(I)+CF+RT(I)
         RSM=RSM+ELS(I)**2
      13:%REPEAT
      NEWLINES(2);SPACES(9)
      %PRINTTEXT'EXPECTED AZIMUTH: ';PRINT(TA,3,2);SPACES(6)
      %PRINTTEXT'EXPECTED APP.VELOCITY: ';PRINT(TV,2,2)
      %PRINTTEXT' KM/S ';NEWLINE;SPACES(9)
```

(AVTS PROGRAM LISTING-CONT.)

```
      %PRINTTEXT'COMPUTED AZIMUTH:'
      PRINT(AZ*180/Π,3,2) %UNLESS AZ<0
      %IF AZ<0 %THEN PRINT(AZ*180/Π+360,3,2);SPACES(6)
      %PRINTTEXT'COMPUTED APP.VELOCITY:';PRINT(AV,2,2)
      %PRINTTEXT' KM/S';NEWLINE;SPACES(9)
      %PRINTTEXT'REF. POINT ERROR:';PRINT(CF,1,4);SPACES(6)
      %PRINTTEXT'VARIANCE (1/WEIGHT)  :';PRINT(1/W,1,8)
      NEWLINES(2);SPACES(8)
      %PRINTTEXT'POINT  EXPEC.TIME  OBS.TIME   L.S.RESID.  T.T.RESID.'
      %PRINTTEXT'   CORR.'
      NEWLINES(2)
      %CYCLE I=1,1,N
         SPACES(10)
         PRINT SYMBOL(R(I));PRINT SYMBOL(P(I));SPACES(4)
         PRINT(TT(I),1,3);SPACES(6)
         PRINT(RT(I),1,3) %UNLESS RT(I)=-10
         %IF RT(I)=-10 %THEN ->50;SPACES(5)
         PRINT(ELS(I),1,3);SPACES(5)
        PRINT((RT(I)-TT(I)),1,3);SPACES(5)
         PRINT(((RT(I)-TT(I))-ELS(I)),1,3)
         50:NEWLINE
      %REPEAT
      NEWLINES(2)
      SPACES(8)
      %PRINTTEXT'MEAN VALUE OF CORRELATION: '
      PRINT(REP/M,2,4)
      NEWLINES(2)
      %PRINTTEXT'        S.R. OF MEAN S.RESIDUAL:'
      PRINT(SQ RT (RSM/M),1,4)
      NEWPAGE
      SELECTOUTPUT(97)
      SPACES(20)
      PRINT((AZ*(180/Π)-TA),4,2) %UNLESS AZ<0
      %IF AZ<0 %THEN PRINT((AZ*(180/Π)+360-TA),4,2)
      PRINT((AV-TV),6,2)
      SPACES(22)
      %CYCLE I=46,1,52
         PRINT SYMBOL(ET(I))
      %REPEAT
      NEWLINE
      %CYCLE I=46,1,52
         PRINT SYMBOL(ET(I))
      %REPEAT
      SPACES(2)
      %CYCLE I=18,1,24
         PRINT SYMBOL(ET(I))
      %REPEAT
      SPACES(3);PRINT(TA,3,2);SPACES(2)
      PRINT(AZ*180/Π,3,2) %UNLESS AZ<0
      %IF AZ<0 %THEN PRINT(AZ*180/Π+360,3,2)
```

```
(AVTS PROGRAM LISTING-CONT.)

      SPACES(3);PRINT(TV,3,2);SPACES(2)
      PRINT(AV,2,2);SPACES(3)
      PRINT(1/W,2,4)
      SELECTOUTPUT(2)
      ->20
%ENDOFPROGRAM
```

COMMAND:CONSOLE DISCONNECTED 21/01/74 16.45.35

AVTS PROGRAM INPUT DATA

```
9
CP      0.000       0.000      0.00
E1      2.426      -0.844      0.00
E3      7.004      -2.435      0.00
E4      9.467      -3.224      0.00
E5     11.846      -4.151      0.00
S1     -0.878      -2.346      0.00
S3     -2.460      -7.080      0.00
S4     -3.280      -9.450      0.00
S5     -4.174     -11.847      0.00
08OCT72 024541.6 5.4  33 WEST CHILE RISE       E 1  1  45.73 231.17 14.1
CP     0.00        1.0000
E1     0.06        0.8129
E3     0.30        0.9496
E4     0.42        0.5981
E5     0.44        0.8607
S1    -0.04        0.9388
S3    -0.32        0.9827
S4    -0.44        0.6680
S5    -0.68        0.9720
08OCT72 024541.6 5.4  33 WEST CHILE RISE       E 1  2  45.73 231.17 14.11
CP     0.00        1.0000
E1     0.08        0.9917
E3     0.22        0.9628
E4     0.40        0.9916
E5     0.42        0.9643
S1    -0.04        0.9977
S3    -0.40        0.9939
S4    -0.56        0.9692
S5    -0.68        0.9878
08OCT72 024541.6 5.4  33 WEST CHILE RISE       E 1  3  45.73 231.17 14.08
CP     0.00        1.0000
E1     0.14        0.9985
E3     0.22        0.9937
E4     0.42        0.9961
E5     0.46        0.9969
S1    -0.02        0.9958
S3    -0.40        0.9879
S4    -0.56        0.9672
S5    -0.68        0.9854
```

AZIMUTH AND APPARENT VELOCITY FROM SAAS DATA

RELATIVE TIME ARRIVALS IN SECONDS FROM CROSS CORRELATION O/P

COORDINATES OF USED POINTS

POINT	X(I)	Y(I)
CP	0.000	0.000
E1	2.426	-0.844
E3	7.004	-2.435
E4	9.467	-3.224
E5	11.846	-4.151
S1	-0.878	-2.346
S3	-2.460	-7.080
S4	-3.280	-9.450
S5	-4.174	-11.847

EVENT DATA

DATE	O.TIME	M	DEP.	REGION	SIGNAL	DIST.
080CT72	024541.6	5.4	33	WEST CHILE RISE	E 1 1	45.73

EXPECTED AZIMUTH: 231.17 EXPECTED APP.VELOCITY: 14.11 KM/S
COMPUTED AZIMUTH: 228.45 COMPUTED APP.VELOCITY: 15.44 KM/S
REF. POINT ERROR:-0.0345 VARIANCE (1/WEIGHT) :-0.01409324

POINT	EXPEC.TIME	OBS.TIME	L.S.RESID.	T.T.RESID.	CORR.
CP	0.000	0.000	-0.034	0.000	0.034
E1	0.096	0.050	-0.066	-0.046	0.019
E3	0.278	0.320	0.051	0.042	-0.009
E4	0.379	0.360	0.005	-0.019	-0.024
E5	0.470	0.410	-0.020	-0.060	-0.039
S1	-0.153	-0.050	0.059	0.103	0.044
S3	-0.450	-0.370	0.019	0.080	0.061
S4	-0.601	-0.480	0.051	0.121	0.071
S5	-0.757	-0.740	-0.063	0.017	0.080

MEAN VALUE OF CORRELATION: 0.8648

S.R. OF MEAN S.RESIDUAL: 0.0458

EVENT DATA

DATE	O.TIME	M	DEP.	REGION	SIGNAL	DIST.
080CT72	024541.6	5.4	33	WEST CHILE RISE	E 1 2	45.73

EXPECTED AZIMUTH: 231.17 EXPECTED APP.VELOCITY: 14.11 KM/S
COMPUTED AZIMUTH: 224.59 COMPUTED APP.VELOCITY: 14.69 KM/S
REF. POINT ERROR:-0.0280 VARIANCE (1/WEIGHT) :-0.01535903

POINT	EXPEC.TIME	OBS.TIME	L.S.RESID.	T.T.RESID.	CORR.
CP	0.000	0.000	-0.028	0.000	0.028
E1	0.096	0.070	-0.033	-0.026	0.007
E3	0.278	0.240	-0.005	-0.038	-0.034
E4	0.379	0.340	0.016	-0.039	-0.055
E5	0.470	0.390	-0.003	-0.080	-0.077
S1	-0.153	-0.050	0.078	0.103	0.025
S3	-0.450	-0.450	-0.017	0.000	0.018
S4	-0.601	-0.600	-0.013	0.001	0.014
S5	-0.757	-0.740	0.006	0.017	0.011

MEAN VALUE OF CORRELATION: 0.9843

S.R. OF MEAN S.RESIDUAL: 0.0311

EVENT DATA

DATE	O.TIME	M	DEP.	REGION	SIGNAL	DIST.
080CT72	024541.6	5.4	33	WEST CHILE RISE	E 1 3	45.73

EXPECTED AZIMUTH: 231.17 EXPECTED APP.VELOCITY: 14.08 KM/S
COMPUTED AZIMUTH: 224.40 COMPUTED APP.VELOCITY: 14.28 KM/S
REF. POINT ERROR:-0.0481 VARIANCE (1/WEIGHT) :-0.02476894

POINT	EXPEC.TIME	OBS.TIME	L.S.RESID.	T.T.RESID.	CORR.
CP	0.000	0.000	-0.048	0.000	0.048
E1	0.097	0.130	0.005	0.033	0.028
E3	0.279	0.240	-0.029	-0.039	-0.010
E4	0.380	0.360	0.009	-0.020	-0.030
E5	0.471	0.430	0.009	-0.041	-0.050
S1	-0.153	-0.030	0.082	0.123	0.041
S3	-0.451	-0.450	-0.023	0.001	0.025
S4	-0.602	-0.600	-0.015	0.002	0.017
S5	-0.759	-0.740	0.009	0.019	0.009

MEAN VALUE OF CORRELATION: 0.9913

S.R. OF MEAN S.RESIDUAL: 0.0349

APPENDIX 3-A

ORIGINAL AZIMUTH AND APPARENT VELOCITY OBSERVED AT SAAS

N.E	N.S	MB	DEP.	TAZ	OAZ	TAV	OAV	PHASE	TFOS
1.-EAST EUROPE-MIDDLE EAST									
A17	1	4.7	33	49.37	49.30	21.75	19.69		
A38	1	5.9	46	51.40	49.74	22.26	19.42		
A38	5	5.9	46	51.40	56.53	22.19	19.36	AP	16
A23	1	4.9	18	37.57	42.56	22.42	20.55		
A23	2	4.9	18	37.57	40.20	22.41	18.12	AP	4
A30	1	5.1	47	52.01	47.51	22.48	18.51		
A46	1	5.0	10	45.39	44.46	23.02	21.61		
A46	3	5.0	10	45.39	42.43	23.01	21.21	AP	5
A28	1	5.0	26	48.20	43.38	23.34	21.63		
A29	1	4.8	28	48.19	44.67	23.34	21.58		
A29	2	4.8	28	48.19	41.78	23.32	19.95	AP	5
A05	1	5.4	33	49.26	53.58	23.76	26.08		
A05	2	5.4	33	49.26	52.13	23.76	24.92	AP	5
A22	1	4.6	136	42.63	61.09	23.84	18.73		
A87	1	4.7	33	49.72	43.56	23.80	21.58		
2.-ATLANTIC OCEAN AND MID-ATLANTIC RIDGE									
E46	1	5.2	33	6.35	0.57	17.02	17.55		
A77	1	5.0	33	15.57	15.73	15.43	14.15		
A55	1	4.8	33	15.67	16.21	16.73	16.02		
A55	3	4.8	33	15.67	15.94	16.71	15.45	AP	10
A54	1	4.8	33	15.73	14.57	16.73	15.07		
A56	2	5.0	33	19.94	15.10	17.01	15.72		
E24	2	4.9	33	26.83	27.50	12.16	7.29		

N.E	N.S	MB	DEP.	TAZ	DAZ	TAV	DAV	PHASE	TFDS
E13	1	5.7	33	27.31	33.40	13.44	13.00		
E13	2	5.7	33	27.31	28.48	13.44	11.91		
E13	4	5.7	33	27.31	34.22	13.42	12.72		
E13	5	5.7	33	27.31	41.74	13.42	12.40		
E13	6	5.7	33	27.31	40.39	13.44	14.14		
E13	7	5.7	33	27.31	30.65	13.44	12.47		
E13	8	5.7	33	27.31	33.48	13.44	12.57		
E13	9	5.7	33	27.31	31.38	13.44	13.09		
E13	10	5.7	33	27.31	37.42	13.44	12.68		
E13	11	5.7	33	27.31	26.45	13.44	11.91		
E13	12	5.7	33	27.31	34.65	13.44	12.37		
E13	13	5.7	33	27.31	25.18	13.44	12.94		
E13	14	5.7	33	27.31	33.16	13.44	13.50		
E13	15	5.7	33	27.31	36.25	13.44	13.42		
E13	16	5.7	33	27.31	35.17	13.44	13.97		
E13	17	5.7	33	27.31	23.99	13.44	12.21		
E13	20	5.7	33	27.31	32.07	13.44	13.35		
E13	21	5.7	33	27.31	26.02	13.44	11.82		
A61	1	4.7	33	41.05	39.24	12.08	10.28		
A15	1	4.3	33	51.12	46.57	12.01	11.40		
E69	1	4.9	33	67.42	63.53	12.91	13.47		
A14	1	5.1	33	98.52	93.30	12.71	12.64		
E33	1	5.2	20	112.76	112.08	18.11	16.75		
3.-SOUTH SANDWICH ISLAND REGION									
A21	1	5.5	33	163.91	158.49	13.66	14.72		
A21	3	5.5	33	163.91	161.68	13.64	14.75	AP	8
A40	1	5.3	33	163.97	159.32	13.66	15.64		
A40	4	5.3	33	163.97	159.29	13.64	15.25	AP	12
A81	1	4.8	33	144.66	140.81	13.79	12.72		
A26	1	5.2	33	152.28	152.53	14.06	14.23		
A13	1	4.9	33	163.87	161.48	14.19	15.79		
E262	2	0.0	33	165.06	157.51	14.25	14.96		
E63	1	5.6	33	163.70	157.98	14.55	15.22	PRE	
E63	2	5.6	33	163.70	157.42	14.55	14.62		

N.E	N.S	MB	DEP.	TAZ	DAZ	TAV	DAV	PHASE	TFDS
4.-EAST PACIFIC DCEAN									
A60	1	5.0	33	216.42	225.08	18.53	22.15		
A44	1	5.4	33	217.84	217.73	19.35	20.92		
E 1	1	5.4	33	231.17	233.07	14.11	16.13	PRE	
E 1	2	5.4	33	231.17	228.80	14.11	15.41		
E 1	3	5.4	33	231.17	228.48	14.08	14.96	AP	7
E 1	4	5.4	33	231.17	231.43	14.11	15.89		
E 1	5	5.4	33	231.17	231.18	14.11	16.23		
E 1	6	5.4	33	231.17	227.00	14.11	41.57	PCP	38
E 1	7	5.4	33	231.17	226.50	11.21	12.49	PP	44
A89	1	5.0	33	238.66	243.76	13.81	15.84		
E12	1	4.4	33	252.89	264.93	12.78	13.15		
E12	3	4.4	33	252.89	265.74	12.76	13.14		
E39	1	5.1	33	263.10	275.23	16.43	14.92		
A79	1	4.6	33	275.19	281.60	15.68	15.15		
A34	1	5.8	33	287.67	291.28	15.56	14.58		
A34	5	5.8	33	287.67	286.24	15.56	29.44	PCP	59
5.-NORTHERN LATIN-AMERICA									
A01	1	5.2	128	329.90	325.44	12.59	12.21		
A45	1	0.0	50	310.35	310.37	12.77	11.89		
A63	1	4.6	193	310.25	308.37	12.82	13.66		
A63	2	4.6	193	310.25	310.04	12.62	11.39	AP	39
A19	1	4.3	164	310.39	308.41	12.85	11.94		
E10	1	3.5	168	310.31	308.36	12.84	12.11		
E37	1	4.4	159	310.29	308.31	12.84	10.73		
E 8	1	4.9	33	303.36	295.61	13.31	13.79		
E 8	2	4.9	33	303.36	298.68	13.29	13.74	AP	4
E28	1	4.9	33	339.78	336.14	13.43	11.20		
A86	1	4.8	33	306.51	306.37	14.37	14.54		

N.E	N.S	MB	DEP.	TAZ	ΔAZ	TAV	ΔAV	PHASE	TFΔS
E34	1	4.6	24	302.21	299.98	14.41	14.99		
E34	3	4.6	24	302.21	302.44	14.40	13.87	AP	8
E34	4	4.6	24	302.21	302.55	14.40	14.03	XP	10
A32	1	4.4	77	303.04	302.22	14.64	13.99		
E60	1	5.6	73	303.18	301.31	14.62	17.05		
E60	2	5.6	73	303.18	302.27	14.62	14.43		
E60	7	5.6	73	303.18	306.31	14.54	14.42	AP	18
E60	8	5.6	73	303.18	298.82	14.54	15.13	XP	25
E60	9	5.6	73	303.18	311.28	14.62	26.86	PCP	85
A03	1	3.9	157	302.55	302.87	14.86	14.47		
A04	1	5.1	85	302.58	301.26	14.83	13.63		
A76	1	4.6	96	302.45	303.44	15.33	14.53		
A76	3	4.6	96	302.45	303.20	15.18	14.19	AP	19
A36	1	5.1	115	303.28	304.70	15.43	14.68		
A36	4	5.1	115	303.28	303.77	15.24	13.41	AP	33
E65	2	4.5	33	301.03	302.05	15.57	14.35		
E52	1	5.5	33	301.63	300.30	15.56	13.65		
E11	1	4.8	42	300.70	302.69	15.69	13.34		
E53	1	4.7	33	300.90	303.71	16.06	13.60		
E14	1	5.7	38	298.56	292.30	17.46	16.17	PRE	
E14	2	5.7	38	298.56	294.89	17.46	18.28		
E14	3	5.7	38	298.56	295.54	17.46	17.47		
E14	4	5.7	38	298.56	296.94	17.46	16.77		
E14	5	5.7	38	298.56	298.23	17.46	15.60		
E14	6	5.7	38	298.56	302.41	17.43	15.76		
E14	7	5.7	38	298.56	298.88	17.43	16.02		
E14	8	5.7	38	298.56	291.35	17.43	17.98		
E14	9	5.7	38	298.56	298.88	17.43	17.87		
E14	10	5.7	38	298.56	298.82	17.43	16.81		
E14	11	5.7	38	298.56	302.86	17.46	17.45		
E14	12	5.7	38	298.56	292.12	17.46	18.62		
E14	13	5.7	38	298.56	299.69	17.46	19.69		
E14	14	5.7	38	298.56	300.32	17.46	19.36		
E14	15	5.7	38	298.56	291.77	17.46	17.07		
E14	16	5.7	38	298.56	291.92	17.46	16.29		
E14	17	5.7	38	298.56	295.57	17.46	16.99		
E14	18	5.7	38	298.56	292.26	17.46	19.22		
E14	19	5.7	38	298.56	289.19	17.46	20.92		
E14	20	5.7	38	298.56	305.21	17.46	16.69		

N.E	N.S	MB	DEP.	TAZ	DAZ	TAV	DAV	PHASE	TFDS
6.-WESTERN SOUTH AMERICA									
E30	1	4.6	19	220.87	213.13	12.64	12.17		
A67	1	4.6	129	224.03	219.48	12.05	13.32	PRE	
A67	2	4.6	129	224.03	218.75	12.05	11.04		
A67	4	4.6	129	224.03	221.07	11.23	11.44	AP	26
A52	1	4.5	112	224.34	217.84	12.44	12.34		
E16	1	4.1	123	226.98	222.21	12.32	14.38	PRE	
E16	2	4.1	123	226.98	222.88	12.32	13.28		
E16	4	4.1	123	226.98	197.24	11.82	11.72	AP	29
E16	5	4.1	123	226.98	220.19	11.82	11.68	XP	41
A06	1	4.6	28	227.58	221.96	12.41	13.16	PRE	
A06	2	4.6	28	227.58	219.59	12.41	12.08		
A25	1	5.3	104	227.53	223.39	12.06	13.80		
A39	1	0.0	121	227.60	223.22	12.32	12.20		
A39	2	0.0	121	227.60	222.03	11.82	11.48	AP	24
A57	1	5.4	40	227.66	221.64	12.42	12.99		
A57	2	5.4	40	227.66	219.99	12.39	12.81	AP	9
A07	1	4.9	40	227.74	225.17	12.42	12.86	PRE	
A07	2	4.9	40	227.74	221.50	12.42	13.16		
A07	3	4.9	40	227.74	213.97	12.42	12.62	AP	10
A07	4	4.9	40	227.74	222.25	12.42	12.56	XP	14
E29	1	4.1	67	227.86	221.74	12.42	12.86		
E29	4	4.1	67	227.86	221.06	12.32	13.32	AP	18
E29	5	4.1	67	227.86	223.62	12.32	12.93	XP	25
A31	1	5.0	88	228.79	222.40	12.37	12.86		
A31	2	5.0	88	228.79	222.93	12.37	12.62	AP	15
A31	3	5.0	88	228.79	221.86	12.37	12.34	XP	20
E45	1	5.5	137	230.05	223.46	11.46	11.09		
E45	2	5.5	137	230.05	225.60	11.46	11.69		
E45	3	5.5	137	230.05	222.70	11.46	10.78		
E45	4	5.5	137	230.05	224.39	11.46	9.32	AP	22
E45	5	5.5	137	230.05	223.84	10.19	10.79	PP	31
A66	1	4.9	40	230.04	224.59	12.31	12.81		
A59	1	5.6	39	231.23	221.01	11.76	10.78		
E 2	2	4.1	173	231.25	223.90	11.27	10.78		

N.E	N.S	MB	DEP.	TAZ	OAZ	TAV	OAV	PHASE	TFOS
E64	1	4.9	47	231.66	226.34	12.32	13.10	PRE	
E64	2	4.9	47	231.66	225.77	12.32	13.28		
E64	3	4.9	47	231.66	229.89	12.32	11.64	AP	9
E64	4	4.9	47	231.66	224.21	12.32	13.51	XP	13
A18	1	4.7	66	232.92	227.27	12.25	13.27		
A18	3	4.7	66	232.92	225.03	12.06	12.56	AP	14
A58	1	4.9	51	233.20	228.56	12.19	12.54		
A58	4	4.9	51	233.20	226.81	12.07	12.66	AP	11
A58	5	4.9	51	233.20	228.27	12.07	13.36	XP	17
A88	2	4.8	53	236.84	231.07	11.98	12.75		
E 19	1	4.5	24	236.89	233.94	11.34	11.18		
A84	2	5.0	4	237.39	235.80	11.96	13.50		
A90	2	4.9	4	237.41	233.86	11.94	12.46		
E66	1	4.6	27	238.34	238.25	11.83	11.13		
A75	1	5.2	34	239.56	235.03	11.64	11.49		
E 3	1	4.7	73	240.42	236.16	10.99	12.14		
E 3	2	4.7	73	240.42	235.18	10.99	11.19		2
E 3	3	4.7	73	240.42	240.36	10.99	12.00		3
E 3	4	4.7	73	240.42	239.83	10.99	13.70		4
E68	1	4.6	33	240.62	237.64	11.47	11.41		
E56	1	4.7	193	241.31	237.75	10.66	11.32		
E56	2	4.7	193	241.31	242.68	10.66	11.89		0.5
E56	3	4.7	193	241.31	243.15	10.66	13.64		2
E36	2	4.4	201	243.00	246.13	10.48	11.98		
E36	3	4.4	201	243.00	241.14	10.48	12.91		3
A64	1	4.5	209	243.46	241.40	9.59	11.46		
A41	1	4.5	215	243.65	243.64	9.42	11.70		
A41	3	4.5	215	243.65	236.49	9.42	9.37		
A80	2	4.8	74	243.77	239.24	11.14	11.79		
A65	2	4.8	195	244.23	243.31	9.60	11.61		
A78	2	4.7	106	245.60	244.27	10.91	11.10		

N.E	N.S	MB	DEP.	TAZ	DAZ	TAV	DAV	PHASE	TFDS
A85	1	4.8	118	246.29	260.00	9.93	12.73	PRE	
A85	2	4.8	118	246.29	248.48	9.93	11.53		
A85	3	4.8	118	246.29	254.14	9.93	12.71		2
E17	1	3.8	275	246.38	241.38	10.33	10.75		
E17	2	3.8	275	246.38	255.92	10.33	14.07		2
E57	1	4.7	191	248.86	259.95	10.13	12.36		
E57	3	4.7	191	248.86	252.19	10.13	12.85		1
E57	4	4.7	191	248.86	253.73	10.13	12.95		3
E57	5	4.7	191	248.86	248.07	10.13	12.07		4
A72	1	4.7	128	250.21	257.56	10.63	11.90	PRE	
A72	2	4.7	128	250.21	256.11	10.63	11.72		
A72	4	4.7	128	250.21	258.71	10.63	12.70		5
A69	1	4.5	121	250.85	261.84	10.75	12.50	PRE	
A69	2	4.5	121	250.85	261.52	10.75	12.18		
A69	3	4.5	121	250.85	261.39	10.75	13.78		3
E55	1	4.8	131	250.93	267.14	10.72	11.34		
E55	2	4.8	131	250.93	260.23	10.72	11.85		1
E55	3	4.8	131	250.93	247.79	10.72	11.90		1.5
E55	4	4.8	131	250.93	243.46	10.72	11.79		4
A20	2	4.7	49	251.70	247.08	11.09	10.95		
E21	1	4.7	124	252.11	260.08	10.72	11.57		
E21	2	4.7	124	252.11	240.31	10.72	10.57		1
E21	3	4.7	124	252.11	266.54	10.72	13.66		3
E61	1	4.6	100	252.41	261.08	10.63	11.03		
A73	1	3.9	126	252.76	266.79	10.69	11.89	PRE	
A73	2	3.9	126	252.76	264.91	10.69	12.25		
A24	1	5.1	33	254.69	268.34	11.26	12.04		
E41	1	5.3	127	256.53	264.31	10.76	11.39	PRE	
E41	2	5.3	127	256.53	263.51	10.76	11.20		
E41	3	5.3	127	256.53	258.69	10.76	11.41		1
E41	4	5.3	127	256.53	268.33	10.76	13.26		3
E47	1	4.0	141	256.59	266.87	10.75	14.11		
E47	2	4.0	141	256.59	257.51	10.75	10.64		1
E47	3	4.0	141	256.59	263.91	10.75	14.07		3
A48	1	4.0	127	257.23	265.39	10.85	11.69		
A48	2	4.0	127	257.23	267.04	10.85	12.70		4

2

N.E	N.S	MB	DEP.	TAZ	ΔAZ	TAV	ΔAV	PHASE	TFOS
A70	1	5.2	132	258.95	263.33	10.85	11.27		
A70	2	5.2	132	258.95	264.12	10.85	11.05		2
A70	3	5.2	132	258.95	268.62	10.85	12.86		3
A12	2	3.6	162	261.12	269.86	11.12	10.44		
A12	3	3.6	162	261.12	267.01	11.12	12.85		4
A51	1	5.0	102	262.49	267.32	9.15	8.68		
A51	2	5.0	102	262.49	269.80	9.15	9.44		4
A51	3	5.0	102	262.49	247.13	9.15	9.66		6
A51	4	5.0	102	262.49	268.62	9.15	10.53		10
A42	1	4.6	50	262.57	266.53	11.48	11.41		
A42	2	4.6	50	262.57	270.61	11.48	12.56		
A71	1	5.4	85	265.78	271.29	12.11	11.80		
E 6	2	4.9	98	267.54	269.09	11.99	12.30		
A16	1	5.2	63	268.70	272.05	12.41	12.07		
E 18	1	5.2	62	277.29	277.71	12.56	12.26		
E44	1	5.0	61	277.34	279.49	12.57	11.67		
A02	1	4.9	33	279.91	281.31	12.42	13.02		
E22	2	4.6	137	282.17	285.44	12.44	12.01		
A09	1	5.4	33	284.21	285.28	12.50	11.83		
A08	1	6.1	64	284.32	286.23	12.51	11.75		
A53	2	4.9	40	286.81	288.47	12.83	11.92		
A49	1	5.4	89	289.95	291.96	12.75	12.08		

N.E = EVENT NUMBER
N.S = SIGNAL NUMBER
TAZ = EXPECTED AZIMUTH AT SAAS
ΔAZ = OBSERVED AZIMUTH AT SAAS
TAV = EXPECTED APPARENT VELOCITY AT SAAS
ΔAV = OBSERVED APPARENT VELOCITY AT SAAS
TFOS = TIME FROM ONSET IN SECONDS
AP = SMALL P - LARGE P
XP = SMALL S - LARGE P
PRE = PRECURSOR PHASE

APPENDIX 3-B

CORRECTED AZIMUTH AND APPARENT VELOCITY OBSERVED AT SAAS

N.E	N.S	MB	DEP.	TAZ	OAZ	TAV	OAV	PHASE	TFOS
1.-EAST EUROPE-MIDDLE EAST									
A17	1	4.7	33	49.37	55.30	21.75	20.77		
A38	1	5.9	46	51.40	55.67	22.26	20.46		
A38	5	5.9	46	51.40	62.72	22.19	20.13	AP	16
A23	1	4.9	18	37.57	48.44	22.42	22.03		
A23	2	4.9	18	37.57	43.62	22.41	19.59	AP	4
A30	1	5.1	47	52.01	53.30	22.48	19.25		
A46	1	5.0	10	45.39	50.79	23.02	23.15		
A46	3	5.0	10	45.39	48.50	23.01	22.79	AP	5
A28	1	5.0	26	48.20	49.64	23.34	23.22		
A29	1	4.8	28	48.19	51.00	23.34	23.10		
A29	2	4.8	28	48.19	47.43	23.32	21.37	AP	5
A05	1	5.4	33	49.26	61.89	23.76	27.63		
A05	2	5.4	33	49.26	59.98	23.76	26.44	AP	5
A22	1	4.6	136	42.63	68.00	23.84	18.87		
A87	1	4.7	33	49.72	50.03	23.80	23.12		
2.-ATLANTIC OCEAN AND MID-ATLANTIC RIDGE									
E46	1	5.2	33	6.35	1.22	17.02	19.50		
A77	1	5.0	33	15.57	17.98	15.43	15.27		
A55	1	4.8	33	15.67	18.82	16.73	17.45		
A55	3	4.8	33	15.67	18.43	16.71	16.79	AP	10
A54	1	4.8	33	15.73	17.06	16.73	16.29		
A56	2	5.0	33	19.94	17.57	17.01	17.11		
E24	2	4.9	33	26.83	29.10	12.16	7.39		

N.E	N.S	MB	DEP.	TAZ	DAZ	TAV	DAV	PHASE	TFOS
E13	1	5.7	33	27.31	36.57	13.44	13.72		
E13	2	5.7	33	27.31	31.12	13.44	12.57		
E13	4	5.7	33	27.31	37.36	13.42	13.41		
E13	5	5.7	33	27.31	45.16	13.42	12.95		
E13	6	5.7	33	27.31	44.24	13.44	14.88		
E13	7	5.7	33	27.31	33.59	13.44	13.20		
E13	8	5.7	33	27.31	36.55	13.44	13.24		
E13	9	5.7	33	27.31	34.47	13.44	13.86		
E13	10	5.7	33	27.31	40.71	13.44	13.31		
E13	11	5.7	33	27.31	28.98	13.44	12.59		
E13	12	5.7	33	27.31	37.73	13.44	13.02		
E13	13	5.7	33	27.31	27.91	13.44	13.84		
E13	14	5.7	33	27.31	36.45	13.44	14.29		
E13	15	5.7	33	27.31	40.07	13.44	14.14		
E13	16	5.7	33	27.31	39.05	13.44	14.63		
E13	17	5.7	33	27.31	26.44	13.44	12.96		
E13	20	5.7	33	27.31	35.27	13.44	14.00		
E13	21	5.7	33	27.31	28.50	13.44	12.50		
A61	1	4.7	33	41.05	41.95	12.08	10.68		
A15	1	4.3	33	51.12	50.14	12.01	11.84		
E69	1	4.9	33	67.42	67.93	12.91	13.73		
A14	1	5.1	33	98.52	97.62	12.71	12.38		
E33	1	5.2	20	112.76	116.58	18.11	15.75		
3.-SOUTH SANDWICH ISLAND REGION									
A21	1	5.5	33	163.91	159.40	13.66	13.55		
A21	3	5.5	33	163.91	162.34	13.64	13.57	AP	8
A40	1	5.3	33	163.97	160.16	13.66	14.35		
A40	4	5.3	33	163.97	160.12	13.64	14.02	AP	12
A81	1	4.8	33	144.66	142.72	13.79	11.94		
A26	1	5.2	33	152.28	153.18	14.06	13.17		
A13	1	4.9	33	163.87	162.15	14.19	14.48		
E262	2	0.0	33	165.06	158.24	14.25	13.71		
E63	1	5.6	33	163.70	158.74	14.55	13.89	PRE	
E63	2	5.6	33	163.70	158.36	14.55	13.50		

N.E	N.S	MB	DEP.	TAZ	DAZ	TAV	DAV	PHASE	TFDS
4.-EAST PACIFIC OCEAN									
A60	1	5.0	33	216.42	219.43	18.53	20.54		
A44	1	5.4	33	217.84	212.93	19.35	19.29		
E 1	1	5.4	33	231.17	228.45	14.11	15.44	PRE	
E 1	2	5.4	33	231.17	224.59	14.11	14.69		
E 1	3	5.4	33	231.17	224.40	14.08	14.28	AP	7
E 1	4	5.4	33	231.17	226.96	14.11	15.18		
E 1	5	5.4	33	231.17	226.64	14.11	15.48		
E 1	6	5.4	33	231.17	216.77	14.11	36.21	PCP	38
E 1	7	5.4	33	231.17	223.15	11.21	11.99	PP	44
A89	1	5.0	33	238.66	238.82	13.81	15.40		
E12	1	4.4	33	252.89	260.30	12.78	13.27		
E12	3	4.4	33	252.89	261.11	12.76	13.27	AP	7
E39	1	5.1	33	263.10	270.34	16.43	15.23		
A79	1	4.6	33	275.19	276.78	15.68	15.61		
A34	1	5.8	33	287.67	286.96	15.56	15.22		
A34	5	5.8	33	287.67	276.84	15.56	31.47	PCP	59
5.-NORTHERN LATIN-AMERICA									
A01	1	5.2	128	329.90	323.81	12.59	13.12		
A45	1	0.0	50	310.35	307.47	12.77	12.57		
A63	1	4.6	193	310.25	305.19	12.82	14.51		
A63	2	4.6	193	310.25	307.25	12.62	12.01	AP	39
A19	1	4.3	164	310.39	305.65	12.85	12.59		
E10	1	3.5	168	310.31	305.56	12.84	12.77		
E37	1	4.4	159	310.29	304.56	12.84	11.37		
E 8	1	4.9	33	303.36	291.72	13.31	14.44		
E 8	2	4.9	33	303.36	294.95	13.29	14.45	AP	4
E28	1	4.9	33	339.78	335.22	13.43	11.96		
A86	1	4.8	33	306.51	302.85	14.37	15.47		

N.E	N.S	MB	DEP.	TAZ	ΔAZ	TAV	ΔAV	PHASE	TFOS
E34	1	4.6	24	302.21	295.96	14.41	15.86		
E34	3	4.6	24	302.21	298.87	14.40	14.64	AP	8
E34	4	4.6	24	302.21	298.75	14.40	14.49	XP	10
A32	1	4.4	77	303.04	298.60	14.64	14.78		
E60	1	5.6	73	303.18	296.79	14.62	18.19	PRE	
E60	2	5.6	73	303.18	298.53	14.62	15.27		
E60	7	5.6	73	303.18	302.81	14.54	15.33	AP	18
E60	8	5.6	73	303.18	294.72	14.54	15.97	XP	25
E60	9	5.6	73	303.18	305.00	14.62	30.44	PCP	85
A03	1	3.9	157	302.55	299.14	14.86	15.44		
A04	1	5.1	85	302.58	297.66	14.83	14.46		
A76	1	4.6	96	302.45	299.74	15.33	15.40		
A76	3	4.6	96	302.45	299.59	15.18	15.01	AP	19
A36	1	5.1	115	303.28	301.04	15.43	15.59		
A36	4	5.1	115	303.28	300.39	15.24	14.16	AP	33
E65	2	4.5	33	301.03	298.32	15.57	15.18		
E52	1	5.5	33	301.63	296.68	15.56	14.37		
E11	1	4.8	42	300.70	299.28	15.69	14.06		
E53	1	4.7	33	300.90	300.28	16.06	14.37		
E14	1	5.7	38	298.56	286.83	17.46	17.15	PRE	
E14	2	5.7	38	298.56	289.62	17.46	19.40		
E14	3	5.7	38	298.56	290.55	17.46	18.51		
E14	4	5.7	38	298.56	292.24	17.46	17.77		
E14	5	5.7	38	298.56	293.94	17.46	16.50		
E14	6	5.7	38	298.56	298.31	17.43	16.77		
E14	7	5.7	38	298.56	294.51	17.43	16.97		
E14	8	5.7	38	298.56	286.01	17.43	18.94		
E14	9	5.7	38	298.56	293.97	17.43	19.06		
E14	10	5.7	38	298.56	294.22	17.43	17.86		
E14	11	5.7	38	298.56	298.32	17.46	18.70		
E14	12	5.7	38	298.56	286.59	17.46	19.69		
E14	13	5.7	38	298.56	294.30	17.46	21.16		
E14	14	5.7	38	298.56	295.07	17.46	20.81		
E14	15	5.7	38	298.56	286.70	17.46	17.96		
E14	16	5.7	38	298.56	287.10	17.46	17.11		
E14	17	5.7	38	298.56	290.72	17.46	17.98		
E14	18	5.7	38	298.56	286.55	17.46	20.36		
E14	19	5.7	38	298.56	282.78	17.46	22.13		
E14	20	5.7	38	298.56	301.05	17.46	17.89		

N.E	N.S	MB	DEP.	TAZ	OAZ	TAV	OAV	PHASE	TFOS
6.-WESTERN SOUTH AMERICA									
E30	1	4.6	19	220.87	210.47	12.64	11.56		
A67	1	4.6	129	224.03	216.24	12.05	12.66	PRE	
A67	2	4.6	129	224.03	216.08	12.05	10.58		
A67	4	4.6	129	224.03	218.21	11.23	10.98	AP	26
A52	1	4.5	112	224.34	214.91	12.44	11.76		
E16	1	4.1	123	226.98	218.10	12.32	13.60	PRE	
E16	2	4.1	123	226.98	219.14	12.32	12.68		
E16	4	4.1	123	226.98	195.16	11.82	11.09	AP	29
E16	5	4.1	123	226.98	216.99	11.82	11.19	XP	41
A06	1	4.6	28	227.58	218.30	12.41	12.56	PRE	
A06	2	4.6	28	227.58	216.32	12.41	11.54		
A25	1	5.3	104	227.53	219.49	12.06	13.17		
A39	1	0.0	121	227.60	220.08	12.32	11.69		
A39	2	0.0	121	227.60	219.12	11.82	11.02	AP	24
A57	1	5.4	40	227.66	218.38	12.42	12.40		
A57	2	5.4	40	227.66	216.85	12.39	12.21	AP	9
A07	1	4.9	40	227.74	221.44	12.42	12.33	PRE	
A07	2	4.9	40	227.74	217.78	12.42	12.53		
A07	3	4.9	40	227.74	210.84	12.42	11.98	AP	10
A07	4	4.9	40	227.74	218.73	12.42	12.02	XP	14
E29	1	4.1	67	227.86	218.50	12.42	12.28		
E29	4	4.1	67	227.86	217.39	12.32	12.70	AP	18
E29	5	4.1	67	227.86	220.28	12.32	12.36	XP	25
A31	1	5.0	88	228.79	219.13	12.37	12.29		
A31	2	5.0	88	228.79	219.70	12.37	12.07	AP	15
A31	3	5.0	88	228.79	218.75	12.37	11.81	XP	20
E45	1	5.5	137	230.05	220.58	11.46	10.67		
E45	2	5.5	137	230.05	222.48	11.46	11.25		
E45	3	5.5	137	230.05	219.93	11.46	10.37		
E45	4	5.5	137	230.05	221.89	11.46	9.02	AP	22
E45	5	5.5	137	230.05	221.03	10.19	10.40	PP	31
A66	1	4.9	40	230.04	221.23	12.31	12.27		
A59	1	5.6	39	231.23	218.30	11.76	10.37		
E 2	2	4.1	173	231.25	221.08	11.27	10.39		

N.E	N.S	MB	DEP.	TAZ	OAZ	TAV	OAV	PHASE	TFOS
E64	1	4.9	47	231.66	222.83	12.32	12.56	PRE	
E64	2	4.9	47	231.66	222.25	12.32	12.71		
E64	3	4.9	47	231.66	226.63	12.32	11.24	AP	9
E64	4	4.9	47	231.66	219.92	12.32	12.59	XP	13
A18	1	4.7	66	232.92	223.68	12.25	12.72		
A18	3	4.7	66	232.92	221.72	12.06	12.05	AP	14
A58	1	4.9	51	233.20	225.00	12.19	12.10		
A58	4	4.9	51	233.20	223.40	12.07	12.15	AP	11
A58	5	4.9	51	233.20	224.61	12.07	12.82	XP	17
A88	2	4.8	53	236.84	227.47	11.98	12.29		
E19	1	4.5	24	236.89	230.25	11.34	10.83		
A83	2	0.0	33	237.35	229.00	11.95	12.60		
A84	2	5.0	4	237.39	231.81	11.96	13.05		
A90	2	4.9	4	237.41	230.24	11.94	12.06		
E66	1	4.6	27	238.34	234.59	11.83	10.88		
A75	1	5.2	34	239.56	231.64	11.64	11.16		
E 3	1	4.7	73	240.42	233.27	10.99	11.63		
E 3	2	4.7	73	240.42	231.87	10.99	10.88		2
E 3	3	4.7	73	240.42	236.67	10.99	11.71		3
E 3	4	4.7	73	240.42	235.66	10.99	13.31		4
E68	1	4.6	33	240.62	234.20	11.47	11.12		
E56	1	4.7	193	241.31	234.34	10.66	11.04		
E56	2	4.7	193	241.31	238.97	10.66	11.64		0.5
E56	3	4.7	193	241.31	238.89	10.66	13.30		2
E36	2	4.4	201	243.00	242.32	10.48	11.76		
E36	3	4.4	201	243.00	237.16	10.48	12.58		3
A64	1	4.5	209	243.46	237.85	9.59	11.21		
A41	1	4.5	215	243.65	239.96	9.42	11.46		
A41	3	4.5	215	243.65	233.68	9.42	9.17		2
A80	2	4.8	74	243.77	235.65	11.14	11.50		
A65	2	4.8	195	244.23	239.67	9.60	11.37		
A78	2	4.7	106	245.60	240.70	10.91	10.88		

N.E	N.S	MB	DEP.	TAZ	DAZ	TAV	DAV	PHASE	TFOS
A85	1	4.8	118	246.29	255.77	9.93	12.71	PRE	
A85	2	4.8	118	246.29	244.76	9.93	11.36		
A85	3	4.8	118	246.29	249.96	9.93	12.59		2
E17	1	3.8	275	246.38	238.04	10.33	10.52		
E17	2	3.8	275	246.38	250.97	10.33	14.01		2
E57	1	4.7	191	248.86	255.83	10.13	12.34		
E57	3	4.7	191	248.86	247.99	10.13	12.69		7
E57	4	4.7	191	248.86	249.47	10.13	12.82		3
E57	5	4.7	191	248.86	244.19	10.13	11.88		4
A72	1	4.7	128	250.21	253.61	10.63	11.85	PRE	
A72	2	4.7	128	250.21	252.23	10.63	11.64		
A72	4	4.7	128	250.21	254.93	10.63	12.60		5
A69	1	4.5	121	250.85	257.42	10.75	12.47	PRE	
A69	2	4.5	121	250.85	257.46	10.75	12.18		
A69	3	4.5	121	250.85	256.80	10.75	13.77		3
E55	1	4.8	131	250.93	263.36	10.72	11.42		
E55	2	4.8	131	250.93	256.28	10.72	11.83		1
E55	3	4.8	131	250.93	243.97	10.72	11.71		1.5
E55	4	4.8	131	250.93	239.58	10.72	11.51		4
A20	2	4.7	49	251.70	243.49	11.09	10.77		
E21	1	4.7	124	252.11	256.23	10.72	11.55		
E21	2	4.7	124	252.11	237.06	10.72	10.34		1
E21	3	4.7	124	252.11	261.99	10.72	13.76		3
E61	1	4.6	100	252.41	257.32	10.63	11.02		
A73	1	3.9	126	252.76	262.84	10.69	11.97	PRE	
A73	2	3.9	126	252.76	260.83	10.69	12.31		
A24	1	5.1	33	254.69	264.34	11.26	12.14		
E41	1	5.3	127	256.53	260.51	10.76	11.43	PRE	
E41	2	5.3	127	256.53	259.78	10.76	11.23		
E41	3	5.3	127	256.53	254.89	10.76	11.38		1
E41	4	5.3	127	256.53	263.92	10.76	13.38		3
E47	1	4.0	141	256.59	262.17	10.75	14.21		
E47	2	4.0	141	256.59	253.98	10.75	10.60		1
E47	3	4.0	141	256.59	259.22	10.75	14.11		3
A48	1	4.0	127	257.23	261.26	10.85	11.72		
A48	2	4.0	127	257.23	262.81	10.85	12.79		4

N.E	N.S	MB	DEP.	TAZ	OAZ	TAV	OAV	PHASE	TFOS
A70	1	5.2	132	258.95	259.57	10.85	11.30		
A70	2	5.2	132	258.95	260.44	10.85	11.09		2
A70	3	5.2	132	258.95	264.35	10.85	12.98		3
A12	2	3.6	162	261.12	266.23	11.12	10.58		
A12	3	3.6	162	261.12	262.50	11.12	13.01		4
A51	1	5.0	102	262.49	264.44	9.15	8.73		
A51	2	5.0	102	262.49	266.68	9.15	9.52		4
A51	3	5.0	102	262.49	244.02	9.15	9.53		6
A51	4	5.0	102	262.49	265.13	9.15	10.61		10
A42	1	4.6	50	262.57	262.73	11.48	11.48		
A42	2	4.6	50	262.57	266.45	11.48	12.70		
A71	1	5.4	85	265.78	267.39	12.11	11.94		
E 6	2	4.9	98	267.54	265.03	11.99	12.41		
A16	1	5.2	63	268.70	267.76	12.41	12.23		
E 18	1	5.2	62	277.29	273.75	12.56	12.51		
E44	1	5.0	61	277.34	275.76	12.57	11.92		
A02	1	4.9	33	279.91	277.01	12.42	13.45		
E22	2	4.6	137	282.17	281.60	12.44	12.43		
A09	1	5.4	33	284.21	281.53	12.50	12.17		
A08	1	6.1	64	284.32	282.51	12.51	12.17		
A53	2	4.9	40	286.81	284.88	12.83	12.31		
A49	1	5.4	89	289.95	288.44	12.75	12.53		

N.E = EVENT NUMBER
N.S = SIGNAL NUMBER
TAZ = EXPECTED AZIMUTH AT SAAS
OAZ = OBSERVED AZIMUTH AT SAAS
TAV = EXPECTED APPARENT VELOCITY AT SAAS
OAV = OBSERVED APPARENT VELOCITY AT SAAS
TFOS = TIME FROM ONSET IN SECONDS
AP = SMALL P - LARGE P
XP = SMALL S - LARGE P
PRE = PRECURSOR TO PHASE

APPENDIX 4

RECOMMENDATIONS TO IMPROVE SAAS BULLETINS IN BRASILIA

The preliminary readings of events detected by SAAS made in Brasilia are very important for the following reasons:

a) They are used in the NOAA and ISC epicentral determinations.

b) They are the basic information for future transcription of SAAS tapes.

The audio method at present used in Brasilia to find seismic events recorded in SAAS tapes has several disadvantages, the most important being the poor quality of the sound amplifier used during the analysis. It has been shown in Chapter 3 that the number of events detected during the preliminary analysis made in Brasilia is far less than the number of events recorded on SAAS tapes.

From the results of the analysis used in 3.2, it is clear that by using the visual method to analyse SAAS tapes is possible to pick up from the tapes a larger number of events that can be detected by audio methods at SAAS. Therefore, it is recommended that the visual method of tape analysis should be adopted to carry out the preliminary analysis of SAAS tapes in Brasilia.

To adopt a visual method of analysis in Brasilia the following improvements must be introduced in the reproduction system used there:

a) Increase the number of frequency band pass filters up to at least 7, and

b) Increase 10 times the gain of the reproduction unit by using a new flutter card to make it compatible with the units operating at Edinburgh.

This last improvement will allow the use of lower gains on the jet-pen recorder to get high amplifications without having to use larger pen gains, which introduce instrumental noise produced by the pen recorder.

Some medium magnitude events ($m_b \approx 5.5$) and most of the events with $m_b > 6$ which occurred in South America saturate the dynamic range of the recording unit used at SAAS. In order to increase the dynamic range of the SAAS recording unit, it would be advisable to decrease the gain of the field amplifiers to X1000 instead of X2000. Earthquakes of very large magnitude ($m_b > 6.5$) from relatively short distances (i.e. less than 40° from SAAS) will saturate the recording system even after having decreased the field amplifiers gain to 1000, but it is not advisable to set the field amplifiers to a lower gain than that recommended here because of the danger of reducing the detection capability of the array. To obtain a complete record of these large earthquakes it is necessary to install an extra vertical short period component at E4 with its field amplifier gain as low as possible (i.e. x 100).

APPENDIX 5

BRAZILIAN EVENTS RECORDED AT SAAS IN THE PERIOD AUG 1967 - FEB 1972

No.	DATE	ORIG. TIME	OBSER. TIME	LAT.	LONG.	m_b	LOCALITY
	1967						
01	05 AUG	09 57 10.2	09 55 20.4	-	-	4.5	Rio de Janeiro (GB)
	1968						
01	07 JAN	02 03 41.9	02 00 36.9	-	-	4.3	Pereiros (CE)
02	09	08 09 42	-	-	-	3.8	Pereiros (CE)
03	13	01 58 57.7	01 55 52.7	5.8 S	38.9W	4.6	Pereiros (CE)
04	16	13 42 39.2	13 39 34.2	-	-	4.4	Pereiros (CE)
05	16	16 27 42.3	16 24 37.3	-	-	4.3	Pereiros (CE)
06	19	18 27 31.9	18 24 26.9	-	-	4.1	Pereiros (CE)
07	04 FEB	23 12 19.9	23.09 14.9	-	-	4.2	Pereiros (CE)
08	10	12 46 45	-	-	-	3.8	Pereiros (CE)
09	17	13 23 55.4	13 20 50.4	6.1 S	39.0W	4.6	Pereiros (CE)
10	22	00 40 51.0	00 37 46.0	-	-	4.1	Pereiros (CE)
11	23	09 13 03.4	09 09 58.4	-	-	4.0	Pereiros (CE)
12	23	12 53 26.6	12 50 21.6	-	-	3.9	Pereiros (CE)
13	23	14 26 05.4	14 23 00.4	6.3S	38.8W	4.9	Pereiros (CE)
14	23	15 24 20.9	15 21 15.9	-	-	3.9	Pereiros (CE)
15	23	15 36 07.9	15 33 02.9	-	-	4.4	Pereiros (CE)
16	23	19 02 56.0	18 59 51.0	-	-	3.9	Pereiros (CE)
17	24	07 32 40.7	07 29 35.7	-	-	4.0	Pereiros (CE)
	1970						
01	12 JAN	04 46 18.9	04 43 00.8	-	-	4.6	Belém (PA)
02	20 APR	13 40 56.6	13 39 31.1	-	-	4.0	Carmo do Cajuru(MG)
03	20	20 00 52	-	-	-	3.7	Carmo do Cajuru(MG)
04	25	01 55 30.0	01 54 01.3	-	-	4.4	Carmo do Cajuru(MG)
05	12 MAY	20 55 12	-	-	-	3.7	Carmo do Cajuru(MG)
06	13 AUG	18 48 49.9	18 47 21.9	-	-	4.2	Carmo do Cajuru(MG)
07	14 -	04 59 56.3	04 59 00.9	-	-	4.0	Tocantins
08	14	13 27 20.0	13 25 54.0	-	-	4.5	Carmo do Cajuru(MG)
09	19	18 46 20	-	-	-	3.7	Carmo do Cajuru(MG)
10	20	13 59 00.3	13 57 30.7	-	-	4.2	Carmo do Cajuru(MG)
11	21	13 25 09.8	13 23 41.7	-	-	4.3	Carmo do Cajuru(MG)

12	22 AUG	13 07 33.5	13 06 06.2	-	-	4.2	Carmo do Cajuru(MG)
13	24	13 27 57.8	13 26 29.1	-	-	4.3	Carmo do Cajuru(MG)
14	26	13 23 43.8	13 22 17.2	-	-	4.5	Carmo do Cajuru(MG)
15	29	13 17 39.1	13 16 11.8	-	-	4.2	Carmo do Cajuru(MG)
16	12 SEP	13 27 06.8	13 25 36.7	-	-	4.3	Carmo do Cajuru(MG)
17	13	13 13 15.1	13 21 47.6	-	-	4.3	Carmo do Cajuru(MG)
18	28	20 00 34.6	19 59 07.7	-	-	4.0	Carmo do Cajuru(MG)
19	06 OCT	18 19 37.1	18 18 09.1	-	-	4.0	Carmo do Cajuru(MG)
20	08 -	01 46 40.6	01 46 08.7	-	-	3.7	190 km de Brasília
21	08	13 14 25.7	13 12 56.3	-	-	3.9	Carmo do Cajuru(MG)
22	10	20 08 26.9	20 06 59.6	-	-	4.0	Carmo do Cajuru(MG)
23	13	13 24 44.0	13 23 18.1	-	-	4.1	Carmo do Cajuru(MG)
24	14	09 30 01.1	09 28 33.1	-	-	3.8	Carmo do Cajuru(MG)
25	14	13 17 15.0	13 15 52.7	-	-	3.9	Carmo do Cajuru(MG)
26	20	13 25 35.6	13 24 07.0	-	-	4.3	Carmo do Cajuru(MG)
27	20	20 06 18.2	20 04 51.0	-	-	4.0	Carmo do Cajuru(MG)
28	23	13 32 02.4	13 30 33.7	-	-	4.2	Carmo do Cajuru(MG)
29	01 NOV	13 48 37.2	13 47 12.0	-	-	4.5	Carmo do Cajuru(MG)
30	06	14 06 53.0	14 05 27.8	-	-	3.9	Carmo do Cajuru(MG)
31	11	13 26 00	-	-	-	3.7	Carmo do Cajuru(MG)
32	16	13 23 30.1	13 22 04.2	-	-	4.4	Carmo do Cajuru(MG)
33	17	13 37 45.0	13 36 18.4	-	-	4.3	Carmo do Cajuru(MG)
34	17	13 48 45.6	13 47 16.6	-	-	4.0	Carmo do Cajuru(MG)
35	20 -	23 56 24.7	23 55 20.3	-	-	4.0	Paranaíba (MS)
36	25	19 49 00.0	19 47 32.0	-	-	4.5	Carmo do Cajuru(MG)
37	26	13 23 53.1	13 22 24.3	-	-	3.8	Carmo do Cajuru(MG)
38	27	13 25 45.3	13 24 17.3	-	-	4.2	Carmo do Cajuru(MG)
39	29	06 33 07	-	-	-	4.3	Carmo do Cajuru(MG)
40	29	06 34 44	-	-	-	3.7	Carmo do Cajuru(MG)
	1972						
01	07 JAN	14 08 55.3	14 07 27.1	-	-	3.9	Carmo do Cajuru(MG)
02	08	13 42 02.2	13 41 35.6	-	-	3.9	Carmo do Cajuru(MG)
03	09	18 29 40.0	18 28 12.7	-	-	4.3	Carmo do Cajuru(MG)
04	09	18 57 58.2	18 56 30.2	-	-	3.8	Carmo do Cajuru(MG)

05	13 JAN	13 26 17.4	13 24 30.5	-	-	3.7	Carmo do Cajuru (MG)
06	15	13 44 35.3	13 42 47.3	-	-	4.5	Carmo do Cajuru (MG)
07	17	13 13 13.1	13 11 45.3	-	-	3.9	Carmo do Cajuru (MG)
08	20	13 37 28.8	13 35 39.4	-	-	4.1	Carmo do Cajuru (MG)
09	21	04 11 09.4	04 09 38.5	-	-	3.7	Carmo do Cajuru (MG)
10	22	13 14 40.1	13 13 12.1	-	-	3.7	Carmo do Cajuru (MG)
11	22	13 24 48.2	13 23 21.6	-	-	3.7	Carmo do Cajuru (MG)
12	22	16 05 52.1	16 04 25.5	-	-	3.7	Carmo do Cajuru (MG)
13	23	13 29 29.2	13 28 02.6	-	-	4.0	Carmo do Cajuru (MG)
14	25	13 47 25.0	13 45 58.4	-	-	3.8	Carmo do Cajuru (MG)
15	26	13 58 01.9	13 56 35.3	-	-	4.1	Carmo do Cajuru (MG)
16	28	13 30 38.5	13 29 10.9	-	-	4.0	Carmo do Cajuru (MG)
17	29	08 56 14.3	08 54 45.6	-	-	3.7	Carmo do Cajuru (MG)
18	30	07 36 23.9	07 34 56.6	-	-	3.7	Carmo do Cajuru (MG)
19	04 FEB	13 29 42.7	13 28 14.0	-	-	3.7	Carmo do Cajuru (MG)
20	04	20 27 01.3	20 25 34.7	-	-	3.7	Carmo do Cajuru (MG)
21	10	13 24 41.1	13 23 13.0	-	-	3.7	Carmo do Cajuru (MG)
22	04 MAR	13 31 43.7	13 30 15.7	-	-	3.7	Carmo do Cajuru (MG)
23	09	14 12 33.0	14 11 03.4	19.63	41.07	4.5	Carmo do Cajuru (MG)
24	16	13 19 53.8	13 18 29.1	-	-	3.9	Carmo do Cajuru (MG)
25	25	14 01 00.0	13 59 30,3	20.45	41.77	4.2	Carmo do Cajuru (MG)
26	29 -	14 44 14.7	-	-	-	3.7	Distância 7°
27	05 APR	06 25 21.1	06 23 53.1	-	-	3.9	Carmo do Cajuru (MG)
28	16	13 30 48.2	13 29 19.5	-	-	4.2	Carmo do Cajuru (MG)
29	19	13 18 50.7	13 17 25.2	-	-	4.1	Carmo do Cajuru (MG)
30	03-MAY	15 33 28.2	-	-	-	4.5	60° W de Brasília
31	06	13 42 16.7	-	-	-	3.7	Carmo do Cajuru (MG)
32	08	17 21 45.0	17 20 20.9	-	-	4.0	Carmo do Cajuru (MG)
33	09	14 13 14.0	14 11 46.0	-	-	4.3	Carmo do Cajuru (MG)
34	11	13 28 05.0	13 26 38.4	20.43	42.07	4.4	Carmo do Cajuru (MG)
35	17 JUN	13 55 24.2	13 53 55.5	-	-	4.1	Carmo do Cajuru (MG)
36	17	18 08 53.1	18 07 24.4	-	-	4.1	Carmo do Cajuru (MG)
37	29	18 09 32.3	-	-	-	3.7	Carmo do Cajuru (MG)
38	28	13 30 53.9	13 29 33.1	-	-	3.9	Carmo do Cajuru (MG)

39	03 JUL	13 49 30.4	-	-	-	3.7	Carmo do Cajuru (MG)
40	01	19 15 48.5	-	-	-	3.7	Carmo do Cajuru (MG)
41	09	13 03 29.7	13 02 00.8	20.3 S	44.0 W	4.5	Carmo do Cajuru (MG)
42	13	13 19 18.4	13 17 39.0	20.4 S	41.6 W	4.2	Carmo do Cajuru (MG)
43	13	13 37 42.9	13 36 14.9	20.4 S	41.9 W	4.4	Carmo do Cajuru (MG)
44	14	13 54 47.2	13 53 19.2	20.4 S	41.6 W	4.4	Carmo do Cajuru (MG)
45	15	13 20 57.4	13 28 25.4	20.4 S	41.8 W	4.1	Carmo do Cajuru (MG)
46	16	13 13 38.1	13 12 10.1	20.2 S	41.5 W	4.2	Carmo do Cajuru (MG)
47	16	13 36 04.7	13 34 39.2	-	-	3.9	Carmo do Cajuru (MG)
48	16	19 51 40.3	19 51 03.5	13.5 S	49.1 W	4.6	Formagem (MG)
49	19	13 48 42.9	13 47 17.4	-	-	4.2	Carmo do Cajuru (MG)
50	22	13 05 14.7	13 03 46.7	20.4 S	41.8 W	4.3	Carmo do Cajuru (MG)
51	23	13 37 47.0	13 36 09.7	20.1 S	41.5 W	4.2	Carmo do Cajuru (MG)
52	24	13 37 44.7	13 36 18.1	20.2 S	41.8 W	4.3	Carmo do Cajuru (MG)
53	29	13 42 20.5	13 40 55.0	-	-	4.1	Carmo do Cajuru (MG)
54	30	15 02 09.9	-	-	-	-	Carmo do Cajuru (MG)
55	04 AGO	13 39 06.9	13 37 36.4	20.2 S	41.5 W	4.2	Carmo do Cajuru (MG)
56	05 -	02 23 54		8.1 S	34.5 W	3.0	Recife (PE)
57	05 -	02 26 28		8.1 S	34.5 W	3.6	Recife (PE)
58	05 -	02 33 38		8.1 S	34.5 W	3.6	Recife (PE)
59	05 -	02 48 05		8.1 S	34.5 W	3.8	Recife (PE)
60	05 -	03 02 00		8.1 S	34.5 W	3.6	Recife (PE)
61	09	13 33 18.3	-	20.2 S	41.3 W	4.3	Carmo do Cajuru (MG)
62	10	13 14 54.5	13 13 23.1	20.4 S	41.6 W	4.2	Carmo do Cajuru (MG)
63	11	13 50 49.4	13 49 18.8	-	-	4.1	Carmo do Cajuru (MG)
64	17	13 13 01.5	-	20.3 S	41.5 W	4.1	Carmo do Cajuru (MG)
65	19	13 13 51.4	13 12 21.9	19.2 S	40.4 W	4.2	Carmo do Cajuru (MG)
66	20	14 02 36.1	14 01 06.7	-	-	4.1	Carmo do Cajuru (MG)
67	21	13 15 17.2	13 14 48.1	20.3 S	41.6 W	4.3	Carmo do Cajuru (MG)
68	27	14 02,24.7	14 00 56.9	20.4 S	41.7 W	4.2	Carmo do Cajuru (MG)
69	28	13 41 27.3	13 39 49.3	20.1 S	41.4 W	4.3	Carmo do Cajuru (MG)
70	01 SET	13 33 24.7	13 31 56.7	19.6 S	40.9 W	4.0	Carmo do Cajuru (MG)
71	04	13 58 40.1	13 57 12.1	20.3 S	41.7 W	4.3	Carmo do Cajuru (MG)
72	27	14 56 52.5	14 55 24.5	-	-	3.9	Carmo do Cajuru (MG)

73	17	OUT	13 24 25.3	13 22 37.3	20.3 S	41.7 W	4.5	Carmo do Cajuru (MG)
74	18		13 22 26.1	13 20 58.1	19.4 S	40.0 W	4.4	Carmo do Cajuru (MG)
75	23		13 53 25.9	13 51 57.9	19.0 S	40.4 W	4.2	Carmo do Cajuru (MG)
76	24		13 13 51.5	13 14 22.1	-	-	3.8	Carmo do Cajuru (MG)
77	25		13 33 42.9	13 32 04.9	20.2 S	41.5 W	4.1	Carmo do Cajuru (MG)
78	28		13 54 22.6	13 52 51.2	20.5 S	41.8 W	4.3	Carmo do Cajuru (MG)
79	28		14 47 55.9	-	-	-	3.7	Carmo do Cajuru (MG)
80	28		22 28 23.2	22 26 48.9	-	-	4.0	Carmo do Cajuru (MG)
81	30		18 35 28.7	18 34 00.0	-	-	4.0	Carmo do Cajuru (MG)
82	01	OUT	14 09 04.6	14 08 35.2	-	-	3.8	Carmo do Cajuru (MG)
83	02		13 37 16.1	13 35 44.4	20.6 S	41.7 W	4.2	Carmo do Cajuru (MG)
84	08		14 04 06.4	14 02 39.1	20.2 S	41.7 W	4.3	Carmo do Cajuru (MG)
85	12		13 34 09.6	13 32 39.2	-	-	4.2	Carmo do Cajuru (MG)
86	12		14 36 58.9	14 35 30.2	-	-	3.8	Carmo do Cajuru (MG)
87	13		18 57 52.3	18 56 24.3	-	-	3.7	Carmo do Cajuru (MG)
88	15		13 35 45.59	13 34 17.59	20.2 S	41.6 W	4.2	Carmo do Cajuru (MG)
89	16		15 56 29.0	15 54 55.7	-	-	3.7	Carmo do Cajuru (MG)
90	17		14 14 45.3	14 13 15.9	-	-	3.8	Carmo do Cajuru (MG)
91	19		13 15 15.4	13 13 47.4	20.3 S	41.6 W	3.9	Carmo do Cajuru (MG)
92	20		13 25 36.8	13 14 08.8	19.7 S	41.0 W	4.1	Carmo do Cajuru (MG)
93	21		13 24 15.8	13 22 48.5	20.4 S	41.8 W	4.1	Carmo do Cajuru (MG)
94	22		17 16 22.1	17 14 52.7	-	-	3.9	Carmo do Cajuru (MG)
95	27		13 40 59.9	13 39 30.5	20.5 S	41.8 W	4.3	Carmo do Cajuru (MG)
96	28		13 15 08.4	13 13 39.0	-	-	4.0	Carmo do Cajuru (MG)
97	04	NOV	12 30 47.0	12 29 19.0	-	-	4.0	Carmo do Cajuru (MG)
98	04		13 33 02.0	13 31 32.6	20.3 S	41.6 W	4.3	Carmo do Cajuru (MG)
99	12		18 28 14.5	-	-	-	3.7	Carmo do Cajuru (MG)
100	13		13 47 23.0	13 45 55.0	-	-	4.2	Carmo do Cajuru (MG)
101	16		19 05 06.7	19 03 39.4	20.3 S	41.8 W	4.3	Carmo do Cajuru (MG)
102	17		13 31 52.8	13 30 24.8	20.1 S	42.0 W	4.1	Carmo do Cajuru (MG)
103	18		18 05 57.8	18 04 29.8	-	-	3.8	Carmo do Cajuru (MG)
104	22		18 51 09.3	18 49 41.3	20.2 S	41.5 W	4.1	Carmo do Cajuru (MG)
105	24		22 29 40.1	22 27 35.2	-	-	3.8	Carmo do Cajuru (MG)
106	29		13 21 30.0	13 19 43.4	-	-	4.2	Carmo do Cajuru (MG)

107	24 DEZ	14 35 05.6	14 33 37.5	-	-	3.8	Carmo do Cajuru(MG)
108	06	13 26 46.5	13 25 18.5	20.3S	41.7W	4.2	Carmo do Cajuru(MG)
109	11	13 23 29.2	13 22 02.6	20.4S	41.9W	4.3	Carmo do Cajuru(MG)
110	13	18 04 52.3	18 03 22.9	-	-	3.9	Carmo do Cajuru(MG)
111	18	13 31 44.1	13 30 16.7	20.1S	41.3W	4.1	Carmo do Cajuru(MG)
112	19	17 44 25.3	-	-	-	3.7	Carmo do Cajuru(MG)
113	21	13 17 35.1	13 15 07.1	20.3S	41.7W	4.2	Carmo do Cajuru(MG)
114	22	18 39 35.1	18 38 06.7	20.3S	41.6W	4.4	Carmo do Cajuru(MG)
115	23	18 44 58.5	18 43 30.5	20.2S	41.5W	3.8	
	1972						
01	02 JAN	02 05 49.0	02 04 20.0	-	-	3.7	Carmo do Cajuru(MG)
02	04	13 51 31.2	13 49 43.8	19.8S	40.9W	4.2	Carmo do Cajuru(MG)
03	06	20 19 57.4	20 18 28.0	-	-	4.4	Carmo do Cajuru(MG)
04	07	23 07 19.4	23 06 41.4	16.0S	57.7W	3.7	Carmo do Cajuru(MG)
05	08	13 42 32.2	13 41 06.1	19.8S	41.4W	4.3	Carmo do Cajuru(MG)
06	14	13 09 20.3	13 07 53.0	20.2S	41.6W	3.9	Carmo do Cajuru(MG)
07	18	13 24 52.9	13 23 00.8	20.3S	41.6W	4.1	Carmo do Cajuru(MG)
08	19	20 17 26.6	20 15 57.9	-	-	3.7	Carmo do Cajuru(MG)
09	21	13 31 26.1	13 29 51.8	20.2S	41.6W	4.3	Carmo do Cajuru(MG)
10	25*	14 00 18.8	13 58 50.8	20.4S	41.8W	4.2 4.3	Carmo do Cajuru(MG)
11	26 -	13 38 25.7	13 36 57.0	18.2S	39.8W	4.1	Itaobim (MG)
12	27	13 23 14.7	13 21 46.7	20.3S	41.7W	4.0	Carmo do Cajuru(MG)
13	27	18 29 29.9	18 28 01.9	20.4S	41.7W	4.0	Carmo do Cajuru(MG)
14	28	13 19 58.5	13 18 48.7	20.0S	41.9W	4.2	Carmo do Cajuru(MG)
15	28	14 04 00.3	14 02 33.7	-	-	3.9	Carmo do Cajuru(MG)
16	29 -	03 35 35.0	03 34 46.3	-	-	3.0	325km oeste de Brasília
17	01 FEB	13 13 39.4	13 12 12.1	20.2S	41.7W	4.1	Carmo do Cajuru(MG)
18	01	19 50 46.6	19 49 19.3	-	-	4.0	Carmo do Cajuru(MG)
19	01	20 05 43.1	20 04 15.1	20.2S	41.6W	3.8	Carmo do Cajuru(MG)
20	02	20 26 21.0	20 24 53.7	20.3S	41.8W	4.1	Carmo do Cajuru(MG)
21	04	14 05 47.6	14 04 21.0	-	-	4.2	Carmo do Cajuru(MG)
22	05	18 17 13.9	18 15 45.9	-	-	3.8	Carmo do Cajuru(MG)
23	06	14 43 47.0	14 42 21.3	20.0S	41.5W	4.3	Carmo do Cajuru(MG)

24	07	13 53 13.4	13 52 12.0	-	-	4.1	Carmo da Cajuru (MG)
25	08	13 11 05.4	13 11 04.2	-	-	4.0	Carmo do Cajuru(MG)
26	08	13 21 54.5	13 20 27.2	-	-	4.0	Carmo do Cajuru (MG)
27	09	13 36 01.1	13 34 47.0	-	-	4.0	Carmo do Cajuru(MG)
28	10	13 59 09.4	13 57 42.0	-	-	4.0	Carmo do Cajuru (MG)
29	10	14 00 16.5	13 58 43.2	20.1S	41.5W	4.1	Carmo do Cajuru (MG)
30	15	13 32 03.4	13 30 36.1	20.3S	41.7	4.1	Carmo do Cajuru (MG)
31	15	13 40 13.1	13 38 45.1	20.3S	41.7W	3.9	Carmo do Cajuru (MG)
32	21	14 00 57.3	13 59 34.3	-	-	4.1	Carmo do Cajuru (MG)
33	22	13 16 14.5	13 14 46.5	-	-	4.1	Carmo do Cajuru (MG)
34	22	20 54 03.2	20 52 34.5	-	-	4.0	Carmo do Cajuru (MG)
35	23	20 06 25.5	20 04 58.2	-	-	4.2	Carmo do Cajuru (MG)

* EVENTS NOT INCLUDED IN THE LISTING:

	OBSER. T	ORIG. T			
08AUG71	13 34 10.5	13 32 39.2	20.4S 41.7W	4.3	Carmo de Cajuru
23JAN72	03 05 16.4	03 03 51.2	20.2S 41.6W	4.7	Carmo de Cajuru

APPENDIX 6

ESTIMATION OF ERRORS IN AZIMUTH AND APPARENT VELOCITY CALCULATIONS

The fundamental equation used to calculate the azimuth (Az) and the apparent velocity (V) from array data is shown in Figure 29 (Chapter 5), where:

$$Az = \arctan (a/b) \qquad (14\text{-a})$$

$$V = 1/\sqrt{a^2+b^2} \qquad (14\text{-b})$$

which are derived from the equations

$$a = \sin(Az)/V \qquad (14\text{-c})$$

$$b = \cos(Az)/V \qquad (14\text{-d})$$

where $\underline{a}$ and $\underline{b}$ are the components of the slowness (s) along the lines 1 and 2 of the array, and

$$s = 1/V = t/x \qquad (A6\text{-}1)$$

where $\underline{t}$ is the time involved for the seismic waves to travel the extension $\underline{x}$ of a line. Note that in equation (14-a), the azimuth is measured from the direction of line 2.

For events coming from azimuths which coincide with the directions of the lines 1 and 2 of an L shaped array, the values of $\underline{a}$ and $\underline{b}$ are

$$a = 0, \text{ and } |b| = 1/V = s \text{ if } Az = K(\pi/2) \text{ and } K = 2,4 \qquad (A6\text{-}2)$$

$$|a| = 1/V = s, \text{ and } b = 0 \text{ if } A = K(\pi/2) \text{ and } K = 1,3 \qquad (A6\text{-}3)$$

if the azimuth of the event is $Az = K(\pi/4)$ and $K = 1,3,5,7$, than:

$$a = b = \sin(\pi/4)/V = \sqrt{2}/2V = s\sqrt{2}/2 \qquad (A6\text{-}4)$$

Considering events with Az = K(π/2), and K = 1,3 the standard error in slowness (da) due to an error (dt) in the estimate of propagation time along line 1, is:

$$da = dt/x \qquad \text{(A6-5)}$$

By definition:

$$V = 1/a \qquad \text{(A6-6)}$$

then, the error in apparent velocity (dVa) is

$$dV = (-1/a^2)da \qquad \text{(A6-7)}$$

or from equation (A6-5)

$$dV = -V^2(dt/x) \qquad \text{(A6-8)}$$

Considering events with Az = K(π/4), and K = 1,3,5,7, this last equation is:

$$dV = -\frac{\sqrt{2}}{2} V^2(dt/x) \qquad \text{(A6-9)}$$

Equations (A6-8) and (A6-9) represent the maximum and the minimum error, respectively, caused to the apparent velocity by dt, in an L shaped array with its lines maximum aperture equal to x.

From equations (14-b) and (14-c), the following relations are obtained:

$$\sin(Az) = (aV) \qquad \text{(A6-10)}$$

$$\cos(Az) = (bV) \qquad \text{(A6-11)}$$

therefore

$$d_1(Az) = (V/\cos(Az)da \qquad \text{(A6-12)}$$

and

$$d_2(Az) = -(V/\sin(Az))da \qquad \text{(A6-13)}$$

are the components of the error in azimuth d(Az) parallel to lines 1 and 2 respectively. Finally

$$d(Az) = V\left[\frac{1}{\sin^2(Az)} + \frac{1}{\cos^2(Az)}\right]^{\frac{1}{2}} dt/x \qquad \text{(A6-14)}$$

which corresponds to the error in azimuth for a given dt, in an L shaped array with its arms extended the distance x.

Figures A6-1 and A6-2 show the expected errors in apparent velocity and in azimuth for typical values of dt, in an L shaped array with x = 12.5 km, similar to that used in the present research.

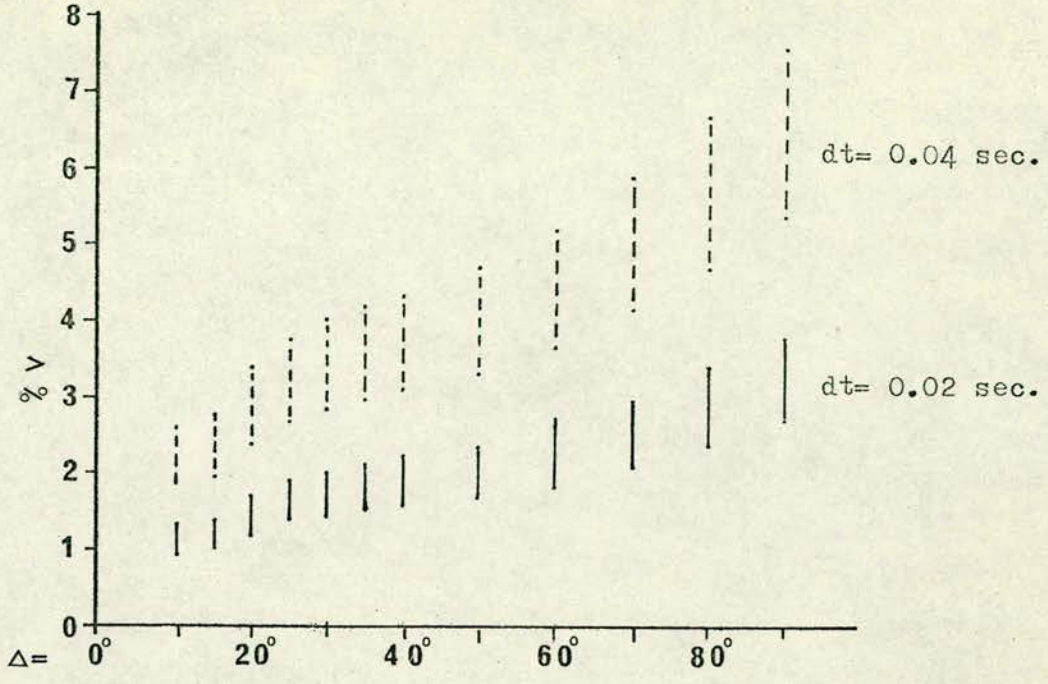

Figure A6-1.- EXPECTED ERRORS AT SAAS IN THE CALCULATIONS OF APPARENT VELOCITY, AS A FUNCTION OF DISTANCE

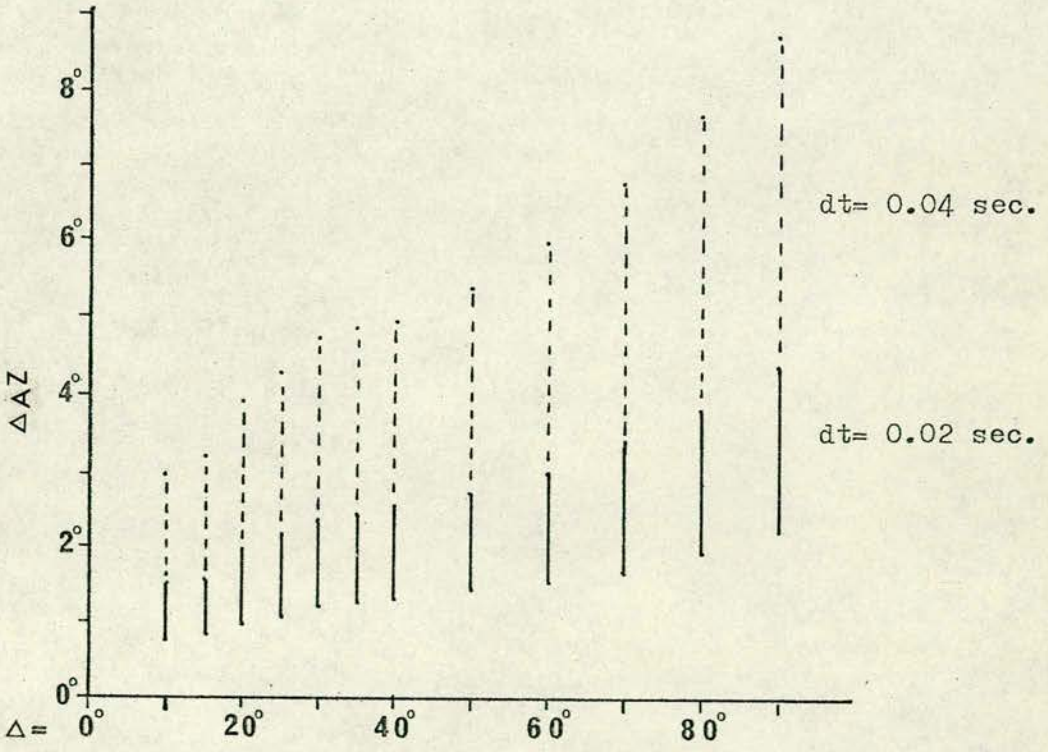

Figure A6-2.- EXPECTED ERRORS AT SAAS IN THE CALCULATIONS OF AZIMUTH AS A FUNCTION OF DISTANCE